Design and control of collaborative, cross and carry mobile robots : C3Bots

Bassem Hichri

No d'ordre : 2601
EDSPIC : 710

Université Blaise Pascal - Clermont II

École Doctorale

Science pour l'Ingénieur de Clermont Ferrand

Thèse

présentée par

Bassem Hichri

Ingénieur Mécatronique

pour obtenir le grade de

Docteur d'Université

Spécialité: Vision pour la robotique

Design and Control of Collaborative, Cross and Carry Mobile Robots: C^{3}Bots

Soutenue publiquement le 5 October 2015 devant le Jury composé de:

Cyril NOVALES	Examinateur	Maître de Conférences à l'Université d'Orléan
Faïz BEN AMAR	Rapporteur	Professeur à l'UPMC de Paris
Ioan DOROFTEI	Examinateur	Professeur à l'UT Georghe Asachi de Iasi, Roumanie.
Jean-Christophe FAUROUX	Co-encadrant scientifique	Maître de Conférences - HDR à l'IFMA
Jean-Pierre DERUTIN	Président du jury	Professeur à l'UBP
Lounis ADOUANE	Co-encadrant scientifique	Maître de Conférences - HDR à l'UBP
Olivier SIMONIN	Rapporteur	Professeur à l'INSA de Lyon
Youcef MEZOUAR	Directeur de thèse	Professeur à l'IFMA

Institut Pascal (UMR CNRS/UBP/IFMA 6602)
Axe Mecaniques, Materiaux et Structures

"Nothing is original. Steal from anywhere that resonates with inspiration or fuels your imagination. Devour old films, new films, music, books, paintings, photographs, poems, dreams, random conversations, architecture, bridges, street signs, trees, clouds, bodies of water, light and shadows. Select only things to steal from that speak directly to your soul. If you do this, your work (and theft) will be authentic. Authenticity is invaluable; originality is non-existent. And don't bother concealing your thievery - celebrate it if you feel like it. In any case, always remember what Jean-Luc Godard said: "It's not where you take things from - it's where you take them to."

[MovieMaker Magazine #53 - Winter, January 22, 2004]" Jim Jarmusch

Abstract: Our goal in the proposed work is to design and control a group of similar mobile robots with a simple architecture, called m-bot. Several m-bots can grip a payload, in order to co-manipulate and transport it, whatever its shape and mass. The resulting robot is called a p-bot and is capable to solve the so-called "removal-man task" to transport a payload. Reconfiguring the p-bot by adjusting the number of m-bots allows to manipulate heavy objects and to manage objects with any shape, particularly if they are larger than a single m-bot. Obstacle avoidance is addressed and mechanical stability of the p-bot and its payload is permanently guaranteed. A proposed kinematic architecture for a manipulation mechanism is studied. This mechanism allows to lift a payload and put it on the m-bot body in order to be transported. The mobile platform has a free steering motion allowing the system manoeuvre in any direction. An optimal positioning of the m-bots around the payload ensures a successful task achievement without loss of stability for the overall system. The positioning algorithm respects the **F**orce **C**losure **G**rasping (**FCG**) criterion which ensures the payload stability during the manipulation phase. It respects also the **S**tatic **S**tability **M**argin (**SSM**) criterion which guarantees the payload stability during the transport. Finally it considers also the **R**estricted **A**reas (**RA**) that could not be reached by the robots to grab the payload. A predefined control law is then used to ensure the **T**arget **R**eaching (**TR**) phase of each m-bot to its desired position around the payload and to track a **V**irtual **S**tructure (**VS**), during the transportation phase, in which each elementary robot has to keep the desired position relative to the payload. Simulation results for an object of any shape, described by a parametric curve, are presented. Additional 3D simulation results with a multi-body dynamic software and experiments by manufactured prototypes validate our proposal.

Keyword: Cooperative mobile robots, Control architecture, Payload transport and co-manipulation, Lifting mechanism, Force closure grasping, Static stability margin, Restricted areas, Obstacle avoidance, Target reaching, Virtual structure navigation.

Résumé: L'objectif du travail proposé est de concevoir et commander un groupe des robots mobiles similaires et d'architecture simple appelés m-bots (mono-robots). Plusieurs m-bots ont la capacité de saisir ensemble un objet afin d'assurer sa co-manipulation et son transport quelle que soit sa forme et sa masse. Le robot résultant est appelé p-bot (poly-robot) et est capable d'effectuer des tâches de déménageur pour le transport d'objets génériques. La reconfigurabilité du p-bot par l'ajustement du nombre des m-bots utilisés permet de manipuler des objets lourds et des objets de formes quelconques (particulièrement s'ils sont plus larges qu'un seul m-bot). Sont considérés dans ce travail l'évitement d'obstacle ainsi que la stabilité du p-bot incluant la charge à transporter. Une cinématique pour un mécanisme de manipulation a été proposée et étudiée. Ce dernier assure le levage de la charge et son dépôt sur le corps des robots pour la transporter. Plusieurs variantes d'actionnement ont été étudiées : passif, avec compliance et actionné. Un algorithme de positionnement optimal des m-bots autour de l'objet à manipuler a été proposé afin d'assurer la réussite de la tâche à effectuer par les robots. Cet algorithme respecte le critère de "Force Closure Grasping" qui assure la stabilité de la charge durant la phase de manipulation. Il maintient aussi une marge de stabilité statique qui assure la stabilité de l'objet durant la phase de transport. Enfin, l'algorithme respecte le critère des zones inaccessibles qui ne peuvent pas être atteintes par les m-bots. Une loi de commande a été utilisée afin d'atteindre les positions désirées pour les m-bots et d'assurer la navigation en formation, durant la phase du transport, durant laquelle chaque robot élémentaire doit maintenir une position désirée par rapport à l'objet transporté. Des résultats de simulation pour un objet de forme quelconque, décrite par une courbe paramétrique, sont présentés. Des simulations 3D en dynamique multi-corps ainsi que des expériences menées sur les prototypes réalisés ont permis de valider nos propositions.

Mots-clés: Robots mobiles coopératifs, Architecture de contrôle/commande, Co-manipulation et transport de charge, Mécanisme de levage, Synthèse dimensionnelle, Force Closure Grasping, Marge de stabilité statique, Évitement d'obstacles, Atteinte des cibles, Navigation en formation.

Acknowledgements

I would never have been able to finish my dissertation without the guidance of my committee members, help from friends, and support from my family and wife.

I would like to express my deepest gratitude to my advisor, Professor Youcef Mezouar, for his excellent guidance, caring, patience, and providing me with an excellent atmosphere for doing research.

I would like to deeply thank Dr. Lounis Adouane and Dr. Jean-Christophe Fauroux for guiding me, spending a lot of their time providing me information and advices that gives a considerable scientific value to my developed research. I would like to thank them also as they, patiently corrected my writing and financially supported my research. I would also like to thank Professor Ioan Doroftei for guiding my research for the past several years and helping me to develop my background in mobile robotics.

My thanks are also dedicated to Professor Faïz BEN AMAR and Professor Olivier SIMONIN because they agreed to report on this thesis.

I like to acknowledge the following entities: LABEX IMobS^3 Innovative Mobility: Smart and Sustainable Solutions, the French National Centre for Scientific Research (CNRS), Auvergne Regional Council and the European funds of regional development (FEDER).

I would like to thank my office colleagues, who as a good friends, were always willing to help and give their best suggestions. It would have been a lonely lab without them. Many thanks to Nesrine, Aicha, Lazher, Seif, Zinou, Khaled, Achraf, Jacqueline and other workers in the laboratory of Pascal Institute for helping me in different situations. My research would not have been possible without their helps.

I would also like to thank my wife, Anissa Awi. She was always there cheering me up and stood by me through the good and bad times.

Finally, I would like to thank my parents, my sister and my brother. They were always supporting me and encouraging me with their best wishes...

Contents

List of Figures

List of Tables

Abbreviations

AGV	**A**utomated **G**uided **V**ehicle
ASRS	**A**utomated **S**torage and **R**etrieval **S**ystem
ATHLETE	**A**ll **T**errain **H**ex-**L**imbed, **E**xtra-**T**errestrial **E**xplorer
C^{3}Bots	**C**ollaborative **C**ross and **C**arry mobile ro**Bots**
CVM	**C**urvature **V**elocity **M**ethod
DGP	**D**orsal **G**eneral **P**ayload transport
DT	**D**orsal **T**ransport
FCG	**F**orce **C**losure **G**rasping
DoF	**D**egrees **o**f **F**reedom
FPS	**F**undamental **P**rinciple of **S**tatic
HPJ	**H**igher-**P**air **J**oint
IED	**I**mprovised **E**xplosive **D**evice
ICR	**I**nstantaneous **C**enter of **R**otation
MMH	**M**anual **M**aterial **H**andling
MWR	**M**odular **W**heeled **R**obot
M-bot	**M**ono-ro**bot**
MOUT	**M**ilitary **O**perations on **U**rbanized **T**errain
P-bot	**P**oly-ro**bot**
PEGASUS	**P**entad **G**rade **A**ssist **S**uspension **S**ystem
PF	**P**otential **F**ield
RA	**R**estricted **A**rea
RSI	**R**epetitive **S**train **I**njuries
RUR	**R**ossum's **U**niversal **R**obot
SSM	**S**tatic **S**tability **M**argin
SRP	**S**tanford **R**obotic **P**latform

TPC	**T**otal **P**ossible **C**onfigurations
TC	**T**ested **C**onfigurations
TR	**T**arget **R**eaching
UGV	**U**nmanned **G**round **V**ehicle
USAR	**U**rban **S**earch **A**nd **R**escue
VDA	**V**irtual **D**eformable **A**rea
VFF	**V**ector **F**orce **F**ield
VFH	**V**ector **F**ield **H**istogram
VS	**V**irtual **S**tructure

Symbols

Indexes	
c	M-bot contact (with the ground (c=g) or with the payload (c=p)).
d	Desired position index.
m	M-bot number/ m $\in [m_{min}, m_{max}]$.
n	Normal contact.
p	Contact point position with the payload.
pl	Payload.
t	Tangential contact.
x	Component w.r.t $\vec{x}$ axis.
y	Component w.r.t $\vec{y}$ axis.
θ	Orientation component.

Symbols		
B	Payload closed boundary.	
C_{pm}	Friction cone.	
$C_{m,c}$	Contact point of m-bot # m with ground (c=g) or payload (c=p).	
$d_{m,m+1}$	Stability margin.	
δ_1	Horizontal clearances parameters.	
δ_2	Vertical clearances parameters.	
e	Robot position error.	
$\vec{F}_{int}$	Force of tightening exerted by an interconnection mechanism.	
$\vec{f}_{m,p,n}$	Normal pushing force exerted by a m-bot on the payload.	N
$\vec{f}_{m,p,t}$	Resulting lifting force exerted by a m-bot on the payload.	N
$\vec{f}_{m,g,n}$	Normal force exerted in m-bot's wheels.	N
$\vec{f}_{m,g,t}$	Tangential force in m-bot's wheels.	N
F_{pm}	Applied force by the payload on the robot body when it is laid on it.	

$\mathcal{G} = \{P_1 ... P_{m_{max}}\}$	A grasp of the poly-robot, defined by the position of all its m-bots.
G_{pl}	Payload center of mass.
G_m	M-bot center of mass.
m	m-bot number.
m_{max}	Maximum number of m-bots in the p-bot.
m_{min}	Minimum number of m-bots in the p-bot.
M	M-bot mass.
M_{pl}	Payload mass.
N_{tP}	Number of total positions.
N_P	Number of tested positions.
Ω	A large set of points representing the external surface of an object.
$\vec{M}$	Torque.
μ_c	Friction coefficient.
$\vec{g}$	Gravity acceleration.
P_m	Punctual contact position m-bot/payload.
$P(\theta)$	Equation of the payload boundary.
X_m	Robot state vector.
X_{dm}	Robot desired pose.
$W = \{\omega_1 ... \omega_{m_{max}}\}$	Set of wrenches.

Chapter 1

Introduction

Until now, robots have shown their effectiveness in different environments and different applications. In the industrial context, robotic manipulators are more and more involved in the assembly lines. They achieve various repetitive tasks with great speed and accuracy. The tasks achieved by those robots can vary depending on the industrial activity sector. In spite of their success, manipulators suffer from a lack of mobility, which means a limited workspace because of their fixed basis. Contrary to robot arms, mobile robots have the ability to move in various environments. In recent years, many researches were oriented to survey and design mobile robotic systems [11, 65, 153, 163], which is relatively young field, gathering different engineering and science disciplines. This blend between those disciplines allows the design of autonomous systems able to interact with the environment without human mediation and also to achieve diverse tasks, infeasible for humans, such as high-risk missions for law enforcement and military applications (*e.g.*, reconnaissance missions, surveillance, neutralization of IEDs – Improvised Explosive Devices), hazardous site clean-ups, and planetary explorations (*e.g.*, Mars Rover). The use of Unmanned Ground Vehicles (UGVs) in Urban Search And Rescue (USAR) and Military Operations on Urbanized Terrain (MOUT) is gaining popularity because the mobile robots can be sent ahead or in place of humans, act on the surroundings with a manipulator arm or other active means attached to an arm, collect data about its surroundings, and send it back to the operator with no risks for the human operators.

Autonomous mobile robots have the ability for sensing and reacting in the environment by acquiring additional abilities. They can also collaborate when a task needs more

than one robot, such as co-manipulation or heavy objects transport [3, 160]. Nowadays mobile autonomous systems are also designed for all terrain exploration [46, 51, 179]. This implies that the robot must have the ability to evolve and to move in different conditions of ground surface, so they can progress in rough terrain and avoid or climb obstacles by using different modes of locomotion [13, 46, 51, 179]. Our goal is to design several Collaborative Cross and Carry mobile roBots (C3Bots), called mono-robots (abbreviated into m-bots) with a simple architecture that will be capable to co-manipulate and transport objects of any shape by connecting together. The resulting robot will be called a poly-robot (abbreviated into p-bot) and will be capable to solve the so-called removal-man task to transport any type of payload. Reconfiguring the poly-robot by adjusting the number of mono-robots allows to grip and manipulate heavy payloads, particularly if they are wider than a single mono-robot.

1.1 Motivation and objectives

The development of an innovative robotic system for co-manipulation and transport of payloads of any shape is a complex process that can be divided into several steps. As a first phase, the ideas concerning the robot mobility have to be surveyed. Then these ideas are converted into a preliminary design. Trade-offs have to be conducted to enable an objective, methodological selection of the best design. After that, detailed properties have to be specified and simulations are run to determine the expected performance. Multiple iterations of detailed design, prototype manufacturing, and testing might be necessary before defining the final solution. In literature, numerous ideas and first prototypes of robots can be found as well as sophisticated models. Unfortunately, there is almost no work concerning a multi-robot system able to interconnect to form a more complex structure ensuring any shape payloads co-manipulation and transport. Therefore, the following scientific topics were set for this thesis:

- design of a mechatronic system for a structured ground equipped with a manipulator,
- static and dynamic models to maximize the poly-robot margin of stability,
- validation of the co-manipulation, transport and control strategies,

- system control to guarantee efficient connections m-bot/m-bot and p-bot/payload,
- optimal reconfiguration of the m-bots for the task (number, poses, cooperation strategies).

1.2 Outline

This thesis is split into five main parts:

- **Chapter 2**: in this chapter the research problematic will be introduced and an overview about existing developed mobile robots will be presented. Different types of existing mobile robots and particularly terrestrial mobile robots will be detailed. Multi-robot systems will be also concerned for collaborative tasks achievement.
- **Chapter 3**: this chapter is dedicated to the design of the mechanical structure of the m-bots. It will consider the definition of an appropriate methodology of co-manipulation and transport for a multi-robot system. It will also present the system specifications and the mobile robots mechanical architecture and design. The lifting capacity of the developed robot will be evaluated using different strategies of manipulator actuation.
- **Chapter 4**: it will provide a review about the mobile robots control architecture and particularly the control approaches for navigation in formation. The focus is made in this chapter on the chosen methodology to obtain sub-optimal positioning of the robots around the payload to lift it and to transport it while maintaining a geometric multi-robot formation.
- **Chapter 5**: this chapter is dedicated to 3D simulations and experimental results in order to validate the proposed mobile robots architecture. It will also present the simulation results for optimal positioning of the robots for a successful task achievement. The target reaching problem and virtual structure navigation will be simulated for a group of m-bots.
- Finally, a conclusion about the achieved works and future works for C^3Bots project.

Chapter 2

Research Problematic and State of the Art

Abstract: *This first chapter is an introduction to the basic problem which consists on mobile robotic systems and their ability in achieving diverse tasks such as all terrain evolving, cooperative tasks achievement, co-manipulation and payloads transport. The main task of our thesis and which will be ensured by a group of collaborative mobile robots is collaborative co-manipulation and transport of payloads of any shape and mass. This task will be ensured using mobile robots equipped with a manipulation mechanism.*

2.1 Introduction

The use of a group of robots versus a single robot is advantageous since, for example in transportation tasks, a payload is distributed among a group of simpler and inexpensive robots. Additionally, the payload handling dexterity may be increased, the defection of a subset of robots may not fail totally the task achievement and the robots may be reconfigured in order to fit a payload of any shape and to fit the environment in which they evolve. There has been a significant research related to payload transportation using multiple robots [3, 8, 80, 92, 96, 187]. Our goal in the C^{3}Bots project (Collaborative Cross and Carry mobile roBots) is to design several mobile robots, called m-bots, with a simple mechanical architecture that will be able to autonomously co-manipulate and transport objects of any shape. The resulting poly-robot system, called p-bot, will be able to solve the so-called removal-man-task [74] to transport any object on the top platform of m-bots (dorsal transport). This particular variant of the C^{3}Bots project will be called C^{3}Bots **DGP** (**D**orsal **G**eneral **P**ayload transport). Reconfiguring the p-bot by adjusting the number of m-bots allows to manipulate heavy objects with any shape, particularly if they are wider than a single m-bot.

Industries is one of our targeted fields, for which we are interested to develop a robotic system for objects or payloads lifting and transport. Such modern innovative technologies ensure better adaptability and productivity. However, dedicated equipments that request a long installation time are still predominant in heavy industry and construction. Different techniques for object lifting in a safe and efficient way are used for **M**anual **M**aterial **H**andling (**MMH**) [77, 134, 139] but can cause **R**epetitive **S**train **I**njuries (**RSI**) [188].

Developed transporting mechanisms and technologies are widely found. Some transport solutions require heavy infrastructure such as Automated Guided Vehicles (AGV) [174] (*e.g.* ground landmarks, guiding rails) or specific stacking racks for storage as for Automated Storage and Retrieval System (ASRS). Human assistance could also be needed to put the object on the transporting platform (*e.g.* scissor [84]). Forklifts [176] use forks to lift and transport the object but they require the preliminary positioning of the object on a pallet for their subsequent transport. Grabbing systems such as robot hand [120] was designed to adapt the manipulated object shape by it limits the manipulated payload size and shape. According to the previous mentioned systems, one can conclude that for a better stability, an object should be better transported on the robot body

[10, 20] or as close as possible to the robot body, to keep the gravity center above the polygon of support and ensure a bigger stability margin.

In this chapter, the problematic and the state of the art about manipulators, mobile robots and the associated locomotion modes will be studied in order to have an overview about the existing technology and to develop an innovative multi-robot system able to co-manipulate and transport payloads of any shape and mass. It will be organized as follows: section 2.2 presents a brief review about robot manipulators and their extensive use in industrial sites. In section 2.3 and section 2.4 an overview about mobile robotic system will be detailed in order to develop an innovative system for payloads manipulation and transport. Finally, section 2.5 will present the specification of the C^3Bots project and the proposed methodology for transportation task achievement.

2.2 Robotic manipulators

Definition

The term "robot" was first introduced by Karel Capek in his theater play "Rossum's Universal Robot (RUR)". Originally the term ROBOTA, "forced work", designated the origin of android machine able to replace human in every task and effectively the robots invade progressively different fields. Obviously, industry is the winning sector from robotic advance. Manipulators are the most used robots. Since their first use (beginning of the 60^s) until today, manipulators of different types were developed (serial, parallel, hybrid), dimensions and specifications [93] are integrated in various applications (automotive industries, high speed manufacturing...)

A robot manipulator is an electronically controlled mechanism. It is made of multiple segments and an end-effector that performs tasks by interacting with its environment. It is also called robotic arm. Robot manipulators are extensively used in the industrial manufacturing and many other specialized applications (*e.g.* the Canadarm (cf. Fig. 2.1) was used on the American space shuttle to manipulate payloads). The study of robot manipulators involves dealing with the positions and orientations of the several segments that make up the manipulators [94].

FIGURE 2.1: Station Remote Manipulator System [9]

Manipulators are composed of an assembly of links and joints. Links are defined as the rigid sections that make up the mechanism and joints are defined as the connection between two links. The device attached to the manipulator which interacts with its environment to perform tasks is called the end-effector.

Manipulators can be classified according to a variety of criteria such as:

Motion Characteristics

- *Planar manipulator*: if all the moving links move in planes parallel to one another,
- *Spherical manipulator*: if all the links perform spherical motions about a common stationary point,
- *Spatial manipulator*: if at least one of the links of the mechanism possesses a general spatial motion.

Kinematic Structure

- *Open-loop manipulator* (or serial robot): characterized by an open-loop chain,
- *Parallel manipulator*: characterized by a closed-loop chain,
- *Hybrid manipulator*: characterized by an open loop and closed loop chains.

In current industries, robotic manipulators are more and more widespread [79] thanks to their distinguishing characteristics such as: workspace, durability, high speed for task

execution, repeatability, positional precision. They are mainly used repetitive assembly tasks where components are always in the same positions and only a position control is needed for the robot. A considerable number of industrial robot applications in industry are existing today. Their application are motivated by technical and economical reasons such as:

- improving the quality of products,
- reducing the waste,
- increasing the uniformity of quality ,
- increasing the operating safety,
- reducing the request for operators in routine and repeatable processes,
- reducing manufacturing costs,

Fig. 2.2 shows examples of robotic manipulators where robots are synchronised in activities with machines for tools changing (cf. Fig. 2.2(a)), workpiece positioning (cf. Fig. 2.2(b)) or gripping tasks (cf. Fig. 2.2(c)) [90].

Robotic manipulators can also achieve collaborative handling in order to manipulate small workpieces either individually (cf. Fig. 2.3(a)) or in a cooperative way (cf. Fig. 2.3(b)) which allows a shorter task duration than when one large size robot is used.

For manipulation tasks, payload prehension is one of the most complex function to be realized in robotic systems. It is supposed to use a controlled mechanical system (manipulator) adapted to object grasping. Sensors integration to a gripper seems to be necessary for many reasons, in particular to determine the gripping configuration, to control the gripping effort and more generally to control the realized action by the gripper. Prehension systems may have diverse forms according to objects to be manipulated and tasks to be accomplished. Grippers may be extremely versatile systems, from human inspired-systems that offers a great capacity of gripping to some very simple specific grippers. When the manipulating operation becomes very simple and repetitive such as in industry, simple gripper can be found with symmetric tightening or prehension systems using adhesion strategy to be connected to object using different effects: electromagnetic for ferrous material, electrostatic for miniaturized objects. PARAGRIP

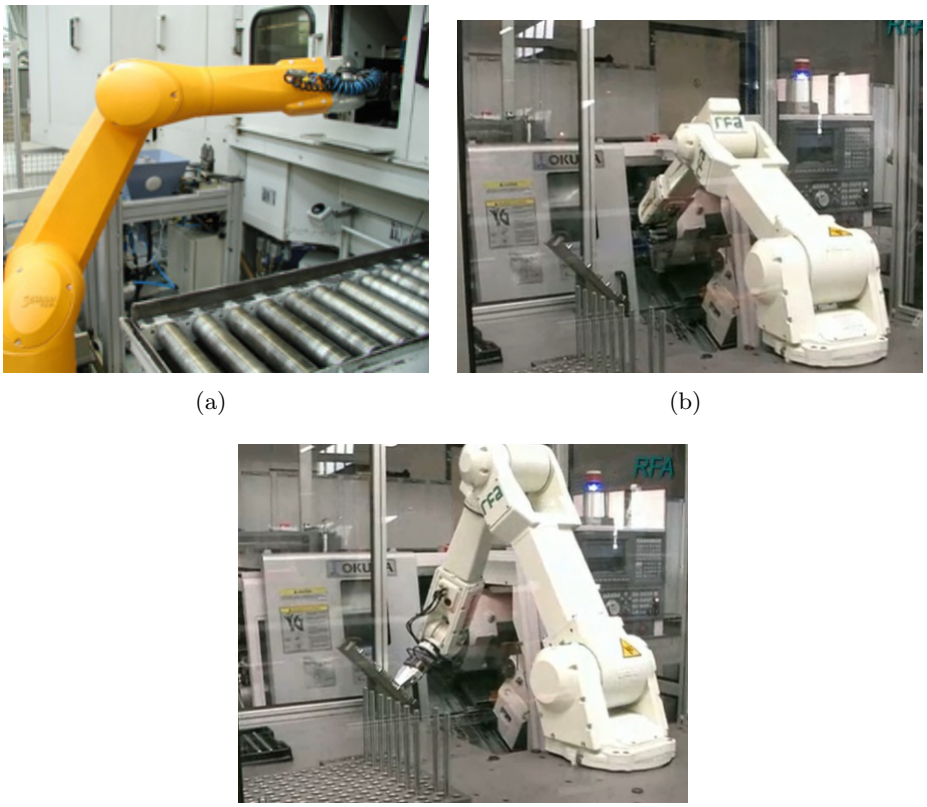

(a) (b)

(c)

FIGURE 2.2: Manipulation tasks [90]: a) tools changing on machine; b) Work pieces positioning; c) Parts griping

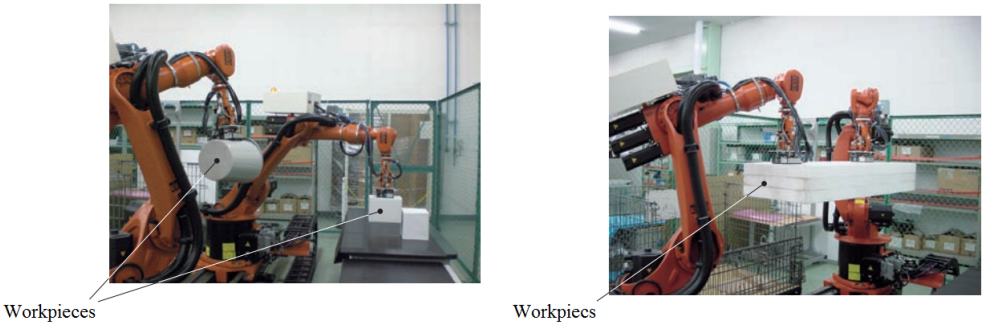

(a) (b)

FIGURE 2.3: cooperative manipulation robots [91]:a) two workpieces are handled by two robots; b) one workpiece is handled by two robots

[143] is a reconfigurable parallel robotic system (Fig. 2.4(a)) using three manipulators and able to manipulate objects in six dimensional Cartesian space using only six actuated joints. The effector of each arm is equipped with a contact element that will ensure the object prehension. The closed loop of the system is formed by the arms and the object after being connected to all the effectors. Another example of human hand inspired gripper [27] is a compliant gripper capable to grasp object with different shapes

illustrated in Fig. 2.4(b). Also Festo [53] has developped a bioinspired compliant gripper (Fig. 2.4(c)) at the end of a souple arm similar to a trunk using pneumatics. This gripper is very efficient to adapt an object shape and grasp it with a high compliance.

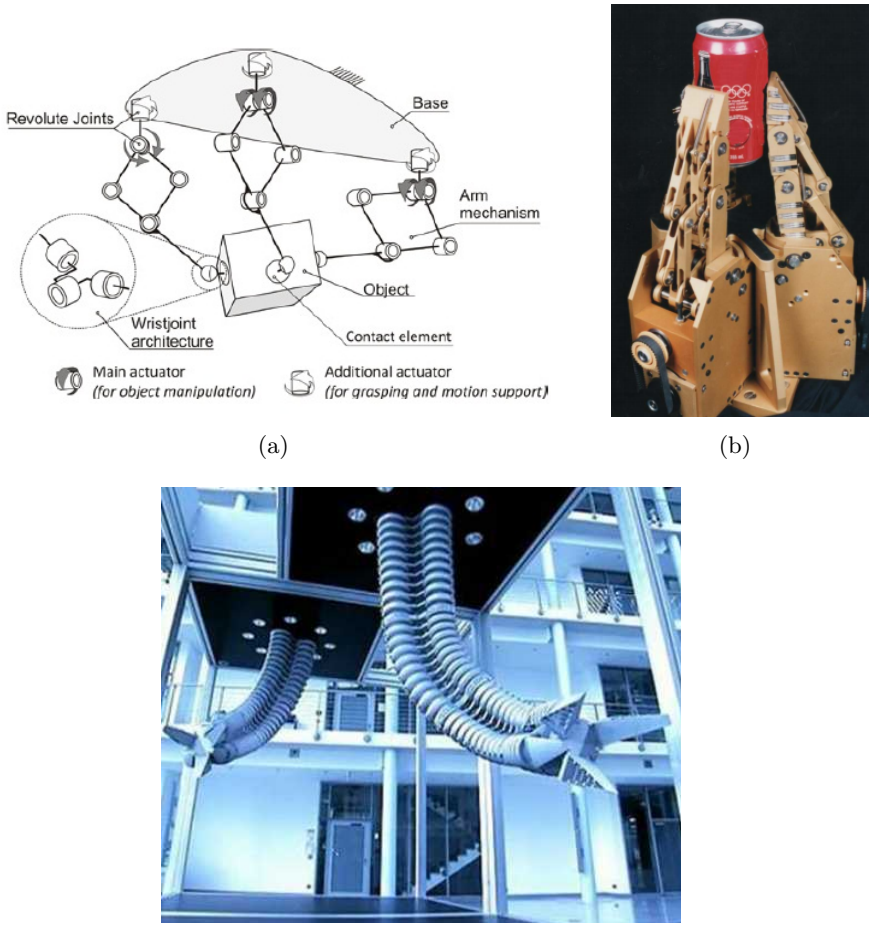

FIGURE 2.4: Prehension Systems: a) PARAGRIP [143]; b) Compliant Gripper [27]; c) Festo Bioinspired Compliant Gripper [53]

In spite of the robotic manipulators performances and wide use in industries, they lack of mobility within the environment. A deep survey of mobile robots will be presented in the next section in the aim of the development of mobile robotic system for manipulation and transportation tasks.

2.3 Mobile robots

Introduction

A variety of mobile robots have been developed depending on the application, velocity, and the type of environment (water, space, terrain with fixed or moving obstacles). Four major categories had been identified [39]:

- Terrestrial robots: Wheeled robots are the most common ones thanks to the wheeled locomotion advantages; others are legged, tracked or crawling vehicles,
- Aquatic robots: These robots operate in water surface or underwater based on water jets or propellers,
- Airborne robots: Flying robots like Robotic helicopters, fixed-wing aircraft, robotically controlled parachutes, and dirigibles,
- Space robots: Those are designed to operate in the microgravity of outer space and are typically envisioned for space station maintenance. Space robots either move by climbing or are independently propelled.

Mobile robots can be classified according to terrain in which they can be designed to evolve. We can then find robots dedicated to flat structured grounds or to all terrain exploration. In this last case, they should be designed with mechatronics architecture allowing additional abilities such as obstacles climbing.

A mobile platform must be able to evolve on structured or rough terrains. A simple base has three degrees of freedom (DOF), (x, y) for its position and its orientation θ. Degrees of freedom may increase for more complex structure, e.g. articulated bases may have two coupled parts. For mobile robot research, most of the used bases have a single body for which position and orientation can be controlled. Even within this framework, there are still a large variety of locomotion methods. In order to choose an adequate locomotion for a mobile robot, its mechatronics structure should be studied. Here we focus only on terrestrial mobile robots moving either using wheels or articulated legs. According to [51, 153], four modes of locomotion can be distinguished:

- Crawling robots (cf. Fig. 2.5) have the ability, by using structure deformation and multiple ground contact points, to move in irregular terrains and cross obstacles but the complexities of their control and the high energy consumption, even for moderate speeds, is a major drawback,

(a) (b)

FIGURE 2.5: Crawling mobile robots: a) Aiko: 7kg, 1.5m long, 20 DOF, 2.5 Nm Obstacle-aided locomotion, slidewinding [165]; b) Active Cord Mechanism ACM-R5: 7.5kg, 1.7m long, 80mm diameter Snake propulsion on ground and water [161]

- Legged robots (cf. Fig. 2.6) have the ability to cross obstacles and progress on rough terrains thanks to their ground contact discontinuity although they are complex not only in terms of mechanical system but also in terms of electronics, sensing and control algorithms. One can cite as examples: Stanford "Sprawlita" [33], Draper "Bug2" [111], Draper "Ratbot" [111], Boston Dynamics "Big Dog" [30], Bremen Robotics Lab "Scorpion" [99],

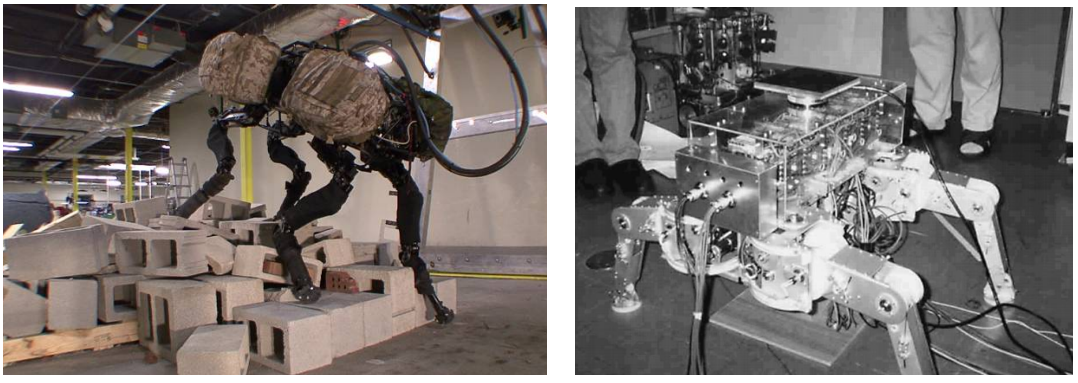

(a) (b)

FIGURE 2.6: Legged mobile robots: a) Boston Dynamics "Big Dog": 75kg, 1m long, 6km/h, 35° slopes, 150kg payload [141]; b) Titan: Four-legged robot with a six-degrees-of-freedom force sensor [10]

- Wheeled systems (cf. Fig. 2.7) can move efficiently on flat and regular surfaces while obstacle climbing is a challenge,

(a) (b)

FIGURE 2.7: Wheeled mobile robots: a) OpenWheel: All terrain four wheeled robot [48]; b) Nomad: Four-wheeled robot [180]

- Tracked robots (cf. Fig. 2.9) which are permanently stable but they present high friction energy loss particularly during steering phases. Some other examples of tracked robots are briefly cited as follow: Foster-Miller "TALON" [178], CMU "Gladiator" [64], Sandia "microcrawler" [22], ESI "MR-1 & MR-5" [44], Remotec's Andros series [118, 181, 182].

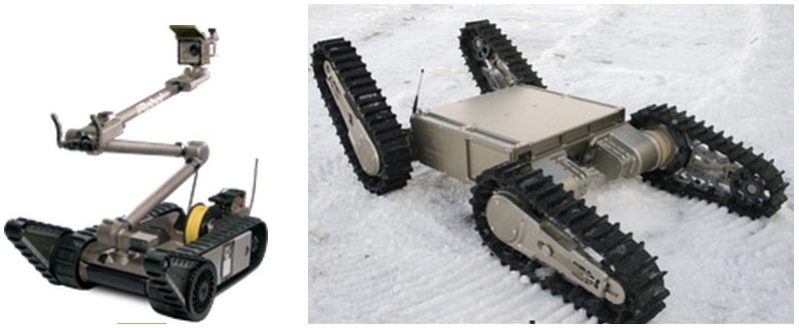

(a) (b)

FIGURE 2.8: Tracked mobile robots: a) Packbot: Tracked robot with auxilliary climbing tracks [60, 82]; b) Chaos mobile robot: autonomous tracked robotic platform designed for high mobility in areas with challenging terrain [43]

Table 2.1 summarizes the different locomotion modes by presenting each mode, the corresponding evolving environment and the characterizing advantages and drawbacks.

Locomotion modes	Locomotion means	Locomotion Environment	Climbed Obstacles	Advantages	Drawbacks
Crawling Robots	Structure deformation Ripple motion	Unstructured and Structured environments	Obstacles with a height lower than the robot length	Great contact points with the ground Fast evolving on rough terrain	High energy consumption High friction Complexity of control
Legged Robots	Legs	Unstructured and Structured environments	Obstacles with a height depending on control type: static or dynamic	High capacity of obstacle climbing High speed locomotion on rough terrains	High energy consumption Complexity of control Discontinuous contact with the ground Complex of stabilisation
Wheeled Robots	Wheels	Structured environments or slightly rough terrain	Obstacles with a height lower than the wheel radius	Energy efficiency High speed on smooth ground	Reduced climbing capacity
Tracked Robots	Caterpillar-tracks	Unstructured and Structured environments	Obstacles with a geometry compatible with the used locomotion	High capacity of obstacles climbing Adaptable to different possible situations	High energy consumption High friction

TABLE 2.1: Mobile robots locomotions characteristics

2.3.1 Flat ground mobile robots

This category of robots is designed for specific applications and tasks, mainly for material transport in an industrial structured environment or for research. Automated Guided Vehicle (AGV) systems are mobile systems, which follow a guided path and are controlled by a centralized or reactive control as explained in [8]. This technology is more detailed in [151] and includes different robot types (cf. Fig. 2.9(a)). We can find also mobile gantry crane or Automatic Storage Retrieval Systems (ASRS), which are widely used than AGVs but restricted to highly structured environment such as warehouses and libraries (cf. Fig. 2.9(b)).

(a) (b)

FIGURE 2.9: Industrial robots: a) BA SYSTEMES "Automated Guided Vehicle (AGV)" [157]; b) Duro Felguera "Automatic Storage Retrieval Systems (ASRS)" [81]

One of the smallest fully autonomous mobile robotsis Alice presented in Fig. 2.10(a). It was developed by Gilles Caprari at the Autonomous Systems Lab at EPFL (Switzerland) [8, 153]. Khepera robot presented in Fig. 2.22(b) is a small mobile robot used for research, with reduced dimensions and which can handle additional modules such as cameras and grippers. It is manufactured and distributed by K-Team SA, Switzerland. It has also infrared proximity and ambient light sensors for environment interaction and obstacle avoidance. Other examples of mobile robots as mentioned in [153] are: RobotCleaner (Fig. 2.10(c)), developed by Alfred Kärcher GmbH & Co and that covers dirty areas with a special strategy until it is really clean. Pioneer robot in (Fig. 2.10(b)), developed at SRI Stanford, is a mobile modular robot offering many equipements such

as on-board camera or an optional gripper. All these systems are efficient on regular terrains but have difficulties on rough terrains.

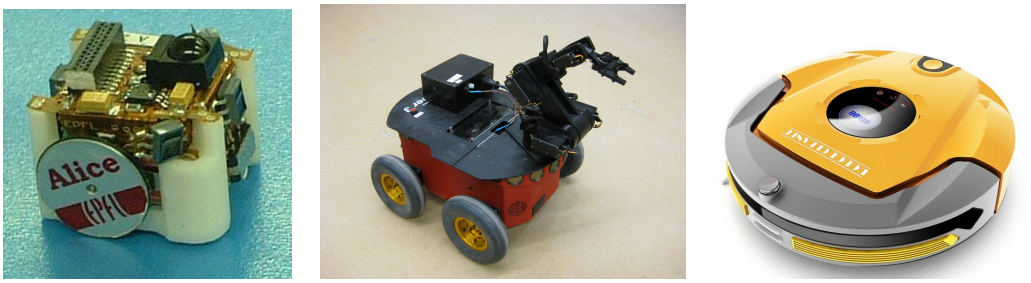

(a) (b) (c)

FIGURE 2.10: Industrial robots: a) Alice module [110]; b) Khepera mobile platform [87]; c) Pioneer [4]; d) Robotcleaner [56]

2.3.2 All terrain mobile robots

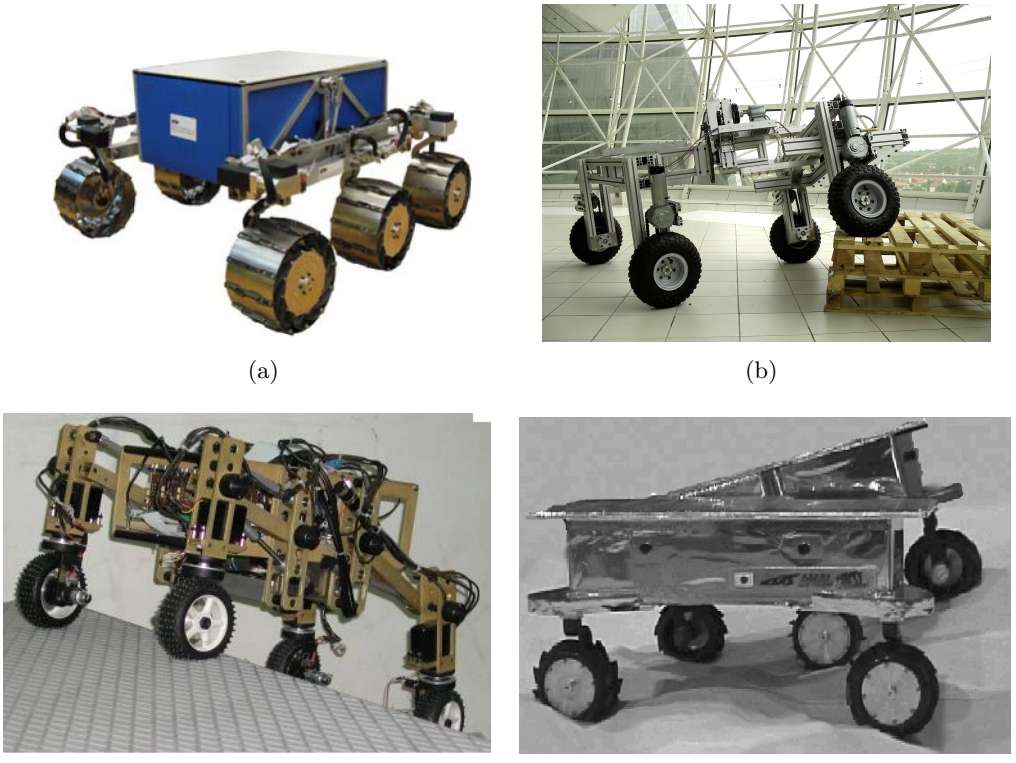

(a) (b) (c) (d)

FIGURE 2.11: All terrain mobile robots: a) CRAB [102]; b) OpenWheel [51]; c) Hylos [13]; d) Micro.5 [105]

Another kind of robots, oriented to all terrain, was studied and developed in many literatures [13, 49, 51, 52, 102, 107]. They are dedicated for planetary or dangerous area exploration. They have different architectures and different modes of locomotion. Fig.

2.11 and 2.12 illustrate some of these systems, which are detailed below. In [102], authors present the torque control as an efficient controller to minimize the wheel slipping by distributing the torque on the wheels for the so-called CRAB robot (cf. Fig. 2.11(a)). This mobile robot has six wheels and its mechanical structure is based on parallelogram bogies which are connected for a better repartition of transmission effort. OpenWheel i3R [51] is a wheeled robot with a deformable frame composed of two axles, four wheels and an inter-axle mechanism including two frames linked by a revolute joint, as illustrated in (cf. Fig. 2.11(b)). This robot is able to move and climb obstacles using the principle of stability on three wheels. It provides interesting crossing capacities, low actuation and a classic four wheel vehicle structure at the price of a complex climbing process. Hylos [13] is a wheel legged robot with sixteen DOF (cf. Fig. 2.11(c)). It has four legs each one combining a two DOF suspension mechanism with steering and driven wheel. It presents great characteristics but requires many actuators and complex control to use its different locomotion modes. Micro 5 [105, 107] is a five wheels mission rover (cf. Fig. 2.11(d)) using a Pentad Grade Assist Suspension System (PEGASUS). Wheels are controlled independently. Steering is achieved by differential left and right wheels. This robot has a good stability that is lower than four wheel vehicles, even though, it does not have compliances on the main structure as explained in [11]. In [152] authors describe Shrimp (cf. Fig. 2.12(a)) which is a mobile robot with fewer actuators. It uses suspensions based on rocker bogies with a parallelogram mechanism. Shrimp has six wheels with a specific articulated body, which permits to keep all of them in contact with the ground. Shrimp can climb over high obstacles and its rear wheel is directly fixed to the frame. The four bars mechanism with the spring makes it an excellent step climber but at the price of reduced stability. Carnegie Mellon University introduces in [175, 179, 180] Nomad (cf. Fig. 2.12(b)), a four wheels drive and four wheels steering mobile robot developed by researchers from the Robotics Institute at Carnegie Mellon University. It can increase its stability by enlarging distances between its wheels, depending on terrain type. The robot is composed of two halves on each wheel that are deployed and steered simultaneously by arms, allowing a chassis reconfiguration so it has two configurations either deployed or stowed. Steering is proven by adjusting a pair of four bars mechanism. Rocky.7 [68, 175] is also a mobile exploration rover (cf. Fig. 2.12(c)) using a rocker bogie suspension mechanism and two steering wheels. This robot has six wheels. It was developed on 1996 by NASA to revisit Mars Planet and to make some tests on the environment with its four-degree-of-freedom arm for sampling soil or

rocks and a solar panel for power supply. Ames Marsokhod Rover [32] is a mobile robot for planet exploration developed by NASA Ames research Center (cf. Fig. 2.12(d)). It consists of three pairs of independently driven titanium wheels, each pair being joined by three degree of freedom passively articulated frame. It is equipped with a five degree of freedom arm developed by MacDonnell Douglas for close up imaging, soil test and sample acquisition. Due to the articulated frame, the payload area is segmented (front/rear). This is unfavorable because it limits the effective payload volume and maximum size of devices. Table 1 summarizes the joints number for mobile robots and the number of actuated joints giving the ability of moving and steering. It also presents estimation for control complexity according to the number of used actuators. Ability for obstacle climbing is also mentioned and concerns obstacles which are greater in height than the robot wheel's radius.

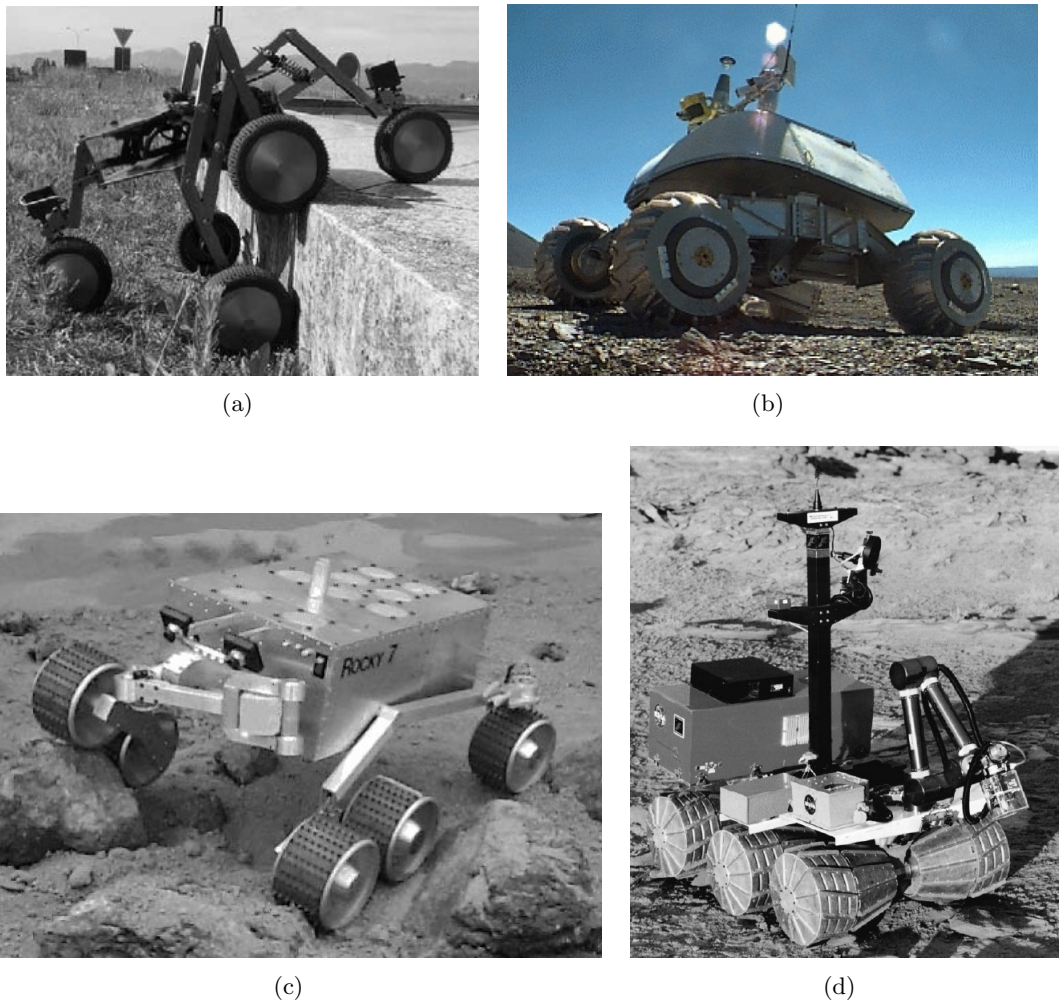

(a) (b)

(c) (d)

FIGURE 2.12: All terrain mobile robots: a) Shrimp [152]; b) Nomad [179]; c) Rocky.7 [175]; d) Marsokhod [32]

2.4 Collaborative mobile robots

Collaborative robots is the synonym of the existence of a group of robots. It states not only to control each robot individually, but also to use an appropriate control strategy in a manner that the assembly of the whole entities generates a coherent and efficient configuration for a desired task achievement.

Generally the use of a group of robots instead of one is motivated by two major factors:

- Either the task to be executed needs imperatively a cooperation between a minimal number of robots, i.e, the task could only be accomplished by the simultaneous intervention of critical number N_c of robots,
- Or to improve certain performances related to the execution of the task to be realized as for example:
  - rapidity: We are looking to reach a high level of performances by paralleling the tasks (*e.g.* the parallel exploration of an unknown environment by a group of mobile robots for cartography tasks [34, 158]). This kind of task could be achieved by only one robot but using a group of robots allows to accelerate the task achievement,
  - robustness-reliability: the control performances may be less affected in case where one agent is broken [119, 129],
  - flexibility: possibility of executing the desired tasks in different manners,
  - emergence: the idea here is to produce a collective performance qualitatively greater than the sum of all unit performances.

In the proposed work the focus is oriented to terrestrial mobile robots in order to design an innovative system for co-manipulation and transport. More informations about the other categories could be found in [11, 39]

In a collaborative task, two main architectural solutions are considered: either using a fully distributed approach in which a robot autonomously cooperates with others for a common goal or by centralizing the management of task allocation. The former solution is often used in collaborative task because it is flexible and fault tolerant [8]. The following sections aim to describe collaborative robotic systems.

2.4.1 Modular robots

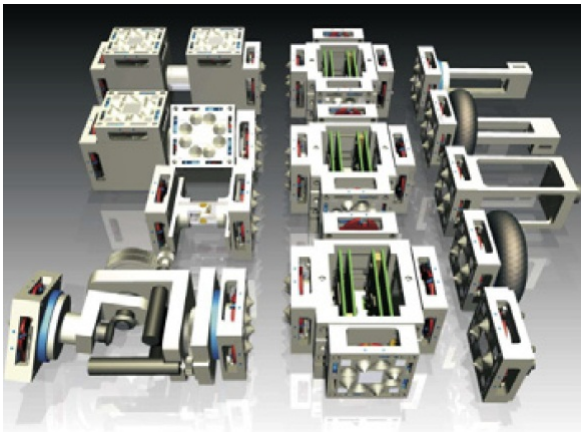

(a) Different modules of SMART robot

(b) Several modular robot configurations for rapid response to a diversity of tasks

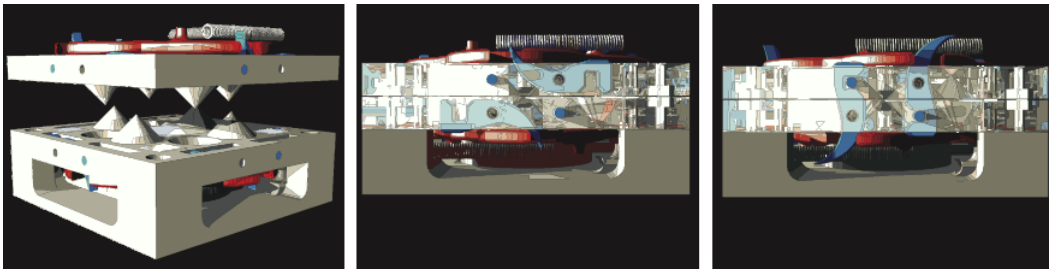

(c) Interconnection system

FIGURE 2.13: Modular robots: SMART modules [16]

A concrete example for collaborative robots is a modular self-reconfigurable robot, which has independent mechatronic modules. SMART robots treated in [16] are described as reconfigurable modular units (cf. Fig. 2.13) mainly composed of joint, power and control modules and other specialized modules. The power modules control the modules actuators. They process the data coming from the robot and manage also the communication between them and the central control unit handled by an operator. The joint module is composed of actuators of different natures (electric, hydraulic, pneumatic) and supplementary components in order to ensure the mechanical interconnection between different modules. The type of used joint module allows to define the formed robot workspace and its configuration. The specialized modules involve sensors, specific tools, passive elements and end effectors. They offer the capacity of manipulation, locomotion... The modules are able to connect using a system of hook and guiding faces (cf. Fig. 2.13(c)). This system allows also to connect the communication network of different modules. The communication between the used modules is necessary to ensure

the synchronisation with the power and control modules distributed in a master-slave architecture.

Authors in [75] have developed Modular Wheeled Robots (MWR) in Fig. 2.14, which mainly consist of a comb shaped body, a single actuated and/or steered wheel and the associated servo motor. An auxiliary module, which has the same geometry, is used to build the structures. The modules are able to inter-connect using a self locking bolt/hook mechanism and guiding faces shapes (cf. Fig. 2.14(b)).

(a)

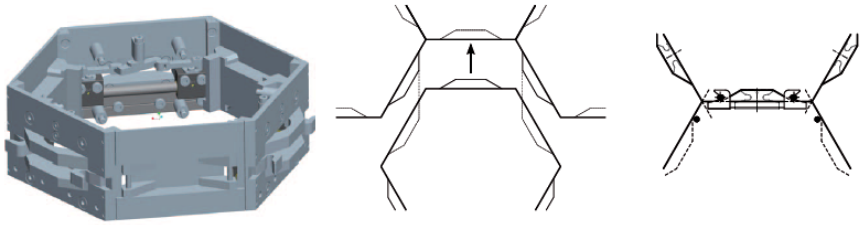

(b) Basic geometry of the interconnection mechanism and its principle

FIGURE 2.14: Modular robots: Modular wheeled robots [75]

In [92], Serge Kernbach presents swarm agents with an interesting form of collective system in a Symbiotic Organism (cf. Fig. 2.15(a)). This robot includes modules, such as MWR and can perform obstacle climbing by interconnecting using a hook system. The previous mentioned robots are used for specific tasks and could evolve in terrain in different configurations. Another interesting structure is given by SLIMEBOTS [83] which use specific modules (cf. Fig. 2.15(b)) equipped with telescopic arms and a friction organ linked to the ground. They are using a gripping material (Velcro strap) for connection to each others. These modular robots are inexpensive but they have non-resistant connections and weak mobility while a simple module is unable to evolve without being connected to other modules.

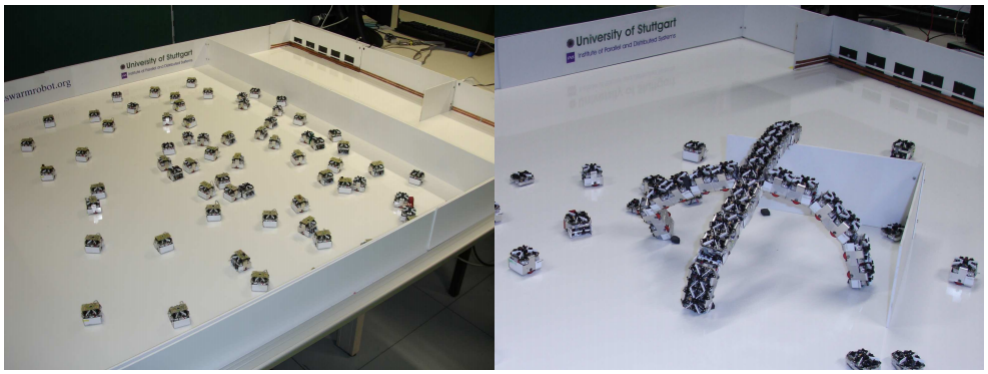

(a)

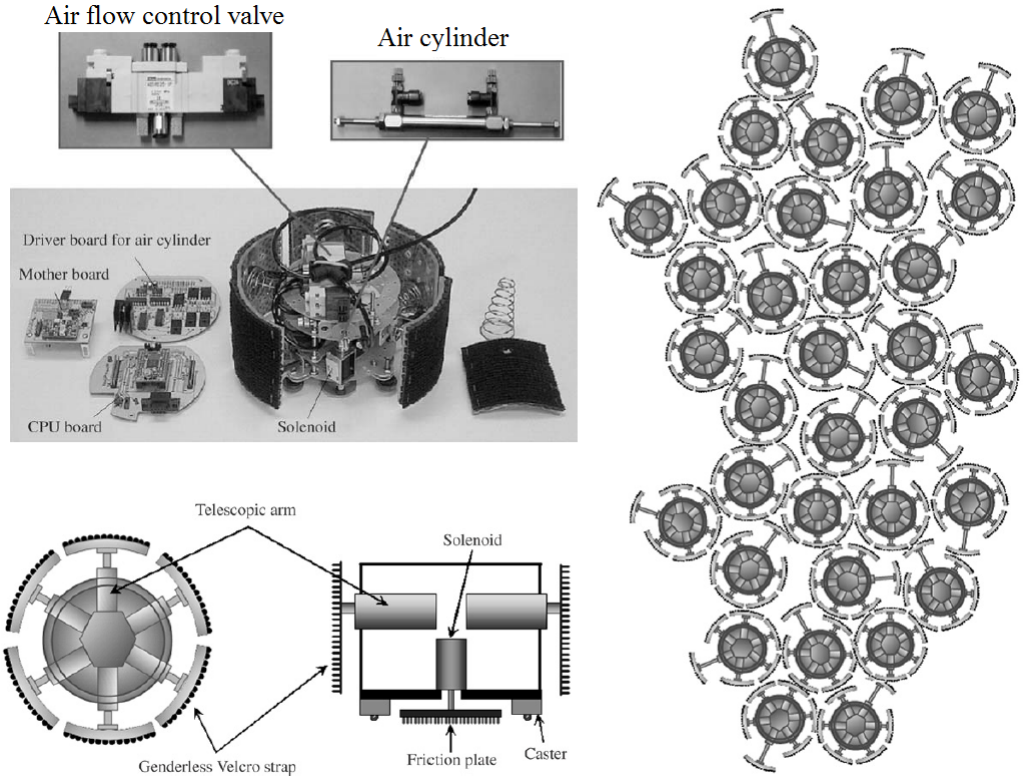

(b)

FIGURE 2.15: Modular robots: a) Symbiotic Robot Organism [92]; b) Slimebots [83]

M-TRAN systems [108, 189] are simple identical modules composed of two blocks (half cubic and half cylindrical) with two rotational DOF and six connection surfaces Fig. 2.16(a). M-TRAN has a simple structure but it presents a lack of stiffness and all modules provide the same torque whereas all the machines and living beings require actuators of various torques, depending on their use. In [86] ATRON (cf. Fig. 2.16(b)) modular systems similar to M-TRAN are presented. It uses modules with rotational actuators around the axis perpendicular to the equatorial plane. All of the presented systems have the ability to disconnect and reconnect between them using an interconnection system

(magnets for the M-TRAN robots and hooks for the ATRON), allowing the robots to reconfigure in a unique structure, enabling the obtained poly-robot to execute tasksthat could not be executed by a single mono-robot.

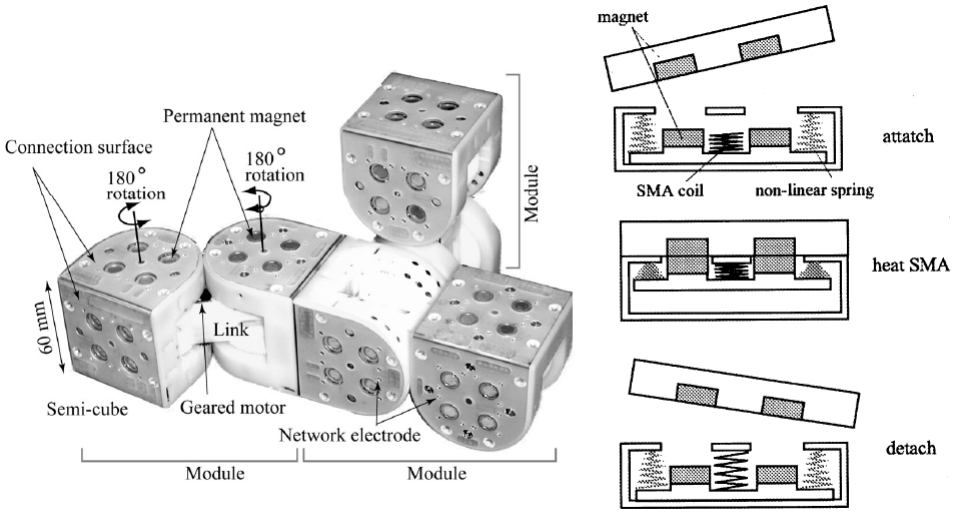

(a)

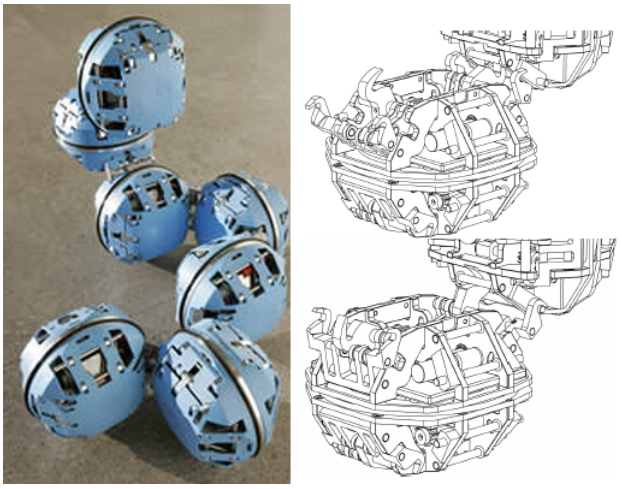

(b)

FIGURE 2.16: Modular robots: a) M-TRAN [108, 189]; b) ATRON [86]

Robot / Criterion	SMART	MWR	Swarm	Slimebots	ATRON	M-Tran	First design	C^{3}Bots
Type of modules	Differentiated	Differentiated	Unique	Unique	Unique	Unique	Unique	Unique
Shape of module	Prismatic	Hexagonal	Cubic	Cylindrical	spherical	Half-cubic Half-spherical	Prismatic	Prismatic
Locomotion mode	Depending on modules	Wheeled	Wheeled	Depending on module kinematic	Depending on module kinematic	Depending on module kinematic	Wheeled	Wheeled
Locomotion module autonomy	No	No	Yes	No	No	Yes	Yes	Yes
Module DOF	Depending on the used module	Depending on the used module	3	7	1	2	4	-
Means of communication	CAN bus	CAN bus	Radio and IR waves		IR diods	IR bus	WIFI	WIFI
Connection locations	4 for P/C 2 for J 1 for S	6	2	6	8	6		
Connection type	Hook	Hook	Hook	Velcro strap	Hook	Magnets	Mechanical	Mechanical
Connection technology	4 hooks + Guiding shapes	1 hook + Guiding shapes	Plier + Ring stowage	Velcro strap	1 hook + Guiding shape	Magnets	Friction contact	Friction contact
Connection actuator	Motor	Motor	Motor	Cylinder	Motor	Shape Memory Alloy spring	Motor	Motor
Connection guiding system	Yes	Yes	No	No	Yes	Yes	No	No

Table 2.2: Table of comparison for modular robots

Table 2.2 summarizes the previously mentioned modular robots. We will take certainly these systems as inspiring models to design an efficient collaborative robotic system. In the next section, we will present the cooperative aspect for object manipulation, which is one of our goals in C^{3}Bots to make a system able to manipulate and transport objects.

2.4.2 Payload manipulation and transport robots

The ability to interact with the environment is an important capability for robotic systems. Indeed, grabbing, lifting, pushing and manipulating objects while navigating is among the main tasks that can be assessed to a group of mobile robots. This kind of systems can undertake various tasks in different fields such as industrial or construction sites. These cooperative robotic systems are used, generally, to improve flexibility and fault tolerance. Many robotic systems used for objects manipulation and transport can be found in literature. For example, Swarm Robots in the Swarmanoid project (cf. Fig. 2.17) are used for collaborative tasks [38]. Authors present three different robots (foot-bot, hand-bot and eye-bot) which have the ability to collectively displace a book in a library. The eye-bot can be attached on the roof in order to describe the environment to the other robots. The foot-bots transport the hand-bot by connecting together using gripping system and the hand-bot is in charge then to manipulate an object using two grippers as end-effectors.

FIGURE 2.17: Payload transport and co-manipulation robot: Swarm robots [38]

Another example of cooperative transport is demonstrated in [185] were two coupled vehicles (cf. Fig. 2.18) are used to transport an object following a trajectory in two different configurations depending on object shape: the V-bed carrier and straight-bed carrier.

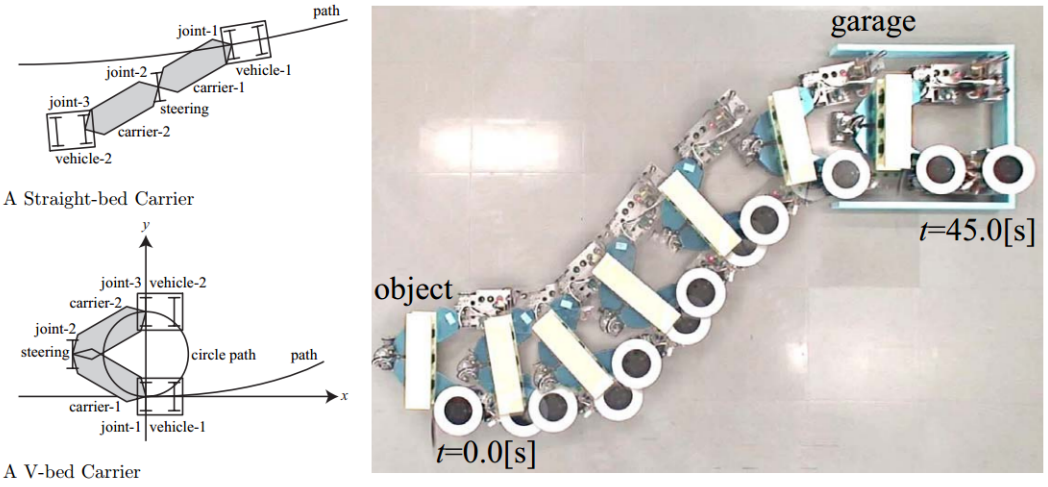

FIGURE 2.18: Payload transport and co-manipulation robot: Coupled Vehicles [185]

In [18] authors made a simulation for S-Bots to present a new control system based on evolutionary robotics for a robot team and their ability to negotiate and interact in order to achieve cooperative tasks and object transport either by connecting directly to it or using a pushing strategy. Authors in [8] apply a fully distributed strategy inspired by a society of insects to perform reactive box pushing task (cf. Fig. 2.19(a)). ARNOLD [3, 160] is a differentially driven wheeled mobile robot (cf. Fig. 2.19(b)) that can team up to cooperatively transport a large common object using a rotative arm moving in the plane parallel to the ground. However, it has not the ability to autonomously lift the object from the ground. The used concept is very interesting to ensure the stability of the transported object. In [80], authors present the example of a group of two to six Khepera robots equipped with gripper turrets to cooperate and pull a stick out of the ground (cf. Fig. 2.19(c)). The used grippers limits the shape of the objects that can be manipulated by the robots. Stanford Robotics Platforms (SRP) [96] are composed of two holonomic mobile platforms equipped with PUMA 560 robot (cf. Fig. 2.19(d)) that can co-manipulate to make cooperative tasks. The used manipulators are equipped with grippers as end-effectors and require a particular payloads shape in order to grip it. Mobile robots can also use tools (cf. Fig. 2.19(e)) for objects manipulation in a cooperative way as it was described on [186, 187] where the robots are using tools such as stick or string for object manipulation. Another interesting strategy used by mobile robotic system was developed and described in [20] for Army Ant cooperative lifting robots (cf. Fig. 2.19(f)). The robots are able to lift the payload by slipping under it and putting it on their bodies. Two generations of these systems have been developed with

different lifting mechanisms based on pneumatic and mechanical systems respectively.

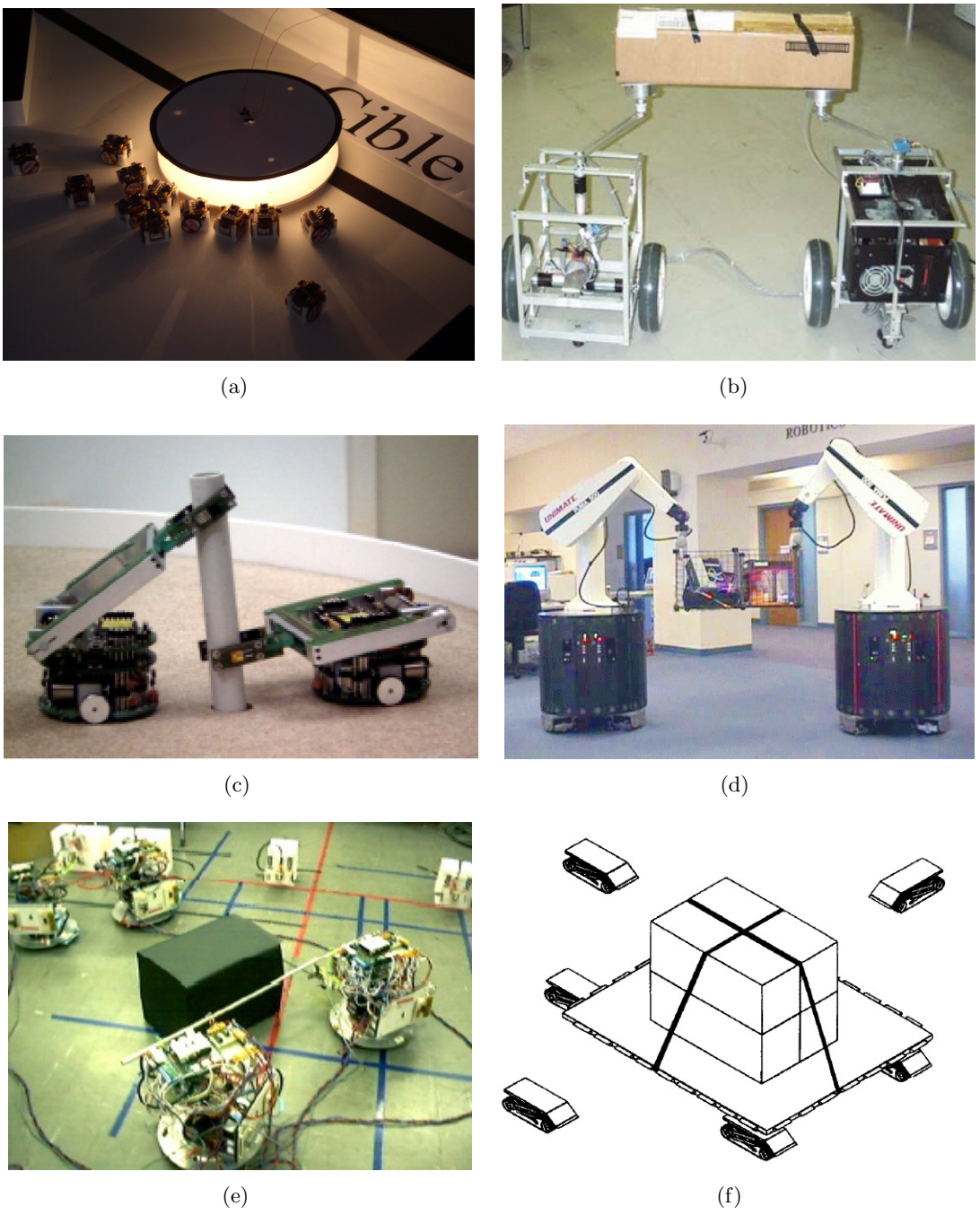

(a) (b) (c) (d) (e) (f)

FIGURE 2.19: Payload transport and co-manipulation robots: a) Alice robots for box pushing [8]; b) ARNOLD for payload co-manipulation and transport [3, 160]; c) Khepera robots for tube pulling from a hole [80]; d) Stanford Robotics Platforms for object co-manipulation [96]; e) mobile robots equipped with tools for object manipulation [186, 187]; f) Army Ants for payloads dorsal transport [20]

Another example of complex structure robots for collaborative manipulation and object transport was described in [183]. The robotic vehicle called ATHLETE "All Terrain Hex-Limbed, Extra-Terrestrial Explorer" was developed by Jet Propulsion Laboratory with

NASA Johnson Space Center, the NASA Ames Research Center, Stanford University and the Boeing Company. Fig. 2.20(a) presents the ATHLETE robot and object co-manipulation. This very complex legged robot uses six wheeled legs with six DOF each, used for rolling or walking depending on the terrain nature, and attached to a hexagon shaped body giving six flat faces, used to dock to similar ATHLETE robots. In [10], authors present the implicit communication based cooperation in which two four legged robots TITAN VIII use their own sensors and plan motions by processing a local information. Fig. 2.20(b) illustrates the cooperation between these robots to transport an object after being posed by a human operator. Table 2.3 presents robot modules complexity according to actuation and mechatronic structure. It also presents an estimation for control complexity for an overall formed structure by modules and the ability for auto reconfiguration and changing the whole structure. Knowledge about these different robotic systems presents an advantage so that we can make development of a new robotic system that can improve manipulation tasks.

(a)

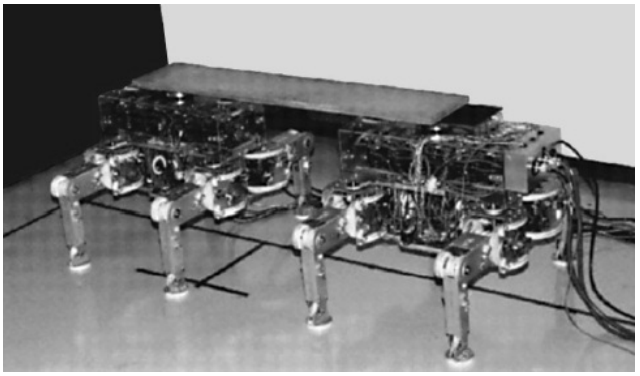

(b)

FIGURE 2.20: Legged mobile robots for object transport: a) ATHLETE [183]; b) TITAN VIII [10]

Criterion \ Robot	Swarmanoid	Coupled vehicles	Swarm	ARNOLD	KHEPERA	SRP	Robots with tools	Army Ant	ATHLETE	TITAN	First design	C3Bots
Type of robot	Wheeled flying	W	W	W	W	W	W	Tracked (T)	Legged (L) W	L	W	W
Manipulation and transport strategy	Gripping (G)	Dorsal Transport (DT)	Pushing		G	G	Pushing Towing	DT	G	DT	DT	DT
End-effector	Grippers (Gr)			Plate	Gr	Gr	Tool		Robot wheels		Plate	Compliant end-effector
Manipulated object	Limited shapes (L-s)	General payload (G-p)	G-p	G-p	Tube	L-s	G-p	G-p	G-p	G-p	G-p	G-p
Human assistance	No	Yes	No	Yes	No	No	No	No	No	Yes	No	No

TABLE 2.3: Table of comparison for Payload co-manipulation and transport robots

Previous mentioned examples of robots for payloads transport use different strategies to ensure the task achievement. Some of them require assistance to put the payload on robot manipulators such as the case of ARNOLD robots and others can achieve the task in a fully autonomous way.

The presented overview about manipulators and mobile robotic systems allows to define the C^{3}Bots project specifications. Next section will be dedicated for the project description.

2.5 C^{3}Bots project

For our application, a wheeled robot structure was privileged since crawling and legged systems require high degrees of freedom, which implies to setup complex hardware and control architecture. Fig. 2.21 shows that, on flat surfaces, wheeled locomotion is one to two orders of magnitude more efficient than legged locomotion. The railway is ideally engineered for wheeled locomotion because rolling friction is minimized on a hard and flat steel surface. But as the surface becomes soft, wheeled locomotion accumulates inefficiencies due to rolling friction whereas legged locomotion suffers much less because it only uses a few contact points with the ground. This is demonstrated in Fig. 2.21 by the dramatic loss of efficiency in the case of a tire on soft ground [164]. Wheeled locomotion efficiency depends greatly on the nature of the environment, particularly the flatness, hardness and cohesion of the ground, whereas the efficiency of legged locomotion depends on the leg mass and body mass.

2.5.1 Wheeled mobile robots

A mobile robot wheel's characteristics (shape, steering angle, radius...) defines the robot's characteristics and its mobility DoF. Thus, one can find omnidirectional robots (well known as holonomic robots). This kind of robots is able to evolve in any direction independently from its orientation. In this category is included the robots with spherical wheels (cf. Fig. 2.24). Opposed to this type of robots, the most common robots for robotic community are the non holonomic robots. Contrary to the previous robots, they lose one DOF corresponding to the instantaneous translation along the wheel axis direction. Principally, there are three main types of non-holonomic robots:

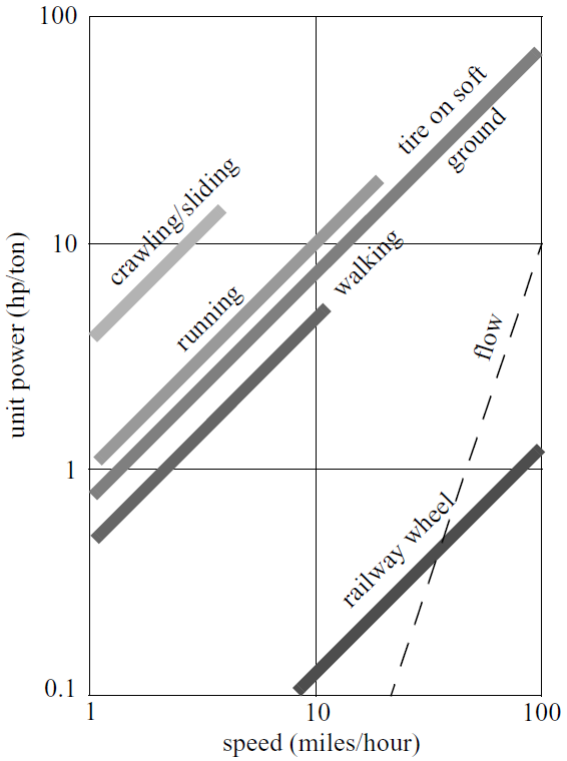

FIGURE 2.21: Specific power versus attainable speed of various locomotion mechanisms [164]

- the tricycle robot: it is composed of two fixed wheels in the same axle and a steering wheel placed on its longitudinal axis. The steering angle of the latter defines the Instantaneous Center of Rotation (ICR) of the robot,
- car-like robot: similar to the tricycle with a difference in the front half which contains two wheels instead of one for a better stability. The term "robot" is associated to the autonomous vehicle that does not require a driver or a remote control. The VIPA autonomous vehicle illustrated in Fig. 2.22(a) belongs to this class of robots,
- unicycle robot: it is actuated by two wheels with independent motorisation. It includes castor wheels for stability insurance. The Khepera (cf. 2.22(b)) robots are unicycle robots that will be used during the C^{3}Bots project later.

More specifications about wheels and rolling will be given in the following.

(a) Robot of type vehicle. (b) Khepera mobile robot.

FIGURE 2.22: Non-holonomic robots

2.5.2 The wheel and rolling

Principle of rolling

A wheel is axi-symmetric about its roll axis and rests on the ground on its contact patch. The contact patch is a small area which is in frictional contact with the ground such that the forces required to cause relative sliding between the wheel and ground are large for linear displacements and small for rotational motions. Thus, we assume that a wheel undergoing pure rolling has a contact point with no lateral or longitudinal slip, yet is free to twist about the contact point [76]. The kinematic constraint of rolling is called a Higher-Pair Joint (HPJ).

Classification of wheels and wheel mountings

Three majors wheel classes could be found in literature. They differ widely in their kinematics, so the choice of wheel type affects the overall kinematics of the mobile robot. The choice of wheel types for a mobile robot is strongly linked to the choice of wheel arrangement, or wheel geometry. The mobile robot designer must consider these two issues simultaneously when designing the locomotion mechanism of a wheeled robot. First of all, there is the standard wheel as shown in Fig. 2.23. This is what most people think of when asked to picture a wheel. The standard wheel has a roll axis parallel to the plane of the floor and can change orientation by rotating about an axis normal to the ground through the contact point. The standard wheel has two DOF. A fixed standard

wheel is mounted directly to the robot body. When the wheel is mounted on a rotational link with the axis of rotation passing through the contact point, we speak of a steered standard wheel. A variation which reduce rotational slip during steering is called the lateral offset wheel. The wheel axis still intersects the roll axis but not at the contact point. The caster offset standard wheel, also know as the castor wheel, has a rotational link with a vertical steer axis skew to the roll axis. The key difference between the steered wheel and the castor wheel is that the steered wheel can accomplish a steering motion with no side effects, as the centre of rotation passes through the contact patch with the ground, whereas the castor wheel rotates around an offset axis, causing a force to be imparted to the robot chassis during steering [76, 153].

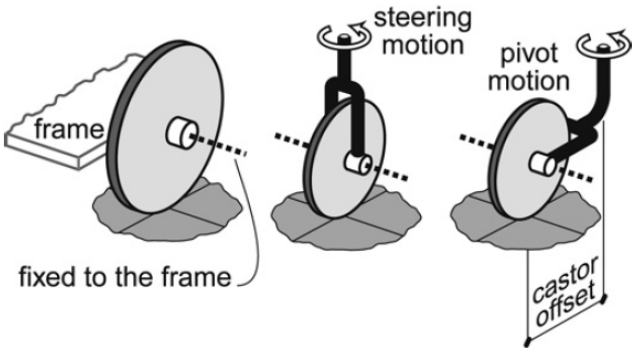

FIGURE 2.23: Different kinds of conventional wheels (from left to right): fixed wheels; steering wheels; castor wheels [19]

The second type of wheel is the omnidirectional wheel. This is a disk with a multitude of conventional standard wheels mounted on its periphery [76, 132] as shown in Fig. 2.24. The omnidirectional wheel has four DOF and works as a normal wheel, but provides low resistance in another direction as well. The angle of the peripheral wheels may be changed to yield different properties. The small rollers attached around the circumference of the wheel are passive and the wheel's primary axis serves as the only actively powered joint. The key advantage of this design is that, although the wheel rotation is powered only along the one principal axis, the wheel can kinematically move with very little friction along many possible trajectories, not just forward and backward [153]. The third type of wheel is the ball or spherical wheel. It has also three DOF. The spherical wheel is a truly omnidirectional wheel, often designed so that it may be actively powered to spin along any direction. There have not been many attempts to build a mobile robot with ball wheels because of the difficulties in confining and powering a sphere. One mechanism for implementing this spherical design imitates the computer

mouse, providing actively powered rollers that rest against the top surface of the sphere and impart rotational force [76, 153].

(a) (b) (c)

FIGURE 2.24: Omnidirectional Wheels: a) Universal [144]; b) Double Universal [144]; c) Swedish 45° [113]

Wheels steering and drive systems

There are a variety of ways to steer or turn a robot. The following are the commonly used for wheeled robots:

- Ackerman steering (typical car cf. Fig. 2.25(a)): Steering wheels are used for vehicle orientation and balancing is ensured by other wheels,
- Differential steering (cf. Fig. 2.25(b)) is based on two independently-driven wheels that are placed on opposite sides of the robot. The platform balancing is ensured by the other wheels of the robot (additional castor wheel, for instance),
- Synchro steering. This is a special type of base devised for mobile robots. The Nomad robot [180] uses this base. It has four driven wheels placed in a triangular pattern supporting the robot. All wheels point in the desired direction of robot when powered. Additionally, the wheels are connected by a belt drive to another motor that turns the wheels synchronously relative to the base. Hence, the robot can change its direction without rotating the base,
- Omni-drive: It is similar to synchro-drive base, but each wheel presents a complex mechanism able to roll in any direction.

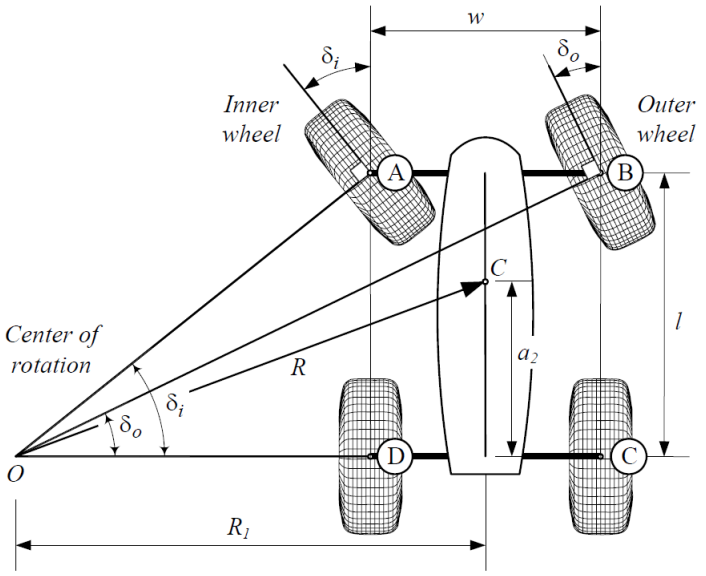

(a)

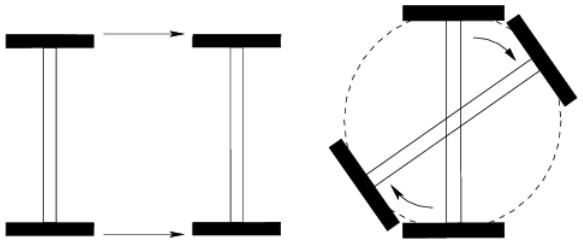

(b)

FIGURE 2.25: a) Ackerman steering [59]; b) Differential drive Pure translation occurs when both wheels evolve at the same angular velocity and pure rotation occurs when the wheels move at opposite velocity [168]

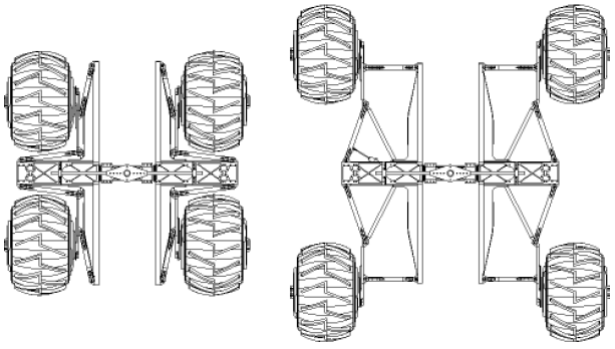

(a)

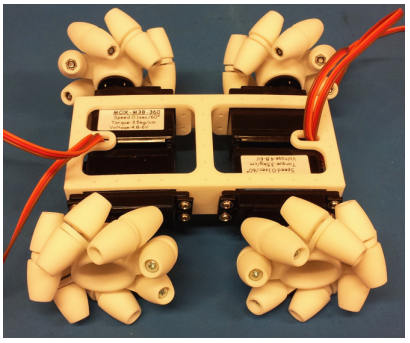

(b)

FIGURE 2.26: a) Synchro-drive base for Nomad robot [180]; b) Omni-drive wheel [126]

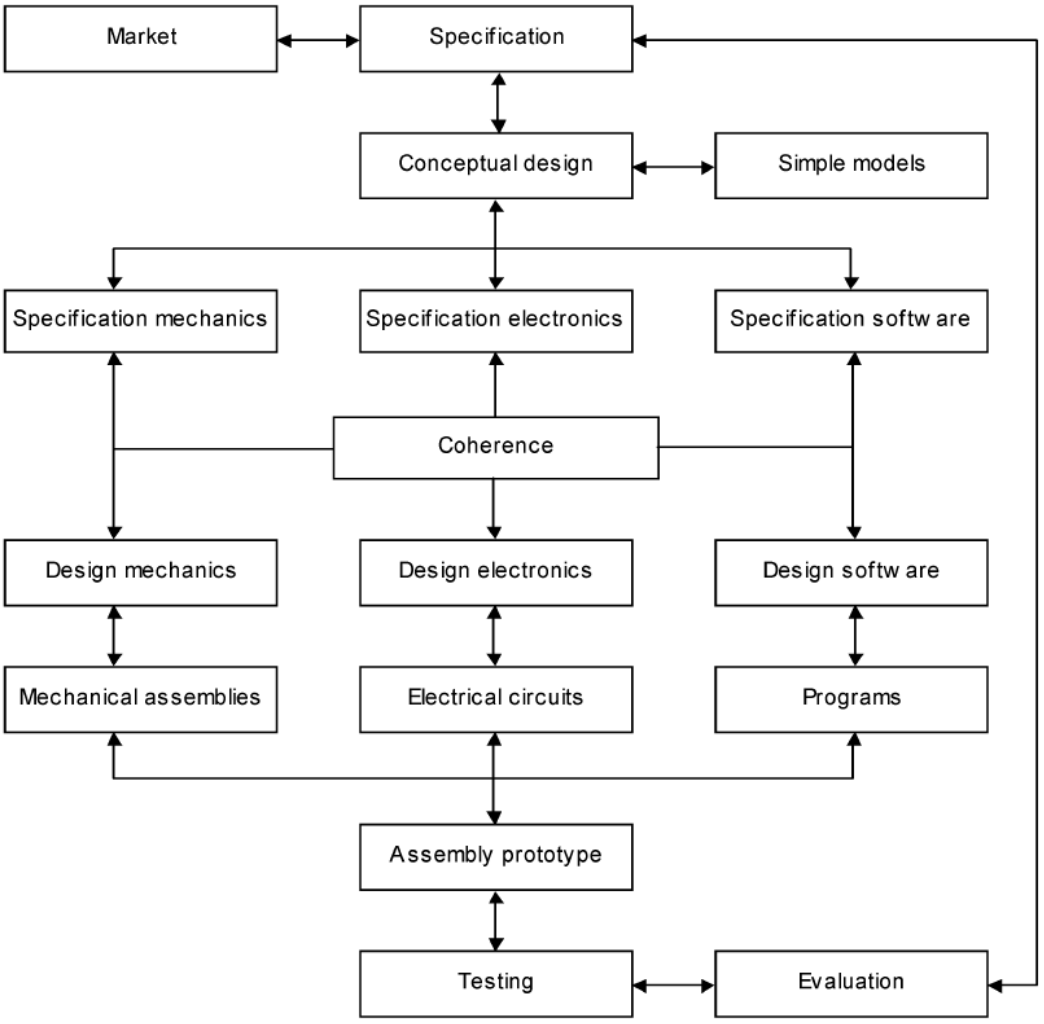

FIGURE 2.27: Mechatronic design process [149]

2.5.3 Mechatronics and robotics design process

In a robotic design project, considered as a mechatronics design project, a team of different disciplines experts work together. The goal of the team is to design products or production systems composed of contributions from various disciplines. These designers must share a common understanding about the design process. A structured approach is essential to offer each of the team members the opportunity to exert some influence (from the start) on design decisions [149].

The general process of designing a robotic system (cf. Fig. 2.27) is not different from other products design process:

- Step one: express the design problematic and formulating the user specification,

- Step two: generating potential (alternative) solutions for solving the design problem and choosing the most promising concept,
- Step three: detailed engineering,
- Step four: prototype manufacturing, experimentation on it and implementation improvements.

The previous four phases (cf. Fig. 2.27) will be described in more details in the following subsections.

Specification phase

The first activity of the design team is to express the design problem. A list of user requirements is formulated in close co-operation with the end user. This may seem a simple task, but most design problems are poorly defined. Finding out exactly what the design problem is can be a major undertaking.

Conceptual design phase

In the conceptual design phase, ideas about how to solve the design problem are generated and evaluated for feasibility. Dependent on the difficulty of the design problem, a more refined breakdown into sub-problems is made in order to obtain a better understanding of the problem. This subdivision into smaller pieces results in a more structured (design) discussion between the team members. Specific design tools are required to understand the technical features of certain concepts in relation to the required system performance. These design tools should provide reliable information about the feasibility of potential solutions [149].

Engineering phase

In the engineering phase, the conceptual design is detailed to the level of drawings of mechanical parts, schemes of electrical wiring and printed circuit boards, and software code. After a conceptual design is adopted, a coherent subset of design tasks is formulated for each of the disciplines involved (Figure 3.2). In the next step, each of the

disciplines fulfils the specified design task. The experts carry out their task more or less independent of one another. However, communication between the experts remains absolutely essential to fine tune the process on a more detailed level. In realising the specific design tasks, each of the experts use their own well-known proven methods and design tools. More details emerge during the engineering phase. Consequently, more refined models can be made, resulting in a better prediction of the performance of the final product [166].

Prototype and test phase

In the last phase of the project, a prototype is realised and tested. First the mechanical and electrical components are realised and assembled. After the assembly is tested, the software is downloaded. In this phase, the different functions of the prototype are tested and debugged. In most cases, additional software fine-tuning is required to compensate mechanical and electrical irregularities or shortcomings [149].

2.5.4 C^{3}Bots project specification

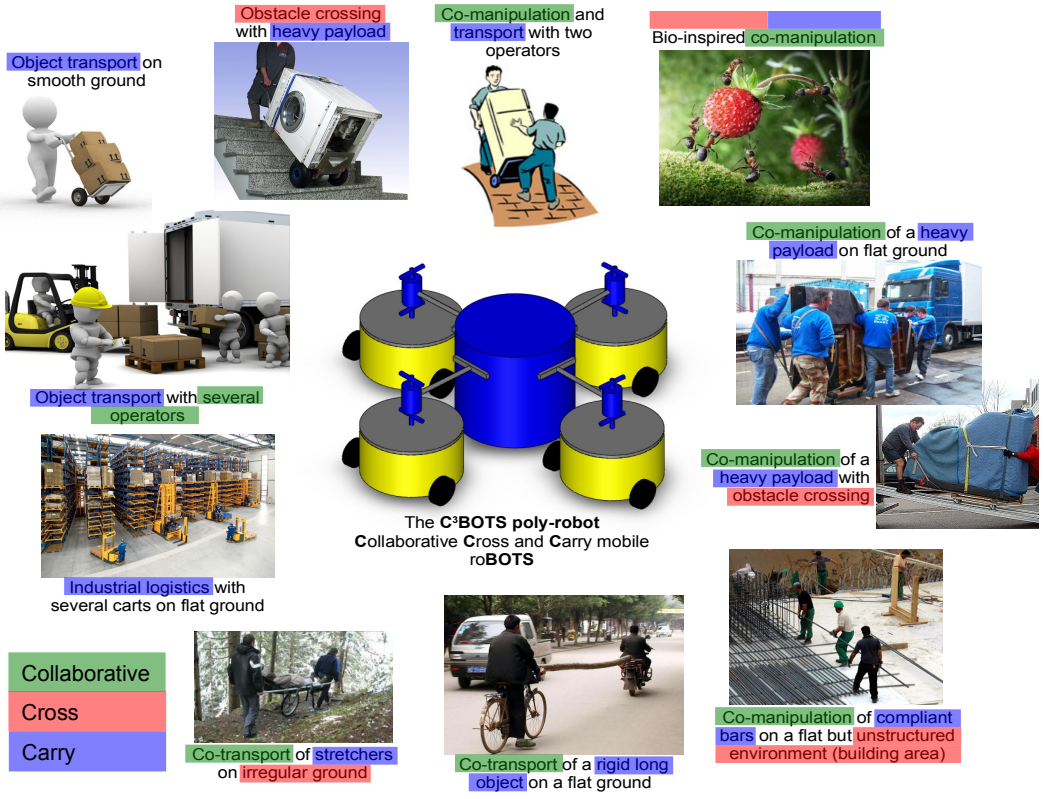

FIGURE 2.28: C^{3}Bots general concepts and achieved tasks

The C^{3}Bots project aims to design identical m-bots equipped with a manipulation mechanism. As presented in Fig. 2.28, the proposed work deals with collaborative tasks in which a group of similar entities are able to cooperate in order to achieve the task. It also considers the obstacle crossing problem in the aim of evolving in all terrain without being in a blocked state. Finally it is dedicated to payloads of any shape co-manipulation and transport. The group of m-bots will be able to lift, co-manipulate and transport a payload which has to be laid on the top platform of each m-bot. Consequently, in addition to an end-effector, the m-bot manipulator has to include a lifting mechanism. The formed p-bot (m-bot + payload) is characterized by its reconfigurability depending on the overall system stability and the success of task achievement. Fig. 2.29 summarizes the main characteristics of the C^{3}Bots project. The proposed work deals with the Dorsal General Payload (DGP) transport and a second variety of C^{3}Bots project, treated in [50, 103], deals with Ventral Long Payloads transport in All Terrain (AT/VLP).

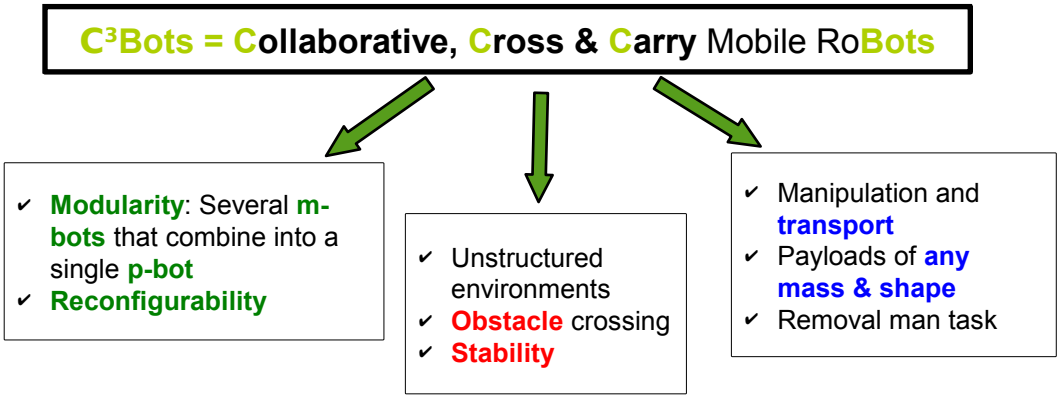

FIGURE 2.29: C^{3}Bots acronym and characteristics

The general architecture of a m-bot is defined with compliance to the following requirements R_i presented in table 2.4 and relative to the environment in which it will operate:

According to the previous requirements, the global co-manipulation method will be described.

2.5.5 C^{3}Bots co-manipulation method

In order to define the co-manipulation method for the task that will be achieved by several m-bots, preliminary ideas were considered and compared. Fig. 2.30 presents the

Requirement	Definition
R_1	Lift a payload in collaboration with similar m-bots using a manipulation mechanism.
R_2	Transport a payload.
R_3	Collision-free payload trajectory from the ground to the top of robot platform with constant orientation.
R_4	Evolve in structured terrain and rough environment (considered in a second part of the project).
R_5	Ensure manoeuvrability.
R_6	Ensure stability.
R_7	Ensure reconfigurability.
R_8	Tighten the contact payload/m-bot.
R_9	Detect other m-bots.
R_{10}	Detect obstacles.

TABLE 2.4: M-bot requirements

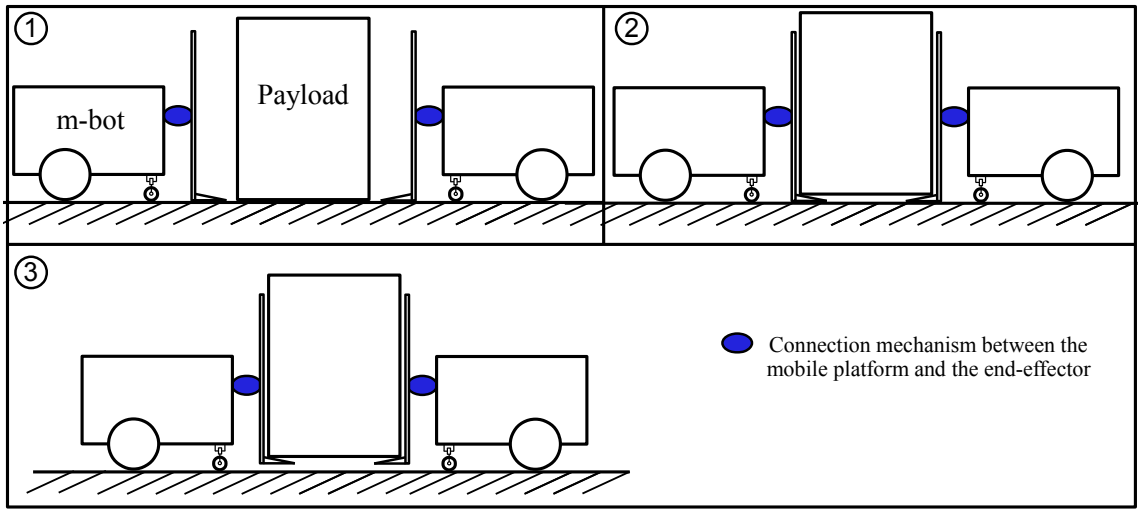

FIGURE 2.30: First mode preliminary idea for payload co-manipulation using forks

first mode of payload co-manipulation using the strategy of forklift trucks which use forks in order to lift an object and transport it. In the case of use of forklifts, a payload must be put on pallets or must require a free space accessible to forks to ensure the payload lifting. The forks may be also inserted under the payload when m-bots are able to exert a high pushing forces, like the strategy of Army Ants [20], that allows to slip the forks under the payload if there is no accessible space.

The kind of tasks targeted by the C^{3}Bots project are the transport of payloads of any shape and the constraints of imposing an accessible space or specified payload shape may limit the generality of tasks that could be achieved by the m-bots. For that reason, the second preliminary mode presented in Fig. 2.31 is proposed where m-bots are using

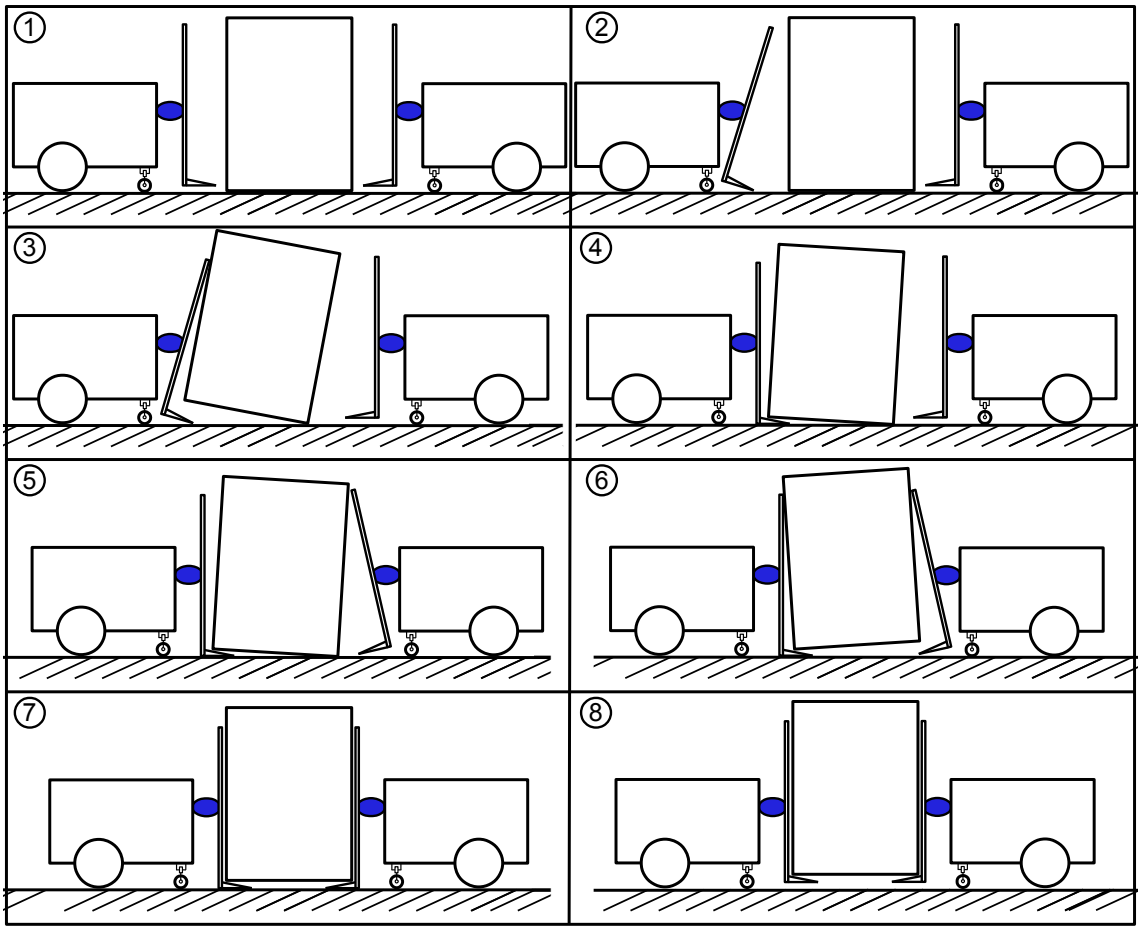

FIGURE 2.31: Second mode preliminary idea for payload co-manipulation using forks

a strategy of payload tilting in order to create the accessible space for the robots forks and to insert them under the payload to lift. This mode is characterised by a longer process and a possibility of loss of stability of the payload if it is much tilted and, in case where the payload mass is considerable, the m-bot may lose its stability. The ideas turned then to a third mode (cf. Fig. 2.32), which consists on using a simple forks (made by only a vertical part) which will apply a pushing force to tighten the payload and then simply lift it. This idea avoid the drawback of the first mode.

For a better stability of the payload and to avoid the risk of payload slipping and falling down between the m-bots end-effectors, the strategy of Army Ants transportation was adopted for putting the payload on the m-bots top platform (cf. Fig. 2.33). Finally the co-manipulation and transportation method was decided and illustrated in Fig. 2.34

The process of co-manipulation and transportation of a payload was initially described in [71–73]. The different phases of payload prehension, lifting and transportation are

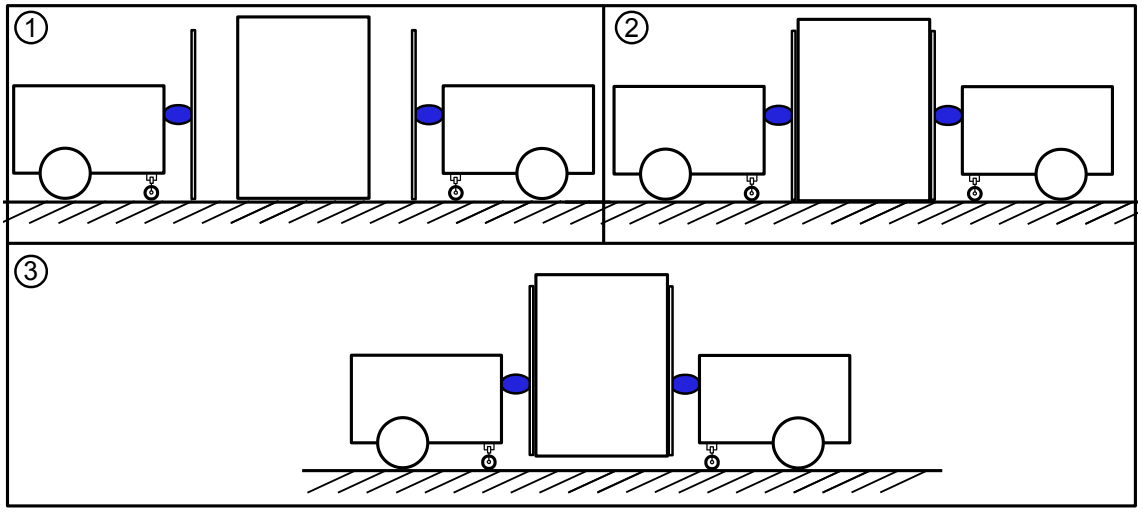

FIGURE 2.32: Third mode preliminary idea for payload co-manipulation with simple vertical forks

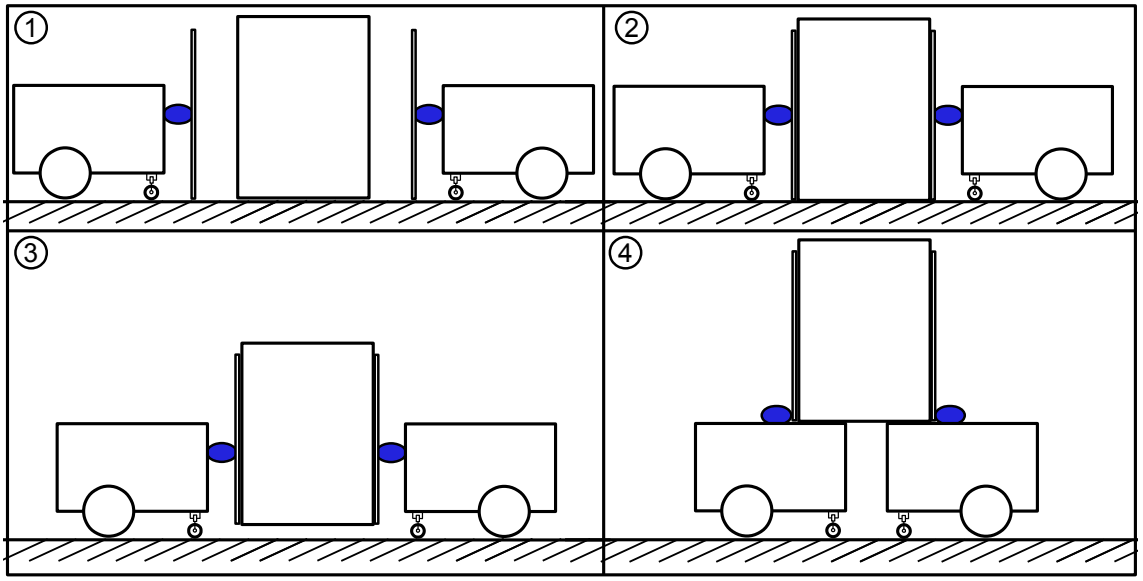

FIGURE 2.33: Fourth mode preliminary idea for payload co-manipulation with simple vertical forks able to put the payload on robot bodies

presented in Fig. 2.34. The first phase consists in locating the payload and surrounding it using distance sensors. The m-bots have to be oriented toward the object in order to face it (cf. Fig. 2.34(a)). Secondly, the payload is held by the m-bots end-effectors which exert a collective pressure using wheel propulsion (Fig. 2.34(b)). Submitted to collective pressure and to the proposed co-lifting manipulation, the object is elevated and laid on the m-bots top platforms (Fig. 2.34(c)). Finally, locomotion and transportation tasks are performed where each m-bot # m is steering by a suitable angle θ_m to ensure to the p-bot a unique Instantaneous Center of Rotation (ICR) (Fig. 2.34(d)).

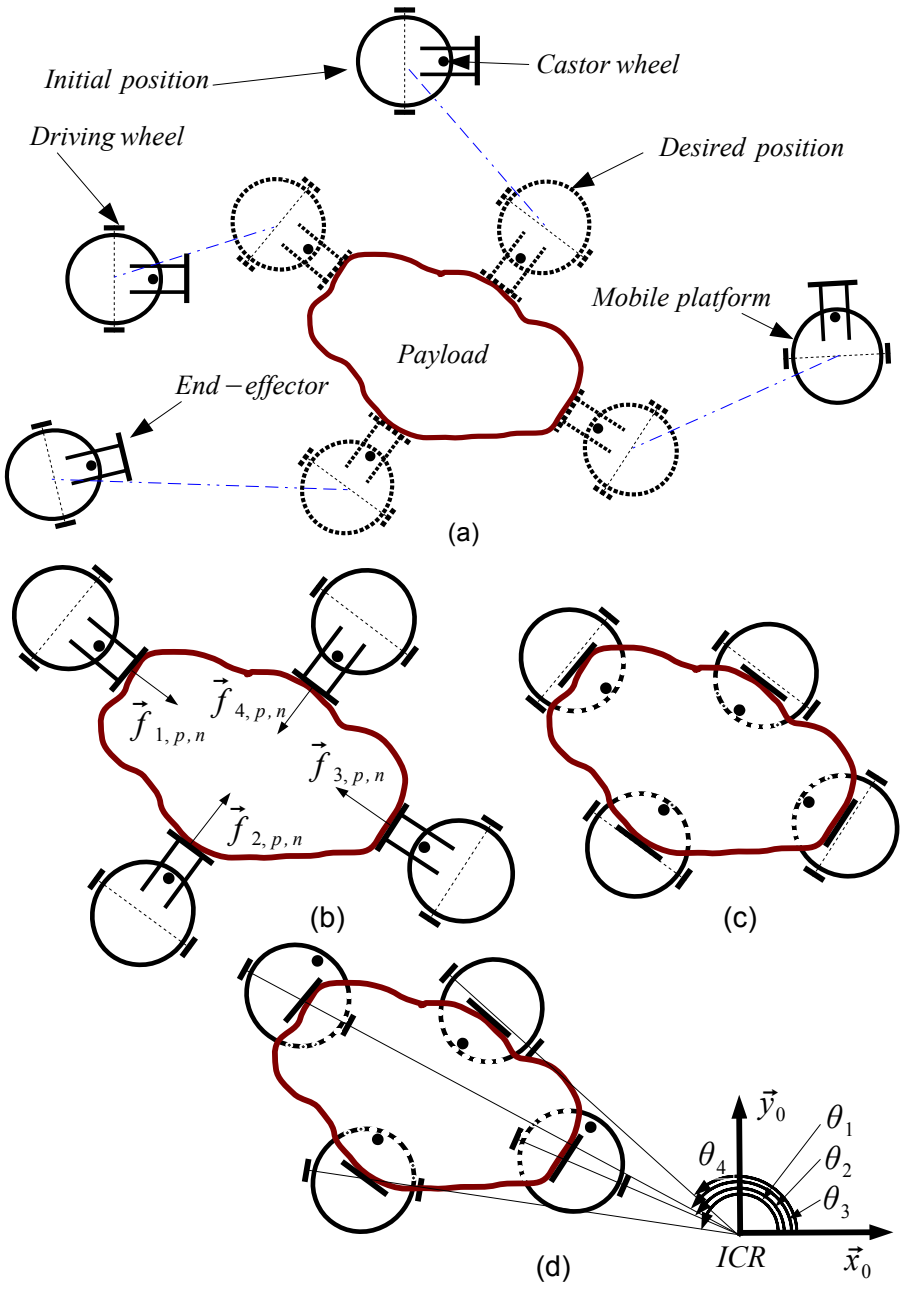

FIGURE 2.34: Co-manipulation method: a) Target reaching; b) Object holding; c) Object set on robot bodies; d) Object transport: a unique Instantaneous Center of Rotation (ICR) requires different steering angles θ_m

2.6 Conclusion

In this chapter, a review of various mobile robots and their categorization according to their structure and locomotion modes have been presented. In addition, some examples from developed systems for regular and irregular terrains have been analysed. Collaborative systems were also described with the associated co-manipulation strategies to transport an object. The aim of this review is to design a robot for all terrain

exploration, object manipulation and transport. From its analysis, the C^{3}Bots innovative system dedicated to object transport on various terrains has been specified. The paradigm of C^{3}Bots is to co-manipulate and transport a payload using several similar m-bots which will form a p-bot. Wheels will be selected for their versatility on various terrains and good efficiency on regular grounds compared to legs and tracks. However, classical robots of Fig. 2.10 lack of mobility on rough and irregular terrains, so advanced architecture such as in Fig. 2.11 and 2.12 should also be considered in the future. One important function for C^{3}Bots is object transportation and may be achieved by robot collaboration as shown in Fig. 2.17, 2.18 and 2.19. Inspiration will also be taken from Army Ants, small robots which transport payloads by laying them on the robot top platforms (Fig. 2.19(f)) and ARNOLD, that has a rotative arm on top of it. We also keep the concept of modularity (Fig. 2.19(b)) and propose to build our robots from two parts: a mobile platform and a manipulation mechanism. The following scientific topics will be concerned in the next chapters:

- Design of a mechatronic system achieving the tasks with minimal DOF,
- Static and dynamic models to maximize the poly-robot margin of stability,
- Control to guarantee efficient connections m-bot/m-bot and p-bot/payload,
- Optimal reconfiguration of the m-bots to achieve the assigned task (number, poses, cooperation strategies).

Chapter 3

Design of Mobile Robots for Co-manipulation and Transportation

Abstract: *The focus is made in this chapter on a developed lifting mechanism based on parallelogram structure mounted on mobile robots to co-manipulate and transport a payload. Structural and dimensional analysis are detailed in order to develop the proposed mechanism. The system performances to lift and maintain the manipulated payload stability is evaluated using various actuation in order to improve the designed structure.*

3.1 Introduction

Diverse mechanisms and technologies are used for objects lifting and transport. Fig. 3.1 presents different systems used for grabbing, lifting or transport objects. Some of them are constraint by the environment or the object position. For our system we have supposed to use a mobile robot on which a manipulation mechanism is going to be mounted and the constraints, as it will be mentioned in the specification table, is that our robot will not be limited to a simple object category but will have to lift and transport objects of any shape and dimensions. So a forklift as shown in Fig. 3.1(c) is excluded because it requires that the object to be transported has been positioned first on a pallet and is accessible to the mobile platform and its manipulating fork. But the idea of using a fork remains very interesting if we use a simplified fork keeping only its vertical part for direct contact with the object. Automated Guided Vehicles (cf. Fig. 2.9(a)) equipped with scissors (cf. Fig. 3.1(b)) would require human assistance to put the object on the platform. Grabbing systems limits the object size and shape and require a crane or supporting arm..

A raw evaluation of the centre of mass shows that, for a better stability, an object is better to be transported on the robot body or as close as possible of the robot body to keep the gravity center in the polygon of support and a bigger stability margin. Many researches in the domain of Manual Material Handling (MMH) prove that operators have a better performance and less body suffering when keeping the payload low and close to the body [58, 77, 134, 139]. To ensure object lifting , a mechanism has to be chosen to ensure the movement of the object from an initial position in the ground to a final position on the robot body. For a better adaptability, a terminal organ ensuring a contact surface with the payload is used and the use of grippers is avoided because it limits he object shapes that can be manipulated and it also requires more actuators. To lift the object from the ground, a variety of mechanisms that can ensure this function with different trajectories can be used. Fig. 3.2 presents different mechanisms for object lifting with linear, circular and complex trajectories. Fig. 3.2(a) presents two mechanisms for object grabbing with grippers and lifting with a linear movement using rack and pinion and a circular movement using a rotational joint. The first one keeps the payload out of the polygon of support, which has an impact on robot stability and the second system brings the payload back into the polygon of support using the revolute

(a) Grab [136]

(b) Scissor

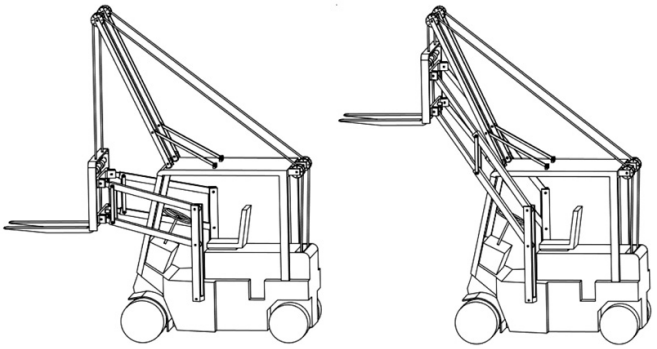

(c) Forklift [176]

FIGURE 3.1: Existing lifting and handling mechanisms

joint. Fig. 3.2(b) presents a mechanism for a linear translation used to displace object or loads in a linear way and can be used for example for lifting tasks. Fig. 3.2(c) presents a robot arm fixed on a robot body which can lift an object using grippers and move them along a complex movement depending on its workspace. This kind of mechanism requires more actuators than previous ones and more complex control. Fig. 3.4(c) presents a parallelogram mechanism with a gripper to lift object in a circular translation movement. Fig. 3.2(e) presents a mechanism for object lifting using a multi-stage system for a higher altitude lifting. The simplest architecture used is the parallelogram mechanism which can ensure the object lifting and, using the circular translation, the object can be brought on the robot body with a constant orientation. This solution allows to ensure the payload stability by putting it on the robot body. So a modelling for this mechanism is required to avoid collision problems and for a better stability of the whole mechanism. In the next section we will present the system specifications and the proposed solutions.

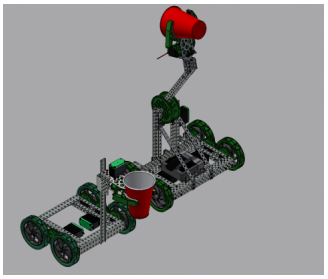

(a) Circular and linear trajectory lifting [40]

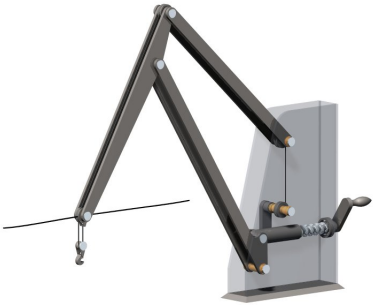

(b) Linear trajectory [1]

(c) Complex manipulation trajectory

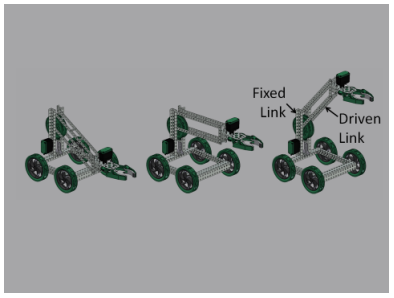

(d) Circular translation trajectory [40]

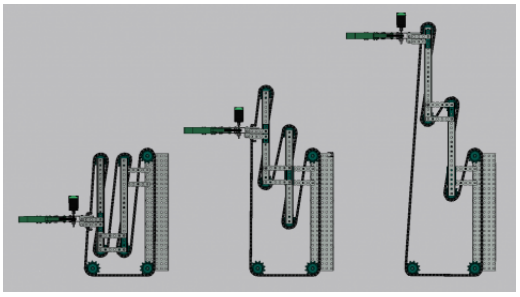

(e) Multi stage lifting mechanism with a linear trajectory [40]

FIGURE 3.2: Object lifting trajectories

Developed transporting mechanisms and technologies are widely found. Some transport solutions require heavy infrastructure such as Automated Guided Vehicles (AGV) [174] (*e.g.* ground landmarks, guiding rails) or specific stacking racks for storage as for Automated Storage and Retrieval System (ASRS). Human assistance could also be needed to put the object on the transporting platform (*e.g.* for scissors elevators [84]). Forklifts [176] use forks to lift and transport the object but require the positioning of the object on a pallet. Grabbing systems such as robot hand [120] limit the manipulated payload size and shape. According to the previous mentioned systems, one can conclude that for a better stability, an object should be better transported on the robot body [10, 20] or as close as possible to the robot body, to keep the gravity center above the polygon of support and as low as possible ensure a bigger stability margin on slopes. Many patented mechanisms for lifting applications with various structures and architectures could be also found (cf. Fig. 3.3). In [131], a lifting mechanism for an articulated bed is described (cf. Fig. 3.3(a)). It is based on two parallel arms, hinged to the chassis and the bed plane, which form an articulated parallelogram with one extendable arm through two segments and equilibrating elastic means. [69] presents another articulated

lifting mechanism comprising a set of arms forming the sides of two rhomboid polygons to lift objects in a vertical direction parallel to the chassis (cf. Fig. 3.3(b)). In [133], the well known lifting jack mechanism (cf. Fig. 3.3(c)), used to lift a vehicle, is presented. Another innovative design [61] is used for a vehicle lifting mechanism using a Y shaped chassis based on a lever, a hydraulic actuator and an articulated support arm (cf. Fig. 3.3(d)). Other example for object lifting and transport is the hand-truck with an innovative design using wheels and a vertical lifter sub assembly [106] (cf. Fig. 3.3(e)). [45] presents a monitoring system for a payload lifting vehicle based on a lifting arm and hydraulic actuators (cf. Fig. 3.3(f)). In [55] a lifting mechanism that could be mounted on the rear of truck is described and presented in Fig. 3.3(g). A mechanism presented in Fig. 3.3(h) for patient lifting and transport is designed in [171]. [84] presents a lifting system for metallic parts in construction sites based on a scissor linkage system with metallic bars and a mechanism ensuring the lift up and down movement (cf. Fig. 3.3(i)). In this paper, a proposed design for modular robots for payload co-manipulation and transport of payloads of any shape is particularly characterized by: its mechanical structure simplicity comparing to [10] and [183], its modularity while using a swarm of elementary robots [8, 38], its adaptability to objects of any shape and mass and its ability to provide a fully autonomous system, without human mediation, contrary for example to robotic system proposed in [160] and [185].

This chapter is organized as follows: section 3.2 presents the specification of the lifting mechanism used for payloads manipulation and the structural and dimensional synthesis of a m-bot. Section 3.3 is dedicated to evaluate the developed mechanism lifting capacity. Section 3.4 presents the determination of the used m-bots to achieve a lifting task successfully in a flat ground.

3.2 Designing a lifting mechanism

The following notations and parameters will be used for the mechanism synthesis:

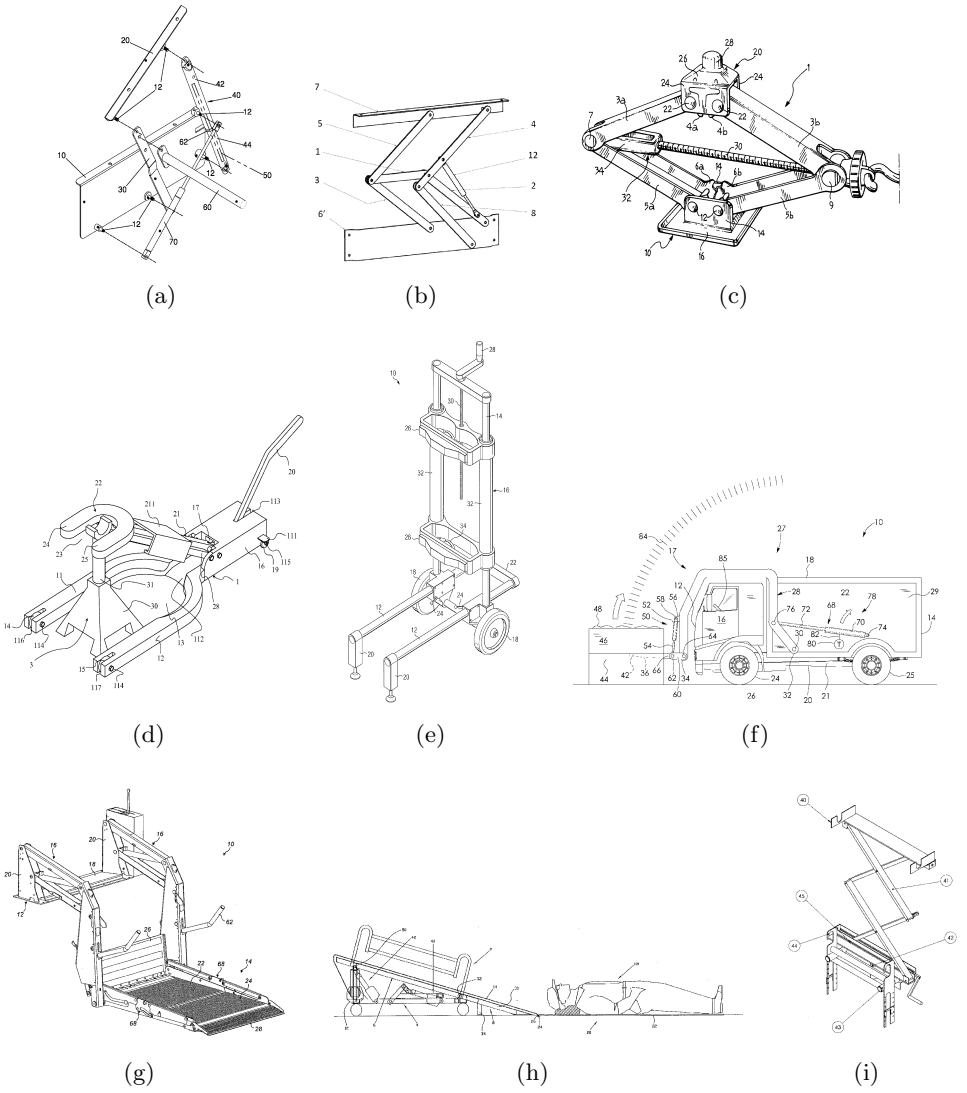

(a) (b) (c)

(d) (e) (f)

(g) (h) (i)

FIGURE 3.3: Selection of patents for lifting systems: a) Lifting mechanism for articulated bed: [131]; b) Lifting mechanism for a storage bed base: [69]; c) A screw and pantograph lifting jack: [133]; d) Lifting mechanism with lift stand accomodation: [61]; e) Multidimensional lifting hand track: [106]; f) Load Lifting vehicle: [45]; g)Truck lifting mechanism [55]; h) Patient lifting device: [171]; i) Scissor: [84]

3.2.1 Specification of the lifting mechanism

The lifting and manipulation mechanism used for object lifting must ensure the following requirements R_{li} presented in table 3.2:

Name	Definition
AB and DC	Parallelogram long bars.
AD and CB	Parallelogram short bars.
α_0	Initial tilting angle of the parallelogram long bars AB or DC.
α_1	Final tilting angle of the parallelogram long bars AB or DC.
d_1	Distance of the castor wheel to the front of the robot.
γ	Tilting angle of the short bars.
δ_1	Horizontal free collision clearance.
δ_2	Vertical free collision clearance.
$\vec{F}_{pm}$	Applied force by the payload on the robot body when it is laid on it.
h	Platform height.
l	Distance between landing position on the platform and the front of the platform.
L_1	Horizontal distance between initial and final positions of the end-effector according to $\vec{x}$ axis.
L_2	Required distance for the manipulation mechanism mounting.
P_1	End-effector lower point position on the ground.
P_2	End-effector lower point position on robot platform.
P_3	End-effector lower point intermediate position.
$\vec{P}_m$	M-bot weight.
$\vec{P}_{pl}$	Payload weight.
ψ	Rotation angle of the manipulation mechanism w.r.t the mobile platform.
r	Trajectory radius.
R_i	M-bot requirement i.
R_{li}	Lifting mechanism requirement i.
s_1	The shortest distance from the free steering center of the mobile platform to the edge of support polygon.
W_b	The wheelbase.
T	Track of the robot.
w_c	Contact point of the robot castor wheel with the ground.
w_l	Contact point of the robot left wheel with the ground.
w_r	Contact point of the robot right wheel with the ground.
ζ	The plane inclination

TABLE 3.1: Design parameters

3.2.2 Structural and dimensional synthesis of the lifting mechanism

Structural selection

The various system requirements R_i (cf. Table 3.1) and manipulation mechanism R_{li} (cf. Table 3.2) will influence directly the kinematics structure. R_5 and R_{l7} can be satisfied by supporting the lifting mechanism on a turret. As a consequence, a revolute joint with z axis will support the mechanism (cf. Fig. 3.4(b)), 3.4(c) and 3.4(d))). R_3 defines the initial and final poses P_1 and P_2 of the lower point P of the end-effector that holds

Requirement	**Definition**
R_{l1}	Manipulate payload via an end-effector.
R_{l2}	Allow object lifting.
R_{l3}	Ensure fittability on the robot mobile platform.
R_{l4}	Avoid collision with robot platform and the ground.
R_{l5}	Tighten contact payload/mechanism using the end-effector.
R_{l6}	Ensure fittability of the robot to the payload.
R_{l7}	Ensure orientability of the robot platform with respect to the payload.
R_{l8}	Put the payload on the robot body.

TABLE 3.2: Manipulation mechanism requirements

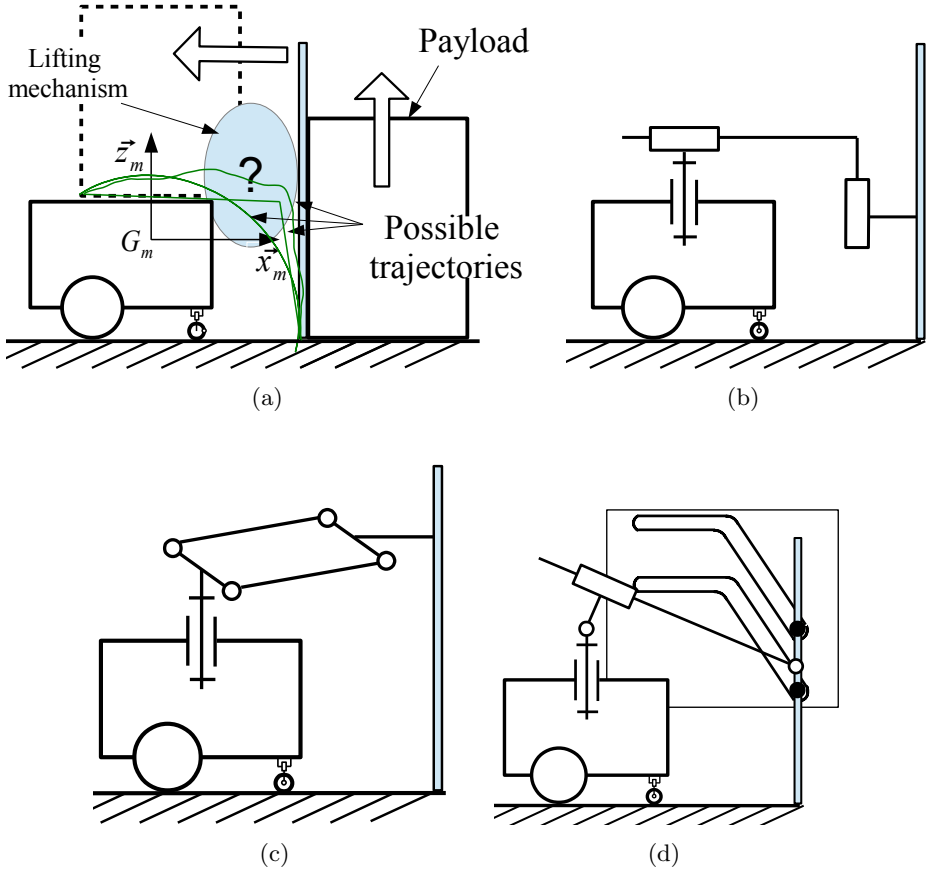

FIGURE 3.4: Elementary lifting systems: a) Payload initial and final position with possible trajectories; b) 2 DOF solution; c) 1 DOF solution based on parallelogram mechanism; d) 1 DOF solution based on cam mechanism

the object. The latter will keep its orientation constant during the lifting motion. The trajectory must start with a vertical lifting motion ($+z_m$) and finish with a backward horizontal motion ($-x_m$) towards the m-bot platform (Fig. 3.4(a)). R_3 and R_{l4} imply not to start the horizontal motion too early in order to avoid collision with the m-bot platform. Different trajectories are allowed (Fig. 3.4(a)) among which the square and the circular motions are the most obvious. A square trajectory could be achieved using

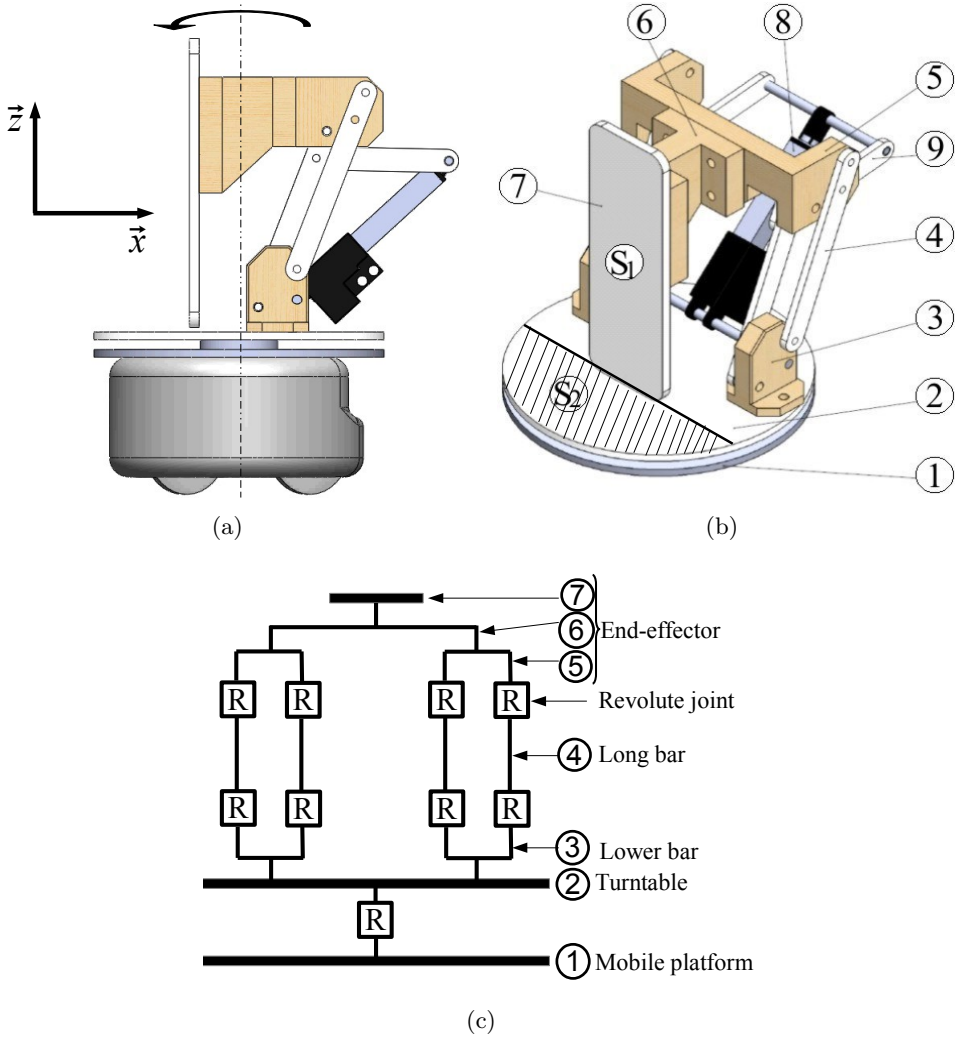

FIGURE 3.5: Elementary lifting systems: a) 3D CAD for a m-bot; b) 3D CAD view for the manipulation mechaism; c) Binding graph

two orthogonal prismatic joints and two actuators (Fig. 3.4(b)). A complex trajectory could also be ensured by using a cam mechanism (Fig. 3.4(d)). A circular trajectory would lead to a simpler solution using only one actuated revolute joint. However, to keep the payload orientation along the circular trajectory, a parallelogram mechanism is preferred (Fig. 3.4(c)) while keeping the control simplicity with a single actuator. The proposed mechanism will be fixed on the top of a unicycle mobile platform.

Structural analysis

Fig. 3.5 describes the proposed lifting mechanism. A turntable (Part *2*) is connected to the base (Part *1* fixed on the mobile platform) via a revolute joint (z_m axis) which

allows the mobile platform of the robot to steer freely when the payload is on robot bodies (laid on surface S_2 on the top of *2*). Two identical parallelogram mechanisms are mounted on *2*. Each one is composed of a lower bar *3*, two long bars *4* and an end-effector support *5, 6, 7*. The payload to be manipulated is hold by the contact surface S_1 of the end-effector. An actuator *8* is used to ensure object lifting and to control the parallelogram mechanism via an additional lever *9*. The actuator allows to maintain the pressure force on the payload.

Dimensional synthesis

Robotic platform and landing position

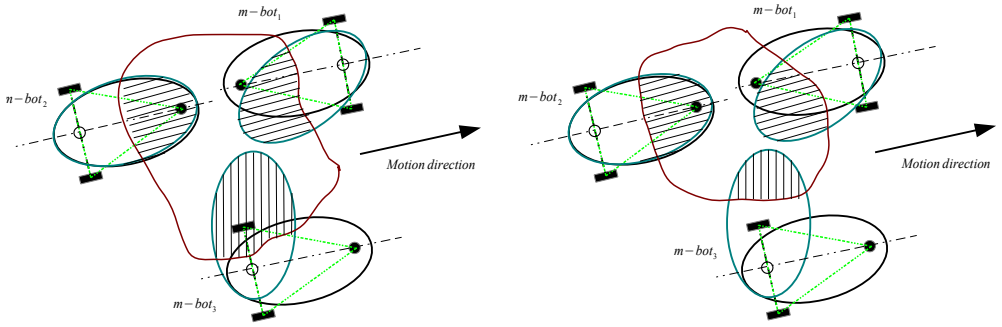

(a) Stable transportation (b) Unstable transportation

FIGURE 3.6: M-bots possible configuration for payload transportation

The choice of a m-bot architecture depends on the system requirements previously defined. It also depends on several criteria to be ensured during the task achievement such as stability. So a m-bot must remain stable during the phase of target reaching and during the lifting and transporting phases. For experiments a three wheel robot existing in our laboratory will be used. This robot architecture is considered then, and is sufficient to ensure stability of the m-bot by maintaining the m-bot center of mass inside its polygon of support, when it evolves in the environment. Its stability margins could be calculated using different developed methods [66, 114, 121, 128]. The adopted strategy for the transport as presented in the co-manipulation method (cf. Fig. 2.34) is based on transportation on robot bodies, and a suitable landing position is another constraint added to ensure the overall system stability. According to Fig. 3.6, one can conclude that depending on the payload positioning on robot body, the m-bot could be

stable or unstable. Depending on the position of landing point P_2, a normal force $\vec{F}_{p,m}$ (cf. Fig. 3.7) applied by the payload on the m-bot, when it is laid on its turntable could either keep its stability or induce the m-bot reversal. A m-bot remains stable if the following conditions are satisfied:

$$\bar{M}_{(w_c w_r)}(\vec{F}_{p,m}) + \bar{M}_{(w_c w_r)}(\vec{P}_m) \geq 0 \text{ if } \psi \in [0, \frac{\pi}{2}] \tag{3.1}$$

$$\bar{M}_{(w_c w_l)}(\vec{F}_{p,m}) + \bar{M}_{(w_c w_l)}(\vec{P}_m) \leq 0 \text{ if } \psi \in [-\frac{\pi}{2}, 0] \tag{3.2}$$

$$\bar{M}_{(w_r w_l)}(\vec{F}_{p,m}) \leq \bar{M}_{(w_r w_l)}(\vec{P}_m) \text{ if } \psi \in [-\frac{\pi}{2}, \frac{\pi}{2}] \tag{3.3}$$

where w_c, w_l and w_r represent respectively the contact points between the castor wheel/-ground, the left wheel/ground and the right wheel/ground. $\vec{F}_{p,m}$ is the force applied by the payload on the robot and $\vec{P}_m$ is the m-bot weight.

In Fig. 3.8(a), the payload is laid on m-bot body in a manner that satisfies equation (3.2) and avoids the robot reversal. However, in Fig. 3.8(b) the generated torque by the payload position is able to make the m-bot$_3$ on the bottom side tip-over if it exceeds the torque generated by its weight. As a conclusion, if both forces $\vec{F}_{p,m}$ and $\vec{P}_m$ are in the same half space separated by the vertical plane passing through $(w_c w_r)$ or $(w_c w_l)$, then the m-bot remains stable during the task. In the other case, if the application points are in two different half spaces than the state of the m-bot will be defined as follow:

$$\begin{cases} \text{The m-bot is stable if } \bar{M}_{(w_i w_j)}(\vec{F}_{p,m}) < \bar{M}_{(w_i w_j)}(\vec{P}_m) \mid i\#j \text{ and } i,j = l,r,c \\ \text{The m-bot is stable if } \bar{M}_{(w_i w_j)}(\vec{F}_{p,m}) = 0 \mid i\#j \text{ and } i,j = l,r,c \\ \text{The m-bot is unstable if } \bar{M}_{(w_i w_j)}(\vec{F}_{p,m}) > \bar{M}_{(w_i w_j)}(\vec{P}_m) \mid i\#j \text{ and } i,j = l,r,c \end{cases} \tag{3.4}$$

The p-bot is developed in order to co-manipulate and transport payload while ensuring the overall system stability and successful task achievement. The payload must be laid in a manner that keeps every m-bot stable. This allows to define and to optimize the landing position P_2 of the payload on the robot turntable with respect to (4.17) and (3.2).

For the optimization problem, an objective function l, which corresponds to the landing

position, is defined as follow, depending on robot parameters (cf. Fig. 3.7):

$$l > d_1 + W_b - s_1 = d_1 + W_b - \frac{W_b T}{2\sqrt{4W_b^2 + T^2}} \tag{3.5}$$

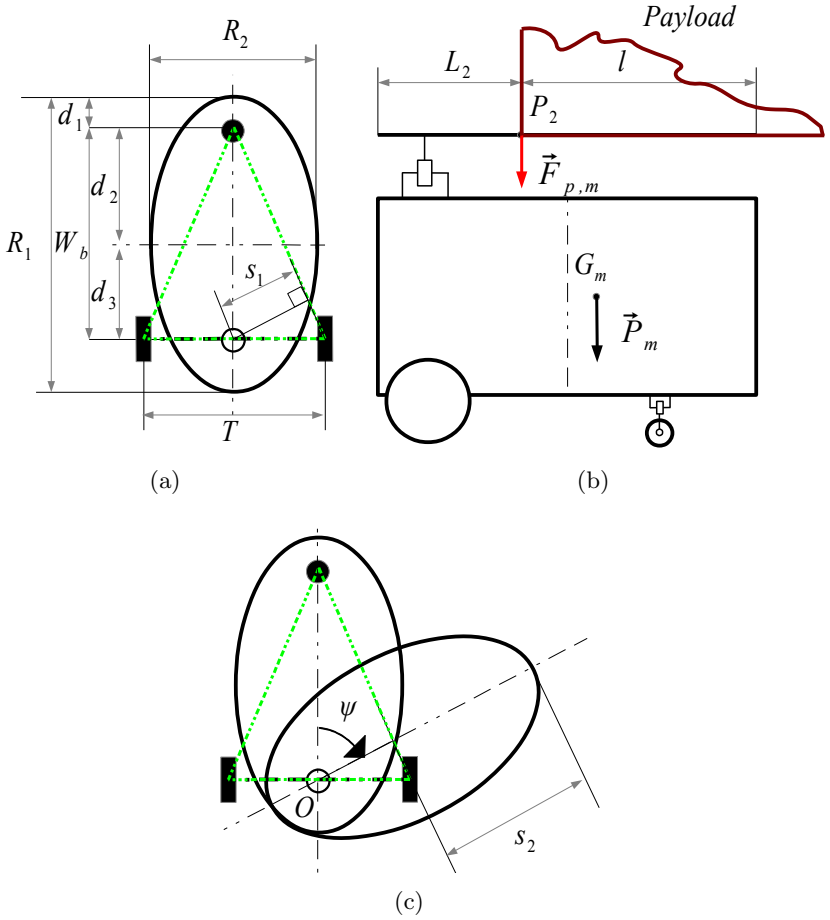

FIGURE 3.7: M-bot parameters: a) mobile platform parameters; b) Payload laid on m-bot body; c) turntable steered by an angle ψ w.r.t the mobile platform

The objective function l must respect the following constraints:

$$l > s_2 = d_1 + W_b - s_1 \tag{3.6}$$

$$l \leq R_1 - L_2 \tag{3.7}$$

$$\psi \in [-\frac{\pi}{2}, \frac{\pi}{2}] \tag{3.8}$$

where L_2 presents the necessary length on the platform, which will be used to mount the manipulation mechanism. This parameter is defined as constant. The decision of the usefulness of a mobile platform depends on this parameter. For a specified platform,

if $L_2 \geq R_1 - W_b - d_1 + s_1$, it will be impossible to use it with the proposed design for the task achievement, because the landing position will be out of the support polygon of the m-bot.

The function l is expressed as follow, with respect to the previous analysis:

$$\begin{cases} l = d_1 + W_b \text{ when it is maximum} \\ l = d_1 + W_b - \frac{W_b T}{2\sqrt{4W_b^2 + T^2}} \text{ when it is minimum} \end{cases} \tag{3.9}$$

Circular mobile platform with centred wheels axis

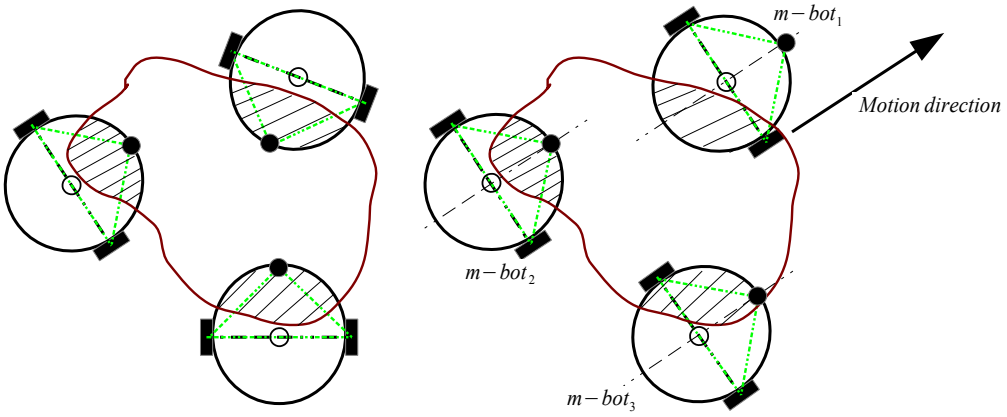

(a) Payload lifting (b) Payload transportation

FIGURE 3.8: Payload transportation by cicular mobile robots

When considering a mobile robot with a circular shape (with a radius R) and centred wheels axis (*e.g.* Khepera mobile robot), fixed parameters are defined such as the distance L_2. To ensure stability, conditions to define P_2 position has to be checked. For a circular robotic platform it is assumed that:

- $d_1 = 0$ - the castor wheel is on the front of the robot;
- $W_b = R$ - the robot rear wheels axis is centred relative to the robot platform;
- $T = 2R$ - the robot wheels are on the robot platform side;
- $L_2 = R$ - the half space on robot body will be used for the manipulation mechanism mounting.

In this case, the landing position P_2 that ensures the m-bot stability during all phases is constrained as follow:

$$R - \frac{R}{\sqrt{2}} \leq l \leq R, \tag{3.10}$$

which is a possible condition that could be ensured. This means the m-bot can support the payload and ensure co-manipulation and transport in a secure way.

In Fig. 3.9 and 3.10, P_2 represents the final landing position of the lower point of the end-effector P. This point is defined according to the analysis of the previous section with respect to the m-bot stability criteria. Two clearance parameters, δ_1 and δ_2, are defined in order to avoid collision between P and the robot platform, during payload lifting at position P_3. Constant and variable parameters are defined in Fig. 3.10.

The position of P_2 is defined according to section 3.2.2 and P_3 is defined by the clearances δ_1 and δ_2. The trajectory radius r is equal to the bar lengths l_{AB} and l_{CD}. Using a geometric construction, the center of trajectory could be determined on the lower side of the robot turntable. Fig. 3.9 presents the geometric construction to obtain the trajectory center and the position of P_1. The trajectory center is obtained by the intersection of both circle C_1 and C_3. α presents the inclination angle of the bars AB and CD during the payload lifting and the initial value α_0 must be well chosen in order to avoid the system blocking state. The normal pushing force generated by robot wheels, is transmitted and converted to a lifting force on the end effector, if and only if $\alpha_0 > 0$. By imposing an initial value of α, P_1 could be found by the intersection of the line passing through the trajectory center and which have an angle α_0 with respect to the horizontal ground. The trajectory radius is then determined as it will be explained in next section.

Trajectory radius determination

To calculate the trajectory radius the method consists in calculating the distances a and b (cf. Fig. 3.11) and solving the following second order equation:

$$r^2 = (h + r\sin\alpha_0)^2 + (a + b)^2. \tag{3.11}$$

The first step is to identify the constant a by using geometrical relations into right angle triangles:

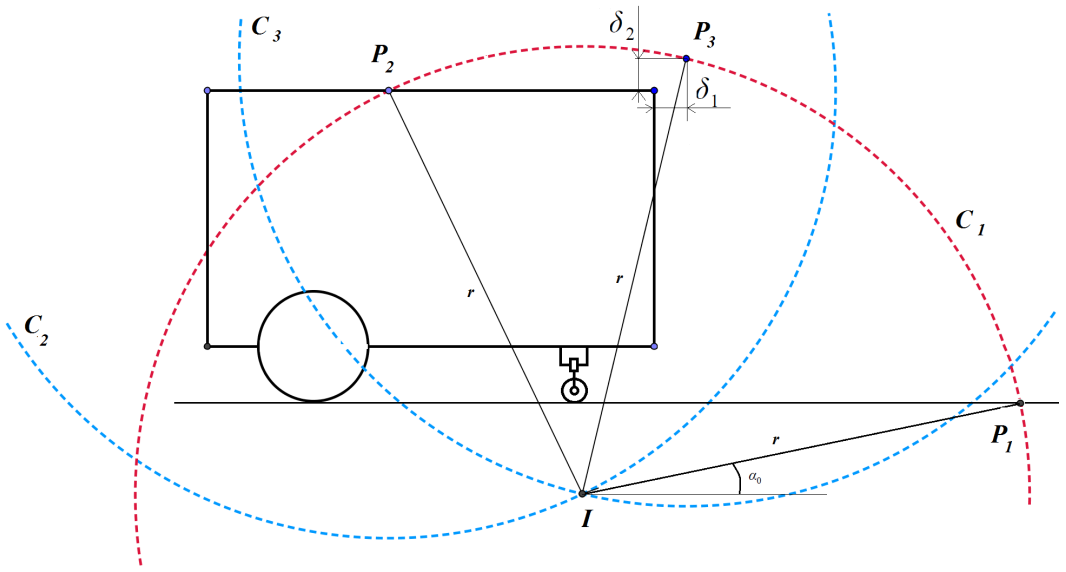

FIGURE 3.9: Determination of the trajectory center and the position of P_1

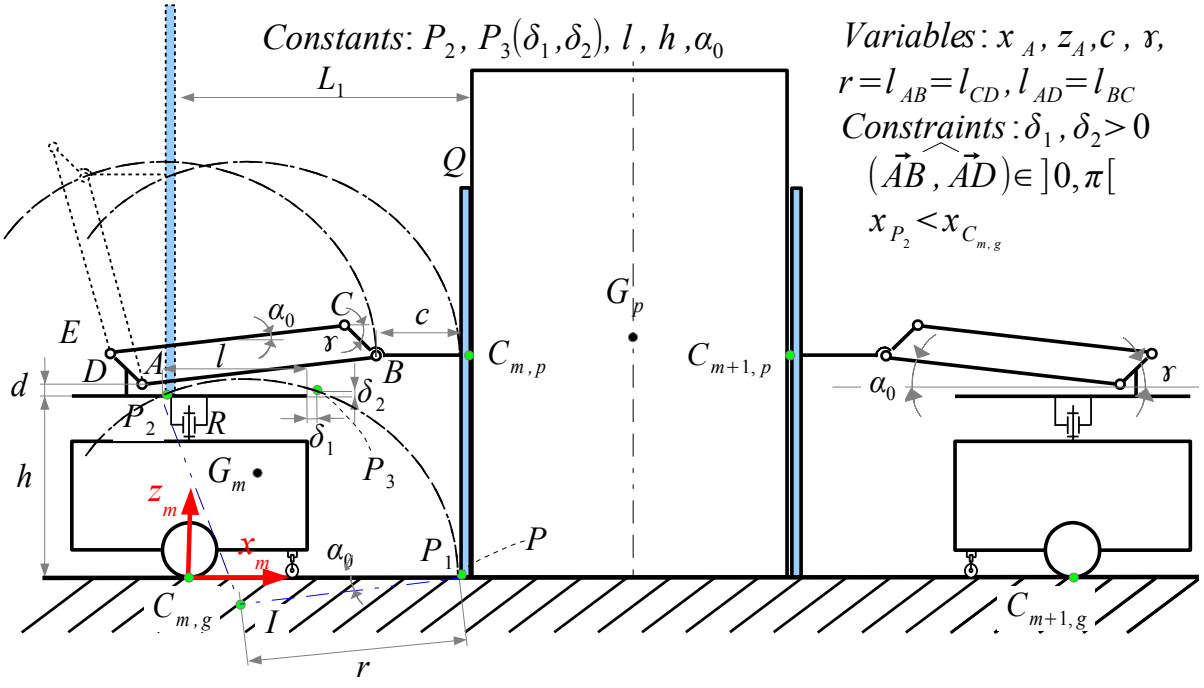

FIGURE 3.10: Dimensions synthesis

In triangle P_2P_3J orthogonal in J,

$$\cos\beta = \frac{l+\delta_1}{l_{P_2P_3}}$$

In triangle P_2EF orthogonal in E,

$$\cos\beta = \frac{\frac{l_{P_2P_3}}{2}}{a}$$

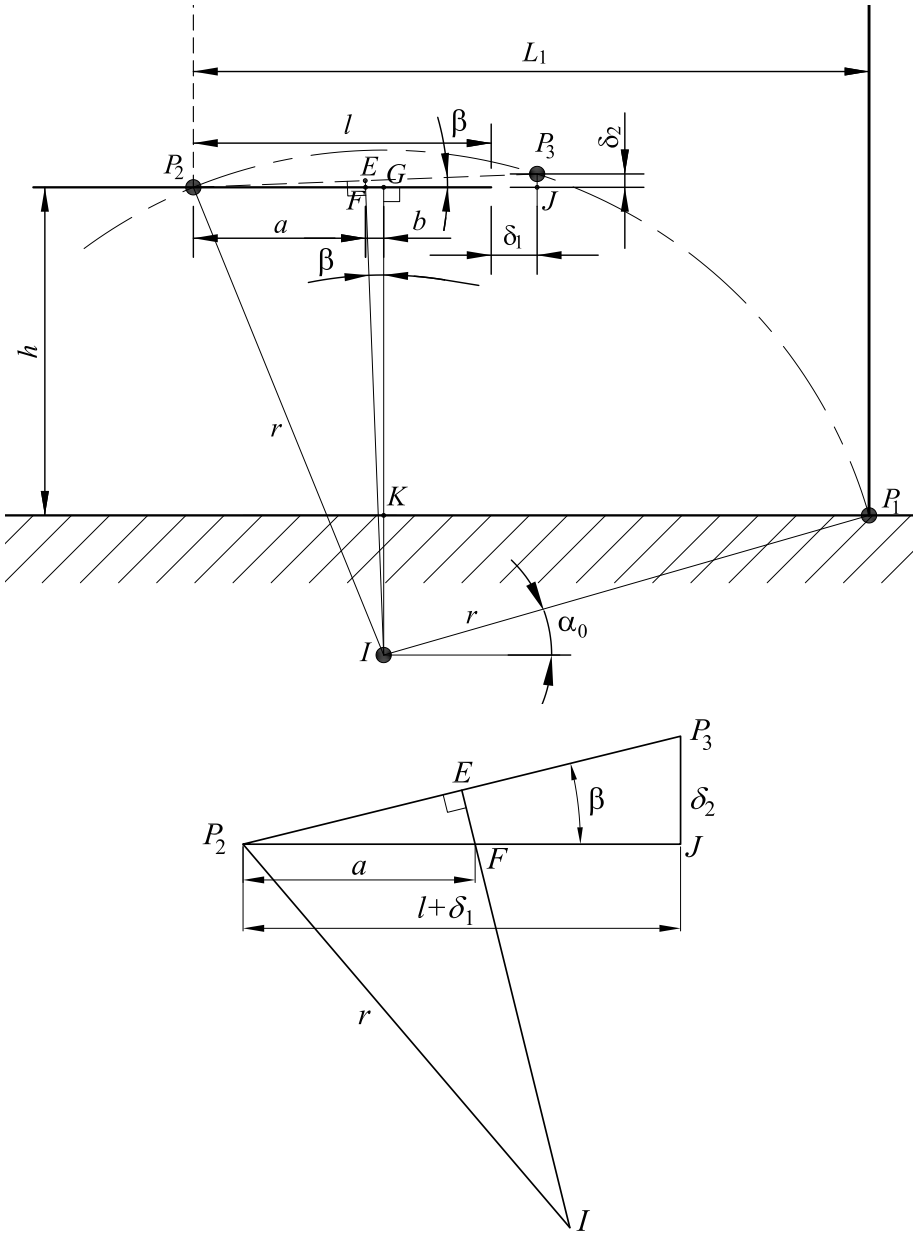

FIGURE 3.11: Determination of the trajectory center I

This means:

$$\frac{l+\delta_1}{l_{P_2P_3}} = \frac{\frac{l_{P_2P_3}}{2}}{a}, \tag{3.12}$$

$$a = \frac{(l+\delta_1)^2 + (\delta_2)^2}{2(l+\delta_1)}. \tag{3.13}$$

The second step is to find the constant b by using geometrical relations into right angle triangles:

In triangle FGI orthogonal in G,

$$\tan\beta = \frac{b}{h + r\sin\alpha_0}$$

In triangle P_2P_3J orthogonal in J,

$$\tan\beta = \frac{\delta_2}{l + \delta_1}$$

which means:

$$\frac{b}{h + r\sin\alpha_0} = \frac{\delta_2}{l + \delta_1}, \tag{3.14}$$

$$b = \frac{\delta_2(h + r\sin\alpha_0)}{l + \delta_1}. \tag{3.15}$$

Now that the constant term $(a + b)$ of eqaution (3.11) is identified, the equation can be reformulated into a second order equation of unknown r. Solving 3.11 means to solve the following equation:

$$mr^2 + nr + p = 0 \tag{3.16}$$

with

$$m = -\frac{[(l + \delta_1)^2 + \delta_2^2](\delta_2 + 2h)\sin\alpha_0}{(l + \delta_1)^2};$$

$$n = \frac{(l + \delta_1)^2\cos^2\alpha_0 - \delta_2^2\sin^2\alpha_0}{(l + \delta_1)^2};$$

$$p = \frac{[(l + \delta_1)^2 + \delta_2^2][(l + \delta_1)^2 + \delta_2^2 + 4h(\delta_2 + h)]}{4(l + \delta_1)^2}$$

Finally r is equal to:

$$r = l_{AB} = l_{CD} = \frac{-m + \sqrt{m^2 - 4np}}{2n} \tag{3.17}$$

The distance between P_1 and P_2 can be deduced in function of constant parameters as follows

$$L_1 = \frac{(l+\delta_1)^2 + (\delta_2)^2 + 2\delta_2(h + r\sin\alpha_0)}{2(l+\delta_1)} + r\cos\alpha_0 \tag{3.18}$$

$$x_{P_1} = x_{P_2} + L_1;\ z_{P_1} = 0 \tag{3.19}$$

Now the position of A and B can be written as:

$$x_A = x_{P_1} - r\cos\alpha_0 - c = x_{P_2} + \frac{(l+\delta_1)^2 + (\delta_2)^2 + 2\delta_2(h + r\sin\alpha_0)}{2(l+\delta_1)} - c \tag{3.20}$$

$$z_A = h + d = z_{P_2} + d \tag{3.21}$$

$$x_B = x_A + r\cos\alpha_0 \tag{3.22}$$

$$z_B = z_A + r\sin\alpha_0 \tag{3.23}$$

Singular positions

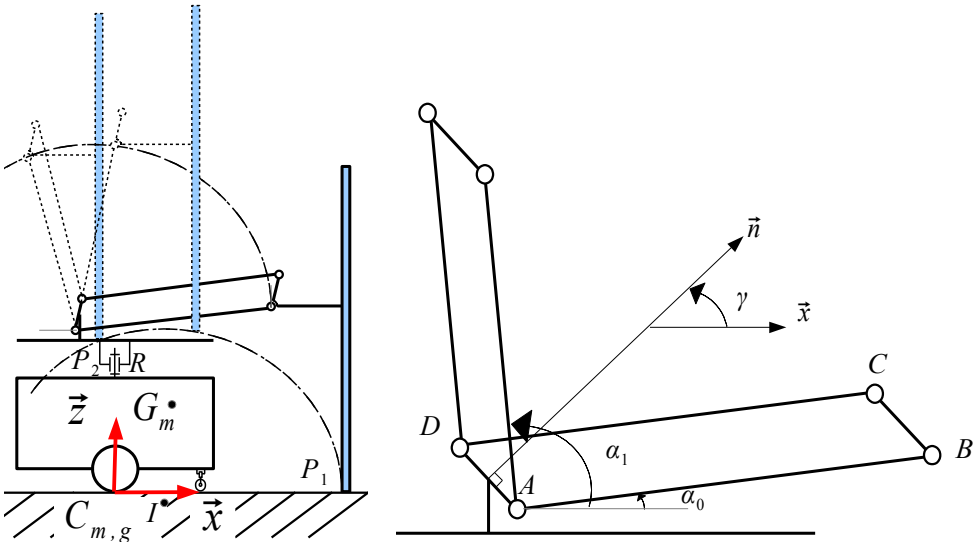

(a) (b)

FIGURE 3.12: Extreme positions of the parallelogram mechanism

To avoid singular positions of the parallelogram mechanism, $\widehat{BAD}$ must satisfy a constraint along the course between α_0 and α_1 which is:

$$\widehat{BAD}] \in 0, \pi[\tag{3.24}$$

When this constraint is satisfied along the trajectory between initial and final positions, the parallelogram mechanism would never have a flattened configuration as presented in Fig. 3.12(a). This constraint implies a suitable choice of γ angle, the angle of the normal vector $\vec{n}$ to segment AB with respect to horizontal.

From Fig. 3.12(b) one can conclude, to avoid the parallelogram flattening, that γ must be less than $\pi - \alpha_1$ and while considering always $\alpha_0 > 0$:

$$\gamma = \frac{\alpha_0 + \alpha_1}{2} \in [0, \pi - \alpha_1] \tag{3.25}$$

where α_0 and α_1 are the extreme angular positions of the link AB.

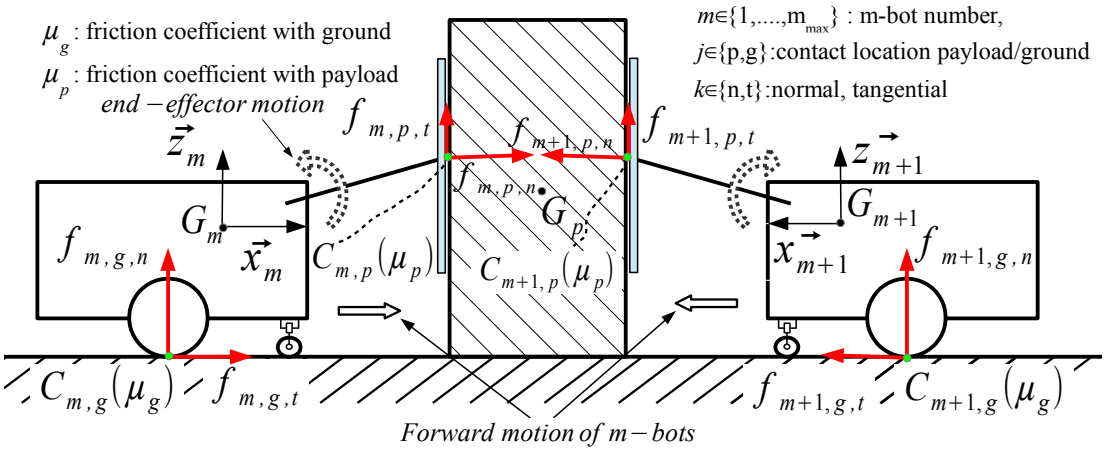

FIGURE 3.13: Payload lifting by two m-bots

3.3 Pre-dimensioning the lifting

In this section it has been considered the lifting capacity of a m-bot. The m-bot # m, with a mass M,is able to apply a normal pushing force $f_{m,p,n}$, which generates a lifting force $f_{m,p,t}$, (Fig. 3.13). The contact point $C_{m,g}$ (m-bot/gound) is characterized by a friction coefficient, μ_g, and the contact point $C_{m,p}$ (m-bot/payload) is characterized by a friction coefficient, μ_p. The maximal lifting force for the m-bot # m will be evaluated according to the manipulation mechanism actuation in the next subsections.

3.3.1 Passive mechanism

In this first case, all the articulations of the manipulation mechanism are left uncontrolled (free joints) (cf. Fig. 3.14). When the mobile platform is moving to push the payload, a normal pushing force $f_{m,p,n}$ appears on the end-effector surface which will generate a lifting force $f_{m,p,t}$. The following notations are considered (cf. Fig. 3.14):

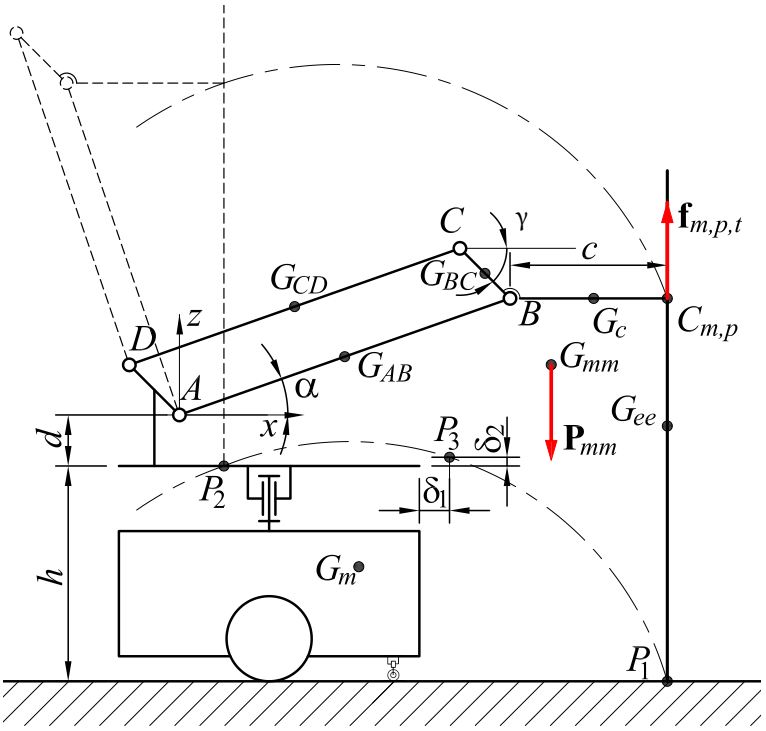

FIGURE 3.14: Passive mechanism

- $L_{AB} = L_{DC} = r$
- $L_{CB} = L_{DA} = r_1$
- G_{AB} and G_{BC} are respectively the center of mass of the bars AB and BC
- G_{CD} and G_{DA} are respectively the center of mass of the bars CD and DA
- G_{ee} denotes the end-effector center of mass and G_c denotes the center of mass for the connecting link between the end-effector and the parallelogram linkage
- G_{mm} denotes the center of mass of the manipulation mechanism

The position of G_{mm} could be found according to the following formula:

$$\vec{AG}_{mm} = \frac{1}{p}\sum_{i=1}^{n} p_i \vec{AG}_i \tag{3.26}$$

where p is the total weight. The generated lifting force is calculated according to:

$$\vec{AG}_{mm} \wedge \vec{P}_{mm} = \vec{AC}_{m,p} \wedge \vec{f}_{m,p,t} \tag{3.27}$$

$$\vec{P}_{mm} x_{G_{mm}} = \vec{f}_{m,p,t}(r_1 \cos\alpha + c) \tag{3.28}$$

Finally $f_{m,p,t}$ could be written as

$$f_{m,p,t} = \frac{P_{mm} x_{G_{mm}}}{r_1 \cos\alpha + c} \tag{3.29}$$

where

$$x_{G_{mm}} = \frac{x_{G_{AB}} m_{AB} + x_{G_{BC}} m_{BC} + x_{G_{CD}} m_{AB} + x_{G_c} m_c + x_{G_{ee}} m_{ee}}{m_{AB} + m_{BC} + m_{AB} + m_c + m_{ee}}$$

with

$$x_{G_{AB}} = \frac{r}{2}\cos\alpha$$

$$x_{G_{CD}} = \frac{r}{2}\cos\alpha - \frac{r_1}{2}\cos\gamma$$

$$x_{G_{BC}} = r\cos\alpha - \frac{r_1}{2}\cos\gamma$$

$$x_{G_c} = r\cos\alpha + \frac{c}{2}$$

$$x_{G_{ee}} = r\cos\alpha + c$$

Finally

$$x_{G_{mm}} = \frac{(2r\cos\alpha - r_1\cos\gamma)(m_{AB} + m_{BC}) + 2(r\cos\alpha + c)(2m_c + m_{ee})}{2(2m_{AB} + m_{BC} + m_c + m_{ee})}$$

The numerator of the previous expression depends on $\cos\alpha$, which decreases in function of robot advance to ensure the payload lifting while α is increasing. The resulting lifting force $\vec{f}_{m,p,t}$ also decreases during the lifting phase which implies a limited performances of m-bots for the task achievement and a risk of payload falling down. This force is expressed as follows

$$f_{m,p,t} = \frac{P_{mm}\left[\frac{(2r\cos\alpha - r_1\cos\gamma)(m_{AB}+m_{BC})+2(r\cos\alpha+c)(2m_c+m_{ee})}{2(2m_{AB}+m_{BC}+m_c+m_{ee})}\right]}{r_1\cos\alpha + c} \tag{3.30}$$

3.3.2 Mechanism with compliant components

Mechanism with helical extension spring

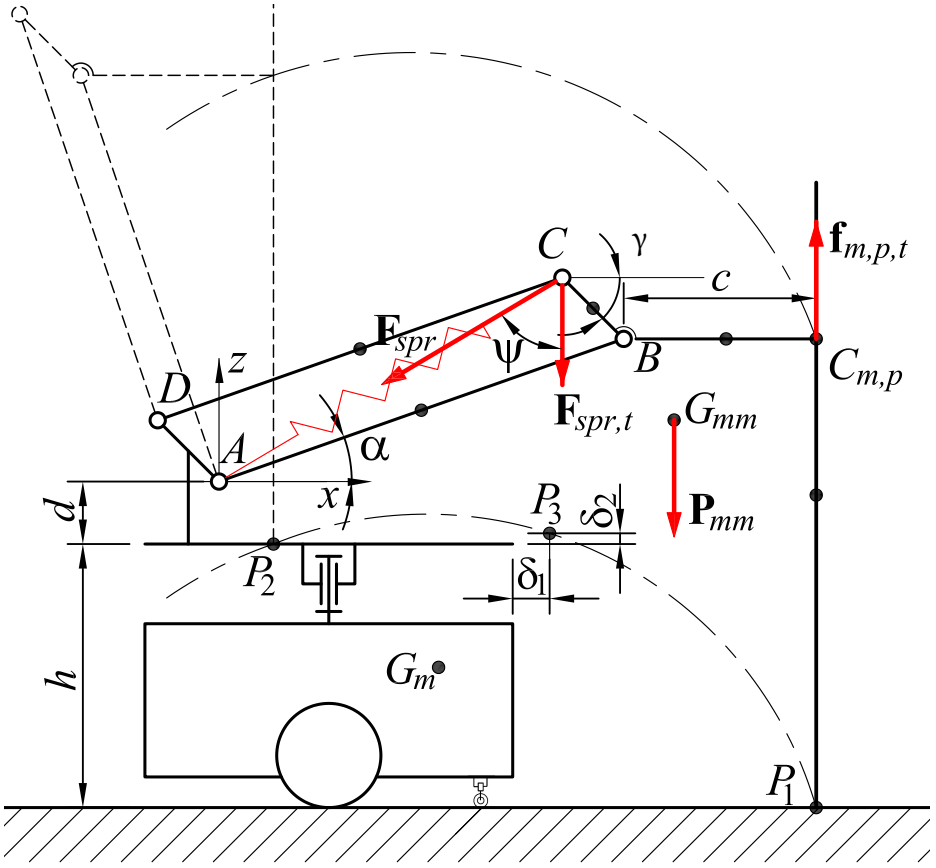

(a)

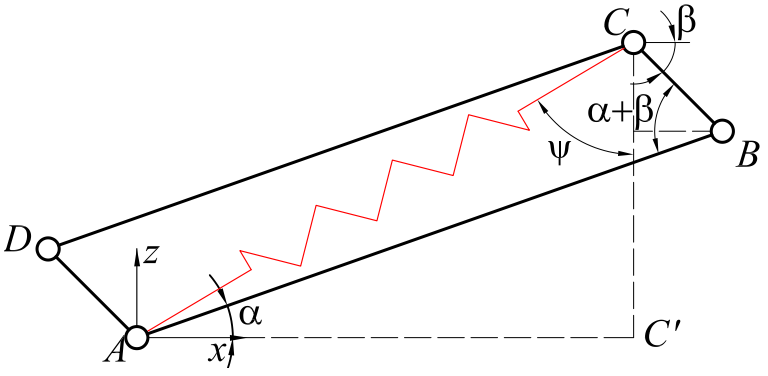

(b)

FIGURE 3.15: Payload lifting using a traction spring

A helical extension spring is used in this case, to evaluate the lifting capacity (cf. Fig. 3.15). The spring is mounted between A and B and the generated spring force F_{spr} during the circular trajectory of any point of the lifting mechanism is expressed as follow:

$$F_{spr} = K\Delta L, \tag{3.31}$$

where K is the spring stiffness

$$\Delta L = L - L_0 = L_{AC} - L_0 = \sqrt{r^2 + r_1^2 - 2rr_1\cos(\alpha+\gamma)} - L_0$$

L_0 is the initial spring length. Finally $\vec{F}_{spr}$ is equal to:

$$F_{spr} = K\sqrt{r^2 + r_1^2 - 2rr_1\cos(\alpha+\gamma)} - L_0, \tag{3.32}$$

By writing the momentum equilibrium in A, the generated lifting force using 3.27 can be written as:

$$f_{m,p,t} = \frac{P_{mm}x_{G_{mm}} + (F_{spr}\cos\psi)L_{AC'}}{r\cos\alpha + c}, \tag{3.33}$$

$$f_{m,p,t} = \frac{P_{mm}x_{G_{mm}} + F_{spr}\frac{r\sin\alpha + r_2\sin\alpha}{\sqrt{r^2+r_1^2-2rr_1\cos(\alpha+\gamma)}}(r\cos\alpha - r_1\cos\alpha)}{r\cos\alpha + c}. \tag{3.34}$$

As in the previous case (helical spring), the term of $\cos\alpha$ figures in the numerator of the resulting lifting force expression $f_{m,p,t}$ but is rectified by the force generated by the spring deformation F_{spr} which increases while the m-bots are lifting the payload. This allows to ensure a system better performances in term of lifting and stability insurance. If the payload mass is assumed to be known and the necessary $f_{m,p,t}$ to lift it is determined, in this case $\vec{F}_{spr}$ and the spring stiffness K could be written as follow:

$$f_{spr} = \frac{f_{m,p,t}(r\cos\alpha + c) - P_{mm}x_{G_{mm}}}{\frac{r\sin\alpha + r\sin\alpha}{\sqrt{r^2+r_1^2-2rr_1\cos(\alpha+\gamma)}}(r\cos\alpha - r_1\cos\alpha)}, \tag{3.35}$$

$$K = \frac{f_{m,p,t}(r\cos\alpha_1 + c) - P_{mm}x_{G_{mm}}}{(\sqrt{r^2 + r_1^2 - 2rr_1\cos(\alpha_1+\gamma)} - L_0)\frac{r\sin\alpha_1 + r\sin\alpha_1}{\sqrt{r^2+r_1^2-2rr_1\cos(\alpha_1+\gamma)}}(r\cos\alpha_1 - r_1\cos\alpha_1)}. \tag{3.36}$$

Mechanism with torsion spring

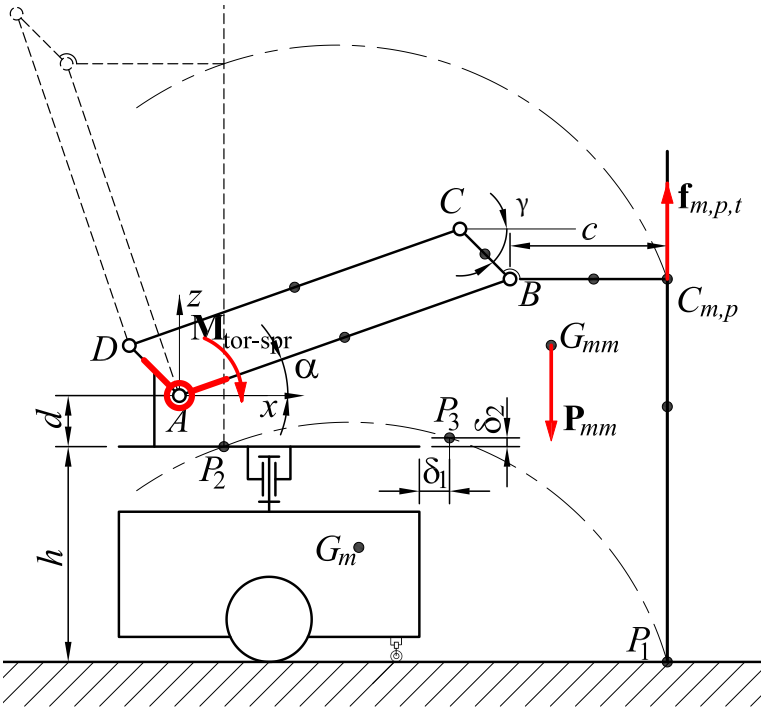

FIGURE 3.16: Payload lifting using a torsion spring

A torsion spring (cf. Fig. 3.16) is able to generate a moment $\vec{M}_{tor-spr}$, when it is deformed. In this case it was considered the use of a torque spring mounted on the joint A and the system response is evaluated in term of resultant normal force, to see the system lifting performance. The sum of all the torques in point A is made in equation (3.37).

$$f_{m,p,t} = \frac{P_{mm} x_{G_{mm}} + M_{tor-spr}}{r \cos \alpha + c}, \tag{3.37}$$

where

$$\bar{M}_{tor-spr} = K(\alpha - \alpha_0), \tag{3.38}$$

k is the torsion spring stiffness and α_0 is the initial value of α angle.

Both cases of use of compliant components are similar by applying an extra lifting force generated by the compliant component deformation which ensures a better performance for the task achievement then the case of use of passive mechanism.

When it is assumed to know the payload mass and the necessary $f_{m,p,t}$ to lift it, then $\vec{M}_{tor-spr}$ and the spring stiffness K could be written as follow:

$$\bar{M}_{tor-spr} = f_{m,p,t}(r\cos\alpha + c) - P_{mm}x_{G_{mm}}, \tag{3.39}$$

$$K = \frac{f_{m,p,t}(r\cos\alpha_1 + c) - P_{mm}x_{G_{mm}}}{\alpha_1 - \alpha_0}, \tag{3.40}$$

3.3.3 Passive mechanism with end effectors interconnection

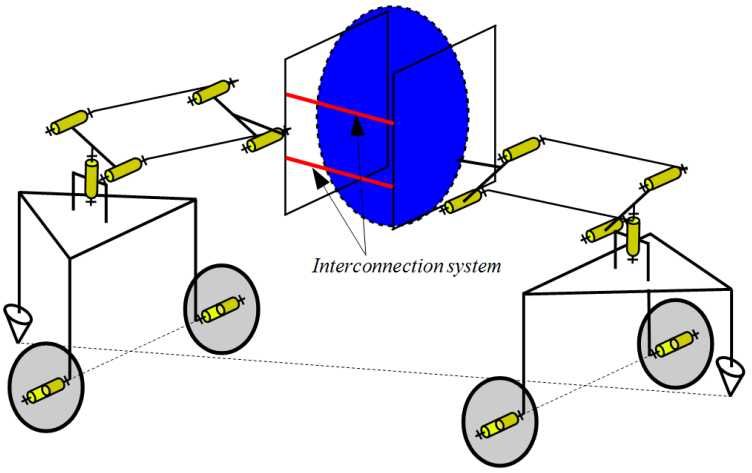

FIGURE 3.17: Interconnection system for payload tightening

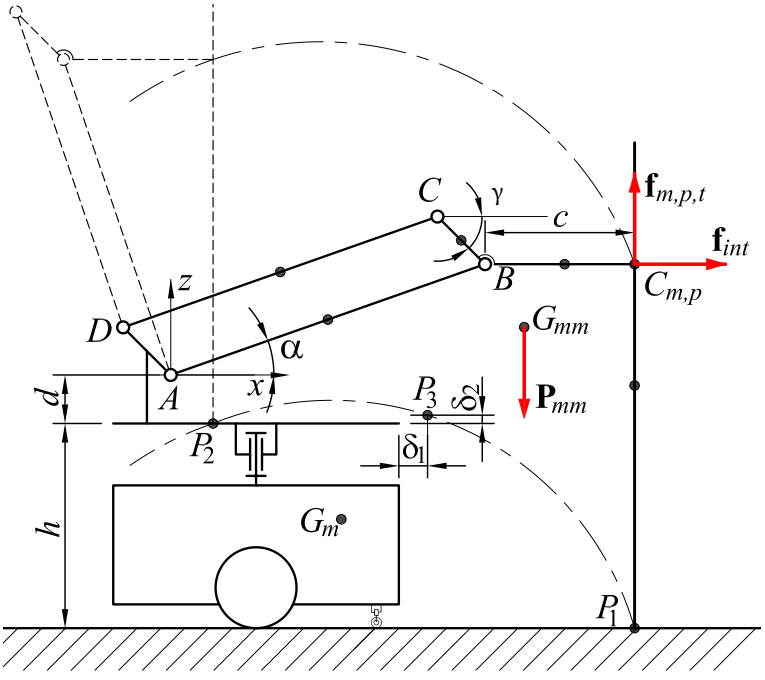

FIGURE 3.18: Payload lifting using an interconnection system

In this case, the group of robots is able to lift a payload proportional to its wheels/ground and its end-effector/payload contact coefficients. The payload is in contact with the m-bots end-effectors thanks to the interconnection mechanism (cf. Fig.3.17). The generated lifting force is then resulted and limited by the wheels propulsion (cf. Fig.3.13). It can be written as:

$$f_{m,p,t} = \mu_p \mu_g M g \tag{3.41}$$

3.3.4 Actuated mechanism with end effectors interconnection

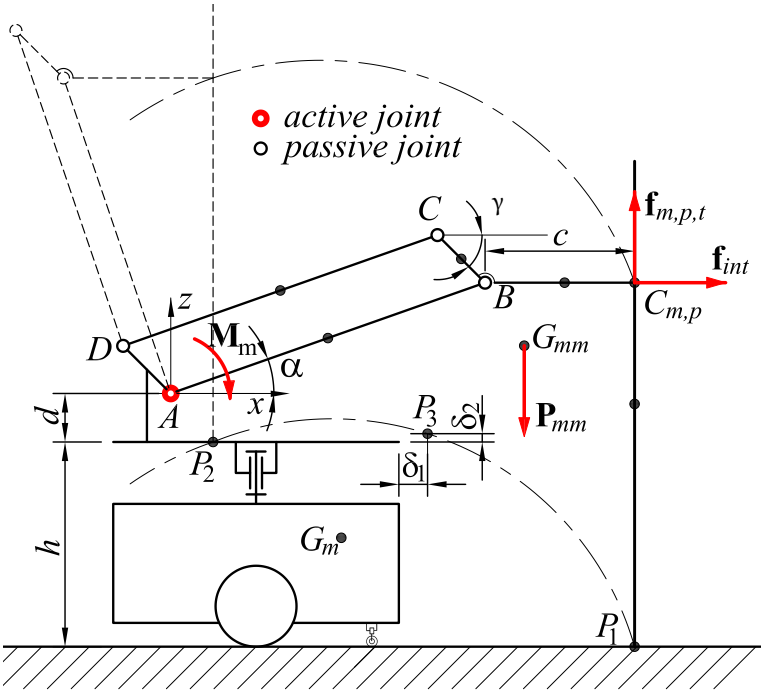

FIGURE 3.19: Payload lifting using an interconnection system and actuated parallelogram system

In the case where an actuator is used for the parallelogram mechanism, the lifting force that allows the payload manipulating will be equal to the lifting force generated by the used actuator:

$$f_{m,p,t} = \frac{M_m - P_{mm} x_{G_{mm}}}{r \cos\alpha + c}, \tag{3.42}$$

An adequate choice of the actuator can ensure this lifting force to transport a payload with a mass equal to:

$$P = \sum_{m=1}^{m_{max}} f_{m,p,t} = m_{max} \left(\frac{M_m - P_{mm} x_{G_{mm}}}{r \cos\alpha + c}\right). \tag{3.43}$$

If the robot are also using their wheel propulsion, then the lifting force expressed in equation (3.41) would be added to the resulting lifting force of equation (3.42).

3.4 Determination of the used number of robots

Payload in flat ground

Passive manipulation mechanism

In the case of use of m-bots in a structured horizontal plane as presented in Fig. 3.20, the number of m-bots that must be used for the task achievement is determined in function of the payload mass and lifting capacity. When considering the cases of m-bots without interconnection system and without manipulator actuation, the lifting capacity is limited by the robot wheels propulsion and the friction coefficients μ_g and μ_p. The minimum number of m-bots that could used is defined as follow:

$$m_{min} = round[\frac{\bar{P}_{pl}}{\mu_p \mu_g M g} = \frac{M_{pl}}{\mu_p \mu_g M}] \tag{3.44}$$

Manipulation mechanism with compliant components

In this case the number of used m-bots allowing the payload lifting and co-manipulation is calculated relative to the force generated by the compliant component deformation. The minimum m-bots number that could be used in case of helical spring is equal to:

$$m_{min} = round[\frac{\bar{P}_{pl}}{\frac{P_{mm} x_{G_{mm}} + F_{spr} \frac{r \sin\alpha + r_2 \sin\alpha}{\sqrt{r^2 + r_1^2 - 2 r r_1 \cos(\alpha+\gamma)}} (r\cos\alpha - r_1 \cos\alpha)}{r\cos\alpha + c}}] \tag{3.45}$$

and in the case of torque spring is equal to:

$$m_{min} = round[\frac{\bar{P}_{pl}}{\frac{\bar{P}_{mm} x_{G_{mm}} + \bar{M}_{tor-spr}}{r\cos\alpha + c}}] \tag{3.46}$$

Actuated manipulation mechanism

In this case the number of used m-bots allowing the payload lifting and co-manipulation is calculated relative to the actuator performance used for the manipulator. The minimum m-bots number that could be used is equal then to:

$$m_{min} = round[\frac{\bar{P}_{pl}}{\frac{\bar{P}_{mm}x_{G_{mm}}+\bar{M}_m}{r\cos\alpha+c}}] \tag{3.47}$$

Payload on a tilted plane ground

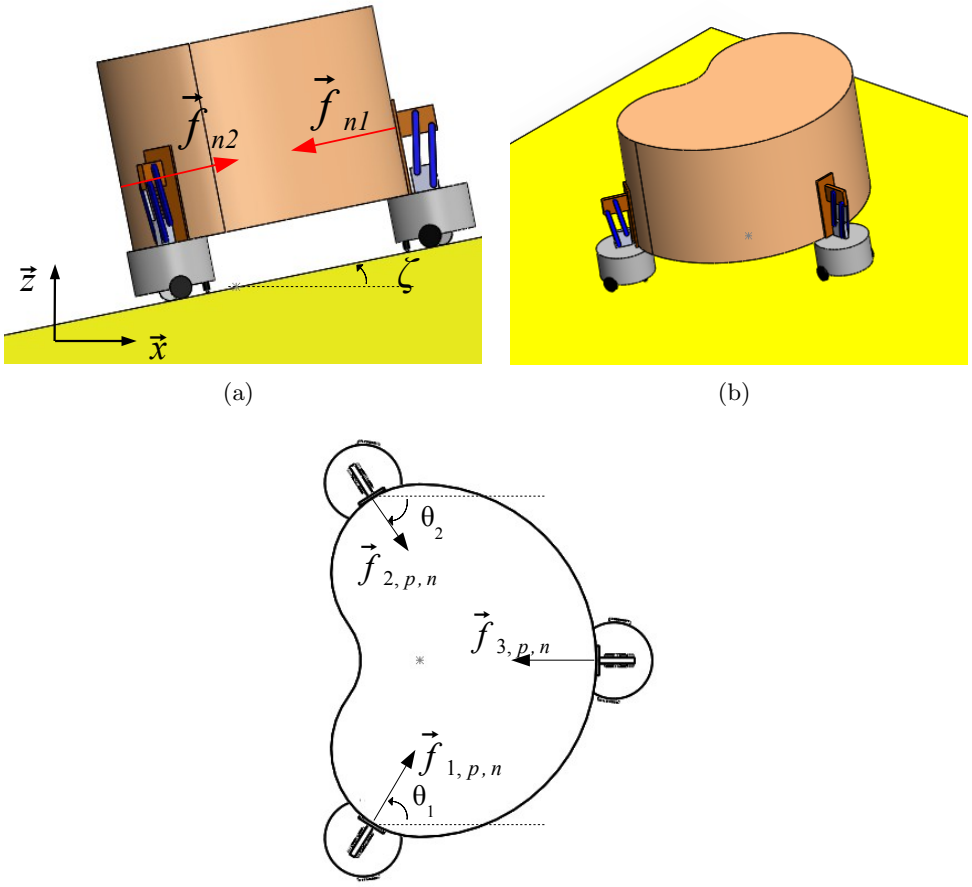

FIGURE 3.20: M-bot lifting and transport in a tilted ground: a) side view; b) perspective; c) top view

If the m-bots are considered to operate in an inclined plane, the repartition of the robots around the payload won't be the same as in the previous case. Fig. 3.20 presents the supposed case. Depending on the angle ζ of the plane inclination the used m-bots in

the both sides, bottom and top, of the payload will be determined. Using the FPS and a simple projection on $\vec{x}$ and $\vec{z}$ axis it has been obtained the following equations:

$$\begin{cases} f_{n1}(\mu_p \sin\zeta + \cos\zeta) + f_{n2}(\mu_p \sin\zeta - \cos\zeta) = \vec{0} \\ P_{pl} + f_{n1}(\mu_p \cos\zeta - \sin\zeta) + f_{n2}(\sin\zeta + \mu_p \cos\zeta) = \vec{0} \end{cases} \tag{3.48}$$

Solving the linear system of two equations with two unknowns f_{n1} and f_{n2} finally gives

$$\begin{cases} f_{n1} = \frac{P_{pl}(\cos\zeta - \mu_p \sin\zeta)}{2\mu_p} \\ f_{n2} = \frac{P_{pl}(\cos\zeta + \mu_p \sin\zeta)}{2\mu_p} \end{cases} \tag{3.49}$$

The number of m-bots in the bottom side are determined in function of f_{n1}, however, m-bots supporting the payload on the top side are determined in function of f_{n2}. The m-bots orientation must be taken into consideration in a way that

$$m_{min_{bottom}} = round[\frac{f_{n1}}{\mu_g Mg \sum_{m=1}^{m_{min}} \cos\theta_m}] \tag{3.50}$$

$$m_{min_{top}} = round[\frac{f_{n2}}{\mu_g Mg \sum_{m=1}^{m_{min}} \cos\theta_m}] \tag{3.51}$$

3.5 Conclusion

In this chapter, it has been considered the problem of payload co-manipulation and transportation using a multi-robot system. The task was defined by several phases achieved by using several m-bots. A m-bot is mainly composed of two parts: a mobile platform and a manipulation mechanism used to lift and put the payload on robot bodies. The overall system composed of the used m-bots and the payload is called p-bot, which is modular and can gather a variable number of m-bots depending on the task to be achieved. The m-bot structure has been studied and the lifting mechanism has been presented in order to obtain a functional system that ensures stability and successful task achievement. The system lifting capacity has been evaluated in a passive way and with using compliant components. It has been demonstrated that the system is more efficient while using springs with a certain limited stiffness in order to avoid loss of

stability. It has been also demonstrated that the system becomes more efficient, in term of payload mass to be manipulated, if the friction coefficients are greater. However, the system efficiency is limited to the wheel propulsion forces and the m-bots mass.

Chapter 4

Control architecture

Abstract: *This chapter addresses optimal positioning of a group of mobile robots for a successful manipulation of payloads of any shape. The focus is made in this chapter on the chosen methodology to obtain sub-optimal positioning of the robots around the payload to lift it and to transport it while maintaining a geometric multi-robot formation. This appropriate positioning is obtained by combining two constraints for stable and safe lifting and transport of the payload. A predefined control law is then used to track a virtual structure in which each elementary robot has to keep the desired position relative to the payload. Simulation results for an object of any shape, described by a parametric curve, are presented. Additional 3D simulation results with a multi-body dynamic software validate our proposal.*

4.1 Introduction

In this chapter cooperative control problem is considered. We are looking then to design an innovative architecture for object lifting and transport in a structured ground in a first part and for all terrain navigation in a second part. To avoid loss of stability or object slipping during the object transport the control problems arise when using a group of mobile robots to perform a task jointly. Using more than one robot as opposed to a single one presents many advantages when considering redundant task, dangerous tasks or a task that scale up or down in time or that require flexibility. In [15], an overview about mobile robots and cooperative control for multi-agent systems was presented. In recent literature the control problem of a group of robot was considered and many works treated the problem of control architectures and control approaches [5, 24, 67, 89, 117, 140, 145, 146, 155, 170]. In this chapter, the first part deals with the state of the art related to robot control architectures. and approaches is presented to treat later the problem of formation control in which we are interested to transport an object from an initial pose (x_i, y_i, θ_i) to a final pose (x_f, y_f, θ_f).

4.2 Mobile robots control

Mobile robots control needs the juxtaposition of three main phases: perception, decision and action. The perception builds a model of the environment where the robot evolves, the decision uses this model to generate the motion instructions. Finally the action transforms these instructions to an adequate control for the robot effectors. A sophisticated control must manage these three phases [5].

It is possible to make an analogy between a task achieved by a robot and a usual representation of an automatic system to enslave. In this case the controller block corresponds to the robot controller, the system bloc corresponds to the robot immersed in its environment. Using its sensors, the robot will collect information from the environment. After a data processing for the collected information in the level of robot controller, a control is produced in order to satisfy the best input dictated to the task to be achieved. The control law execution by the robot effectors allows to modify the robot state and the global system state (modification of the output), which contains the feedback loop [5].

The targeted tasks in the C^{3}Bots project are dedicated for a group of mobile robots, this means that the mobile robot control won't depend only on its proper perception and objectives, but also it will take into consideration a certain information related to the global evolution of the multi-robot system. Obviously this will add a certain level of complexity to the mobile robot controller. This complexity is related to:

- The dynamics of the interaction between the robot entities in the environment. These interactions, if they are not well mastered, may influence in a harmful way the system evolution. The robots can be blocked, embarrassed, desynchronized,
- The number of variables governing the system evolution, resulting from the raising of the number of used systems (robots) in the environment,
- The complexity of the inherent control of one robot that has to act in function of his own received instructions coming from the environment and also has to adapt its behaviour to the other entities. That means that the robot will try to converge to a viable or even optimal equilibrium for the cooperative task execution,
- The perceptual uncertainties of the robot which can add more complexity for the robot control for a large number of sensors.

These mentioned points are the most important ones that render up more complex the multi-robot system control.

The control scheme in Fig. 4.1 was extended for the case of multi robot system. We can conclude that the robots share the same environment and that the decisions (control) generated by each controller are influenced by the interactions with the other robots.

4.3 Centralized control architecture versus distributed control architecture

An extremely important point to take into consideration before designing a control architecture for a group of mobile robots is the choice of centralizing the control or distributing it for the robotic entities.

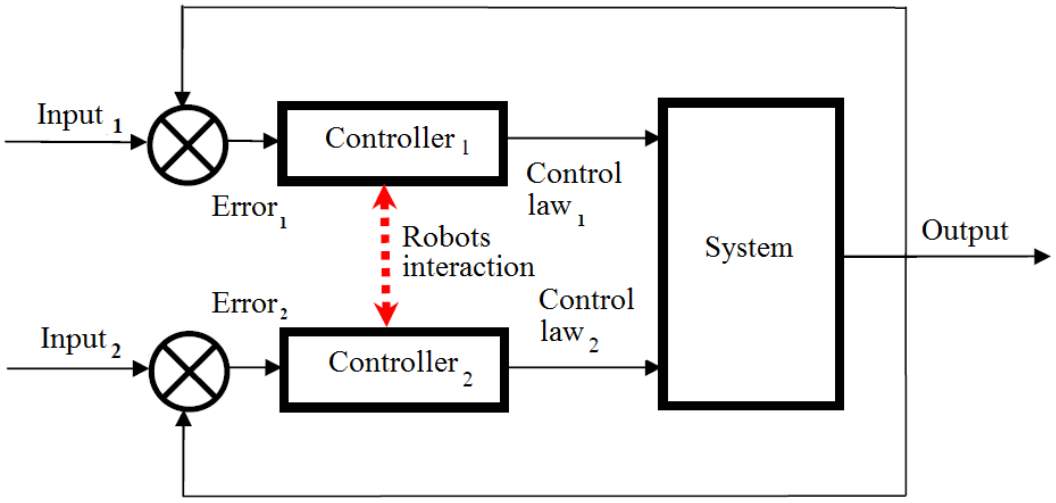

FIGURE 4.1: Control architecture for a multi-robot system [5]

Centralized control [5, 89] is often synonym to the *Top-Down* approach. It is based on a single controller relocated from the physical structure of a robot that processes all the information needed to achieve the desired control objectives. Thus in a centralized control, both the individual member and the whole group can improve superior performance and optimal decisions. This architecture implies a global knowledge of each element of the system, it requires high computational power, massive information flow and it is not robust due to the dependence on a single controller. In contrast with centralized control, in a **decentralized control** [5, 89], often synonym to the *Bottom-Up* approach, each element of the system has its own controller and is completely autonomous in the decision process. This implies a reduced number of communicated signals and information. Decentralized controllers are then more flexible and require less computational effort. It is also needed to provide some degrees of centralization for human operator for programming tasks and to monitor the system. Twinning both control architectures makes a **hybrid architecture** where a central processor applies high level control over autonomous entities.

In the proposed work, both centralized and decentralized architectures will be used.

4.4 Target reaching and navigation in formation

4.4.1 Target reaching (TR)

When a mobile robot aims to reach a desired position, which is denoted as Target Reaching (TR) phase, the problem of path planning arise. Path planning problem treats the calculation of an optimal path without collision from an initial configuration to a final configuration in a free space. Three methods in the literature are detailed below to solve this problem:

- cellular decomposition method [150];
- potential field (PF) [95];
- graph constructing [125].

The notion of completeness differentiates these approaches. We distinguish the complete planner (or exact method) which guarantees to find a solution or to inform that it does not exist. It is the first developed method to solve the problem of path planning (e.g. Piano remover [31, 150]). Complete planner in resolution are based on the configuration space discritization. It gives a solution if it exists but with a unique given resolution. Finally the probabilist completeness planner which can give a solution if it exists but in a defined time.
Trajectory generation has as main function to calculate the position or situation evolution in function of time. This trajectory of reference defines the control system input. The problem of trajectory generation for manipulators was widely treated in literature [26, 29]. In our case we treat the problem of trajectory generation between two points which is a point to point problem. We can define, in function of the imposed constraints (e.g. geometric or kinematic kinematic constraints), a type of trajectory presentation (polynomial curve of degree 2, cubic...)

Obstacle avoidance

Obstacle avoidance is a crucial behaviour that must figure in the use of mobile robots. In fact the mobility characteristic imposes that the mobile robot evolves in a dynamic and

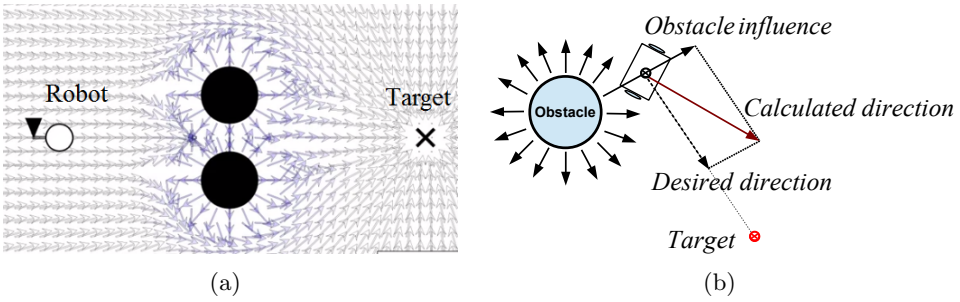

FIGURE 4.2: Obstacle avoidance using Potential Field method: a) the obstacle generates repulsive virtual forces and the target generates attractive virtual forces; b) Virual forces affect the robot direction

over constrained environment. That is why all mobile robots are equipped with sensors allowing obstacles detection (Laser sensors, Ultra sound, Infra red...). Many methods were developed in literature for obstacle avoidance (based on local perception of the environment). *Potential Field* method (PF) is one of the most widespread methods in literature. The idea behind this technique is to imagine virtual forces acting on the robot [14, 95]: the obstacles apply repulsive forces on the mobile robot and the desired position to reach applies an attractive force (cf. Fig 4.17(a)). The sum of these forces defines the final direction and the evolving speed of the robot. This method is easy to be implemented and that is why a considerable number of works use this framework [104, 124, 162]. Although this method has some drawbacks such as:

- in case of null resultant of the applied forces on the robot, the mobile platform is blocked in a local minimum where its speed is null. Some of the proposed solution for this problem was the introduction of noise in the sum of applied force [156] or by adding a circular PF countering the obstacle;
- like any obstacle in the robot environment, the generated forces would affect the robots figuring in its neighbourhood. This means that in some cases, a non annoying obstacle can affect the robot orientation and speed (cf. Fig 4.17(b)).

The *Vector Field Histogram* (VFH) [101] comes to replace *Virtual Force Field* (VFF) [28] based on PF and facing the same problems. VFH uses a local occupation grid constructed by the robot sensors. Each cell of the grid is associated to a number (value and certitude). A histogram representing the environment occupation around the robot is constructed thanks to this occupation grid (cf. 4.3). For that, the grid is discretized in angular sectors. The sum of the values of cells in each sector is calculated. The

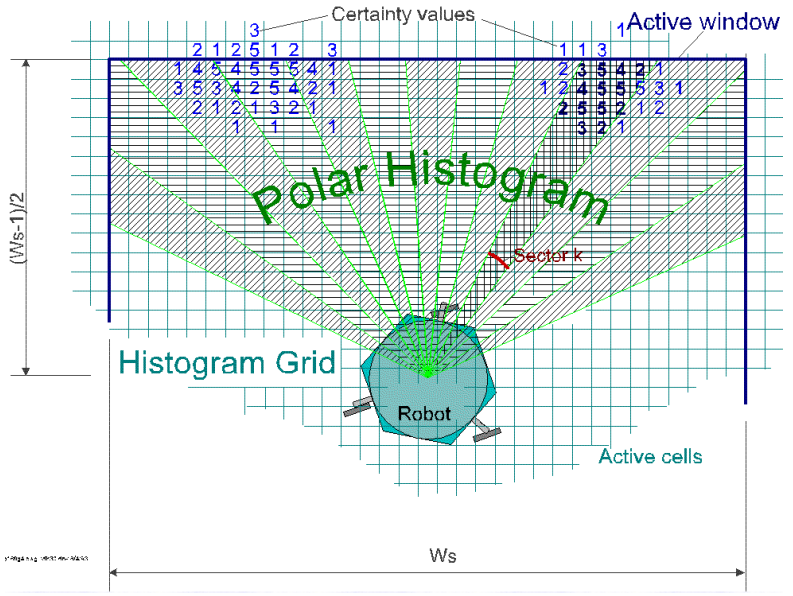

FIGURE 4.3: Obstacle avoidance using Vector Field Histogram method [85]

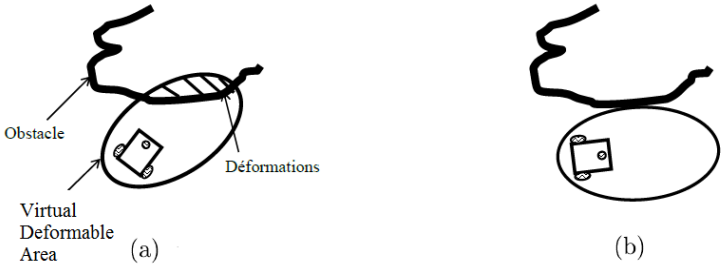

FIGURE 4.4: Obstacle avoidance using Virtual Deformable Area method [191]

sum values which are less than a determined margin present a tolerated direction to the robot. This method was improved and called VFH+ [167] taking into account the robot dimensions.

The *Virtual Deformable Area* (VDA) is also very efficient and is adaptable to any obstacle shape. It consists on assuming that the robot is encountered by a deformable area protecting it using proximity sensors (cf. 4.4). In the case of use of mobile robot, this area is customizable in function of its velocity and mostly in function of its sensors data. The aim is then to control the robot and to minimize these deformations which means to avoid the obstacle. This method uses a distributed control of the multi-robot system ensuring a secure navigation [63]. It has also drawbacks related to the local minima corresponding to the symmetry of the virtual zone [191].

There are other approaches based on constraints optimization. One can mention Curvature Velocity Method (CVM) [137, 154], Lane Curvature Method [100], Dynamic

Window [57, 127],... The general principle of these methods is to select a cople of linear and angular velocities (V, ω) which satisfies the different constraints considering obstacle avoidance. Such couple produces a trajectory for which all the constraints satisfaction are evaluated. The relevant choice is selected by comparing all the evaluations for all possible trajectories.

4.4.2 Navigation in formation

Formation control is more and more considered in recent literature [21, 24, 35, 130, 140, 145, 170, 184] and is classified into three main approaches: the behavior-based approach, the leader-follower approach and the virtual structure approach. In the **behavior-based** approach [17, 24, 173] a so called behavior or motion primitives for each entity is designed (e.g. obstacle avoidance, formation keeping, target seeking, trajectory tracking). Then a more complex motion patterns can be generated by using a weighted sum of the relative importance of these behaviors and the interaction of several robots. Although, the main drawback of this approach is the complexity of the dynamics of the group and as a consequence the desired formation configuration cannot be guaranteed. **Leader-follower** approach [35, 62, 115, 130, 140, 142] is a strategy in which a robot will be the leader while others act as followers. The main advantage of using this approach is the reduction of the strategy to a tracking problem where stability of the tracking error is shown through standard control theoretic techniques: the leader will aim to track a predefined trajectories and the followers track its transformed coordinates with some prescribed offset. A disadvantage of this approach is that there is no feedback from followers to the leader so that if a follower is perturbed then the formation cannot be maintained which involve a lack of robustness to this strategy. The final approach is **Virtual-structure** (VS) [122, 145, 170] in which the entire formation is considered as a rigid body and the notion of hierarchy do not exist. The control law for each entity is derived by defining the VS dynamic and then translated to the motion of the VS into the desired motion of each vehicle. The main advantages of this approach are its simplicity to prescribe the coordinate behavior of the group and the maintain of the formation during maneuvers. However, the possible application will be limited if we aim to maintain the same VS especially when the formation shape needs to be frequently reconfigured.

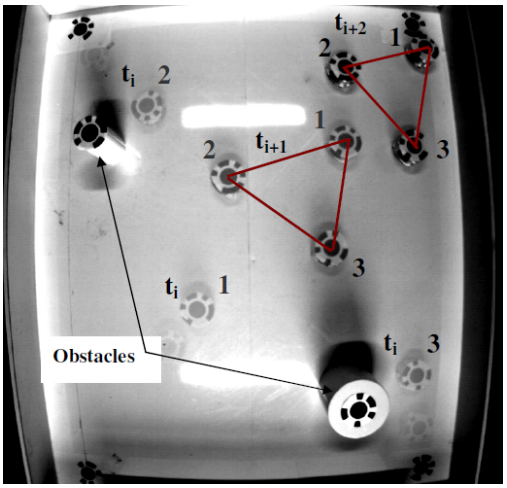

FIGURE 4.5: Triangular Virtual structure navigation using Khepera mobile robots [170]

In [140] authors presented a control law for formation control for the flocking problem. A kinematic model for a car like system was developed and a modelling for attraction to a target was achieved considering the obstacles avoidance problem. The proposed control law was developed based on a defined Lyapunov function. It was validated by simulation results. In [145, 169, 170] the different approaches toward cooperative control of mobile robots were introduced and the aim was to develop and design a virtual structure controller using the so called mutual coupling terms between robots by introducing coupling parameters relating the robots in the control law function.

In [24] a work combining behaviour based approach and virtual structure method to build a distributed control architecture is proposed. Obstacle avoidance and attraction to a dynamic target were considered (cf. Fig 4.5). Unicycle robot model was used and navigation in formation problem was modelled to make a control law architecture based on Lyapunov function which was validated by simulation and experiments.

In [130] the leader-follower formation control for non-holonomic mobile robot was considered based on bioinspired neurodynamics based approach. In this paper trajectory tracking for a single robot was extended to formation control based on backstrepping technique in which the follower can track in real time the leader by the proposed kinematic controller. In backstepping control it was used the derivative of the reference orientation instead of the reference orientation.This technique ensures the tracking controller stability and simplicity. As a typical biological model, the shunting model was adopted for this work. Autonomous navigation of vehicle in an urban environment was considered in [173]. This paper presents a control law based on a novel definition of

control variables and Lyapunov function based on the distance error, orientation and a new parameter related to angle between robot and target positions. This control law was designed for point stabilization (reach a point with a certain orientation) and trajectory tracking problem (track a time parametrized reference). A modelling for tricycle was presented and the control law was developed based on Lyapunov function definition. This work was validated by simulation and experimentation. [62] presents works for leader follower motion coordination. Trajectory tracking controller was designed to make followers track a virtual vehicle using neural network approximation in combination with backstepping and Lyapunov direct design techniques. In the paper [35] also the leader follower formation problem was studied and a control law was developed in which the control input were forced to satisfy suitable constraints between robots and which must be respected to maintain the desired formation. In [142] authors presented a distributed formation control architecture that accommodates an arbitrary number of group leaders and arbitrary flow among vehicles. Authors in [115] presents the problem of modelling and controlling leader-follower formation control of mobile robots and developed a controller based on feedback linearisation and a sliding mode compensator to stabilize the overall system including the internal dynamics.

In [97] various time varying and time invariant controllers for unicycle mobile robots were presented and implemented on Khepera robots is presented.In [36] the problem of controlling two wheeled mobile robots is considered and a feedback control scheme able to cope with dynamic environments. [122] considered the creation of algorithm for a group of robot coordination. It employs coordination and trajectory following techniques. The developed control law was based on Lyapunov technique and graph theory embedded in the virtual structure. In [135] it was considered the design of point to point control algorithm to drive a robot from any arbitrary position to another position. The control variables are derived using Lyapunov's stability technique. In [88] a new control law using an appropriate Lyapunov function was presented. The model of unicyle robot and the configuration of error were modelled to finally deduce a control law and to prove the stability of the Lyapunov function.

4.5 Proposed control strategy for co-manipulation and transport

4.5.1 Overall control architecture

The proposed overall cooperative manipulation and transport strategy, for any payload shape, by a group of m-bots is presented in Figure 4.6. This figure gives the most important steps to be achieved during this cooperative task. The details of the chosen criteria for cooperative manipulation and transportation are given in sub-section 4.5.4.

Step 1 (cf. Fig. 4.6) presents the first phase of the task which consists in payload detection and estimation of its mass and gravity center position. Step 2 consists in determining the minimum number of m-bots (m_{min}) that could be used to ensure the payload lifting and transport. Step 3 presents the main contribution of this chapter. It is detailed by the flowchart in the right side of Fig. 4.6 and will be precisely discussed in sections 4.5.4. The algorithm details are presented in Appendix B. The authors in [148] treated a similar problem for optimal robots positioning taking into account two criterion: the payload stability and the energy consumption. It was considered that the positioning is optimal when the payload is statically stable and the robots consume the minimum of energy (according to the data received from the robots sensors). In the proposed strategy, the m-bots positioning is optimal when Force Closure Grasping (FCG) and Static Stability Margin (SSM) are ensured. The former criterion is a common concept used mainly for manipulation tasks and was used in our proposal to ensure the stable contact payload/end-effector and the latter is used generally for stability during locomotion and was used here for ensuring a stable wheel/ground contact. Finally, Step 4 corresponds to target reaching phase and multi-robot transport of the payload toward the assigned final pose.

4.5.2 Robot model and control law

Definition

Let $R(\mathcal{O}, \vec{x}, \vec{y}, \vec{z})$ be a fixed frame in the ground where $\vec{z}$ is in the vertical direction. $R_m(G_m, \vec{x_m}, \vec{y}_m, \vec{z}_m)$ a mobile frame associated to the robot.

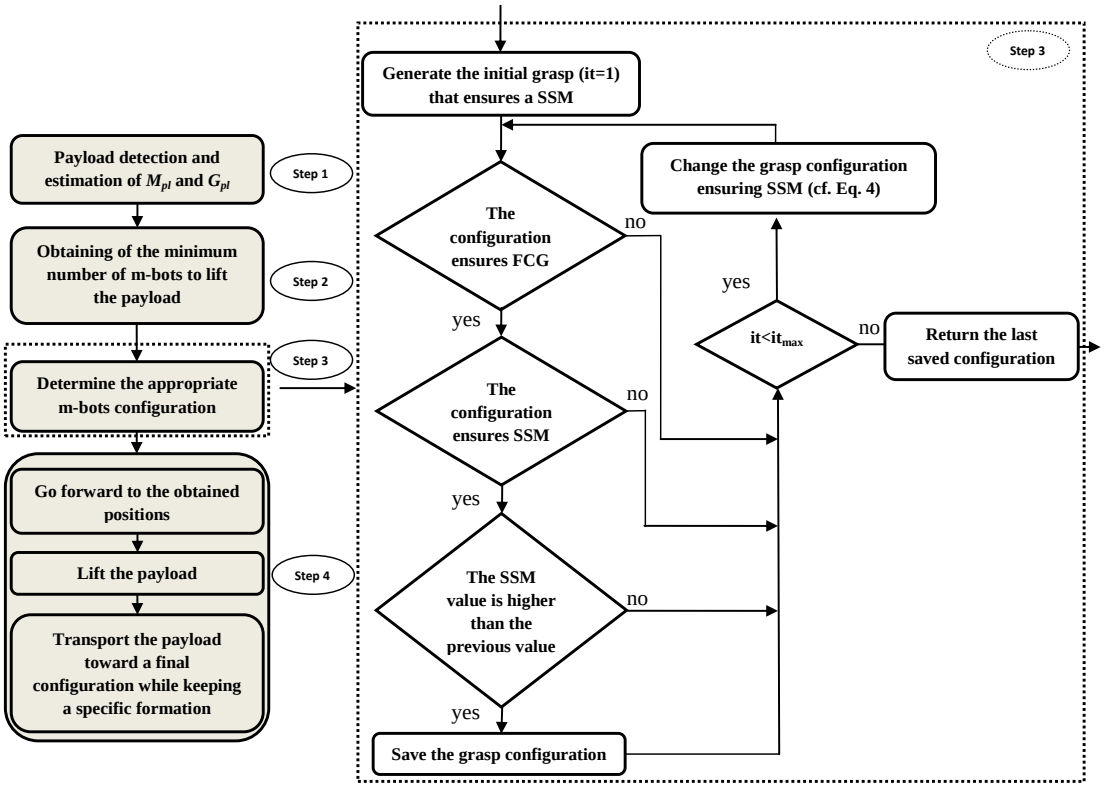

FIGURE 4.6: Flowchart given the sequenced steps for the co-manipulation and transportation of any payload shape

We call robot posture the vector

$$X_m = \begin{pmatrix} x \\ y \\ \theta \end{pmatrix}$$

where x and y are respectively the m-bot center of mass denoted G_m coordinates in the reference frame R and θ is the angle $(\widehat{\vec{x}, \vec{x}_m})$ (cf. Fig. 4.7)

Rolling without slipping

The wheel/ground contact has an important impact in the robot movement properties. We suppose that the mobile robots are rolling without slipping which means that the relative velocity of the wheel with respect to the ground is zero. Theoretically, to check this condition we have to make two assumptions:

- wheel/ground contact is punctual;

- wheels are non-deformable with a radius equal to r.

Practically wheel/ground contact is a surface which allow some slipping. In our modelling we keep the previous assumptions.

Unicycle robot modelling

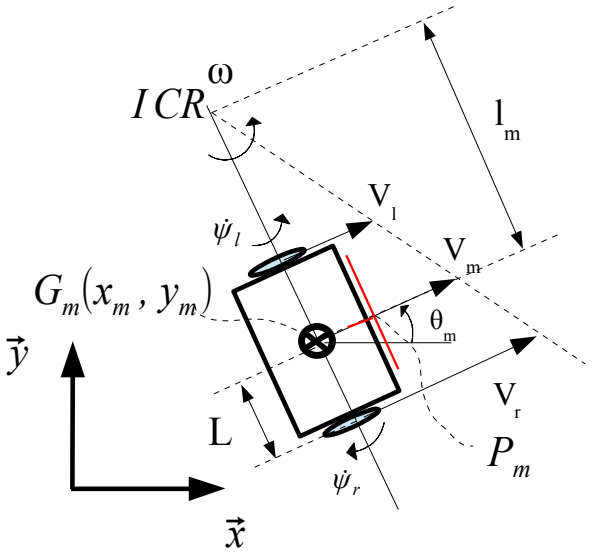

FIGURE 4.7: Unicycle model

In our study for a first part we consider a unicycle mobile robot as it is presented in Fig. 4.7. The state vector q=col(x, y, θ) denotes the position of the robot center of mass (x, y) and its orientation θ with respect to the horizontal axis. The control input are the forward velocity V and the angular velocity ω.

Let's now consider n non-holonomic mobile robots with identical kinematics. Let J $= 1, 2, ..., m_{min}$ denote the set of indices of robots in the formation. Let the state vector q_m=col(p_m, r_m) where p_m=col(x_m, y_m) denotes the Cartesien position of a representative point of the robot i and r_m is the remaining part of the state vector which is in our case for a unicycle robot $r_m = \theta_m$. For each unicycle robot the associated kinematic model is

$$\begin{aligned} \dot{x_m} &= V_m \cos\theta_m \\ \dot{y_m} &= V_m \sin\theta_m \\ \dot{\theta_m} &= \omega_m \end{aligned} \tag{4.1}$$

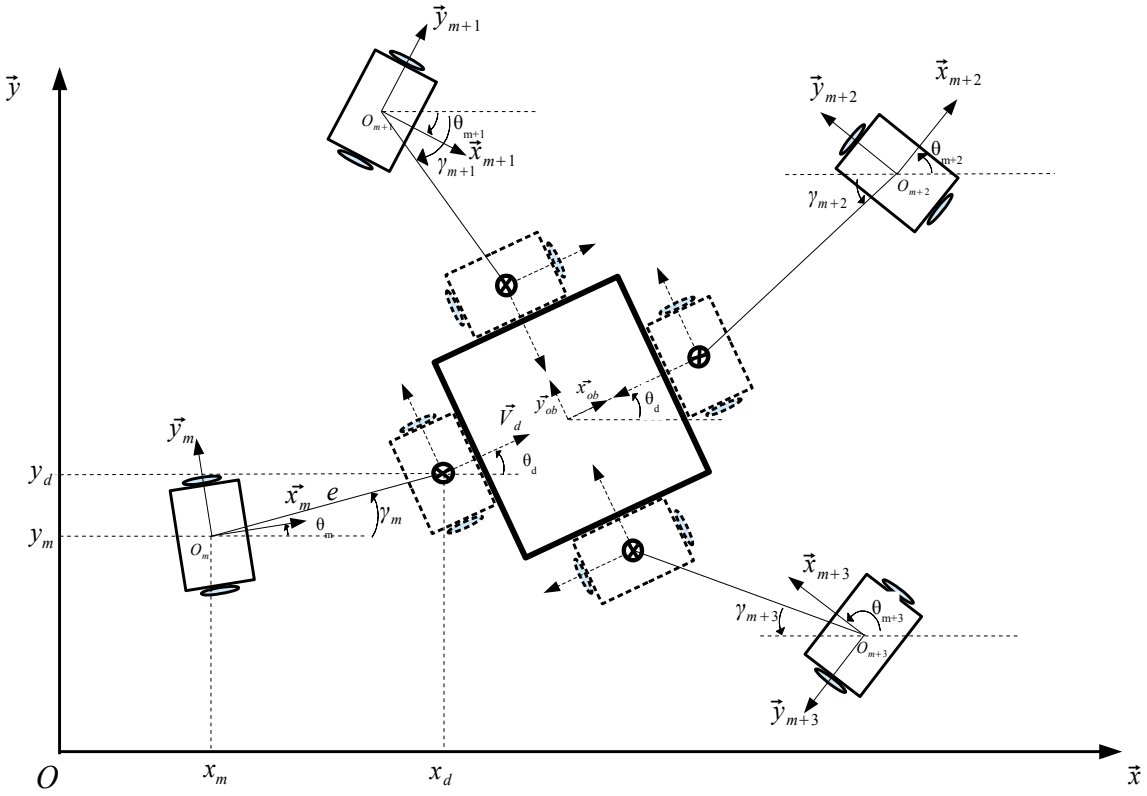

FIGURE 4.8: Scenario of target reaching for a group of m-bots in order to manipulate and lift a payload

Fig. 4.8 presents the scenario of our focus, a group of four robots is supposed to transport a box (presented by a bold black curve) from an initial position to a desired position. First, each robot has to be positioned in a desired position next to the object which we denote by the couple of coordinates (x_d, y_d) for robot m as example.

Fig. 4.9 allows to define the position errors according to the desired position relative to the object. We define the errors (e_x, e_y, e_θ) as

$$\begin{aligned} e_{x_m} &= x_d - x_m = e\cos\gamma_m \\ e_{y_m} &= y_d - y_m = e\sin\gamma_m \\ e_\theta &= \theta_d - \theta_m \end{aligned} \tag{4.2}$$

We denote e the position error defined as

$$e = \sqrt{e_{x_m}^2 + e_{y_m}^2} \tag{4.3}$$

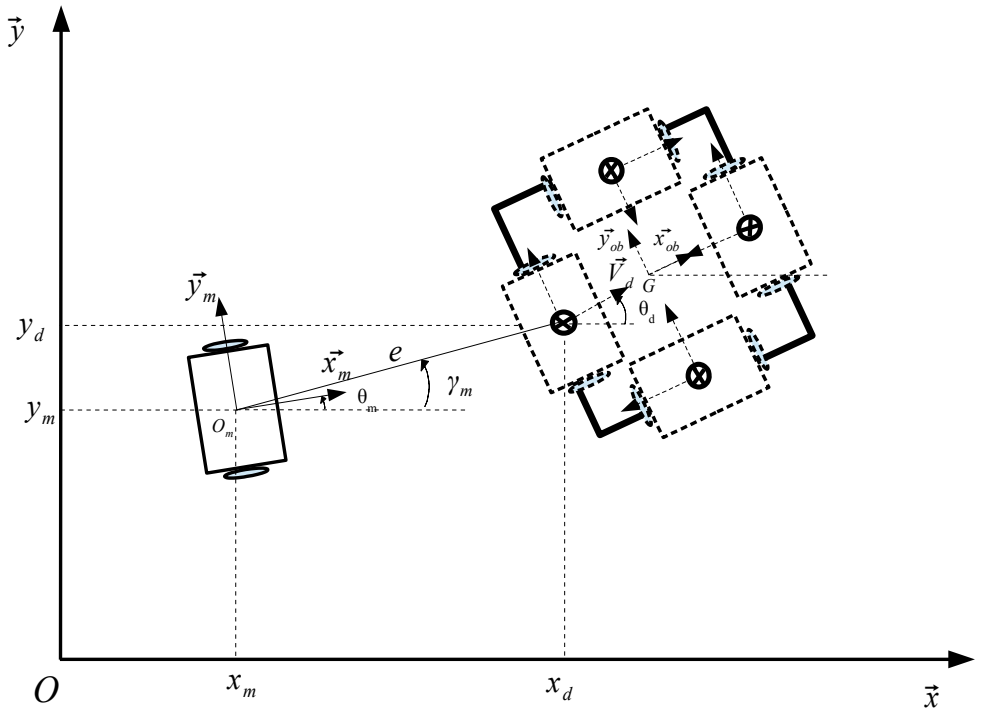

FIGURE 4.9: Attraction to a desired position

By differentiating e we obtain

$$\dot{e} = V_d.\cos(\gamma_m - \theta_d) - V_d.\cos(\gamma_m - \theta_m) \tag{4.4}$$

V_d and θ_d are respectively the m-bot desired speed and orientation in the targeted position. γ_i denotes the current robot angle according to its desired target.

$$\gamma_m = \arctan \frac{e_{y_m}}{e_{x_m}} \tag{4.5}$$

Its derivative is

$$\dot{\gamma_m} = \frac{(\frac{\dot{e_{y_m}}}{e_{x_m}})}{1 + \frac{e_{y_m}}{e_{x_m}}^2} \tag{4.6}$$

Using the previous equations, we obtain

$$\begin{aligned} \dot{e_{x_m}} &= \dot{x_d} - \dot{x_m} = V_d \cos\theta_d - V_m \cos\theta_m \\ \dot{e_{y_m}} &= \dot{y_d} - \dot{y_m} = V_d \sin\theta_d - V_m \sin\theta_m \\ \dot{e_{\theta_m}} &= \dot{\theta_d} - \dot{\theta_m} \end{aligned} \tag{4.7}$$

and

$$\dot{\gamma_m} = \frac{V_d . \sin(\theta_d - \gamma_m)}{e} - \frac{V_m . \sin(\theta_m - \gamma_m)}{e} \tag{4.8}$$

It is considered to keep γ_m constant, *i.e* | $\dot{\gamma_m}$=0

$$\frac{V_d . \sin(\theta_d - \gamma_m)}{e} - \frac{V_m . \sin(\theta_m - \gamma_m)}{e} = 0 \tag{4.9}$$

This allows to determine the angle [25] that the robot must reach to satisfy equation 4.9

$$\theta = \arcsin(\frac{V_d}{V_m} \sin(\theta_d - \gamma_m)) + \gamma_m \tag{4.10}$$

4.5.3 Formation control for object transport

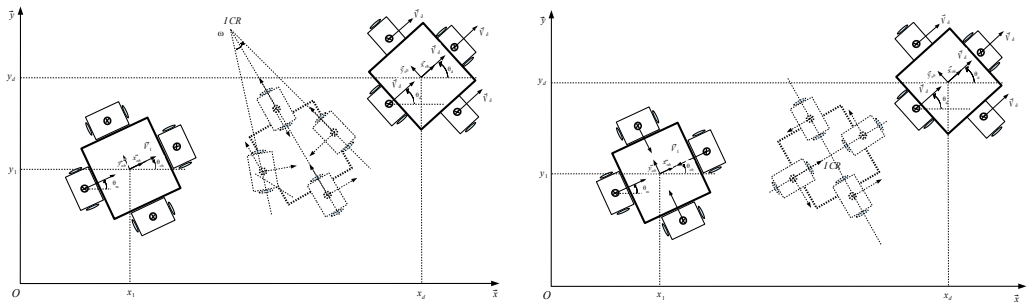

(a) $ICR \neq G_{pl}$ (b) $ICR = G_{pl}$

FIGURE 4.10: Formation object transport

In this section we study the formation control to transport an object using a set of robots. According to the previous section, the group of robots engaged to transport the object were positioned around it and they are equipped with the lifting mechanism developed in the previous chapter. They can lift the object and put it on their bodies. Now the robots have as main task to transport the object from its initial position to

the desired position with a desired orientation as it is shown in Fig. 4.10(a) and Fig. 4.10(b). To ensure the object transport the robots have to keep he formation during the transport and they have to avoid singularities.

If the robots evolve in the same direction following a linear trajectory then the different entities should have the same forward velocities to avoid object slipping and fell down. For another global motion in which the system has to make a rotation to change the object orientation then the robot should ensure the same angular velocities ω. By defining the Instantaneous Center of Rotation ICR (cf. 4.10) position by a couple of coordinates (x_{ICR}, y_{ICR}), the robots evolution is divided into a couple of motions: the first one is a static motion in which the robots have to turn around themselves until the ICR become aligned with the unicycle axis and the second motion is the robot evolving by applying the used control law. It is important to note that the robots motions are synchronised thanks to the applied control law which allows to guarantee the overall system stability. Let l_i be the distance separating the robot i center from the common ICR (cf. 4.7).

$$l_i = \sqrt{(x_{I_{cc}} - x_i)^2 + (y_{I_{cc}} - y_i)^2} \tag{4.11}$$

We know that for a unicycle we have

$$\begin{aligned} l_i &= L\frac{\dot{\psi}_{ri} + \dot{\psi}_{li}}{\dot{\psi}_{ri} - \dot{\psi}_{li}} \\ \omega &= r\frac{\dot{\psi}_{ri} + \dot{\psi}_{li}}{2L} \end{aligned} \tag{4.12}$$

r is the robot wheel radius and L is the spacing.
For each robot we can determine, from equation 4.12, the imposed velocities on wheels to avoid system singularity.

$$\begin{aligned} \dot{\psi}_{ri} &= -Lr\omega(\frac{l_i}{L} + 1) \\ \dot{\psi}_{li} &= -Lr\omega(\frac{l_i}{L} - 1) \end{aligned} \tag{4.13}$$

At any moment of the formation motion we can determine the robots positions with respect to the object position and orientation. During the transportation phase, the robots have to track a dynamic target defined with respect to the payload center of mass.

Used control law

Considering a unicycle mobile robot, the state vector $X_m = (x_m, y_m, \theta_m)^T$ denotes the position of the m^{th} robot center of mass $G_m(x_m, y_m)$ and its orientation θ_m with respect to $\vec{x}$ axis of the global frame. The m-bot control inputs are the forward velocity V and the angular velocity ω.

Let e be the error between the m-bot current pose and the desired pose defined by $X_{dm} = (x_{dm}, y_{dm}, \theta_{dm})^T$: $e = X_{dm} - X_m$.

The used control law [25] is given by (4.14):

$$\begin{aligned} V_m &= V_{max} - (V_{max} - V_d)e^{-(d_m^2/\sigma^2)} \\ \omega_m &= \omega_{Sm} + k\theta_m \end{aligned} \tag{4.14}$$

- V_m and ω_m are the linear and angular velocities of the m-bot,
- V_{max} is the maximum linear speed of the m-bot,
- V_d is the desired velocity of the p-bot and it is considered as constant,
- $d_m = \sqrt{e_x^2 + e_y^2}$ is the current distance between the m^{th} robot and its desired target,
- ω_{Sm} is the angular velocity of set point angle θ_{Sm} applied to the robot in order to reach the desired goal: $\omega_{Sm} = \dot{\theta}_{Sm}$,
- σ, k are positive constants (control law gains).

4.5.4 Positions determination according to multi-criteria task constraints

Since the features of the payload are known (step 1 in Fig. 4.6) the minimum number of m-bots (m_{min}) is obtained while using the equations of section 3.4 (step 2 in Fig. 4.6),

the group of m-bots must be well positioned around the payload (step 3) to permit to safely lift it and to maintain the stability of the payload in the top of the p-bot during the transportation phase (step 4). During this manipulation phase (sub-step 2 in step 4), FCG (cf. sub-section 4.5.4.1) as well as SSM (cf. sub-section 4.5.4.2) must be thus ensured to lift and transport safely the object (cf. details given for Step 3 in Figure 4.6).

4.5.4.1 Force Closure Grasping (FCG)

A grasp is considered stable when a small disturbance on the position of the manipulated object or contact force, generates a restoring wrench that brings the system back to a stable configuration. Force closure grasping problem is extensively studied for objects manipulation using multi fingered robotic hand [116, 190]. This problem was adapted to mobile robot co-manipulation and transport in C^{3}Bots project to ensure lifting and transport task.

Robotic grasping has thrived since few decades. In the aim of ensuring object stability, which is the goal of any used grasping strategy, several methods and algorithms have been developed using diverse approaches. Some grasping configurations have been considered much more better and efficient than others when considering the system equilibrium by applying minimal forces to compensate every external ones. Avoiding too large forces allows to reduce the power for the manipulator actuation and the deformation of the manipulated object. Nguyen in [123] presents an algorithm for stable grasps construction and he proved the possibility of making stable all 3D force closure grasps. In literature, form closure and force closure conditions may be confused. The former implies stability when the contacts position ensures the object immobility and for the latter when the applied forces ensure object immobility. According to [42, 147], a grasping strategy should ensure stability, task compatibility and adaptability to novel objects.

To ensure a stable grasping, analytical and empirical approaches were developed in the literature. Analytical approaches choose the manipulator configuration and contact positions with kinematical and dynamical formulation whereas empirical approaches use learning to achieve a grasp depending on the task and on the geometry of the object. Diverse analytical methods were developed to find a force closure grasp: In [116] force closure configuration for n contacts is synthesized by fixing *n-1* contacts and searching the nth contact position using linear parametrization of a point on an object facet.

Ding et al. [37] presented an algorithm to form force closure starting by a random configuration for grasp and checking if it is force closure. If it is not the case, the finger contact changes its position using the linear parametrization of a point on the object facet. In [112], an algorithm based on geometrical analysis was developed: the intersection of friction cones and the position of the wrench space center according to the convex hull.

Empirical approaches avoid the complexity of computation by attempting to mimic human strategies for grasping. Datagloves hand were used by researchers for empirical approaches to learn the different joint angles [41, 54], hand preshape [109]. Vision based approach is also used to demonstrate grasping skills. A robot can track an operator hand for several times to collect sufficient data [2, 12, 78].

The co-manipulation problem is restricted to a 2D problem in plane $(O, \vec{x}, \vec{y})$ while robots are acting simultaneously and applying a tightening forces on the payload with a contact points in the same plane (Fig. 4.11).

The aim of this part is to ensure force closure grasping when choosing the m-bots positions which returns to fully constraint the payload motion with m_{min} m-bots. In other words, the static equilibrium must be ensured while positioning the group of mobile robots. The problem of force closure grasping is studied under the following assumptions (cf. Fig. 4.11(c)):

- A contact force lies inside the friction cone centred about the normal direction to the contact surface with half angle α,
- The tangent of α represents the friction coefficient,
- The friction cone of the m^{th} contact is denoted C_{pm}.

A necessary and sufficient condition to have force closure is that the intersection of three friction cones is not empty [112]. This condition was extended to m_{min} m-bots. In [112], the treated problem concerns multi-fingered hand grasping although the problem treated in this project focuses on co-manipulation using a group of modular mobile robots. The proposed algorithm aims to ensure force closure if forces and moments equilibrium satisfy (4.15) and when the payload center of mass is inside the friction cones intersection (4.16). The latter condition allows to reduce the momentum generated

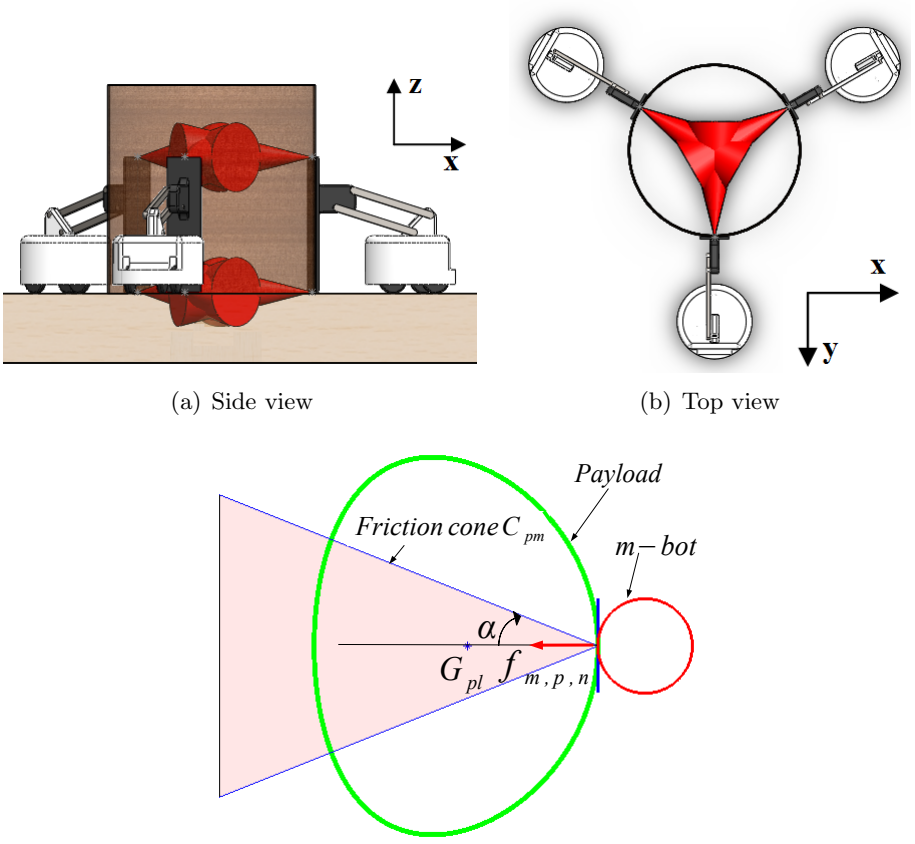

(a) Side view

(b) Top view

(c) m-bot planar contact

FIGURE 4.11: Applied tightening forces on the payload

around the payload center of mass by the m-bots while applying the pushing forces in order to tighten the payload and lift it.

$$\sum_{m=1}^{m_{min}} (P_m \vec{G}_{pl} \wedge \vec{f}_{m,p,n}) = 0; \sum_{m=1}^{m_{min}} \vec{f}_{m,p,n} = 0 \tag{4.15}$$

$$G_{pl} \in Convexhull(\cap C_{pm}) \mid m = 1..m_{min} \tag{4.16}$$

Where C_{pm} denotes the friction cone for the contact force on P_m and $f_{m,p,n}$ is the applied normal on the payload (cf. Fig. 4.11(c)). The condition presented in equation 4.16 offers the ability to apply a normal force in both sides of the payload center of mass as presented in Fig. 4.12(b). In case if it is not satisfied, the system could be in an unstable configuration where robots are applying a normal force that generates a torque around G_{pl} (cf. Fig. 4.12(a)) and then the lifting and manipulation phase risks to be unstable and the task achievement will fail.

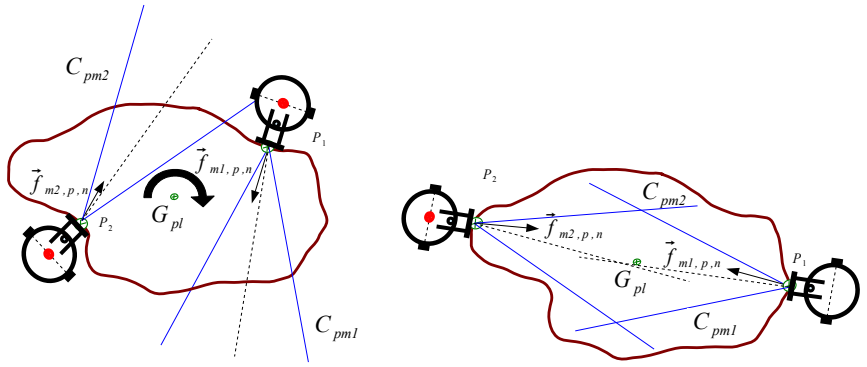

(a) (b)

FIGURE 4.12: M-bots positioning in order to apply a normal force: a) Generated torque around G_{pl}; b) Stable configuration

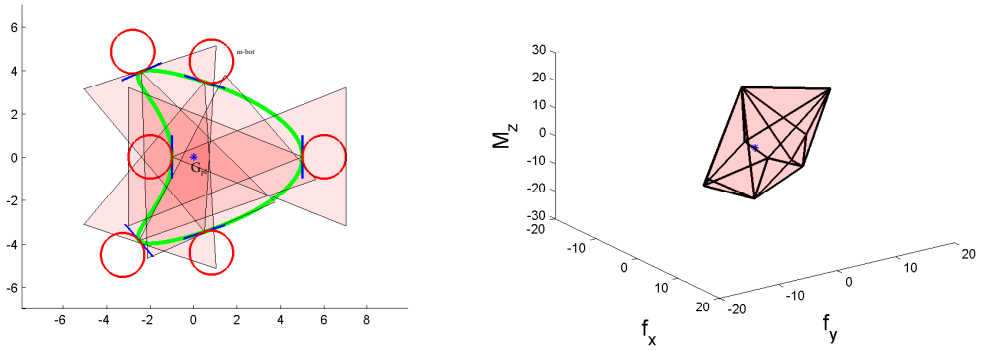

(a) (b)

FIGURE 4.13: M-bots positioning simulation for payloads ensuring a Force Closure Grasping (FCG): a) six m-bots positioned ensuring (4.16); b) corresponding system of wrenches

Fig. 4.13 presents the simulation results for six m-bot positioning w.r.t equation (4.16).

4.5.4.2 Static Stability Margin (SSM)

In this part, Static Stability Margin (SSM) is considered to ensure the payload stability during the transporting phase. Stability margins were extensively studied for walking mobile robots [47, 138, 177]. In the investigated work, to ensure a stable payload transport, the Static Stability Margin (SSM) is a crucial criterion for a successful task achievement. Before describing the proposed algorithm for m-bots positioning ensuring an optimal SSM during object transport using m-bots, let us detail the following assumptions (cf. Fig. 4.14):

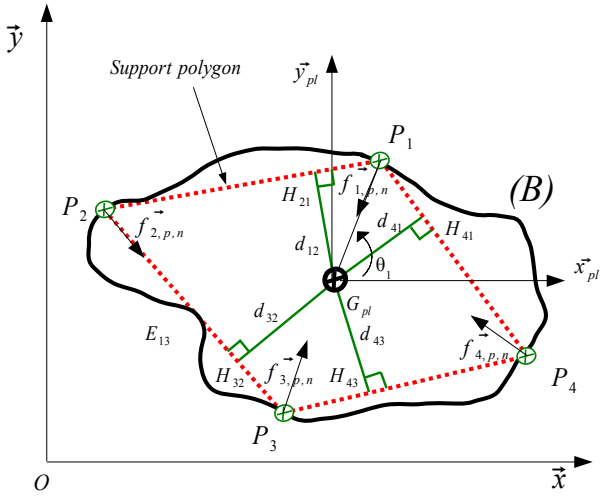

FIGURE 4.14: Support polygon formed by four robots positioned at $P_{m|m=1..4}$

- The payload shape from the top view is a closed curve (B) and parametrized using polar coordinates by $P(\theta)$; $\theta \in [0, 2\pi]$.
- In function of the payload mass M_p, m_{min} is the minimum number of m-bots allowing to lift and transport the object.
- The payload center of mass is denoted G_{pl}.

Let $R(G_{pl}, \vec{x}_{pl}, \vec{y}_{pl}, \vec{z}_{pl})$ be the frame linked to the payload with respect to the reference frame $R(O, \vec{x}, \vec{y}, \vec{z})$ (cf. Fig. 4.14). Cartesian coordinates will be used in the proposed algorithm. As given in section 2, $P(\theta)$ is the parametric description of the payload closed boundary (B). $P_{m|m=1..m_{min}}$ are the m-bots positions, $H_{m,m+1}$ is the projection of the payload center of mass G on the edge linking two consecutive points P_m and P_{m+1} and $d_{m,m+1}$ is the stability margin on the same edge. P_m and $P_{m_{min}+1}$ are confounded and as a consequence $d_{m,m_{min}+1}$ is equal to $d_{m_{min},1}$.

The idea behind the algorithm is to run through (B) and to find the set of points P_m ensuring a maximal SSM while maximizing the objective function (4.17). The constraint imposed by (4.18) must be satisfied for m_{min} m-bots$\geq$3 which gives a necessary condition to keep the center of mass G_{pl} inside the polygon $(P_1..P_m)$

$$f(\theta_m, ..\theta_{m_{min}}) = \text{Min}(d_{m,m+1}) \mid m = 1..m_{min} \tag{4.17}$$

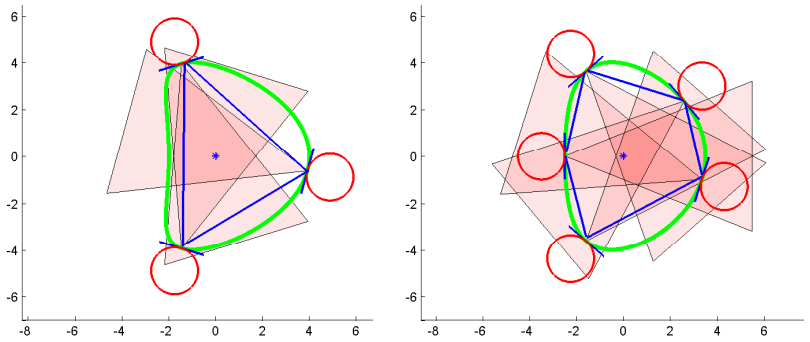

(a) (b)

FIGURE 4.15: M-bots positioning simulation for payloads ensuring a maximum Static Stability Margin (SSM)

$$\theta_{m+1} - \theta_m < \pi \ | m = \{1...m_{min}\} \tag{4.18}$$

In the case where we have only two m-bots to co-manipulate the object, the constraint expressed by (4.18) is not considered and the robots are positioned in opposed positions which means $\theta_{m+1} - \theta_m = \pi$. For each configuration where the minimum number of used m-bots $m_{min} \geq 3$, the algorithm aims at determining the equation of the line $P_m P_{m+1}$ and at computing the shortest distance of $G_{pl}(x_{G_{pl}}, y_{G_{pl}})$ from it.

Then $d_{m,m+1}$ is calculated using equation (4.19) which represents the stability margin with respect to each edge and the static stability margin SSM given by equation (4.17). The coordinates of P_m are expressed in $R(G_{pl}, \vec{x}_{pl}, \vec{y}_{pl}, \vec{z}_{pl})$ (cf. Fig. 4.14).

$$d_{m,m+1} = d(G, (P_m P_{m+1})) = \frac{x_G \frac{y_{P_{m+1}} - y_{P_m}}{x_{P_{m+1}} - x_{P_m}} - y_G + y_{P_m} - x_{P_m} \frac{y_{P_{m+1}} - y_{P_m}}{x_{P_{m+1}} - x_{P_m}}}{\sqrt{(\frac{y_{P_{m+1}} - y_{P_m}}{x_{P_{m+1}} - x_{P_m}})^2 + 1}} \tag{4.19}$$

Fig. 4.15 presents the algorithm result for different payloads shapes and shows a result that respects the constraint of SSM. The corresponding system of wrenches (according to the criterion developed in [112]) allows to validate our proposal (cf. Fig. 4.16).

The proposed algorithm allows to reduce the number of tested configurations for robots positioning w.r.t the condition of equation 4.18. Let assume that the number of total positions denoted N_{tp} according to a chosen *step* is equal to $round(\frac{\pi}{step})$. The Total

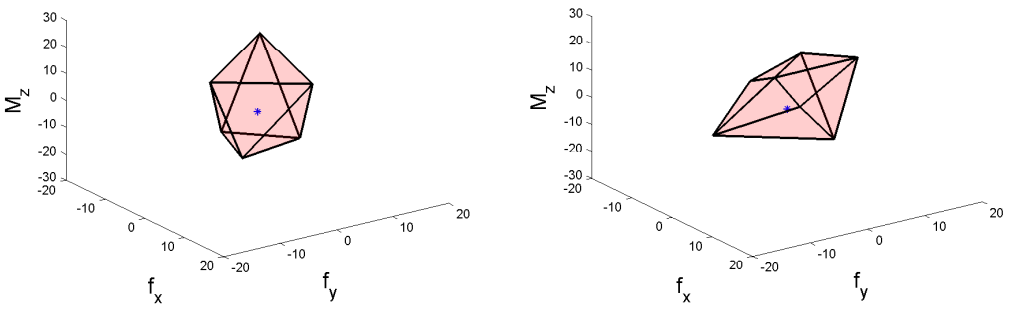

(a) (b)

FIGURE 4.16: Systems of wrenches corresponding to the force-closure grasps shown in Fig. 4.15 respectively, with their convex hull shown as a polyhedron

Possible Configurations TPC is then equal to the following:

$$TPC = \prod_{k=1}^{m_{min}} C^1_{N_{tp}} \tag{4.20}$$

Let's denote N_p the number of positions tested for each m-bot which is equal to $round(\frac{N_{tp}}{m_{min}})$. The Tested Configurations TC is then equal to the following:

$$TC = \prod_{k=1}^{m_{min}} C^1_{N_p} \tag{4.21}$$

For example if $N_{tp} = 180$ and the number of used m-bot is 3, then the tested configurations (TC) is equal to 216.000 instead of 5.832.000 total possible configurations (TPC). This allows to reduce the time of calculation and generates a faster result depending on the chosen step.

4.5.4.3 Restricted Area (RA)

In some cases, the payload could be positioned in a manner that the m-bots could not reach all the positions around it (cf. Fig. 4.17). The proposed algorithm takes into consideration this constraint and allows to find the optimal robots positions that ensures the previous constraints and the task achievement without loss of stability. The RA is presented by a portion of the payload curve and is not considered while searching the optimal positions. This portion is denoted by $\overline{B}$.

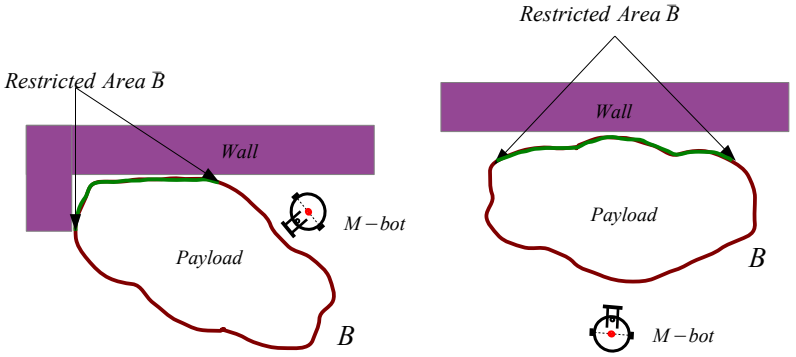

FIGURE 4.17: Payload positioned against a wall and presents restricted and unreachable zones to the m-bots

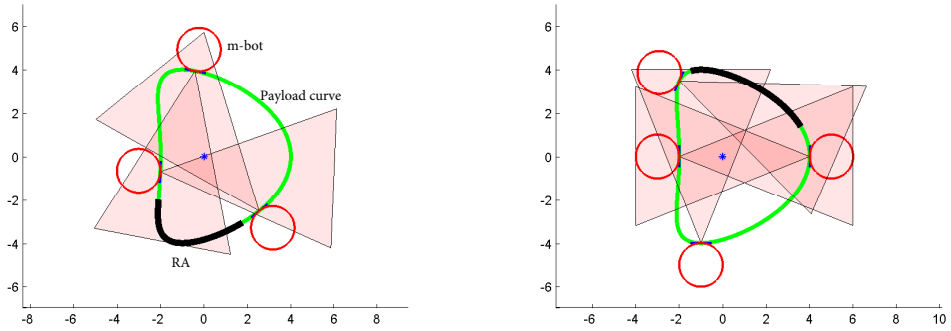

FIGURE 4.18: M-bots positioning simulation for payloads with restricted areas

Fig. 4.18 presents the algorithm result for a payload with a restricted area presented in bold black curve. The corresponding system of wrenches allows to validate our proposal (cf. Fig. 4.19).

4.5.5 Limit-Cycle method for target reaching and navigation in formation

After determining the desired positions of each m-bot, the first phase of the task consists in target reaching for the group of m-bots. Each m-bot is informed about its desired position to reach and must find the optimal trajectory taking into consideration the existing obstacles in the environment.

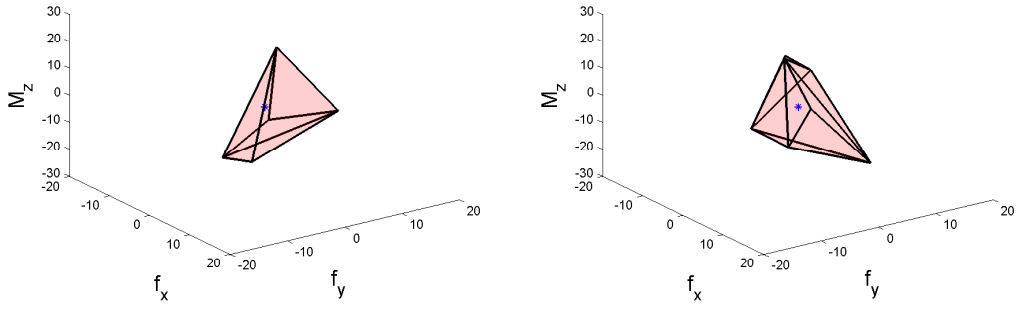

(a) (b)

FIGURE 4.19: Systems of wrenches corresponding to the force-closure grasps shown in Fig. 4.18 respectively, with their convex hull shown as a polyhedron

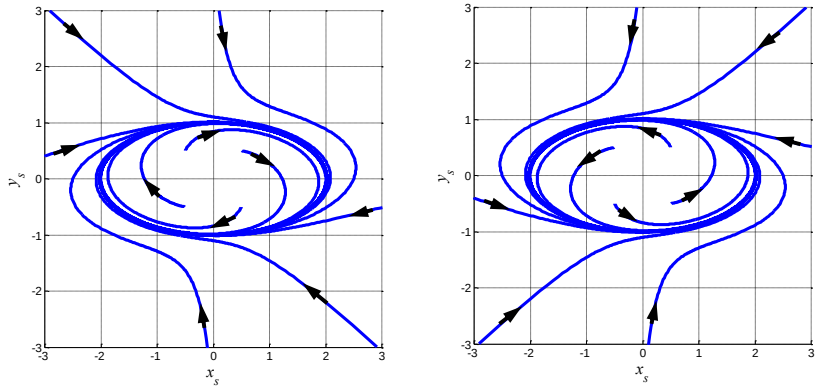

(a) (b)

FIGURE 4.20: Limit-Cycle possible directions [6, 7]: a) clockwise direction; b) counter clockwise direction

The control law used to simulate the obstacle avoidance for desired targets reaching in the proposed work uses the Limit Cycle method [6, 98, 172] which is one of the trajectory methods defined by differential equations [159].

The differential equations of the elliptic limit-cycles are:

$$\begin{aligned} \dot{x}_s = &\quad m(By_s + 0.5Cx_s) + x_s(1 - Ax_s^2 - By_s^2 - Cx_sy_s) \\ \dot{y}_s = &\quad -m(Ax_s + 0.5Cy_s) + y_s(1 - Ax_s^2 - By_s^2 - Cx_sy_s) \end{aligned} \tag{4.22}$$

with $m = \pm 1$ according to the avoidance direction (clockwise or counter-clockwise (cf. Fig. 4.20). (x_s, y_s) corresponds to the position of the m-bot according to the center of

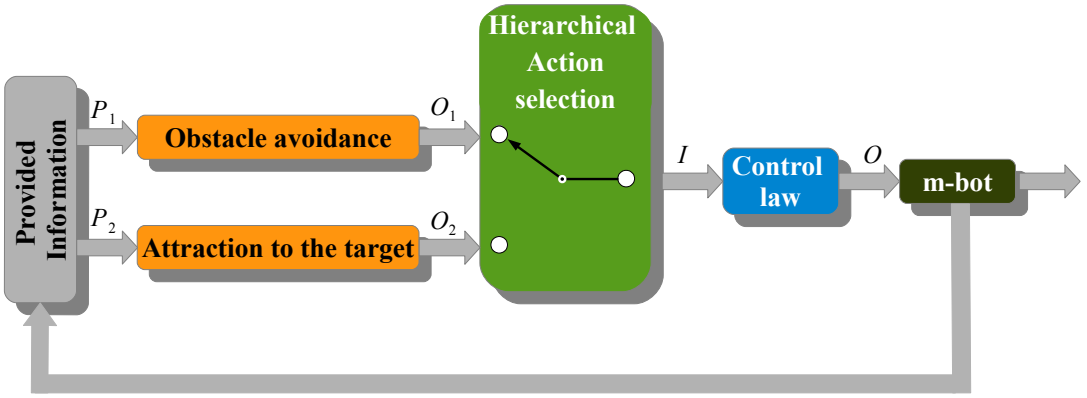

FIGURE 4.21: Control architecture for mobile robot navigation during the target reaching phase (cf. the first phase of step 4 in Fig. 4.6)

the ellipse. The variables A, B and C are given by:

$$A = (\sin(\Omega)/b_{lc})^2 + (\cos(\Omega)/a_{lc})^2 \tag{4.23}$$

$$B = (\cos(\Omega)/b_{lc})^2 + (\sin(\Omega)/a_{lc})^2 \tag{4.24}$$

$$C = (1/a_{lc}^2 - 1/b_{lc}^2)\sin(2\Omega) \tag{4.25}$$

where a_{lc} and b_{lc} characterize respectively the major and minor elliptic semi-axes and c gives the ellipse orientation when it is not equal to 0.

The set point angle that the robot must follow to avoid the obstacle is given by:

$$\theta_{S0a} = \arctan(\frac{\dot{y}_s}{\dot{x}_s}) \tag{4.26}$$

In addition to obstacle avoidance, it defines a security distance to keep between the robot and the obstacle which ensures a non collision. In addition to that and knowing the goal position, the robot can choose the optimal side of obstacle avoidance allowing a faster target reaching. The control architecture for the m-bot navigation is presented in Fig. 4.21. This architecture, with specific elementary controller blocks (attraction to the target, obstacle avoidance), aims to manage the interactions among elementary controllers (target reaching and obstacle avoidance) while guaranteeing the stability of the overall control to obtain safe and smooth navigation.

The robots must avoid the collision with the payload if its target is not apparent to it. The limit-cycle method was adopted to avoid the m-bots collision with the payload as presented in Fig. 4.22. The payload is assumed to be surrounded by an ellipse and

an obstacle, if exists, also is surrounded by an ellipse. These ellipses are presented in Cartesian form with an orientation Ω and semi-axes a_{sur} and b_{sur} (cf. Fig. 4.22(a)). An ellipse of influence is then defined having the same center and orientation of the ellipses surrounding the payload or the obstacle with a semi axes a_{inf} and b_{inf} respecting the following equation:

$$\begin{aligned} a_{inf} &= a_{sur} + R + Marg \\ b_{inf} &= b_{sur} + R + Marg \end{aligned} \tag{4.27}$$

Where R is the robot radius and $Marg$ is a security margin to avoid the collision between m-bots and the payload or obstacle.

The m-bot will proceed by the payload avoidance using the limit-cycle method until a position error ϵ, between the robot real position and the projection of the desired position on the ellipse of influence, is satisfied. This error, if it is satisfied, allows to switch the robot controller from obstacle avoidance to target attraction (the intermediate projected position is presented by red points in Fig. 4.22(b)). In case where the desired position is apparent to the m-bot, then the robot will be attracted first to the intermediate position and then goes to its target. The intermediate position are defined in function of the final desired orientation of the robot. This condition allows the m-bots to reach the final position with the required orientation.

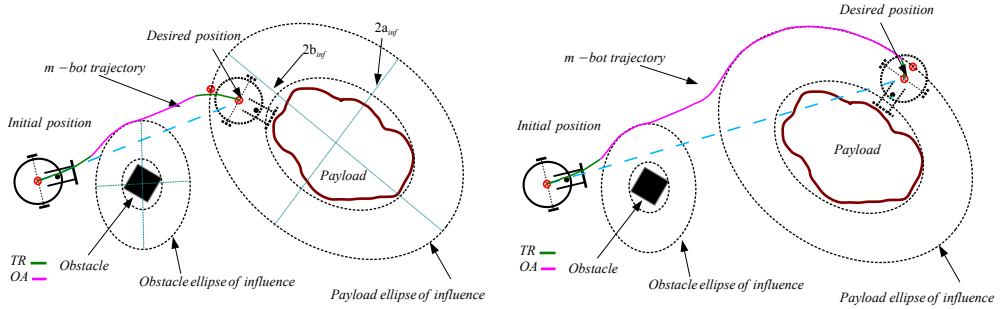

FIGURE 4.22: Target Reaching strategy with obstacle avoidance: a) apparent position reaching; b) hidden position reaching

In order to ensure a smooth and secure m-bot evolving during the target reaching phase, a suitable choice of ϵ is required. As presented in Fig. 4.22(a), the payload is surrounded by an ellipse of influence that will be followed by the m-bot during the attraction to the target if the desired position is not apparent. ϵ is defined as follow: If ϵ is equal to zero,

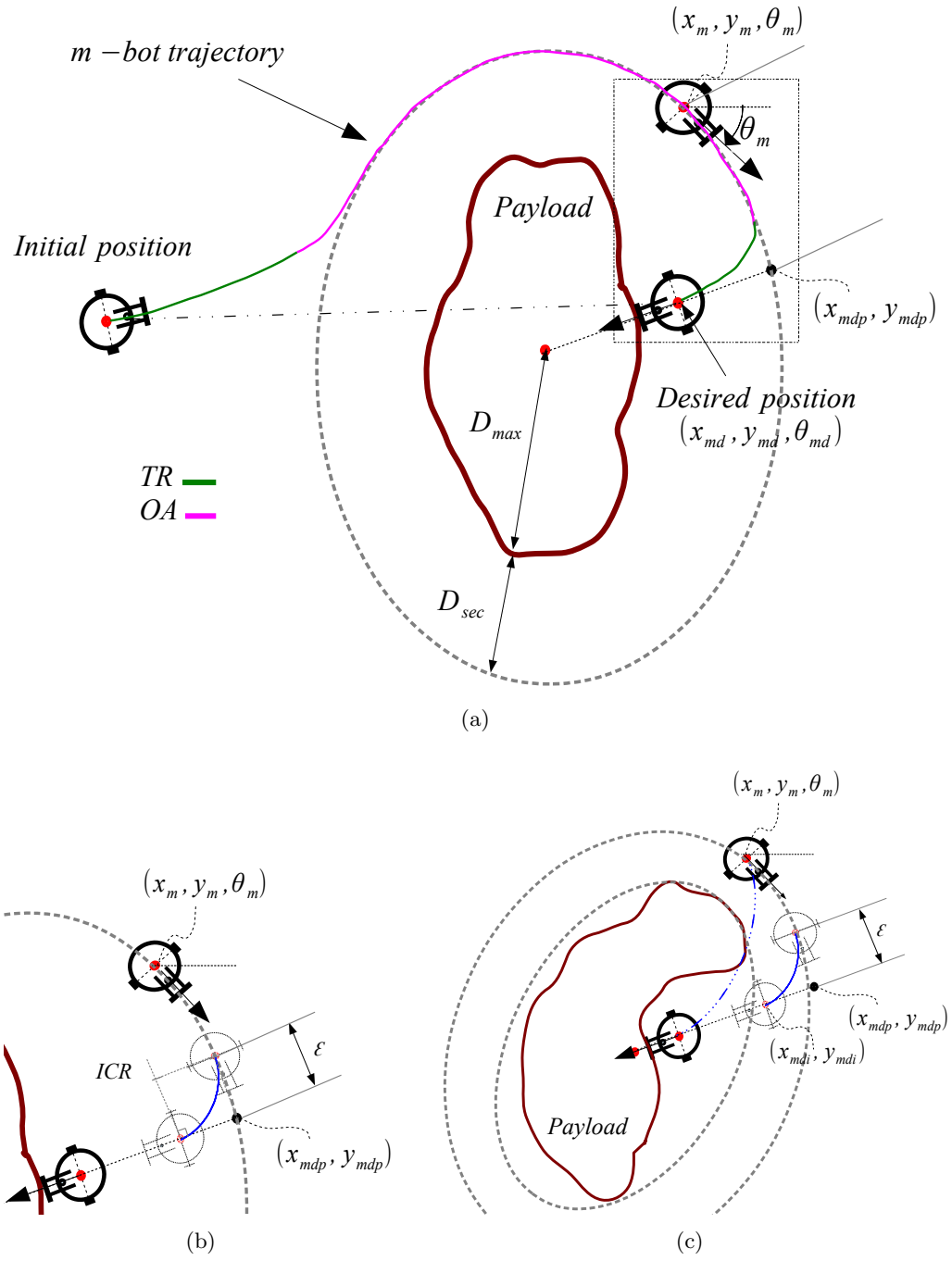

FIGURE 4.23: General principle of smooth target Reaching

then the robot would reach the position of the projection of desired target and then turn around itself to reach the final goal. This allows to have a discrete motion of the robot. In order to avoid this, ϵ is chosen with a strictly positive value that does not exceed the robot platform radius. The reasons why this value is limited to R is that the robot is not so far from the position of controller switch and to avoid the collision between the robot and the payload during the final desired target reaching (cf. Fig. 4.23(b)).

Navigation in Formation: After positioning the m-bots, they must keep their desired position (x_{dm}, y_{dm}) with respect to the payload center of mass G_{pl} and must respect the following conditions during the task achievement:

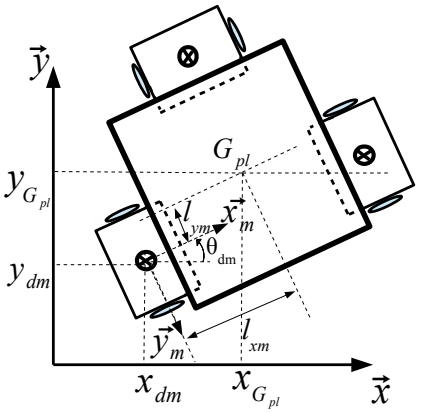

FIGURE 4.24: Robot position relative to the object

$$\begin{aligned} x_{dm} &= x_{G_{pl}} + l_{xm}\cos\theta_{dm} - l_{ym}\sin\theta_{dm} \\ y_{dm} &= y_{G_{pl}} + l_{xm}\sin\theta_{dm} + l_{ym}\cos\theta_{dm} \end{aligned} \tag{4.28}$$

where l_{xm} and l_{ym} (cf. Fig. 4.10(a), Fig. 4.10(b) and Fig. 4.24) are the relative distances $G_m G_{pl}$ according the axis $\vec{x}_m$ and $\vec{y}_m$ respectively. These two distances define rigid links maintaining the robot position with respect to G_{pl}. It is to be noted that the mobile platform has a steering mobility around its vertical axis z (cf. Fig. 3.5(a)). This mobility allows to each robot to rotate around itself ($V_m = 0$ and ω_m=Constant (cf. equation (9)) while maintaining the payload static on its top. According to this effector new degree of freedom, the group of mobile robots could ensure easily the payload approach, lifting and transportation.

In our research problem we aim to control a group of robots for a co-manipulation and transport tasks. Navigation in formation is considered then and it mainly consists simultaneously on:

- reach the target;
- avoid static obstacles;
- avoid other robots;

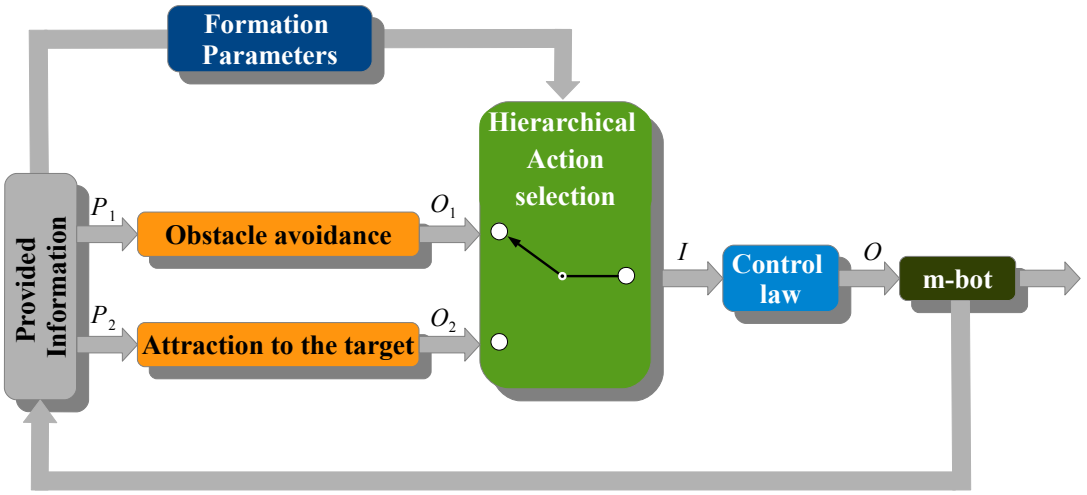

FIGURE 4.25: Control architecture for p-bot navigation (cf. the third phase of step 4 in Fig. 4.6)

- maintain the formation.

The limit cycle method that was used for target reaching problem was extended to the case of a group of m-bots transporting a payload. The dimensions of the ellipse of influence in case of obstacle avoidance (a_{sur} and b_{sur}) are increased according to the formation shape. The advantage is to maintain the shape of the whole formation and avoid the payload slipping. The principle is illustrated in Fig. 4.26.The control architecture for the p-bot navigation is presented in Fig. 4.21. The formation parameters block gives the information of the virtual target w.r.t the local frame (m-bot frame) that must to be kept by the robot

4.6 Conclusion

The main challenge addressed in this chapter is to estimate the optimal robots' configuration around the object to achieve the co-manipulation and the co-transportation while maximizing the stability of the achieved task [73]. The system stability is ensured using the Force Closure Grasping (FCG) criterion which ensures the payload stability during the co-manipulation phase and the Static Stability Margin (SSM) criterion which allow payload stability during the co-transportation phase. Several elementary navigation functions have been used to deal with this cooperative task. Among them, the Obstacle avoidance controller, based on limit-cycles, which is used for two aspects:

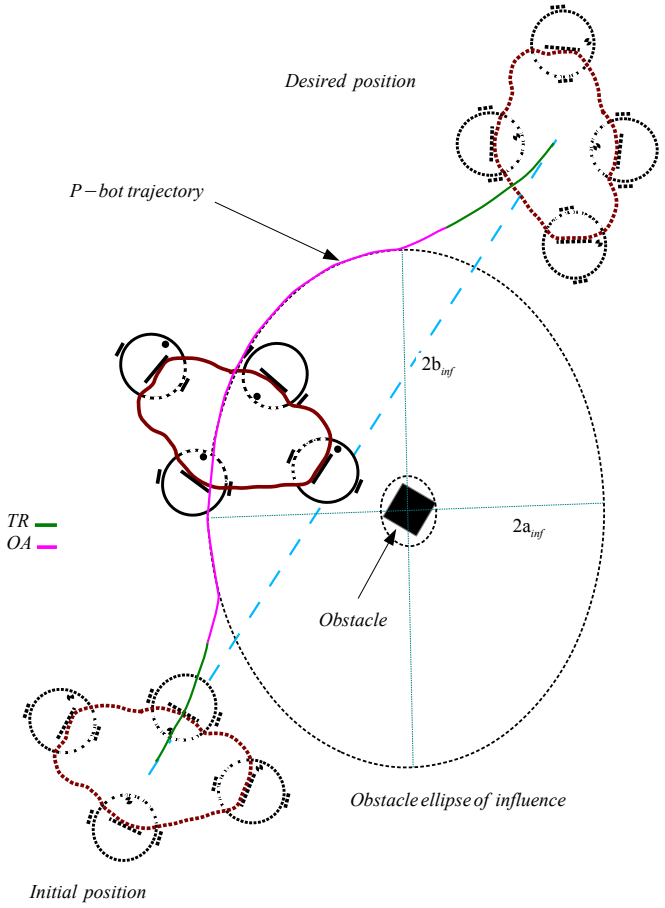

FIGURE 4.26: P-bot obstacle avoidance using limit-cycle method

firstly when each elementary robot aims to reach its position around the payload (the robot can need to avoid other robots or any other obstacles to reach its assigned position); secondly when the overall poly-robot (the robots with the transported payload) is in the navigation phase and has to avoid any obstructing obstacle. This poly-robot navigation arises also interesting issues related to multi-robot navigation in formation. The poly-robot is considered as an overall robot with several constraints induced by the robots' wheels composing the poly-robot [71, 72].

Chapter 5

Simulations and Experimental Results

The focus is made in this chapter on validating the theoretical developments presented in the previous chapters using a multi-body dynamic system and simulation results.

5.1 Mechanical simulations and experimental results

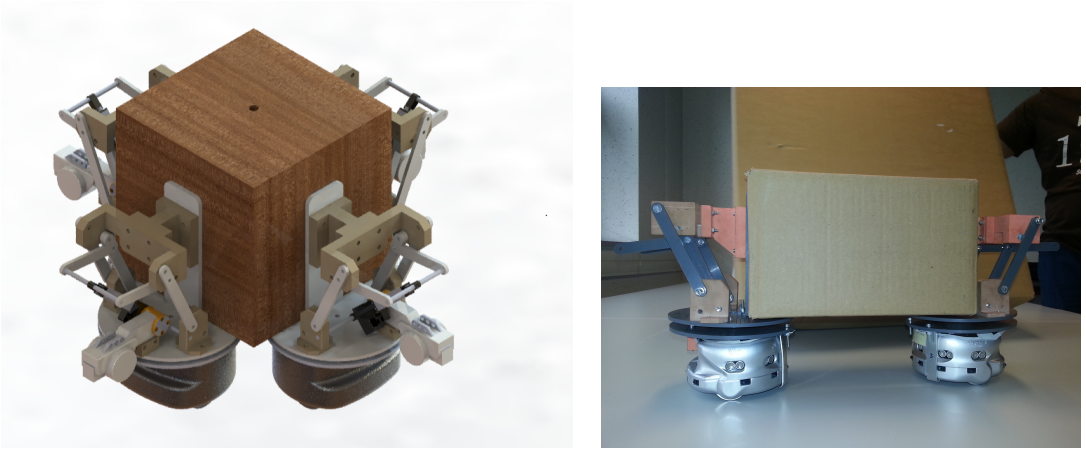

(a) 3D CAD (b) Manufactured prototypes

FIGURE 5.1: Proposed design of the p-bot and manufactured system

In order to validate our proposal for the co-manipulation and lifting strategy using a multiple robot system for payloads transportation, a multi-body dynamic simulation software was used in addition to an experimental test-bench. Simulation and experimental results are presented in following subsections. Fig. 5.1 presents the designed 3D CAD of the proposed system and two real prototypes for future experiments.

5.1.1 Multi-body dynamic system results

The simulation results were based on real physical parameters which were defined as follows:

- static friction coefficient end-effector/payload (rubber/steel), $\mu_p = 0.65$;
- static friction coefficient wheel/ground (rubber/asphalt), $\mu_g = 0.8$;
- m-bot mass, $M = 1.4kg$. A constant torque was imposed on the m-bot wheels in order to impose the mobile platform propulsion and ensure the contact between the robots end effectors and the payload. The different cases previously studied in chapter 3 are illustrated and validated in the next subsections.

5.1.1.1 Simulations for payload putting on m-bots bodies

Fig. 5.2 presents the simulation results for different configurations of payload landing position in order to validate the theoretical analysis of section 3.2.2. It has been demonstrated that if the payload is put on robot turntable in manner that its landing position P_2 is inside the support pattern of the m-bot, then the m-bot remains stable. Consequently, the p-bot in this case is able to successfully achieve the transportation task without loss of stability while keeping the payload on a secure transporting base (cf. Fig. 5.2(c)). In the contrary case, if P_2 is outside the m-bot support pattern, then the system falls down and the task fails (cf. Fig. 5.2(a)). When P_2 is on the edge of the m-bot support pattern, then the m-bot remain stable but if the payload moves during the transportation task, loss of stability may occur if P_2 comes out of the support pattern (cf. Fig 5.2(b)).

(a) Instable configuration for m-bot which generates its reversal

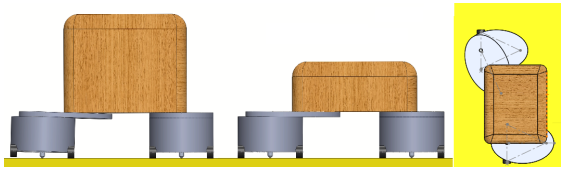

(b) Limit stability of the m-bots when the payload is positioned on the edge of its support polygon

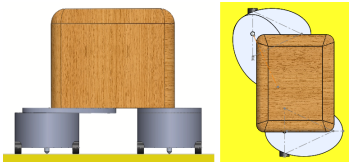

(c) Stable positioning of the payload which allows a secure task achievement

FIGURE 5.2: Simulation for m-bots stability according to the payload landing position

5.1.1.2 P-bot simulation for payload lifting

P-bot simulation using passive lifting mechanism

Fig. 5.3 shows the simulation results for a poly robot lifting a payload in order to put it on the top of m-bots bodies. Fig. 5.3(a) presents the successful task of lifting for a limited payload mass and a high friction contact payload/end-effector. Contrary to the previous simulation, a higher payload mass produce a loss of stability with a decreasing applied tightening force with the variation of inclination angle of the parallelogram

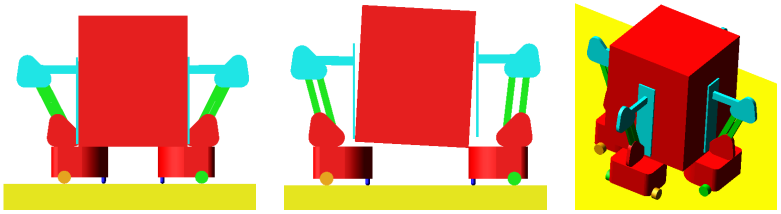

(a) (b) (c)

FIGURE 5.3: Payload lifting using a passive mechanism: a) two m-bots succeed to lift a payload; b) two m-bots fails to support a payload; c) four m-bots are supporting a payload

linkages (cf. Fig. 5.3(b)). Fig. 5.3(c) presents a successful limited payload mass lifting while using four m-bots. The system is able to lift a payload with a mass around $0.2kg$ with two m-bots (cf. Fig. 5.3(a)) and around $0.4kg$ with four m-bots (cf. Fig. 5.3(c)). Fig. 5.4 shows the resultant normal force applied for the payload tightening realized by MSC ADAMS software.

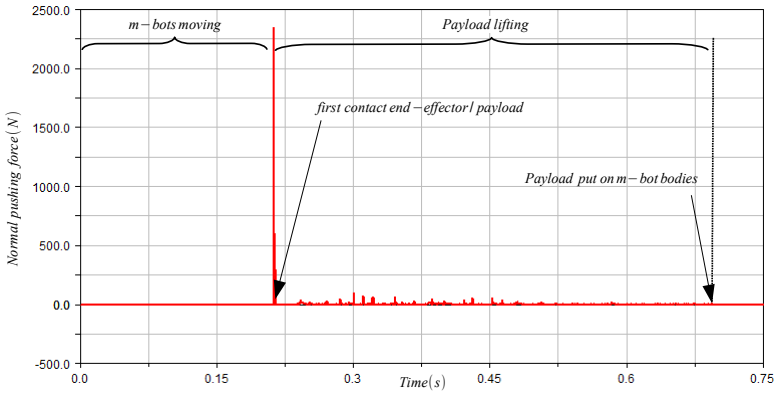

FIGURE 5.4: Resultant normal force for payload tightening with a passive mechanism

P-bot simulation using a manipulation mechanism with helical spring

Fig. 5.5 presents the simulation results for a payload co-manipulation using a helical extension springs with different stiffnesses. In the case of Fig. 5.5(a), the used spring generates a normal force relative to its deformation that allows the p-bot to maintain the payload tightening and the overall system stability. The payload is put on robot bodies and the lifting phase is successfully achieved. The payload is able to slip when using a helical spring with a weak stiffness (Fig. 5.5(b)). However, Fig. 5.5(c) presents the simulation results using a higher stiffness spring that generates a normal force greater than the m-bot wheels propulsion which leads to the robots reversal. Using a helical

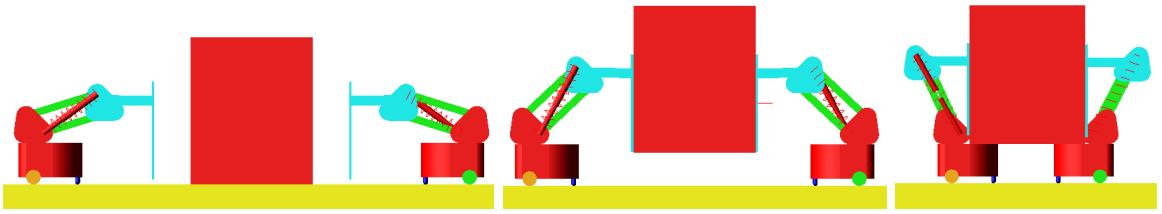

(a) Successful lifting of the payload

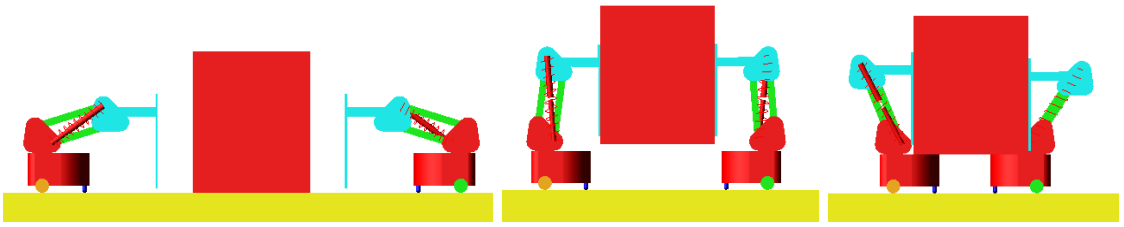

(b) Payload lifting with a low stiffness helical spring (the payload is able to slip because the generated tightening force is not sufficient to maintain it)

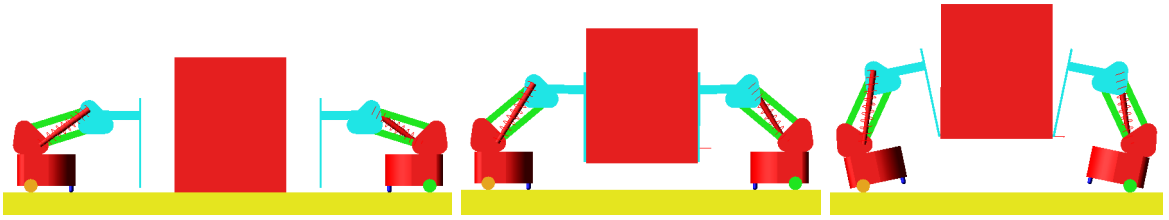

(c) The m-bots tip over when the deformation of used springs generate normal forces that exceeds the pushing forces generated by the robot's wheels propulsion

FIGURE 5.5: Multi-body dynamic simulation for payload lifting using helical extension springs

spring, the system is able to lift in this case a payload with a mass around $0.4kg$ with two m-bots.

The contact force evolution during both simulation cases are presented in Fig. 5.6. The contact is maintained until putting the payload on robot bodies (cf. Fig. 5.6(a) and Fig. 5.6(b)) or until the loss of stability (cf. Fig. 5.6(c)). When using a helical spring with a weak stiffness, the payload may slip during the lifting phase (cf. Fig. 5.5(b)).

P-bot simulation using a manipulation mechanism with torsion spring

The simulation results behavior for the case of the use of torsion spring is similar to the case of helical torsion spring with a lifting capacity about $0.4kg$. In Fig. 5.7(a) the m-bots keep on holding the payload until it lands on robot bodies and in Fig. 5.7(b) the stability is lost because of the use of higher stiffness torsion spring. The contact force

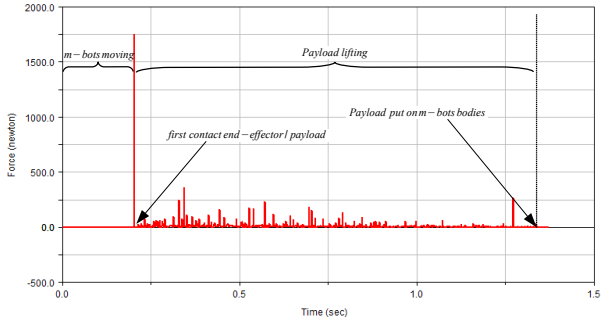

(a) The used helical spring is able to maintain the payload tightening without loss of stability of the whole system

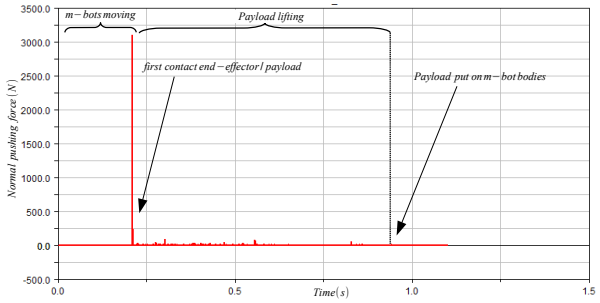

(b) The payload is slipping during the lifting phase when using a less stiffness helical spring

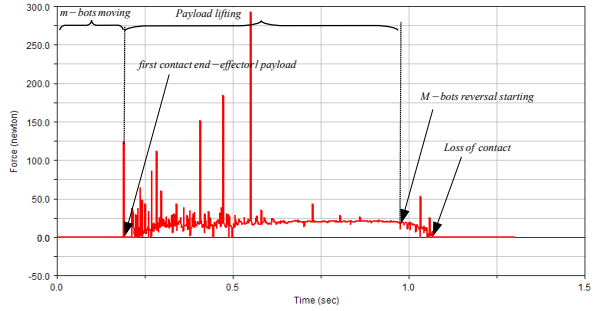

(c) The deformation of used torsion spring generates a normal force greater than the robot's wheels propulsion

FIGURE 5.6: Resultant normal force for payload tightening using helical extension spring

evolution are presented in Fig. 5.8. The contact is maintained until putting the payload on robot bodies (cf. Fig. 5.8(a)) or until the loss of stability (cf. Fig. 5.8(b)).

The m-bots are more efficient in term of payload to be lifted using compliant components. However, if the components stiffness exceeds the value expressed in equation (3.40), loss of stability could occur and the m-bots fall down.

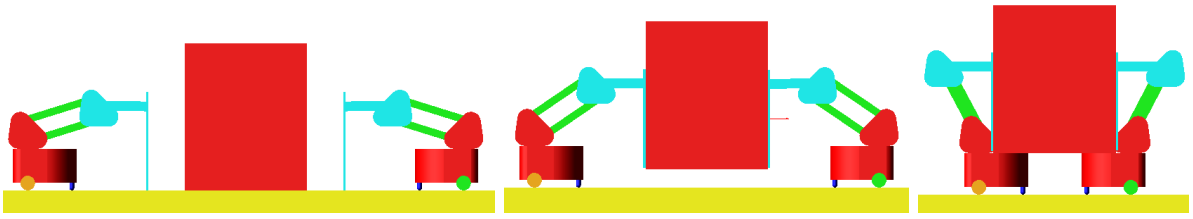

(a) Successful payload lifting

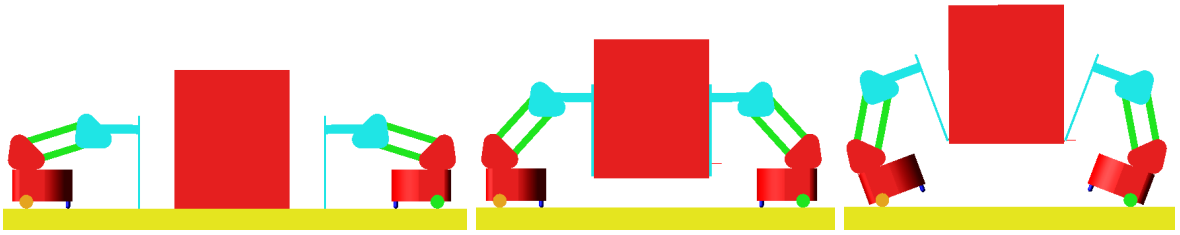

(b) The generated normal force by the torsion spring deformation is greater than the robot's wheels propulsion which generates the m-bots reversal

FIGURE 5.7: Multi-body dynamic simulation for payload lifting using torsion springs

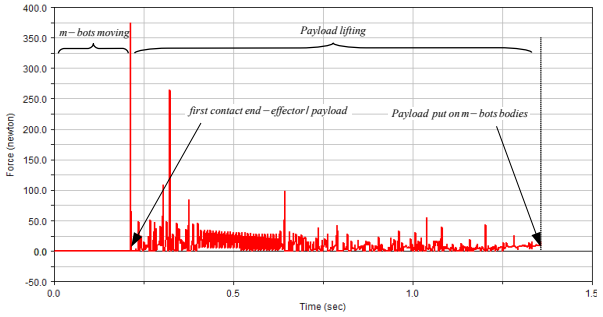

(a) The used torsion spring is able to maintain the payload tightening without loss of stability of the whole system

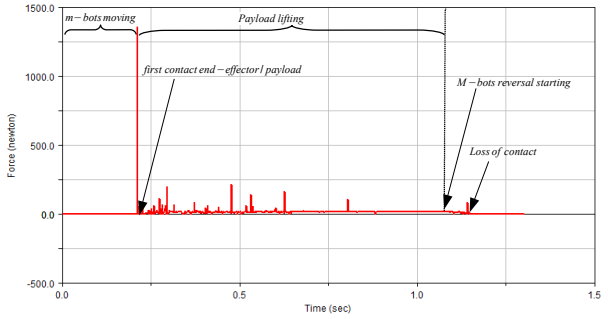

(b) The deformation of used torsion spring generates a normal force greater than the robot's wheels propulsion

FIGURE 5.8: Resultant normal force for payload tightening using a torsion spring

P-bot simulation using an interconnection mechanism

Using an interconnection system allows to ensure the payload tightening during the different phases without loss of stability and without considering the risk of its slipping.

The m-bots are able to lift the payload and put it on their platform. The payload lifting capacity is limited to the applied pushing forces by the m-bots when the manipulation mechanism is not actuated. In the case where the parallelogram mechanism is actuated, the payload mass can reach the total weight of the used m-bots. In Fig. 5.9, the m-bots end-effectors and the payload have the same color as if they are a unique component and connected to each other. The simulation results have shown that, by ensuring this interconnection and by actuating the lifting mechanism allow to have a system considerable performances. Two m-bot, of 1.4 kg each, can lift a payload of 3 kg.

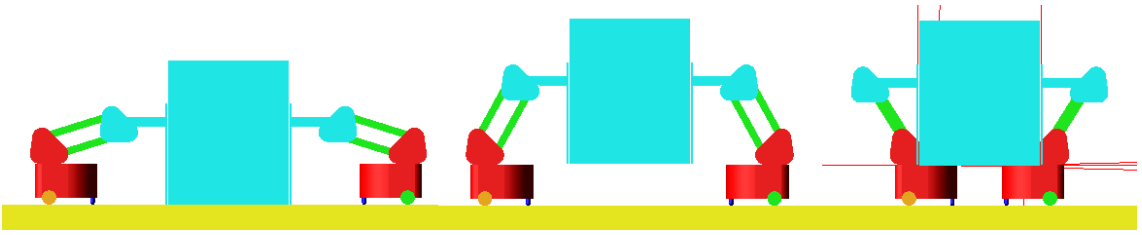

FIGURE 5.9: Payload lifting using an interconnection system and actuated parallelogram system

5.1.2 Test-bench results

A test-bench was developed to validate the theoretical results using passive joints and spring actuation. The mechanism is made of a basis frame and two parallelogram systems in the case of two m-bots that can co-manipulate to lift a payload. The lifting capacities are evaluated according to various payload/end-effector friction coefficients. Fig. 5.10 presents the experimental mechanism with the different parts.

Two 6 V_{cc} Firgelli linear actuators with a maximal force of 23N were used to obtain the tangential forces applied by the wheels of two m-bots. The actuators are controlled by a unique NXT automaton in order to synchronize the forward motion of both lifting mechanism. The real pushing force is measured using a compression force sensor (Vernier Dual-Range Force Sensor DFS-BTA). The results where evaluated according to the lifting capacity using different contact materials in a passive way and with helical extension spring. The following table presents the obtained results:

It is obvious with experiments that the system is more efficient when considering a higher contact friction coefficients. The friction coefficient of rubber-rubber contact is higher

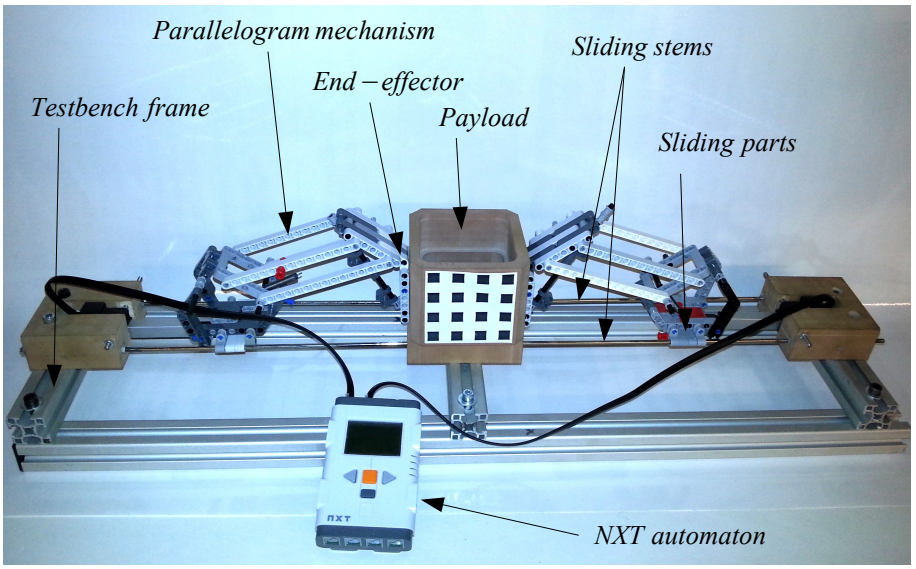

FIGURE 5.10: Testbench for lifting performances evaluation

Type of contact	**Type of actuation**	**Lifting capacity**
Rubber-rubber	Passive mechanism	0.6kg
Rubber-rubber	Helical spring mechanism	0.82kg
Rubber-composite	Passive mechanism	0.17kg
Rubber-composite	Helical spring mechanism	0.5kg
Plastic-composite	Passive mechanism	0.07kg
Plastic-composite	Helical spring mechanism	0.18kg

TABLE 5.1: Testbench lifting results

than plastic-composite contact. Experiments also proved that the use of compliant components improves the system efficiency in term of manipulated payload.

5.1.3 Manufactured prototypes results

Two versions of prototypes were manufactured in order to validate the proposed strategy of co-manipulation and transport. Fig. 5.11(a) presents the first prototype of manipulation mechanism mounted on Khepera mobile robot and Fig. 5.11(b) presents the second prototypes tested for lifting and transport for both m-bot and p-bot. The lifting and transport process by two m-bots is presented in Fig. 5.12.

The proposed co-manipulation strategy and transport were validated using the manufactured prototypes an the videos for experiments could be found in [70].

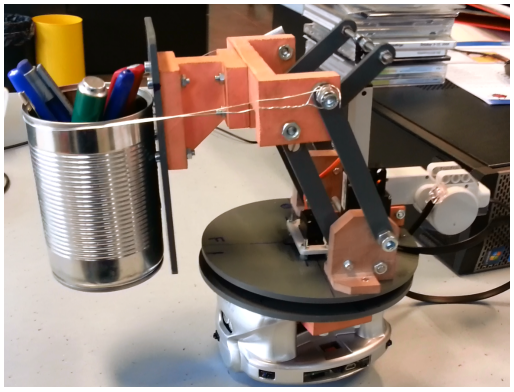

(a) M-bot composed of Khepera mobile platform and the first manufactured prototype

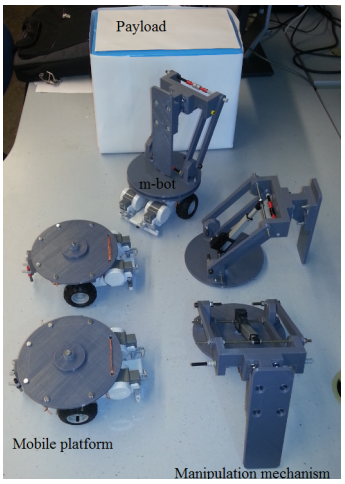

(b) Second manufactured prototype composed of unicycle mobile platform and an actuated lifting mechanism

FIGURE 5.11: Manufactured prototypes

(a) Payload prehension

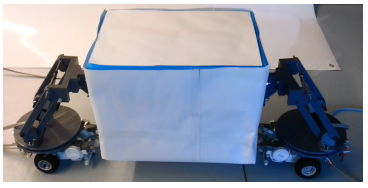

(b) Payload lifted

(c) Payload posed on robot bodies to be transported

FIGURE 5.12: Payload lifting and transport by two m-bots

5.2 Optimal positioning simulations

The proposed algorithm presented in chapter 4 allows to determine a sub-optimal configuration for a group of mobile robots in order to lift and transport a payload of any shape. Two criteria have been respected (FCG and SSM) which reduces the total configurations to be tested by the algorithm. The Algorithm was simulated by using an Intel Core i5 2400 CPU 3.1 GHz system. Fig. 5.13, 5.15, 5.16, 5.17 and 5.18 present the simulation results for the developed algorithm for different numbers of robots positioning in order to guarantee an optimal static stability margin respecting the force closure condition.

The friction cones sides are presented by a thin curves and the intersection is presented by contrasted area resulted by the superposition of friction cones. It is shown how the algorithm keeps the payload center of mass G_{pl} inside the intersection area and it allows to build a polygon of support ensuring the payload stability during the transport. The duration to find results depends on the chosen steps of θ_m to run throw the payload curve (less than 10s). The results were also checked using the developed criterion of Liu in [112]. It was demonstrated for each configuration that the origin of the wrenchspace is inside the convex hull of intersection of the wrenchspaces of each contact force (cf. Fig. 5.13, 5.15, 5.16, 5.17 and 5.19).

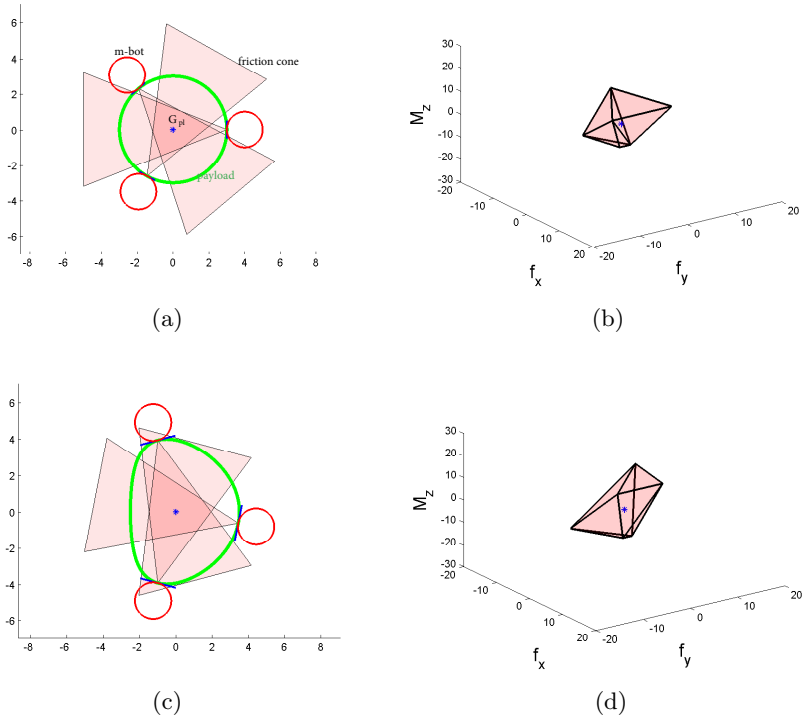

FIGURE 5.13: Three robots positioning simulation for different shapes of payload and systems of six wrenches corresponding to the force closure grasps

The payload stability during the lifting phase was simulated with respect to both criteria (SSM and FCG) using ADAMS multi-body dynamic software to validate the proposed algorithm (cf. Fig. 4.6) while testing the m-bots performances when they are positioned to co-manipulate the object. Fig. 5.14 shows that the robots ensure the payload lifting without loss of stability of the lift. Videos for simulation are visible under [70].

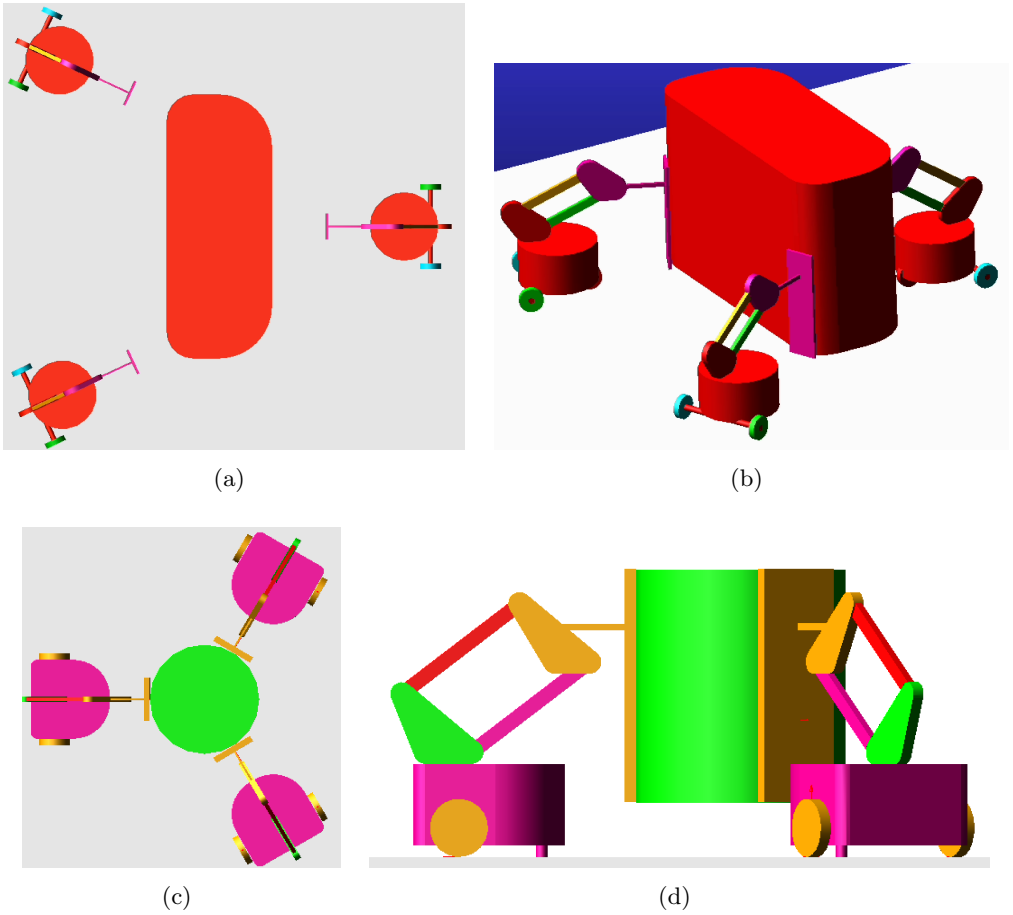

(a) (b)

(c) (d)

FIGURE 5.14: Multibody simulation results for 3 m-bots with ADMAS software: Top view (a and c), and 3D lifting phase (b and d)

Fig. 5.15 presents the simulation results for a group of four m-bots positioning using the proposed algorithm. One can note that the constrained criteria are respected. More results could be found in Appendix C.

Fig. 5.16 presents the simulation results for a group of five m-bots positioning using the proposed algorithm. One can note that the constrained criteria are respected.

Fig. 5.17 presents the simulation results for a group of six m-bots positioning using the proposed algorithm. One can note that the constrained criteria are respected.

In the last addressed case, it was considered that a zone of the payload is restricted and the m-bots are not able to reach it (the bold black curve in Fig. 5.18). The algorithm takes into account this information for robots positioning and generates the optimal positions with respect to SSM and FCG. Our proposal is validated according to Liu Criterion (cf. Fig. 5.19).

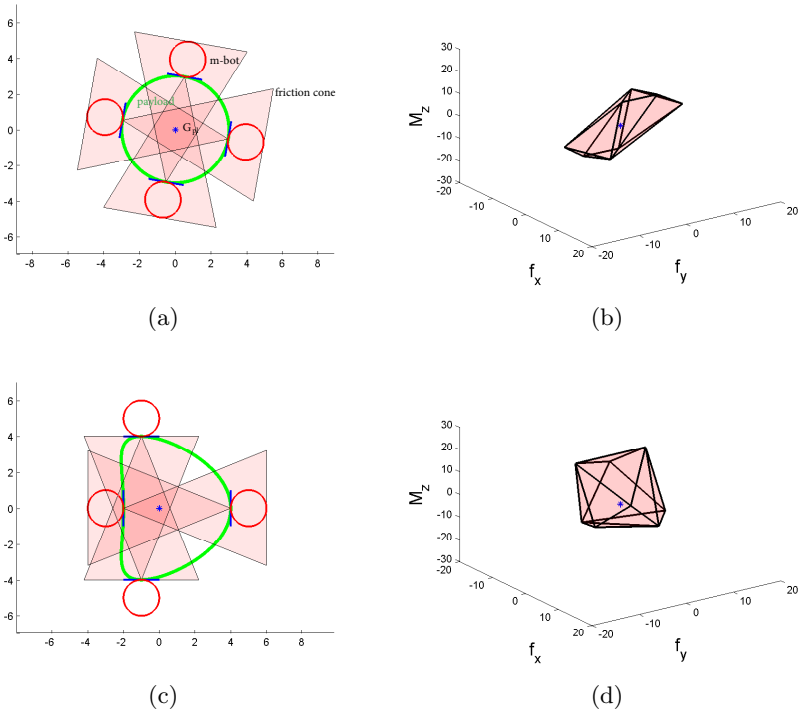

FIGURE 5.15: Four robots positioning simulation for different shapes of payload and systems of eight wrenches corresponding to the force-closure grasps

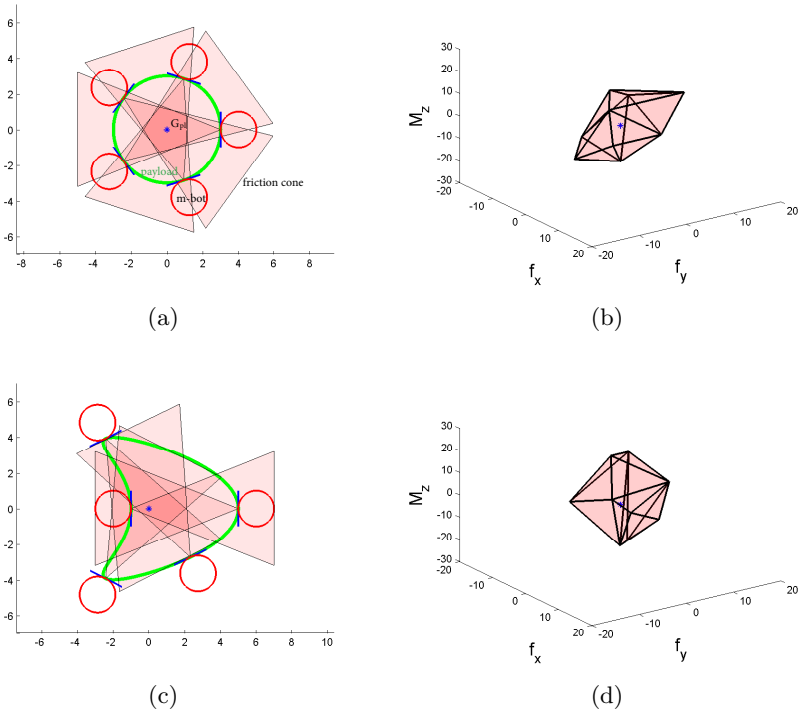

FIGURE 5.16: Five robots positioning simulation for different shapes of payload and systems of ten wrenches corresponding to the force-closure grasps

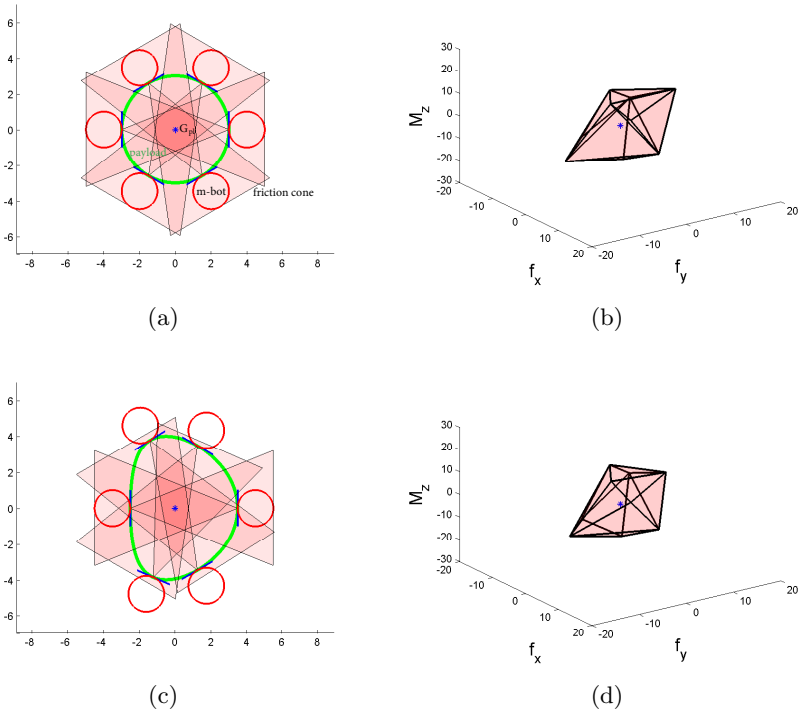

(a) (b)

(c) (d)

FIGURE 5.17: Six robots positioning simulation for different shapes of payload and systems of twelve wrenches corresponding to the force-closure grasps

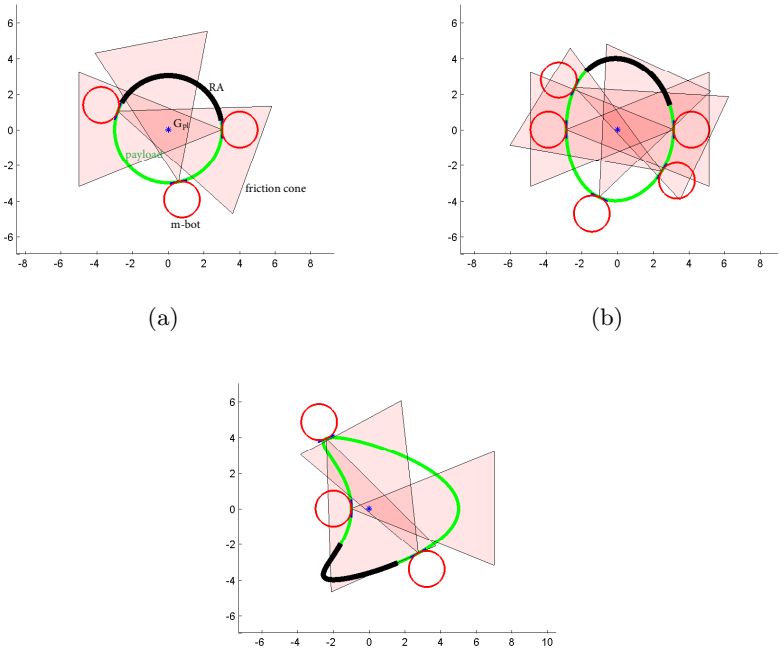

(a) (b)

(c)

FIGURE 5.18: M-bots positioning simulation for different shapes of payload with restricted areas

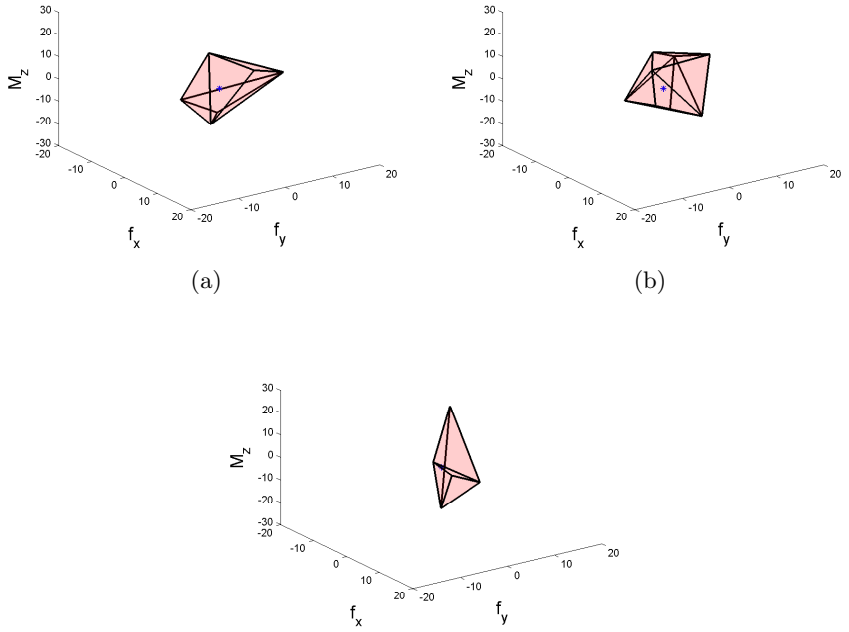

FIGURE 5.19: Systems of wrenches corresponding to the force-closure grasps shown in Fig. 5.18 respectively, with their convex hull shown as a polyhedron

5.2.1 M-bots control for transportation task achievement

5.2.1.1 Target reaching simulations

After lifting the payload, which is positioned now on the top of the p-bot, the group of m-bots must transport the payload toward a final configuration. During this last phase (Step 4 in Fig. 4.6), and in order to guarantee the payload stability, the p-bot should navigate as rigid formation shape and for this, a virtual structure architecture was used [23]. After the end of Step 3, each m-bot receives its attributed position which ensures the sub-optimal p-bot positioning that permits to ensure Force Closure Grasping (FCG) and to maximize the Static Stability Margin (SSM) during the transport.

For transport task, the m-bots have to reach their goals. After reaching the desired positions, the transport task starts considering that the payload lays on robots bodies. To avoid payload slippage, the group of m-bots has to track a fixed position relative to the object when it follows a trajectory. In this section, a control law has been used to solve the target reaching problem (P_m in section. 4.5.4.2) and the navigation as Virtual

Structure (VS) of the set of m-bots. In VS approach [23, 145], the entire formation is considered as a rigid body and the notion of hierarchy do not exist. The control law for each entity is derived by defining the VS dynamics and then translate the motion of the VS into the desired motion of each elementary robot. The main advantages of this approach are its simplicity to prescribe the coordinate behavior of the group and the maintaining of the formation during manoeuvres.

The control law was simulated for a group of m-bots transporting an object with k=22 and $\sigma = 0.1$ (cf. section 4.5.2). The goal reaching problem for one m-bot is illustrated in Fig. 5.20(a) without considering an obstacle and in Fig. 5.22(a) and 5.24(a) while considering obstacle avoidance by the robot. Fig. 5.20(b), 5.22(b) and 5.24(b) show the m-bot trajectory, the convergence of the position error e to zero and the evolution of angular error during target reaching phase. Fig. 5.21(a), 5.23 and 5.25(a) show the m-bot velocities and accelerations for both cases.

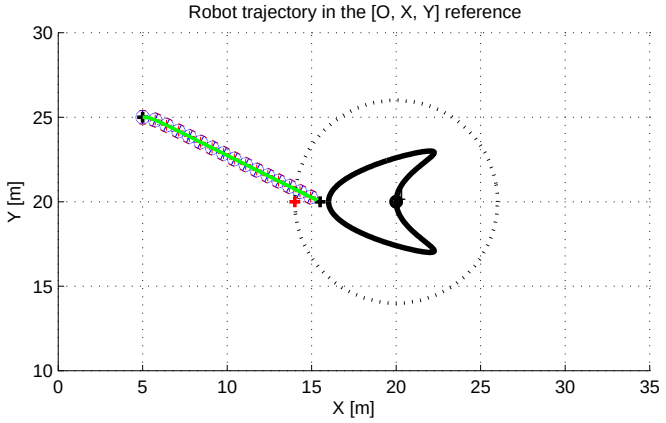

(a)

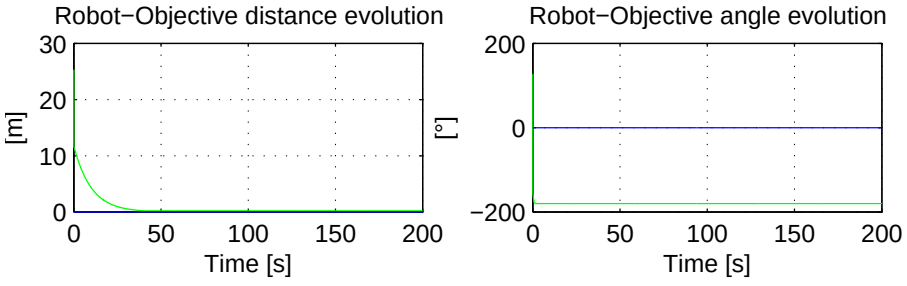

(b)

FIGURE 5.20: Target Reaching (TR) for an apparent desired position: a) m-bot trajectory; b) M-bots position errors and orientation evolution during TR phase

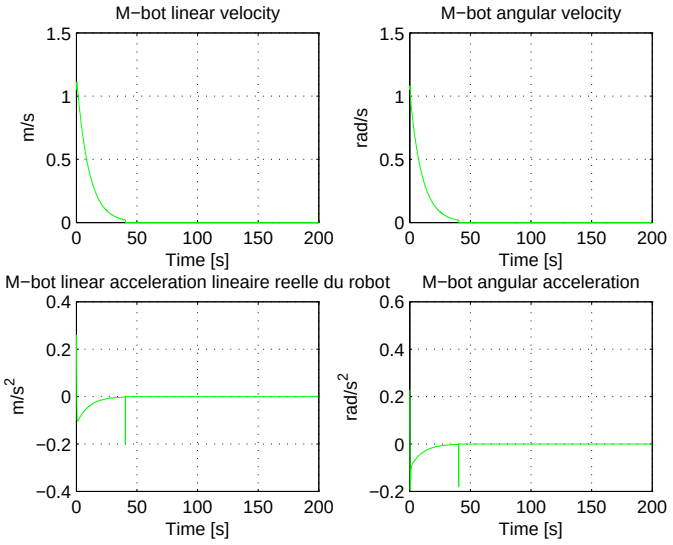

(a)

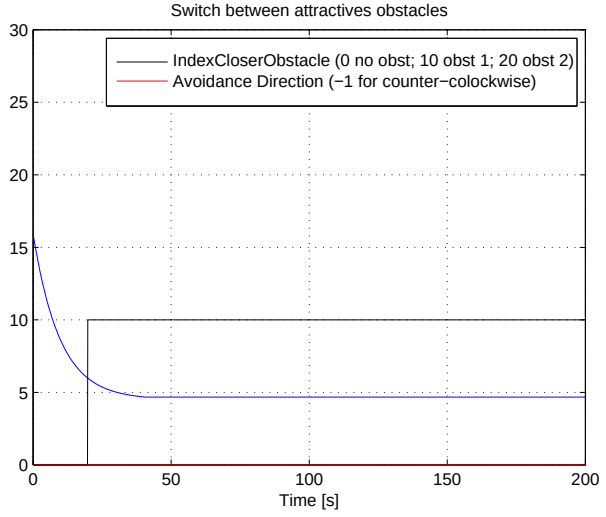

(b)

FIGURE 5.21: Target Reaching (TR) for an apparent desired position: a) m-bot linear and angular velocities and accelerations; b) circle of influence detection by the m-bot

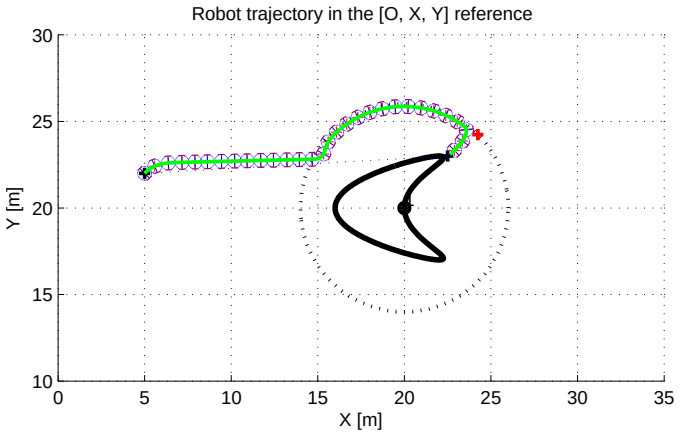

(a)

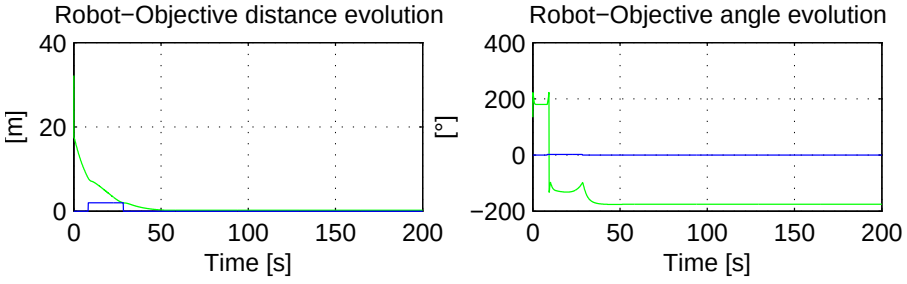

(b)

FIGURE 5.22: Target Reaching (TR) for a hidden desired position: a) m-bot trajectory; b) M-bots position errors and orientation evolution during TR phase

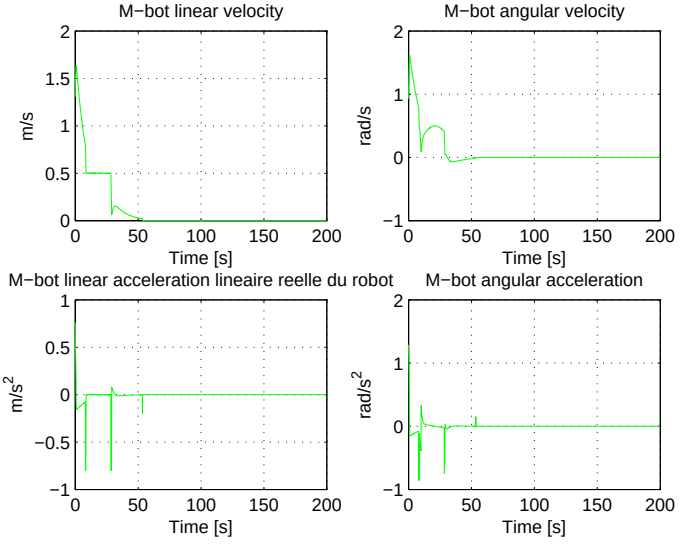

FIGURE 5.23: M-bot linear and angular velocities and accelerations

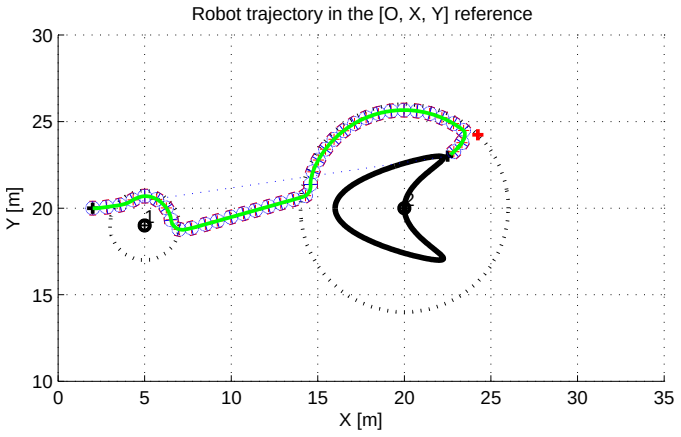

(a)

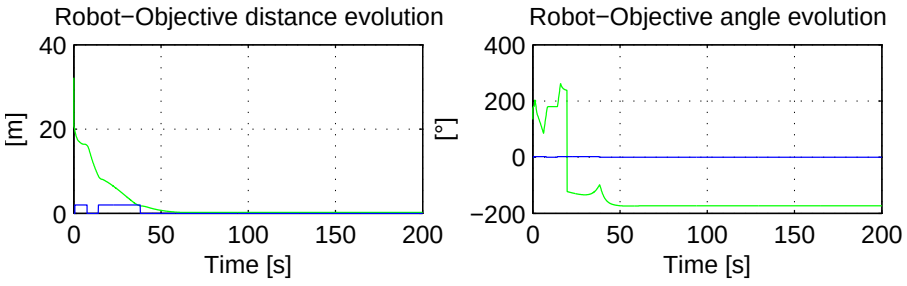

(b)

FIGURE 5.24: Target Reaching (TR) for a hidden desired position and obstacle avoidance: a) m-bot trajectory; b) M-bots position errors and orientation evolution during TR phase

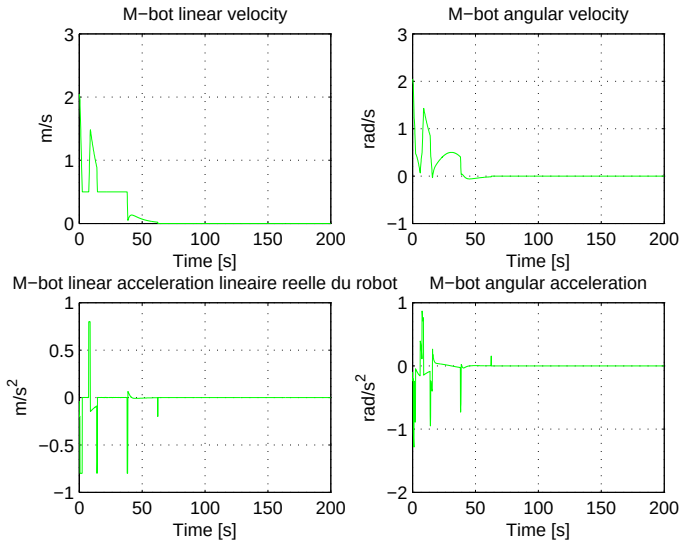

(a)

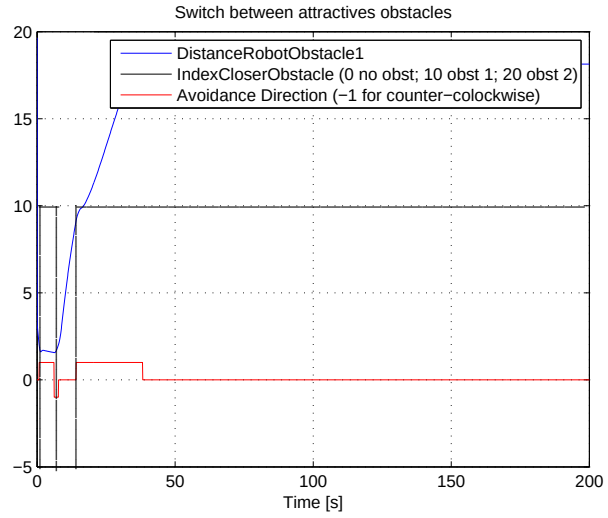

(b)

FIGURE 5.25: Target Reaching (TR) for a hidden desired position and obstacle avoidance: a) m-bot linear and angular velocities and accelerations; b) Obstacle and payload detection by the m-bot

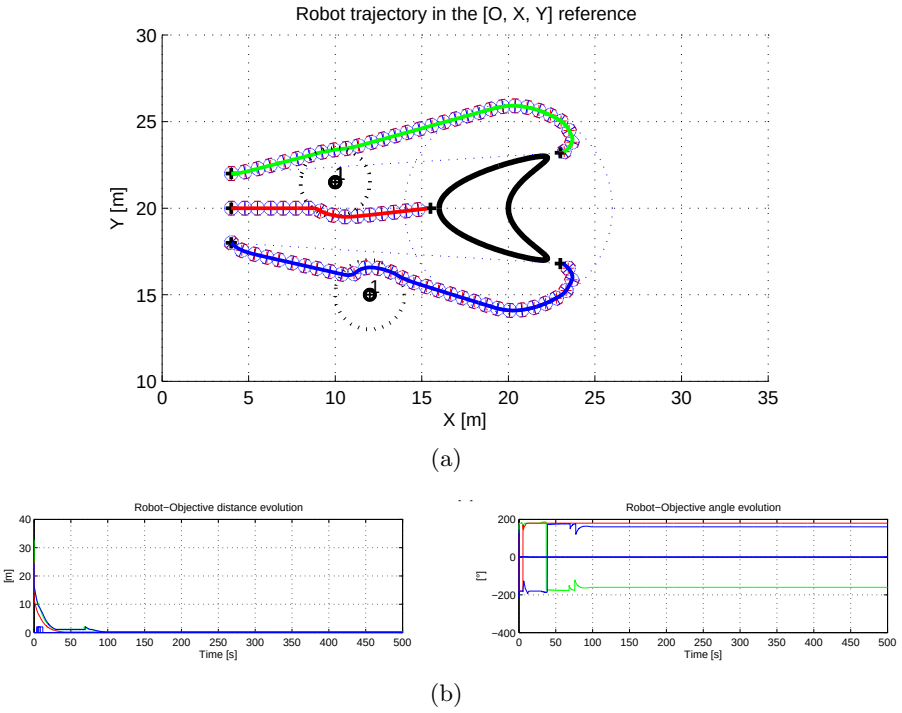

FIGURE 5.26: Target Reaching (TR) for three m-bots while considering limit cycle method for obstacle avoidance and desired hidden target reaching: a) m-bot trajectories; b) M-bots position errors and orientation evolution

Fig. 5.26(a) illustrates the target reaching phase of three m-bots. The positions errors and angle evolutions are shown in Fig. 5.26(b). The m-bots velocities are illustrated in Fig. 5.27. While considering obstacle avoidance, Fig. 5.28 presents the way how each m-bot avoids the obstacle.

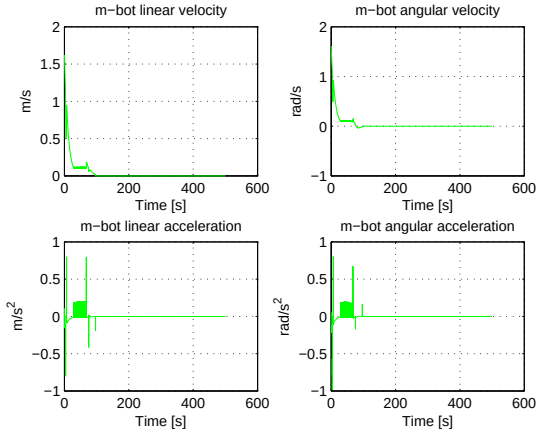

(a)

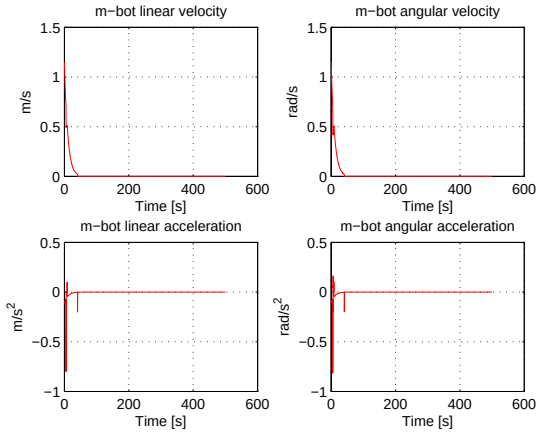

(b)

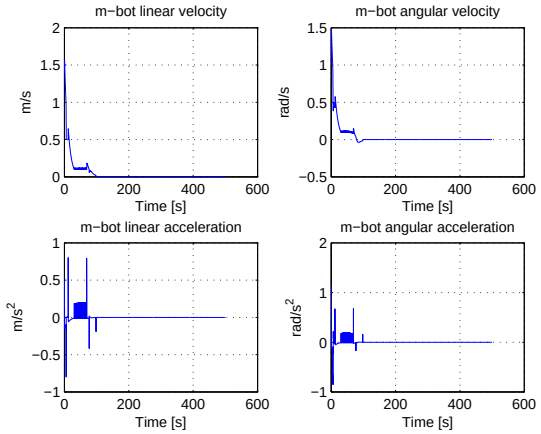

(c)

FIGURE 5.27: M-bots linear and angular velocities and accelerations: a) m-bot$_1$; b) m-bot$_2$; c) m-bot$_3$

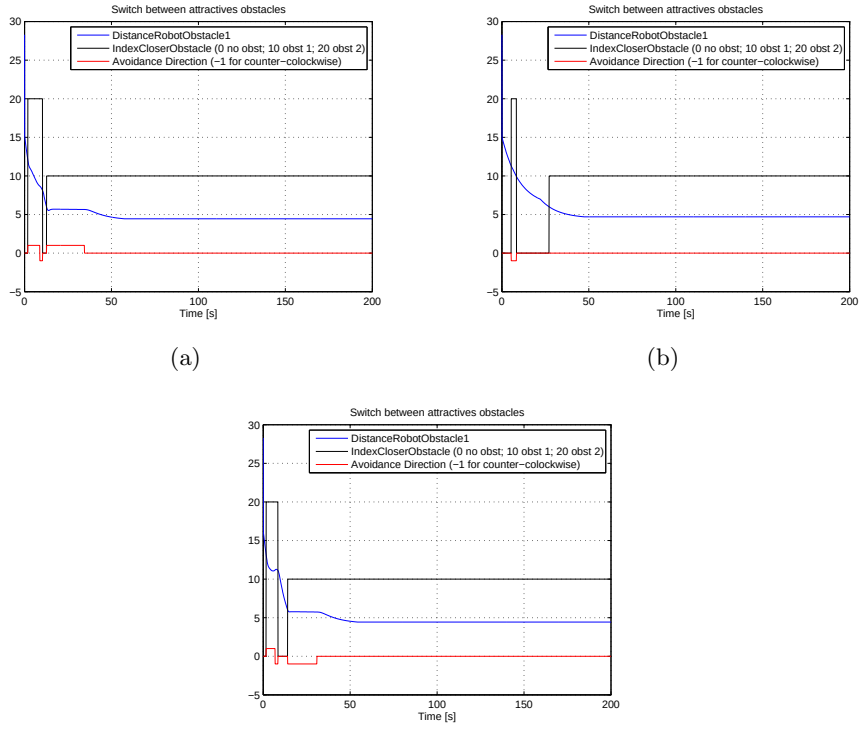

FIGURE 5.28: Obstacle avoidance by the m-bots: a) m-bot$_1$; b) m-bot$_2$; b) m-bot$_3$

5.2.1.2 Payload collective transport

One can note that all m-bots keep a null position errors which means that the formation is properly maintained and that the risk of payload fall down is avoided. It is important to notice, that in the proposed work, we suppose a centralized control of the fleet of robots, thus, the movement of the virtual structure and its dynamic are already defined according to the configuration of the environment. Indeed, the focus is made here on the presentation of the virtual structure and the way how each elementary robot keeps the desired position relative to the payload center of mass.

Fig. 5.29(a) and 5.30(a) present a payload transport using three m-bots in a linear trajectory while keeping its same orientation. The payload centre of mass linear and angular velocities and acceleration are presented in Fig. 5.29(b). The position errors relative to the payload center of mass for the fleet of m-bots are presented in Fig. 5.30(b).

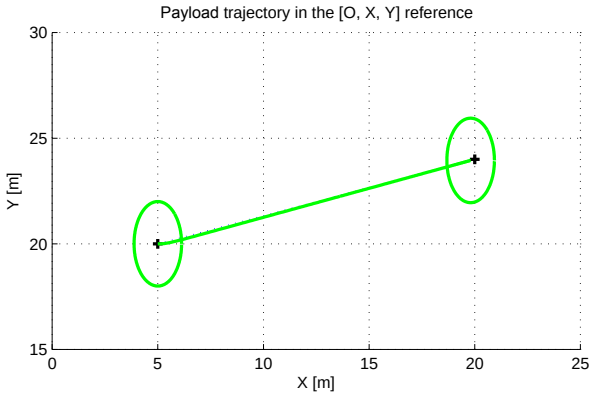

(a)

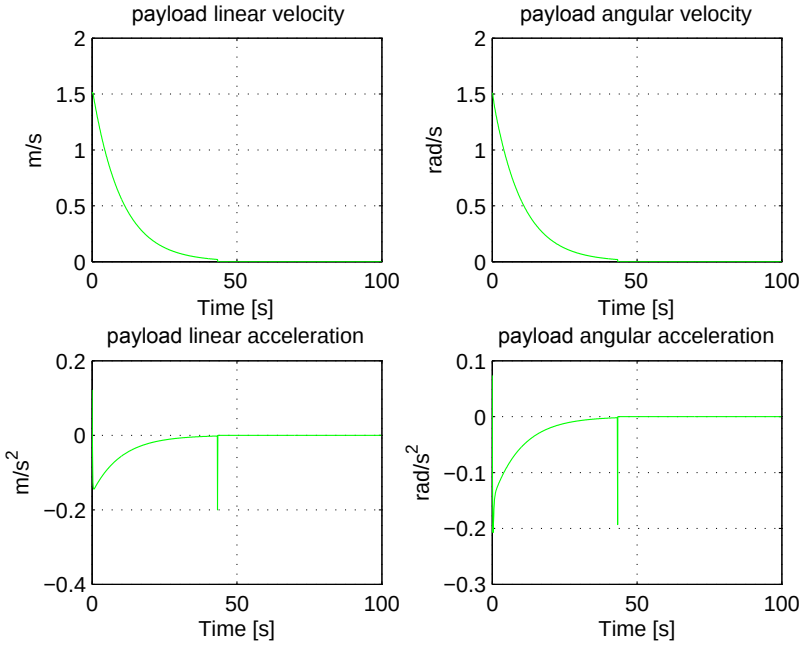

(b)

FIGURE 5.29: Payload transport while keeping the same orientation: a) payload trajectory; b) linear and angular velocities and accelerations of payload center of mass

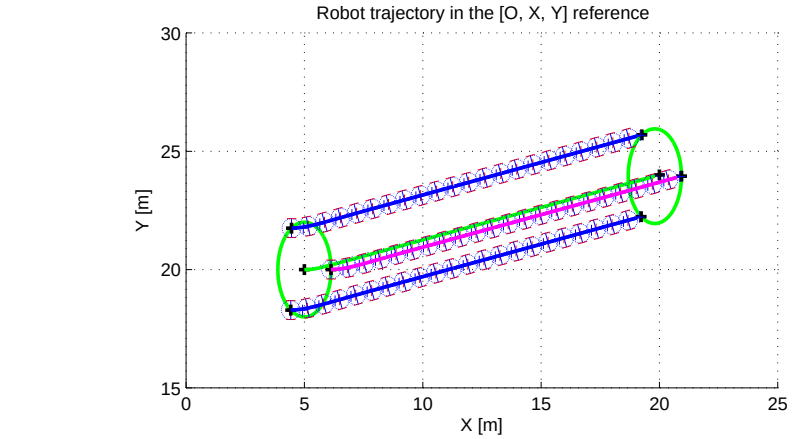

(a)

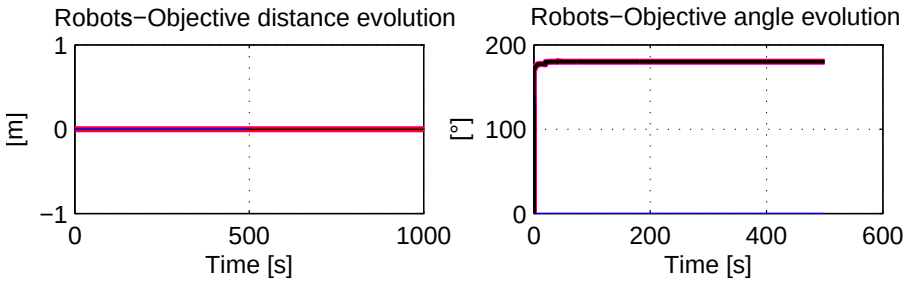

(b)

FIGURE 5.30: Payload transport while keeping the same orientation: a) payload and m-bots trajectories; b) M-bots position errors and orientation evolution during VS navigation

Fig. 5.31(a) presents a payload transport using two m-bots in a linear trajectory while changing its orientation. The position errors relative to the payload center of mass for the fleet of m-bots are presented in Fig. 5.31(b).

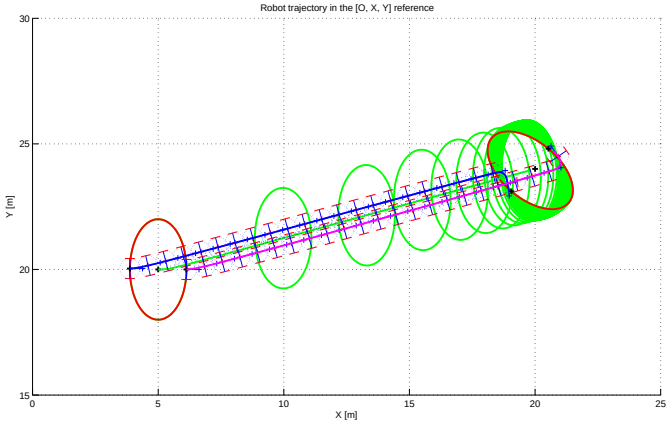

(a)

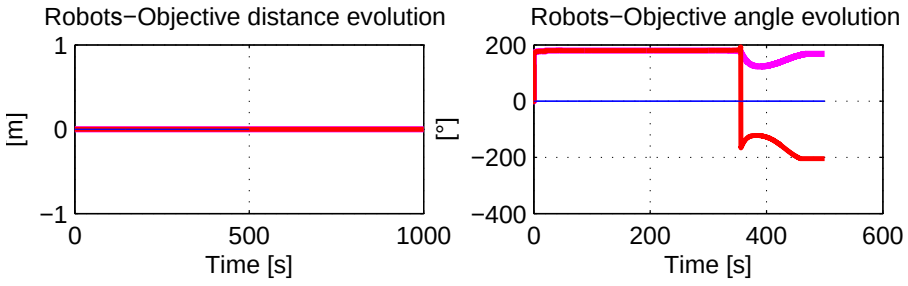

(b)

FIGURE 5.31: Payload transport while changing its orientation: a) payload and m-bots trajectories; b) M-bots position errors and orientation evolution during VS navigation

While considering the case of collective transport in an environment with obstacles, the fleet of m-bots must take this constraint into consideration and as explained in the previous chapter, during the transportation phase, the robots use the limit-cycle method in order to avoid obstacles. Fig. 5.32 and Fig. 5.33 present the case where an obstacle is involved between the initial and final position of the payload. In Fig. 5.32, the payload is transported while keeping its initial orientation while in Fig. 5.33, the payload is transported and its orientation is changed. For both cases, three m-bots were used to transport it and their position errors and orientation evolution are presented respectively in Fig. 5.32(b) and Fig. 5.33(b)

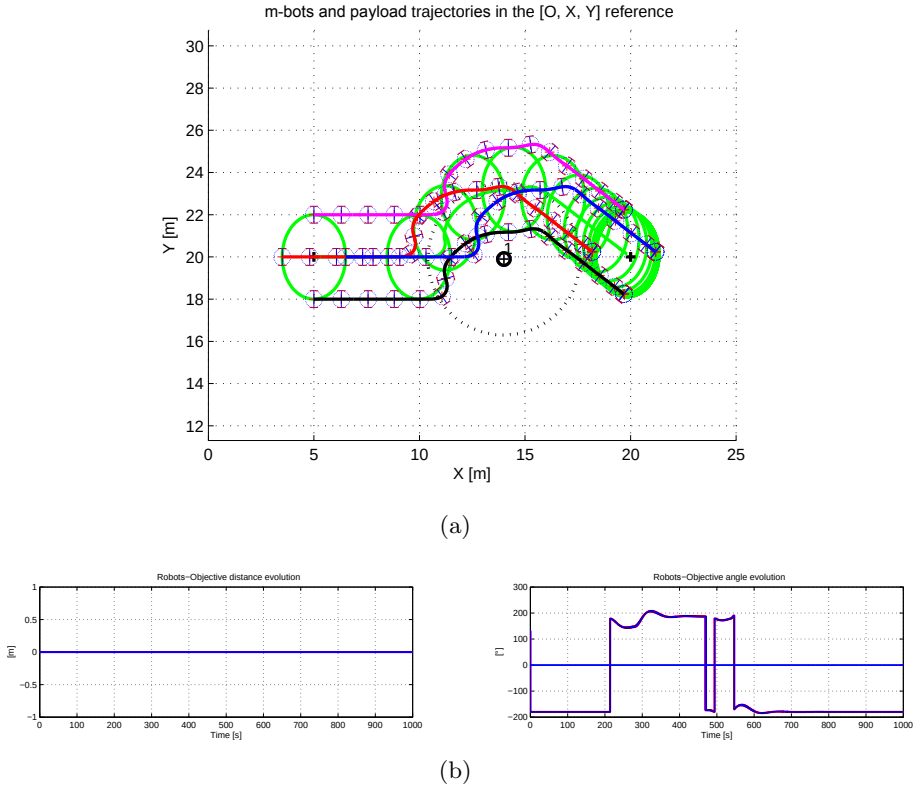

(a)

(b)

FIGURE 5.32: Payload transport with obstacle avoidance while keeping the same orientation: a) payload and m-bots trajectories; b) M-bots position errors and orientation evolution during VS navigation

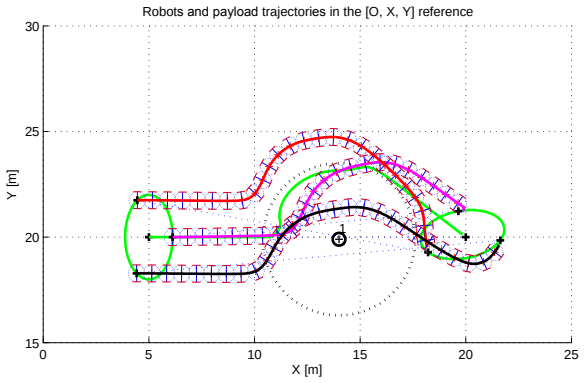

(a)

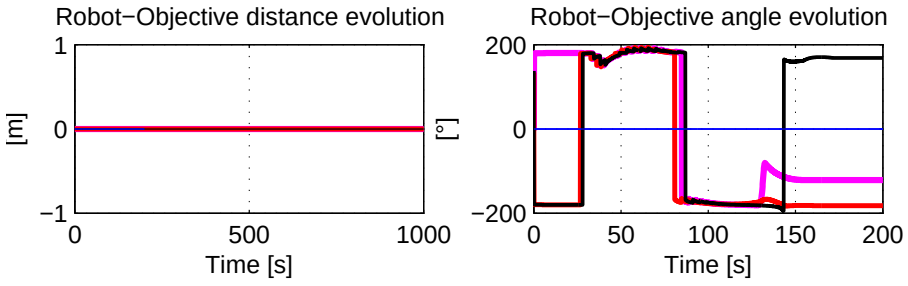

(b)

FIGURE 5.33: Payload transport with obstacle avoidance while changing its orientation: a) payload and m-bots trajectories; b) M-bots position errors and orientation evolution during VS navigation

5.3 Conclusion

In this chapter the theoretical development was validated in both experiments and simulations. The first part presented a multi-body dynamic system simulations that allows to validate our proposal concerning the choice of the mobile platform and landing position. The p-bot lifting capacity using different actuations was also validated and proved that the system efficiency depends on the choice of manipulator actuation. A developed test bench allows also to give similar results while considering the friction coefficients between the robots end-effectors and the payload in addition to the manipulator actuation. Simulation results using Matlab allows to validate the proposed strategy for a group m-bots positioning in order to ensure a Static Stability Margin (SSM) and Force Closure Grasping (FCG) Criteria with respect to reachable areas. The target reaching phase and collective transport were simulated using a pre developed control law and it

was shown how the task could be achieved successfully using the Virtual Structure (VS) approach for p-bot navigation in formation.

Chapter 6

General conclusion and Future Works

General conclusion

The focus of the achieved works in this thesis were made on making innovative multi-robot system able to autonomously co-manipulate and transport payloads of any shape using a manipulation system. A group of robots with a simple architecture called *m-bots* are able to collaborate and form a poly-robot called *p-bot* characterized by its reconfigurability to adapt itself to the varied payloads (shape, mass) and to ensure the overall system stability. The co-manipulation methodology consists in two main phases: lifting phase and transportation phase.

In chapter 2, a review about manipulators and mobile robots was detailed. The state of the art was particularly pointed on mobile robots and collaborative system for objects co-manipulation and transport. It was considered the general architectures for existing developed mobile robots, their locomotion modes and their dedicated evolving environments. The different strategies for collaborative systems were analysed and described in order to synthesis the existing strategies and inspire a suitable transporting mode for the proposed multi-robot system. The project specification was established and the C^3Bots project paradigm was described. The system requirements were defined and the proposed methodology was detailed. Thus, the study of the state of the art allows to choose the wheeled locomotion mode for the proposed design of the mobile robots

thanks to its advantageous characteristics compared to legged or tracked locomotions. It also allowed to define the co-manipulation and transportation methodology based on lifting the payload and putting it on mobile robots bodies for a better stability during the transport.

Chapter 3 presented the m-bots design based on a mobile platform equipped with a manipulation mechanism with a parallelogram structure. This architecture was adopted because it satisfies the function of lifting the payload with constant orientation from the ground to put it on top of robot body. A study for existing lifting mechanism was done and the manipulation mechanism specification was defined. Structural and dimensional synthesis were performed for both, the chosen mobile platform and the lifting system. The landing position of the payload was optimized in order to ensure the m-bots stability during the lifting phase and to ensure the poly-robot stability during the transport. The system variables were determined according to the specifications and to the constant parameters fixed during the design process. Singular positions were studied to avoid the system malfunction. The lifting capacity is than evaluated for the lifting mechanism using different modes (passive, using compliant organs, using actuators, using interconnection).

Chapter 4 presented the proposed control architecture for the multi-robot system. The architectures of mobile robots control were introduced and the proposed system control was presented. An algorithm was developed in order to find the sub optimal positions of the m-bots around the payload according to multi-criterion task constraints. First, the *Force Closure Grasping (FCG)* criterion which is commonly used for multi-fingered hand grasping for manipulation tasks and which ensure the payload stability during the lifting phase. The robots must be positioned in a manner that FCG is respected to avoid loss of stability or payload slippage during the lifting phase. Second, the *Static Stability Margin (SSM)* was also respected. This criterion is commonly used for legged robots and it ensures the robot stability by introducing the support pattern of the robots and it allows to evaluate the robot stability during the locomotion phase. This criterion was taken in consideration for the positioning algorithm in order to ensure the p-bot stability during the transportation phase. The payload can be arranged sometimes in a certain pose and the robots sometimes do not have the accessibility to all the positions around the payload, so a criterion of restricted areas was also included in the algorithm. After finding the optimal positions using the previous described algorithm and which

are calculated in centralized control, each m-bot will be in charge to reach its desired pose $(x_{dm}, y_{dm}, \theta_{dm})$, lift the payload and transport it in a final pose in a decentralized control.

In chapter 5, multi body dynamic simulations validated the theoretical development of the robots design. A test bench was also developed and two prototypes confirmed the proposed strategy and the proposed mechatronic architecture of the system. Simulation results for the positioning algorithm and for the used control law also validated the proposed overall control architecture.

Future work

The achieved works in this thesis allowed opening varied and extended perspective relative to the addressed research theme, that can be found in the list below:

- optimize the existing developed design according to the system evaluation during the experimental phase;
- evaluate the system performances with respect to stability criteria.
- develop a large scale system;
- develop new strategies of collaboration between robots by inspiring from human beings;
- develop an interconnexion mechanism that ensures the interconnection between robots in order to tighten the payload during manipulation phase;
- develop a compliant end effector that allows to adapt the payload shape and ensures a higher contact surface;
- evaluate the required force to be applied by each m-bot to ensure the wole system equilibrium during the different phases of task achievement;
- during the transportation phase and in order to avoid any slippage of the payload, design a compliant sub assembly allowing the m-bot to rectify any slipping motion of the payload if it happens.

- include different sensors on the developed design to make a fully autonomous system and evaluate the robots behavior in maintaining the payload during the different phases of task achievement.
- make experiments with different number of m-bots and for different payloads shapes.
- develop a mechanical system oriented for all terrain will also be considered. A preliminary design is presented in Fig. 6.1 (cf. videos in [70]).

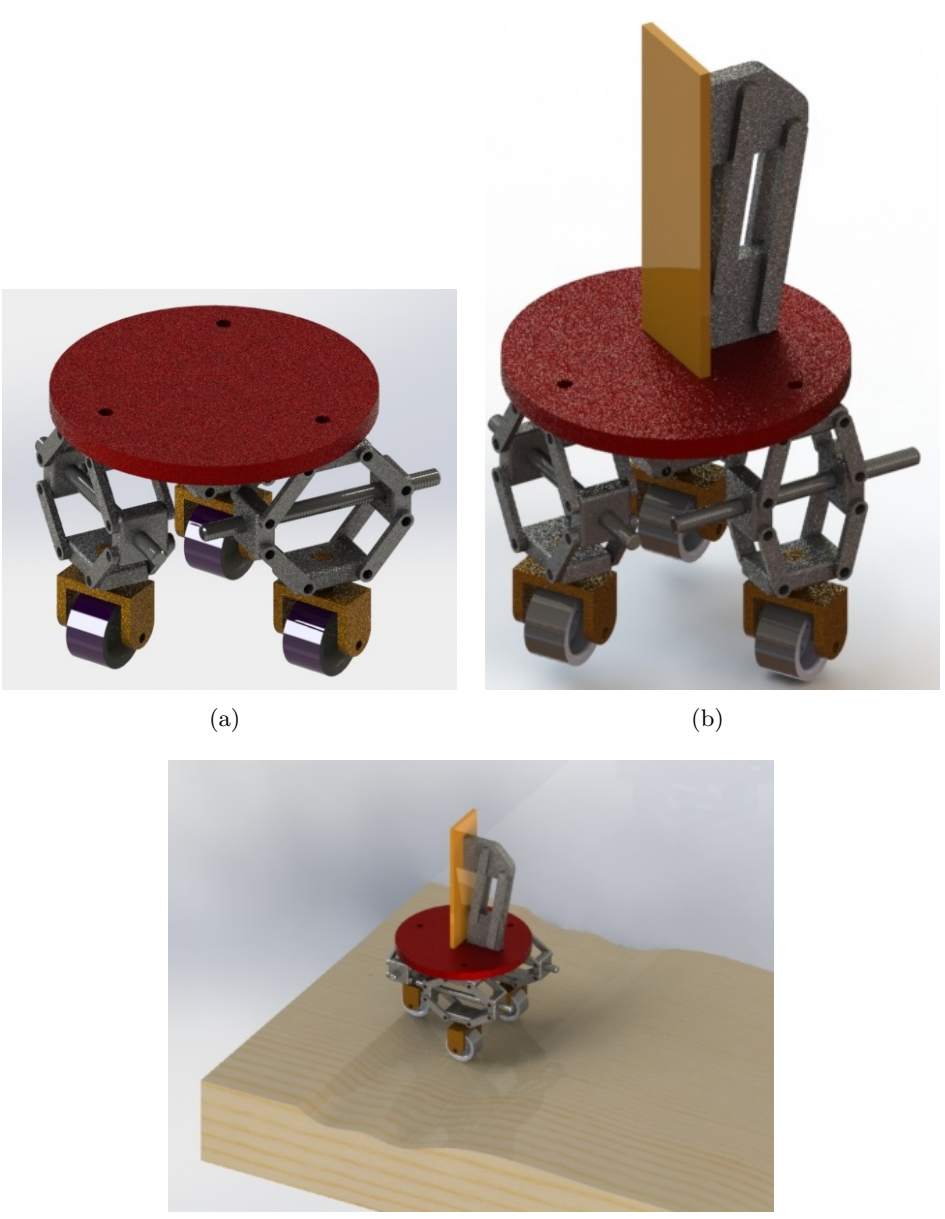

(a) (b)

(c)

FIGURE 6.1: All terrain preliminary design: a) mobile platform for unstructured ground; b) m-bot with manipulator; c) a m-bot evolving in unstructured ground

Appendix A

Mobile Robots for Payloads Co-manipulation and Transport in Structured Terrains

Abstract: *This appendix presents the part and assembly drawings for a robotic system operating in a structured flat ground for payloads of any shape co-manipulation and transport.*

The part drawings and assembly drawings are detailed here:

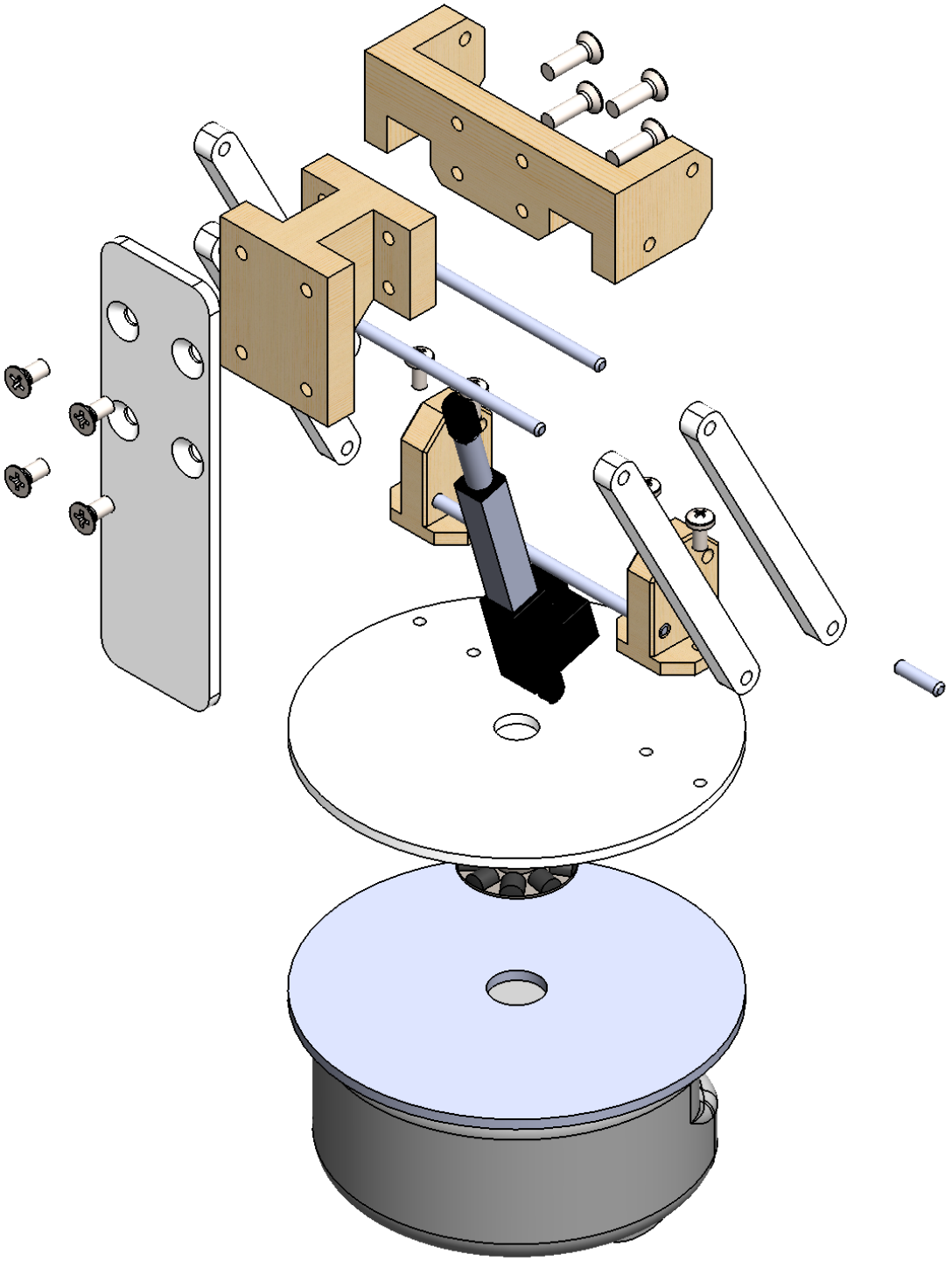

FIGURE A.1: M-bot assembly: exploded view

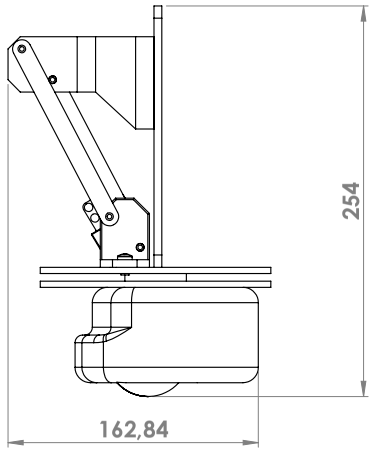

Transporting Position

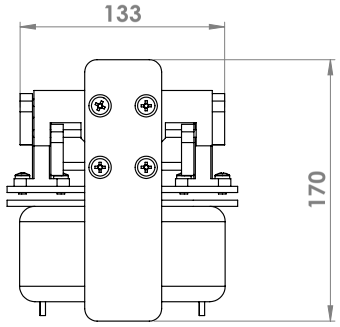

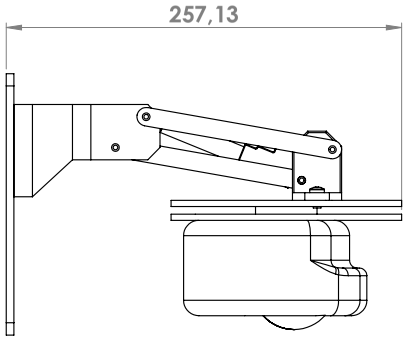

Prehension Position

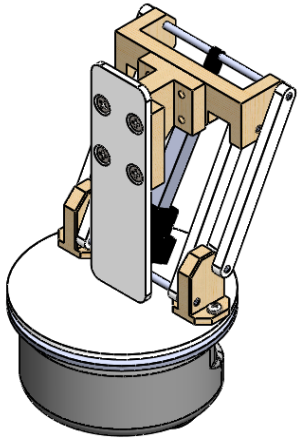

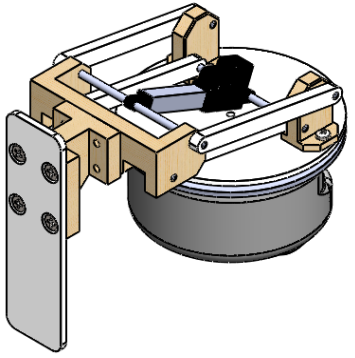

SAUF INDICATION CONTRAIRE: LES COTES SONT EN MILLIMETRES ETAT DE SURFACE: TOLERANCES: LINEAIRES: ANGULAIRES:		FINITION:				CASSER LES ANGLES VIFS	NE PAS CHANGER L'ECHELLE	REVISION
	NOM	SIGNATURE	DATE				TITRE:	
AUTEUR								
VERIF.								
APPR.								
FAB.								
QUAL.				MATERIAU:			No. DE PLAN	A3
							M-bot assembly	
				MASSE:			ECHELLE:1:3	FEUILLE 1 SUR 1

FIGURE A.2: M-bot assembly

FIGURE A.3: End-effector support part1

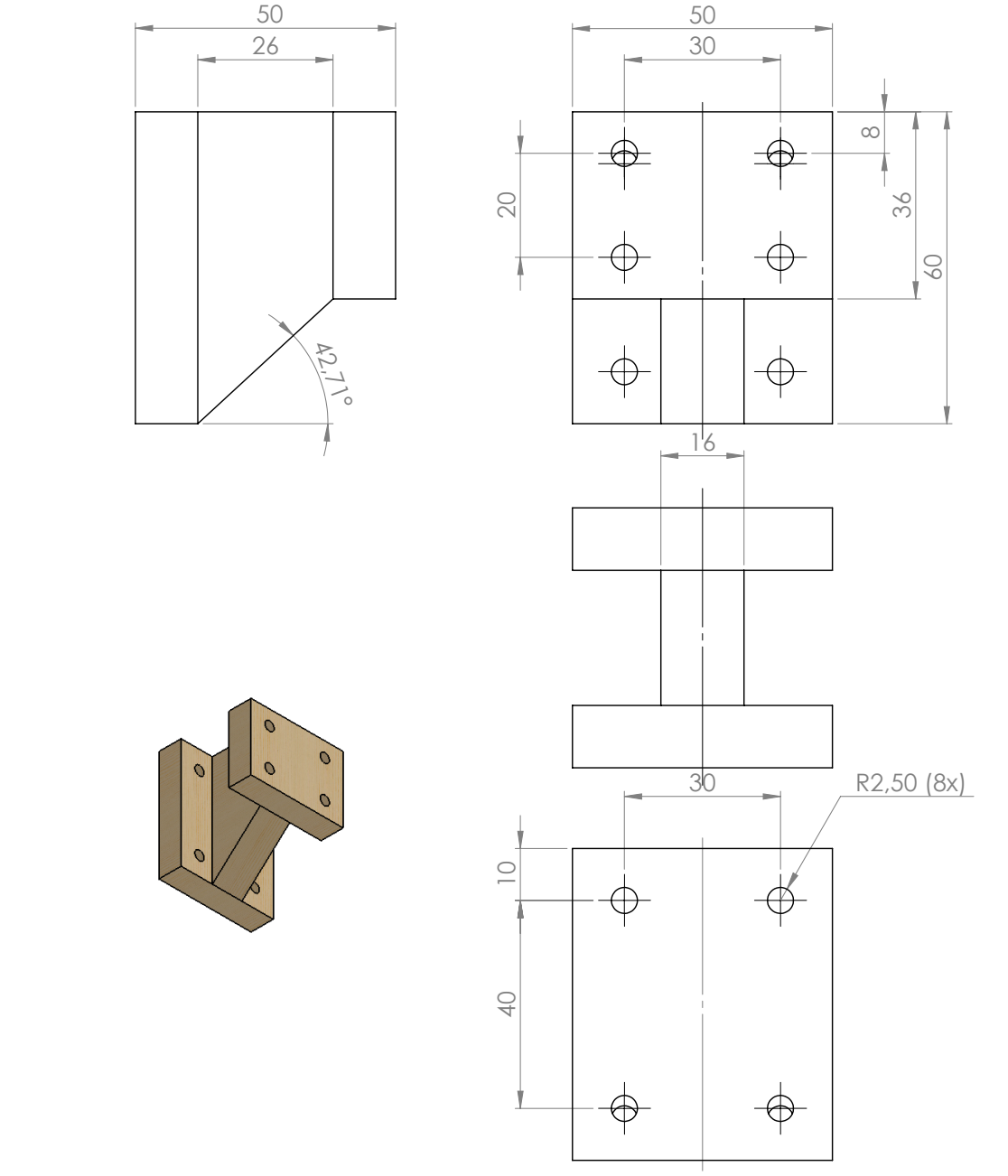

FIGURE A.4: End-effector support part2

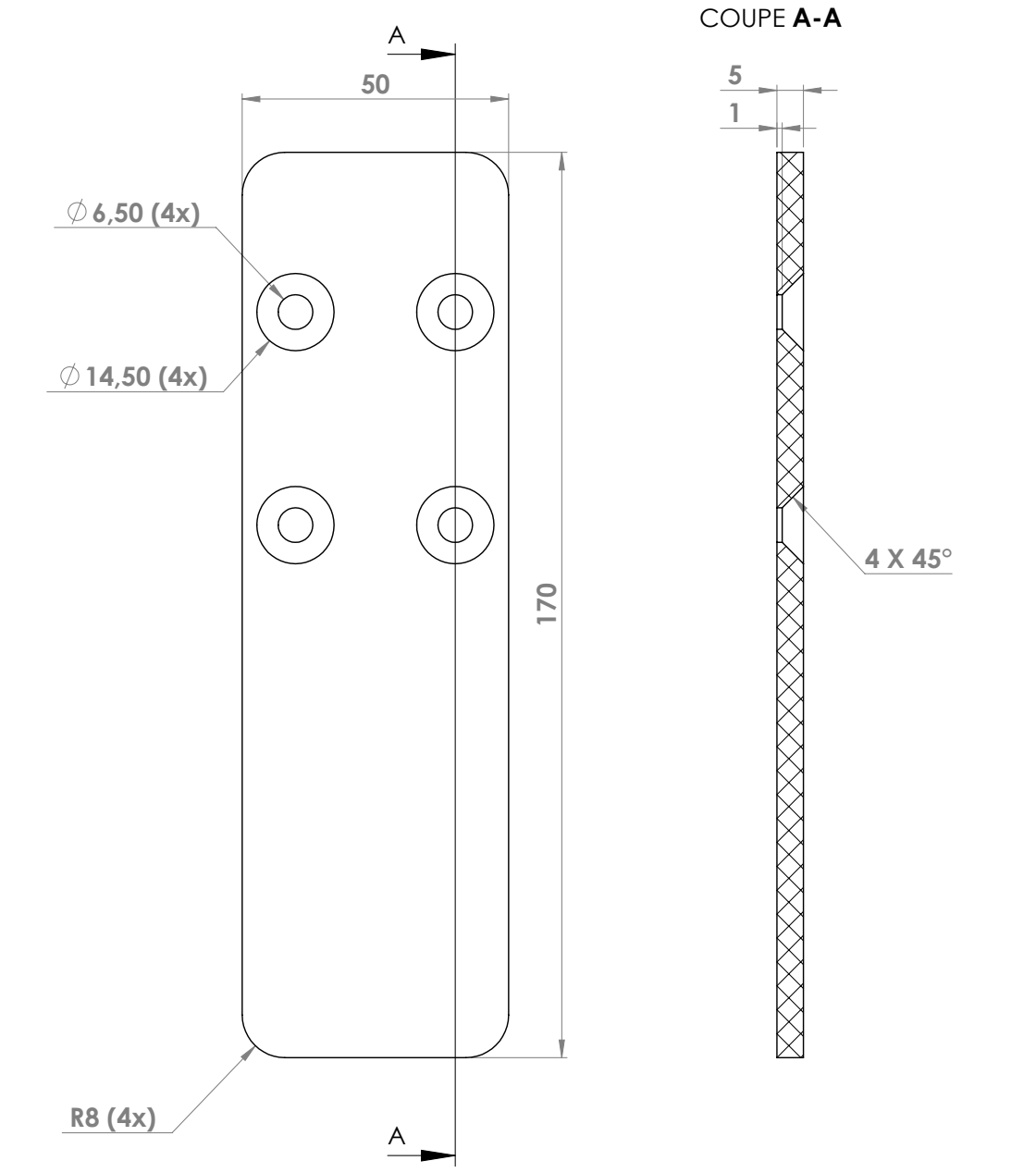

FIGURE A.5: M-bot effector

FIGURE A.6: Lower bar of the manipulation mechanism

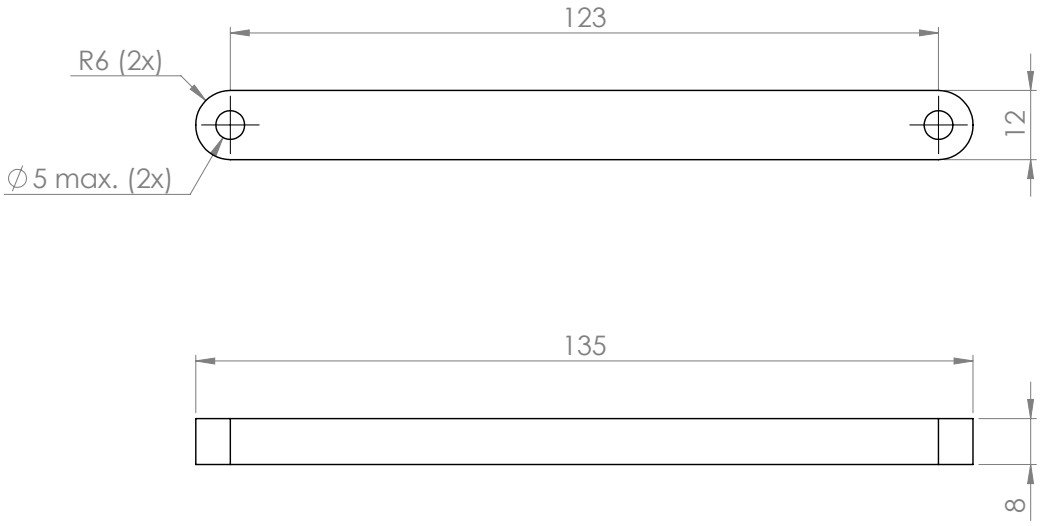

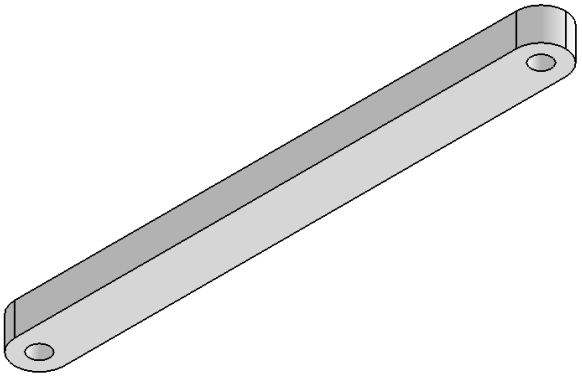

SAUF INDICATION CONTRAIRE: LES COTES SONT EN MILLIMETRES ETAT DE SURFACE: TOLERANCES: LINEAIRES: ANGULAIRES:		FINITION:		CASSER LES ANGLES VIFS		NE PAS CHANGER L'ECHELLE	REVISION
	NOM	SIGNATURE	DATE			TITRE:	
AUTEUR							
VERIF.							
APPR.							
FAB.							
QUAL.				MATERIAU:		No. DE PLAN	A4
				MASSE:		ECHELLE:1:1	FEUILLE 1 SUR 1

long bar

FIGURE A.7: Long bar of the manipulation mechanism

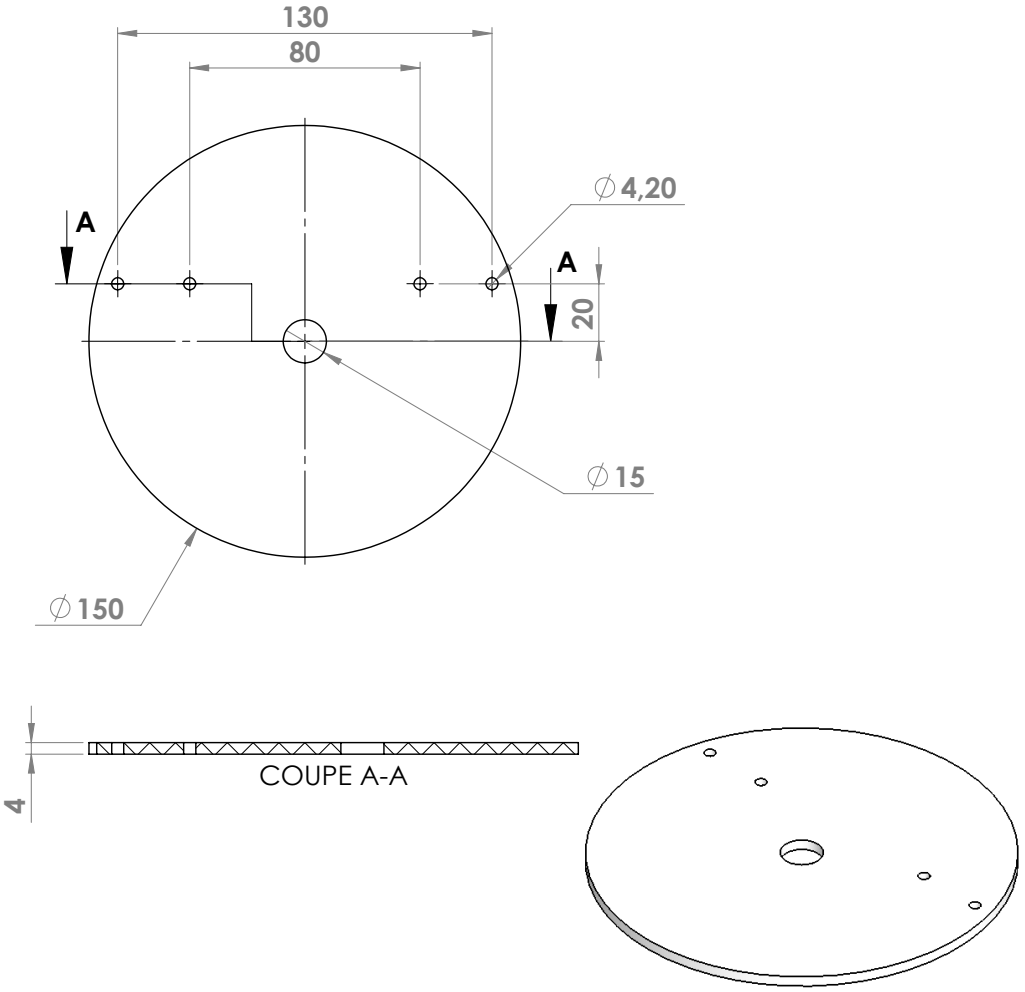

SAUF INDICATION CONTRAIRE: LES COTES SONT EN MILLIMETRES ETAT DE SURFACE: TOLERANCES: LINEAIRES: ANGULAIRES:	FINITION:				CASSER LES ANGLES VIFS	NE PAS CHANGER L'ECHELLE	REVISION
	NOM	SIGNATURE	DATE			TITRE:	
AUTEUR							
VERIF.							
APPR.							
FAB.							
QUAL.				MATERIAU:		No. DE PLAN	A4
						turn-table	
				MASSE:		ECHELLE:1:2	FEUILLE 1 SUR 1

FIGURE A.8: M-bot turn-table

Appendix B

Algorithms for m-bots Positioning

This appendix is dedicated for the developed algorithm in order to find the suboptimal positions of the m-bots to ensure a successful co-manipulation and transport of the payload.

Principle of positioning algorithm

Let $\mathcal{B}(\theta)$ be the parametric description of an object boundary ($\mathcal{B}(\theta)$ is a closed boundary) and Ω a large set of points representing the external surface of the object.
The following function allows to define the payload boundary $\mathcal{B}(\theta)$.

$Beginfunction$
$X = f(\theta)$
$Y = g(\theta)$
$Endfunction$

The second function presented below allows to define the normal and tangent direction by returning the derivative values for a given point P_i.

$Beginfunction$
$\dot{X} = diff(f(\theta))$
$\dot{Y} = diff(g(\theta))$
$Endfunction$

Let $\mathcal{G} = \{P_1...P_n\}$ be a given grasp and we consider $\mathcal{G} \subset \Omega$.
The wrenches applied throught the contact points on the object are grouped in a wrench set $W = \{\omega_1...\omega_n\}$
Let's consider $f_{m,p,t}$ and $f_{m,p,n}$ to be the tangential and normal force vectors respectively.

$$\omega_i = \begin{pmatrix} f_{m,p,t} \\ \tau_i \end{pmatrix} = \mu_p \begin{pmatrix} f_{m,p,n} \\ p_i \times f_{m,p,n} \end{pmatrix}$$

with $f_{m,p,t} = \mu_p f_{m,p,n}$ is the normalized applied force at P_i and τ_i the generated torque relative to the center of mass of the object expressed as follow.

$$f_{m,p,t} = \frac{f_{m,p,n}}{\|f_{m,p,n}\|}; \tau_i = P_i \times f_i$$

μ_p is the magnitude of the grasping force.
The aim of this part is to present an algorithm to determine a set of grasp points that ensures an object lifting to be transported using unicycle mobile robots. The m-bots are equipped with a manipulation mechanism and using robot wheel's propulsion it applies a force f_i to the object via an end effector. We assume hat the contact is punctual

for instance and the applied force is parallel to the environment plane. The number of required m-bots to lift and transport the object is determined in function of the payload mass M. $\mathcal{R}(\mathcal{O}_{pl}, \vec{x}_{pl}, \vec{y}_{pl}, \vec{z}_{pl})$ the reference linked to the object. The idea of the algorithm is to run through $\mathcal{B}(\theta)$ and to find the set of points P_i in which the curve tangent is perpendicular to GP_i (G is the center of mass of the payload) which means that if a normal force is applied on P_i then the generated momentum relative to G is null.
For each point P_i we associate an angle $\theta_i \Rightarrow P_i = \mathcal{B}(\theta_i)$
If the number of m-bots n is determined then we can determine the set of positions according to n that allows the object grasping and we calculate the wrench associated to each m-bot that ensures the following condition.

$$\sum_{i=1}^{n} \omega_i = \vec{0}$$

Which means that each robot will apply a wrench on the object ensuring collaboration to lift and co-manipulate to transport the payload without an excessive force generating a momentum relative to the center of mass G

$$\sum_{i=1}^{n} \omega_i = \begin{pmatrix} \sum_{i=1}^{n} f_{m,p,n} \\ \sum_{i=1}^{n} \tau_i \end{pmatrix} = \begin{pmatrix} 0 \\ 0 \end{pmatrix}$$

Algorithm. 3 consists on testing all the possible configurations of points ensuring the object center of mass G inside the formed polygon. Then it calculates the stability margin on each edge and determines the static stability margin SSM (the minimum of the calculated margins).

$$d_{ij} = d(G, (P_i P j)) = \frac{x_G \frac{y_{P_j} - y_{P_i}}{x_{P_j} - x_{P_i}} - y_G + y_{P_i} - x_{P_i} \frac{y_{P_j} - y_{P_i}}{x_{P_j} - x_{P_i}}}{\sqrt{(\frac{y_{P_j} - y_{P_i}}{x_{P_j} - x_{P_i}})^2 + 1}} \tag{B.1}$$

To find the optimal SSM the algorithm selects the formation with the maximum SSM. the aim than is to maximize the minimum of the SSM.

$$\Rightarrow Max(Min(d_{ij})) \tag{B.2}$$

The first point P_1 runs from $\theta = 0$ to $\theta = \frac{2\pi}{m_{max}}$ and for each position of P_1, $P_i + 1$ is going to run from $\theta_i + \epsilon$ to $\theta_i + \pi$ so that we ensure that G is always inside the polygon of support and to avoid that the next point runs through $\theta > 2\pi$ we test if $\theta_i + \pi - \epsilon > 2\pi$ and if it is the case then $P_i + 1$ is going to run from $\theta_i + \epsilon$ to $2\pi - \epsilon$. The last point $P_{m_{max}}$ must ensure one condition that it must run through $\theta_1 + \pi + \epsilon$ and 2π if $\theta_{m_{max}-1} < \theta_1 + \pi$

else it will run through $\theta_{m_{max}-1}$ and 2π.

Input parameters

Number of used m − bots

Restricted zones

$\mathcal{B}(\theta)$

Output parameters $\mathcal{G} = \{P_1 ... P_{m_{max}}\}$

if *n=2* **then**
| $\theta_2 = \theta_1 + \pi$

else
| $\theta_1 = 0 : \pi - \epsilon$
| $\theta_2 = \theta_1 + \epsilon : \theta_1 + \pi - \epsilon$
| **for** *i=3:n-1* **do**
| | **if** $\theta_{i-1} < pi$ **then**
| | | $\theta_i = \theta_{i-1} + \epsilon : \theta_{i-1} + \pi - \epsilon$
| | **else**
| | | $\theta_i = \theta_{i-1} + \epsilon : 2\pi - \epsilon$
| | **end**
| **end**
| **if** $\theta_{m_{max}-1} < \theta_1 + \pi$ **then**
| | **if** $\theta_{m_{max}-1} + \pi < 2\pi$ **then**
| | | $\theta_{m_{max}} = \theta_1 + \pi + \epsilon : \theta_{m_{max}-1} + \pi - \epsilon$
| | **else**
| | | $\theta_{m_{max}} = \theta_1 + \pi + \epsilon : 2\pi$
| | **end**
| **else**
| | $\theta_{m_{max}} = \theta_{m_{max}-1} + \epsilon : 2\pi$
| **end**
| $\mathcal{G}$=$\{\mathcal{B}(\theta_1), \mathcal{B}(\theta_2), ..., \mathcal{B}(\theta_n)\}$
| For each configuration generated by n points $\mathcal{G}$ calculate the static stability margin SSM d_i.
| Find the Max(min(d_i)).
| Check if the FCG condition is satisfied
| Return the values of θ_i
end

Algorithm 1: Robot positions for a maximal SSM

According to these condition the center of mass of the object G is always inside of the polygon of support while

$$\theta_{i+1} - \theta_i < \pi \mid i = \{1...m_{max} - 1\}$$

Using these conditions we are able to get the set of optimal configurations ensuring a maximum static stability.

In a second part we are supposed to study the Force Closure grasping and to determine the required forces and momentum applied by the robots to ensure object lifting and transport (FC). It is assumed in this phase that the the required robot number n is determined and the desired positions for optimal SSM is defined by the algorithm described in previous section. It is also assumed that the contact is punctual for instance and that each robot i is applying a normal force to the object f_i

$$f_i \in [0, f_{max}] = [0, \mu\mu' m_r g]$$

f_{max} is determined in function of friction coefficient end-effector-object and wheel ground of the robot. In a general case the robots are not acting in the same way if the object has a random shape. Therefore, in order to succeed the manipulation and lifting task we are supposed to determine the required force and momentum generated by each robot with respect to the force constraint. According to the previously described algorithm a form closure maintaining the gravity center of the payload is generated and now it is important to determine the normal and tangential forces to be applied by each robot in order to lift and maintain the object. The study consists of solving the following problem:

$$\begin{pmatrix} \sum_{i=1}^{n} t_i \\ \sum_{i=1}^{n} n_i \\ \sum_{i=1}^{n} \tau_i \end{pmatrix} = \begin{pmatrix} \sum_{i=1}^{n} \mu n_i \\ \sum_{i=1}^{n} n_i \\ \sum_{i=1}^{n} GP_i \times f_i \end{pmatrix} = \begin{pmatrix} M_p g \\ 0 \\ 0 \end{pmatrix}$$

Appendix C

Algorithm results for m-bots positioning

Abstract: *This appendix is dedicated to present the results for mobile robots positioning around a payload of any shape respecting the criteria developed in Chapter 4.*

C.1 Optimal positioning simulations

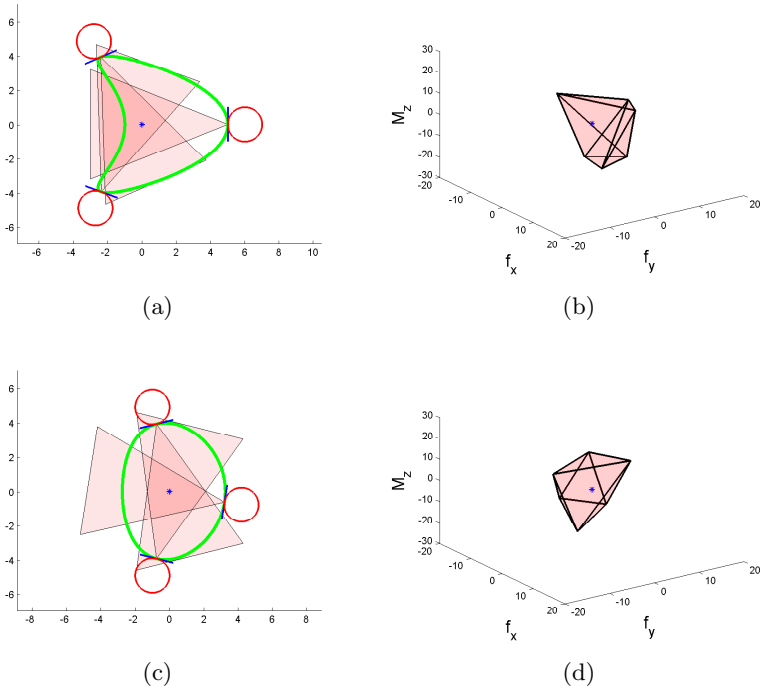

FIGURE C.1: Three robots positioning simulation for different shapes of payload and systems of six wrenches corresponding to the force closure grasps

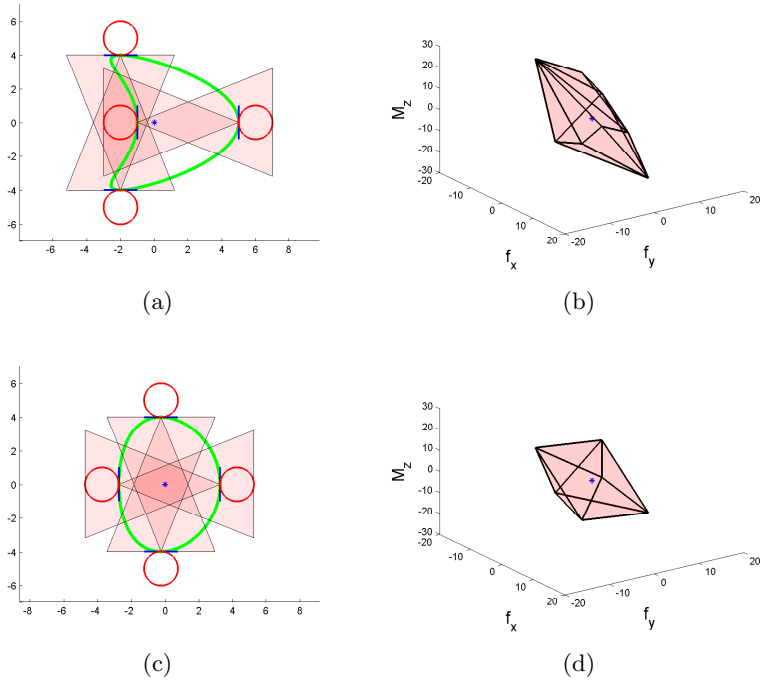

FIGURE C.2: Four robots positioning simulation for different shapes of payload and systems of eight wrenches corresponding to the force-closure grasps

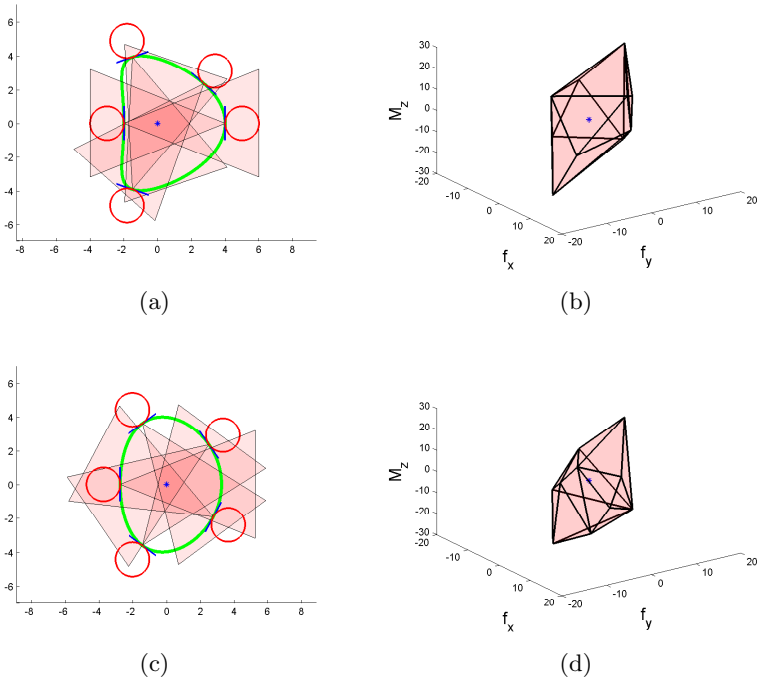

FIGURE C.3: Five robots positioning simulation for different shapes of payload and systems of ten wrenches corresponding to the force-closure grasps

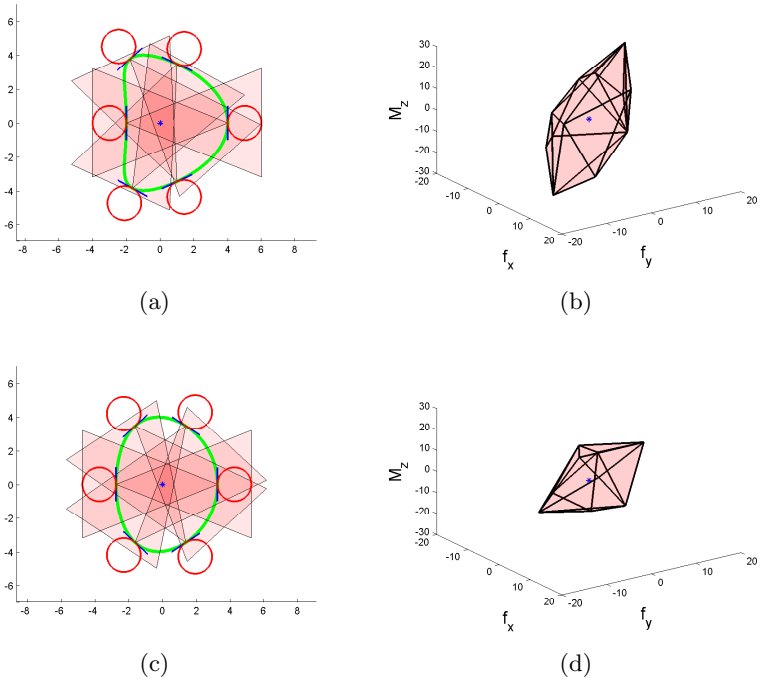

FIGURE C.4: Six robots positioning simulation for different shapes of payload and systems of twelve wrenches corresponding to the force-closure grasps

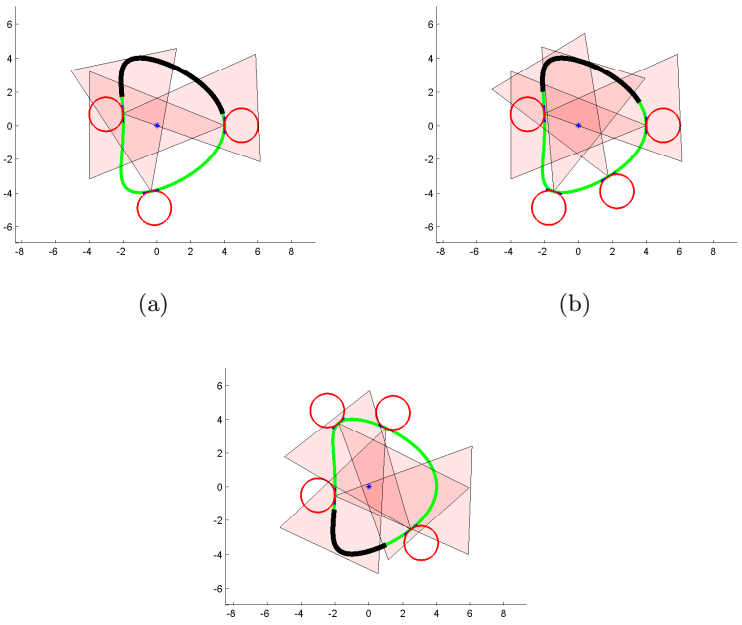

(a) (b)

(c)

FIGURE C.5: M-bots positioning simulation for different shapes of payload with restricted areas

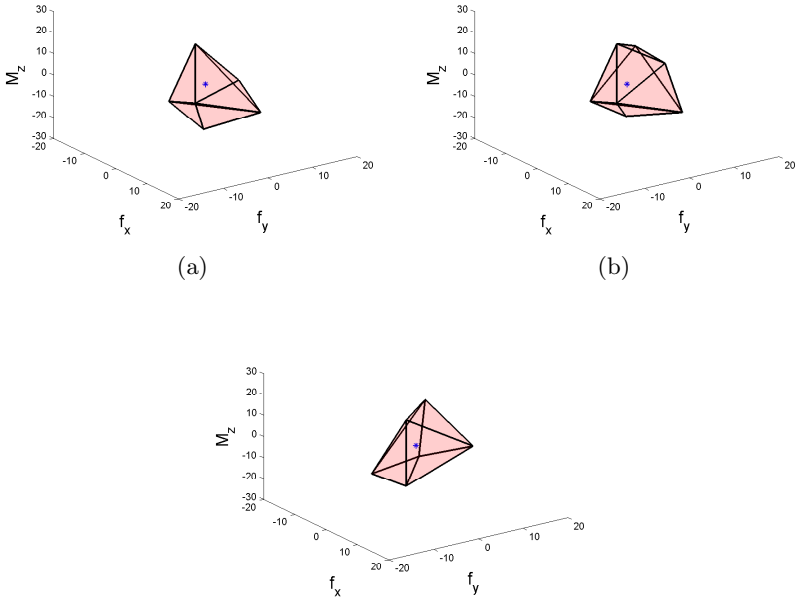

(a) (b)

(c)

FIGURE C.6: Systems of wrenches corresponding to the force-closure grasps shown in Fig. 5.18 respectively, with their convex hull shown as a polyhedron

Bibliography

[1] R. Aachen. rocker harbour crane. http://www.dmg-lib.org/dmglib/main/portal.jsp?mainNaviState=browsen.mecdesc.viewer&id=9025, 2014.

[2] D. Aarno, J. Sommerfeld, D. Kragic, N. Pugeault, S. Kalkan, F. Wörgötter, D. Kraft, and N. Krüger. Early reactive grasping with second order 3d feature relations. In *Recent Progress in Robotics: Viable Robotic Service to Human*, pages 91–105. Springer, 2008.

[3] M. Abou-Samah and V. Krovi. Optimal configuration selection for a cooperating system of mobile manipulators. In *ASME 2002 International Design Engineering Technical Conferences and Computers and Information in Engineering Conference*, pages 1299–1306. American Society of Mechanical Engineers, 2002.

[4] Adept. Research mobile robot. http://www.mobilerobots.com/researchrobots/pioneerp3dx.aspx, Aug. 2014.

[5] L. Adouane. *Architectures de contrôle comportementales et réactives pour la coopération d'un groupe de robots mobiles.* PhD thesis, Université de Franche-Comté, 2005.

[6] L. Adouane. Orbital obstacle avoidance algorithm for reliable and on-line mobile robot navigation. In *9th Conference on Autonomous Robot Systems and Competitions*, 2009.

[7] L. Adouane, A. Benzerrouk, and P. Martinet. Mobile robot navigation in cluttered environment using reactive elliptic trajectories. In *18th IFAC World Congress*, Milano-Italy, August 28, September 2 2011.

[8] L. Adouane, L. Fort-Piat, et al. Hybrid behavioral control architecture for the cooperation of minimalist mobile robots. In *Robotics and Automation, 2004.*

Proceedings. ICRA'04. 2004 IEEE International Conference on, volume 4, pages 3735–3740. IEEE, 2004.

[9] C. S. Agency. Station remote manipulator system. http://www.asc-csa.gc.ca/eng/iss/canadarm2/evolution.asp, 2014.

[10] Y. Aiyama, M. Hara, T. Yabuki, J. Ota, and T. Arai. Cooperative transportation by two four-legged robots with implicit communication. *Robotics and Autonomous Systems*, 29(1):13–19, 1999.

[11] S. A. Ali, E. Hall, M. Ghaffari, and X. Liao. *Mobile robotics, moving intelligence*. INTECH Open Access Publisher, 2006.

[12] P. K. Allen, A. T. Miller, P. Y. Oh, and B. S. Leibowitz. Integration of vision, force and tactile sensing for grasping. In *Int. J. Intelligent Machines*. Citeseer, 1999.

[13] F. B. Amar, C. Grand, G. Besseron, and F. Plumet. Performance evaluation of locomotion modes of an hybrid wheel-legged robot for self-adaptation to ground conditions. In *Proceedings of the 8th ESA Workshop on Advanced Space Technologies for Robotics and Automation, Noordwijk*, pages 1–7. Citeseer, 2004.

[14] J. R. Andrews and N. Hogan. control of manufacturing processes and robotic systems. In *ASME Winter Conference Boston*, pages 243–251, 1983.

[15] T. Arai, E. Pagello, and L. E. Parker. Editorial: Advances in multi-robot systems. *IEEE Transactions on robotics and automation*, 18(5):655–661, 2002.

[16] J. Baca, M. Ferre, and R. Aracil. A heterogeneous modular robotic design for fast response to a diversity of tasks. *Robotics and Autonomous Systems*, 60(4):522–531, 2012.

[17] T. Balch and R. C. Arkin. Behavior-based formation control for multirobot teams. *Robotics and Automation, IEEE Transactions on*, 14(6):926–939, 1998.

[18] G. Baldassarre, S. Nolfi, and D. Parisi. Evolution of collective behavior in a team of physically linked robots. In *Applications of evolutionary computing*, pages 581–592. Springer, 2003.

[19] J. A. Batlle and A. Barjau. Holonomy in mobile robots. *Robotics and Autonomous Systems*, 57(4):433–440, 2009.

[20] J. S. Bay. Design of the "army-ant" cooperative lifting robot. *Robotics & Automation Magazine, IEEE*, 2(1):36–43, 1995.

[21] R. W. Beard, J. Lawton, F. Y. Hadaegh, et al. A coordination architecture for spacecraft formation control. *IEEE Transactions on control systems technology*, 9(6):777–790, 2001.

[22] P. BEN-TZVI. *Hybrid mobile robot system: interchanging locomotion and manipulation.* PhD thesis, University of Toronto, 2008.

[23] A. Benzerrouk. *Architecture de contrôle hybride pour systémes multi-robots mobiles.* Theses, Université Blaise Pascal - Clermont-Ferrand II, Apr. 2011.

[24] A. Benzerrouk, L. Adouane, L. Lequievre, and P. Martinet. Navigation of multi-robot formation in unstructured environment using dynamical virtual structures. In *Intelligent Robots and Systems (IROS), 2010 IEEE/RSJ International Conference on*, pages 5589–5594. IEEE, 2010.

[25] A. Benzerrouk, L. Adouane, and P. Martinet. Stable navigation in formation for a multi-robot system based on a constrained virtual structure. *Robotics and Autonomous Systems (RAS)*, 62(12):1806 – 1815, 2014.

[26] L. Biagiotti and C. Melchiorri. *Trajectory planning for automatic machines and robots.* Springer, 2008.

[27] L. Birglen and F. Herbecq. Self-adaptive compliant grippers capable of pinch preshaping. In *ASME 2009 International Design Engineering Technical Conferences and Computers and Information in Engineering Conference*, pages 249–257. American Society of Mechanical Engineers, 2009.

[28] J. Borenstein and Y. Koren. Real-time obstacle avoidance for fast mobile robots. *Systems, Man and Cybernetics, IEEE Transactions on*, 19(5):1179–1187, 1989.

[29] M. Brady. *Robot motion: Planning and control.* MIT press, 1982.

[30] M. Buehler, R. Playter, and M. Raibert. Robots step outside. In *Int. Symp. Adaptive Motion of Animals and Machines (AMAM), Ilmenau, Germany*, pages 1–4, 2005.

[31] J. Canny. *The complexity of robot motion planning*. MIT press, 1988.

[32] D. Christian, D. Wettergreen, M. Bualat, K. Schwehr, D. Tucker, and E. Zbinden. Field experiments with the ames marsokhod rover. In *Field and Service Robotics*, pages 96–103. Springer, 1998.

[33] J. E. Clark, J. G. Cham, S. A. Bailey, E. M. Froehlich, P. K. Nahata, R. J. Full, and M. R. Cutkosky. Biomimetic design and fabrication of a hexapedal running robot. In *Robotics and Automation, 2001. Proceedings 2001 ICRA. IEEE International Conference on*, volume 4, pages 3643–3649. IEEE, 2001.

[34] W. W. Cohen. Adaptive mapping and navigation by teams of simple robots. *Robotics and autonomous systems*, 18(4):411–434, 1996.

[35] L. Consolini, F. Morbidi, D. Prattichizzo, and M. Tosques. Leader–follower formation control of nonholonomic mobile robots with input constraints. *Automatica*, 44(5):1343–1349, 2008.

[36] M. Deng, A. Inoue, K. Sekiguchi, and L. Jiang. Two-wheeled mobile robot motion control in dynamic environments. *Robotics and Computer-Integrated Manufacturing*, 26(3):268–272, 2010.

[37] D. Ding, Y.-H. Liu, and S. Wang. Computing 3-d optimal form-closure grasps. In *Robotics and Automation, 2000. Proceedings. ICRA'00. IEEE International Conference on*, volume 4, pages 3573–3578. IEEE, 2000.

[38] M. Dorigo, D. Floreano, L. M. Gambardella, F. Mondada, S. Nolfi, T. Baaboura, M. Birattari, M. Bonani, M. Brambilla, A. Brutschy, et al. Swarmanoid. *IEEE Robotics & Automation Magazine*, 1070(9932/13), 2013.

[39] G. Dudek and M. Jenkin. *Computational principles of mobile robotics*. Cambridge university press, 2010.

[40] V. EDR. Elavator. http://curriculum.vexrobotics.com/curriculum/lifting-mechanisms/elevators, 2014.

[41] S. Ekvall and D. Kragic. Interactive grasp learning based on human demonstration. In *Robotics and Automation, 2004. Proceedings. ICRA'04. 2004 IEEE International Conference on*, volume 4, pages 3519–3524. IEEE, 2004.

[42] S. El-Khoury, A. Sahbani, and P. Bidaud. 3d objects grasps synthesis: A survey. In *13th World Congress in Mechanism and Machine Science*, pages 573–583, 2011.

[43] Elmo-Motion-Control. Autonomous solutions. http://www.elmomc.com/applications/high-mobility-robot.htm, Aug. 2014.

[44] O. C. Engineering Services Inc., Toronto. http://www.esit.com, 2015.

[45] D. A. Eppert. Load-measuring, fleet asset tracking and data management system for load-lifting vehicles, May 11 2012. US Patent App. 14/004,884.

[46] T. Estier, Y. Crausaz, B. Merminod, M. Lauria, R. Piguet, R. Y. Siegwart, B. Merminod, B. Merminod, R. Y. Siegwart, and R. Y. Siegwart. *An innovative space rover with extended climbing abilities*. ETH-Zürich, 2000.

[47] J. Estremera, J. A. Cobano, and P. Gonzalez de Santos. Continuous free-crab gaits for hexapod robots on a natural terrain with forbidden zones: An application to humanitarian demining. *Robotics and Autonomous Systems*, 58(5):700–711, 2010.

[48] J. Fauroux, B. Bouzgarrou, and F. Chapelle. Experimental validation of stable obstacle climbing with a four-wheel mobile robot openwheel i3r. In *Proceedings of International Conference on Mechanisms and Mechanical Transmissions, MTM*, volume 8, pages 8–10, 2008.

[49] J.-C. Fauroux, B.-C. Bouzgarrou, N. Bouton, P. Vaslin, R. Lenain, and F. Chapelle. Agile wheeled mobile robots for service in natural environment.

[50] J.-C. FAUROUX, B.-C. BOUZGARROU, and M. KRID. Unité robotique de transport de charges longues, 2015. PCT patent. IFMA 23p.

[51] J.-C. Fauroux, F. Chapelle, and B. Bouzgarrou. A new principle for climbing wheeled robots: Serpentine climbing with the open wheel platform. In *Intelligent Robots and Systems, 2006 IEEE/RSJ International Conference on*, pages 3405–3410. IEEE, 2006.

[52] J.-C. Fauroux, F. Chapelle, B.-C. Bouzgarrou, P. Vaslin, M. Krid, and M. Davis. Mechatronic design of mobile robots for stable obstacle crossing at low and high speeds.

[53] Festo. Compliant manipulator. http://www.robaid.com/bionics/festo-bionic-handling-assistant-inspired-by-elephants-trunk.htm, Nov. 2014.

[54] M. Fischer, P. van der Smagt, and G. Hirzinger. Learning techniques in a dataglove based telemanipulation system for the dlr hand. In *Robotics and Automation, 1998. Proceedings. 1998 IEEE International Conference on*, volume 2, pages 1603–1608. IEEE, 1998.

[55] S. Fletcher and D. Agg. Lift for a vehicle, Aug. 28 2013. EP Patent App. EP20,130,156,587.

[56] P. for global wholesale trade. http://www.alibaba.com/product-detail/3-in-1-robot-vacuum-cleaner_413047693/showimage.html, Aug. 2014.

[57] D. Fox, W. Burgard, and S. Thrun. The dynamic window approach to collision avoidance. *IEEE Robotics & Automation Magazine*, 4(1):23–33, 1997.

[58] R. R. Fox and J. L. Smith. A psychophysical study of high-frequency arm lifting. *International Journal of Industrial Ergonomics*, 2012.

[59] T. free encyclopedia Wikipedia. Ackermann steering geometry, 2014.

[60] T. Frost, C. Norman, S. Pratt, B. Yamauchi, B. McBride, and G. Peri. Derived performance metrics and measurements compared to field experience for the packbot. *NIST Special Publication*, (990):201–208, 2002.

[61] T. J. Galla. Lifting mechanism with lift stand accommodation, Apr. 1 2014. US Patent 8,684,332.

[62] J. Ghommam, H. Mehrjerdi, and M. Saad. Robust formation control without velocity measurement of the leader robot. *Control Engineering Practice*, 21(8):1143–1156, 2013.

[63] A. Gil-Pinto, P. Fraisse, R. Zapata, et al. A decentralized adaptive trajectory planning approach for a group of mobile robots. In *TAROS'05: Towards Autonomous Robotic Systems*, pages 65–72, 2005.

[64] R. i. Gladiator Mobile Robot. http://www.ri.cmu.edu, 2015.

[65] K. Goris. Autonomous mobile robot mechanical design. *VrijeUniversiteitBrussel, Engineering Degree Thesis, Brussels, Belgium*, 2005.

[66] C. Grand, F. Benamar, F. Plumet, and P. Bidaud. Stability and traction optimization of a reconfigurable wheel-legged robot. *The International Journal of Robotics Research*, 23(10-11):1041–1058, 2004.

[67] E.-H. Guechi. *Suivi de trajectoires d'un robot mobile non holonome: approche par modéle flou de Takagi-Sugeno et prise en compte des retards.* PhD thesis, Université de Valenciennes et du Hainaut-Cambresis, 2010.

[68] S. Hayati, R. Volpe, P. Backes, J. Balaram, R. Welch, R. Ivlev, G. Tharp, S. Peters, T. Ohm, R. Petras, et al. The rocky 7 rover: A mars sciencecraft prototype. In *Robotics and Automation, 1997. Proceedings., 1997 IEEE International Conference on*, volume 3, pages 2458–2464. IEEE, 1997.

[69] S. Herrera. Lifting mechanism for a storage bed base and storage bed base provided with the same, July 11 2012. EP Patent 2,338,382.

[70] B. HICHRI. Simulation and experimental results for a group of mobile robots manipulating a payload. https://www.dropbox.com/sh/cvw6e52fwo7wsr7/AAAVKQ7rFbFcKtpZrs4oOlbka?dl=0, July 2015.

[71] B. Hichri, L. Adouane, Fauroux, , and I. Mezouar, Y Doroftei. Cooperative mobile robot control architecture for lifting and transportation of any shape payload. In *Distributed Autonomous Robotic Systems.*

[72] B. Hichri, J.-C. Fauroux, L. Adouane, I. Doroftei, and Y. Mezouar. Lifting mechanism for payload transport by collaborative mobile robots. In *New Trends in Mechanism and Machine Science*, pages 157–165. Springer, 2015.

[73] B. Hichri, J. C. Fauroux, L. Adouane, Y. Mezouar, and I. Doroftei. Design of collaborative, cross & carry mobile robots" c3bots". *Advanced Materials Research*, 837:588–593, 2014.

[74] K. A. H. K. H. Hirata, Y. Kosuge and K. Kawabata. Transportation of an object by multiple distributed robot helpers in cooperation with a human. 68(668):1207–1214, 2002.

[75] M. Hofbaur, M. Brandstotter, S. Jantscher, and C. Schorghuber. Modular reconfigurable robot drives. In *Robotics Automation and Mechatronics (RAM), 2010 IEEE Conference on*, pages 150–155. IEEE, 2010.

[76] R. Holmberg. *Design and Development of Powered-Castor Holonomic Mobile Robots*. Stanford University,, 2000.

[77] S. M. Hsiang, G. E. Brogmus, and T. K. Courtney. Low back pain (lbp) and lifting technique:a review. *International Journal of Industrial Ergonomics*, 19(1):59–74, 1997.

[78] M. Hueser, T. Baier, and J. Zhang. Learning of demonstrated grasping skills by stereoscopic tracking of human head configuration. In *Robotics and Automation, 2006. ICRA 2006. Proceedings 2006 IEEE International Conference on*, pages 2795–2800. IEEE, 2006.

[79] IFR. World robotics 2014 industrial robots, 2015.

[80] A. J. Ijspeert, A. Martinoli, A. Billard, and L. M. Gambardella. Collaboration through the exploitation of local interactions in autonomous collective robotics: The stick pulling experiment. *Autonomous Robots*, 11(2):149–171, 2001.

[81] D. S. S. INC. Automatic storage retrieval systems (asrs). http://www.dynamicstorage.com/asrs.html, Aug. 2014.

[82] IRobot. Robots de défense et sécurité. http://www.irobot.fr/a-propos-d-irobot/defense-securite, Aug. 2014.

[83] A. Ishiguro, M. Shimizu, and T. Kawakatsu. A modular robot that exhibits amoebic locomotion. *Robotics and Autonomous Systems*, 54(8):641–650, 2006.

[84] C. J-P. Elevateur pour mise en place des equipements de chantier, Sept.

[85] B. Johann and K. Yoram. Vector field histogram method. http://www-personal.umich.edu/~johannb/vff&vfh.htm, 2015.

[86] M. W. Jorgensen, E. H. Ostergaard, and H. H. Lund. Modular atron: Modules for a self-reconfigurable robot. In *Intelligent Robots and Systems, 2004.(IROS 2004). Proceedings. 2004 IEEE/RSJ International Conference on*, volume 2, pages 2068–2073. IEEE, 2004.

[87] K-Team. The khepera ii mobile platform. http://www.k-team.com/mobile-robotics-products/old-products/khepera-ii, Aug. 2014.

[88] Y. Kanayama, Y. Kimura, F. Miyazaki, and T. Noguchi. A stable tracking control method for a non-holonomic mobile robot. In *Intelligent Robots and Systems' 91.'Intelligence for Mechanical Systems, Proceedings IROS'91. IEEE/RSJ International Workshop on*, pages 1236–1241. IEEE, 1991.

[89] K. Kanjanawanishkul. Formation control of mobile robots: survey. *eng. ubu. ac. th*, pages 50–64, 2005.

[90] I. Karabegović, E. Karabegović, and E. Husak. Industrial robots and their application in serving cnc machine tools.

[91] O. KAZUYA, H. TOSHIHIRO, F. MASAKAZU, S. NOBUHIRO, and S. MITSUHARU. Development for industrial robotics applications. *IHI Engineering review*, 42(2):103–107, 2009.

[92] S. Kernbach, E. Meister, F. Schlachter, K. Jebens, M. Szymanski, J. Liedke, D. Laneri, L. Winkler, T. Schmickl, R. Thenius, et al. Symbiotic robot organisms: Replicator and symbrion projects. In *Proceedings of the 8th Workshop on Performance Metrics for Intelligent Systems*, pages 62–69. ACM, 2008.

[93] W. Khalil and E. Dombre. *Modélisation, identification et commande des robots*. Hermès science publ., 1999.

[94] W. Khalil and E. Dombre. *Modeling, identification and control of robots*. Butterworth-Heinemann, 2004.

[95] O. Khatib. Real-time obstacle avoidance for manipulators and mobile robots. *The international journal of robotics research*, 5(1):90–98, 1986.

[96] O. Khatib, K. Yokoi, O. Brock, K. Chang, and A. Casal. Robots in human environments: Basic autonomous capabilities. *The International Journal of Robotics Research*, 18(7):684–696, 1999.

[97] B. KIM and P. TSIOTRAS. Experimental comparison of control laws for unicycle-type mobile robots. *sat*, 1(2):9.

[98] D.-H. Kim and J.-H. Kim. A real-time limit-cycle navigation method for fast mobile robots and its application to robot soccer. *Robotics and Autonomous Systems*, 42(1):17–30, 2003.

[99] B. Klaassen, R. Linnemann, D. Spenneberg, and F. Kirchner. Biomimetic walking robot scorpion: Control and modeling. *Robotics and autonomous systems*, 41(2):69–76, 2002.

[100] N. Y. Ko and R. G. Simmons. The lane-curvature method for local obstacle avoidance. In *Intelligent Robots and Systems, 1998. Proceedings., 1998 IEEE/RSJ International Conference on*, volume 3, pages 1615–1621. IEEE, 1998.

[101] Y. Koren and J. Borenstein. Potential field methods and their inherent limitations for mobile robot navigation. In *Robotics and Automation, 1991. Proceedings., 1991 IEEE International Conference on*, pages 1398–1404. IEEE, 1991.

[102] A. Krebs, T. Thueer, E. Carrasco, R. Y. Siegwart, R. Y. Siegwart, and R. Y. Siegwart. *Towards torque control of the CRAB rover*. Eidgenössische Technische Hochschule Zürich, Autonomous Systems Lab, 2008.

[103] M. Krid, J. Fauroux, and B. Bouzgarrou. Modular cooperative mobile robots for ventral long payload transport and obstacle crossing. In *New Trends in Mechanism and Machine Science*, pages 211–219. Springer, 2015.

[104] B. H. Krogh and C. E. Thorpe. Integrated path planning and dynamic steering control for autonomous vehicles. In *Robotics and Automation. Proceedings. 1986 IEEE International Conference on*, volume 3, pages 1664–1669. IEEE, 1986.

[105] T. Kubota, Y. Kuroda, Y. Kunii, and I. Nakatani. Small, light-weight rover "micro5" for lunar exploration. *Acta Astronautica*, 52(2):447–453, 2003.

[106] S. H. Kunkel and J. M. Leatherman. Multidimensional lifting handtruck, Aug. 31 2009. US Patent App. 12/550,778.

[107] Y. Kuroda, K. Kondo, K. Nakamura, Y. Kunii, and T. Kubota. Low power mobility system for micro planetary rover micro 5. In *Artificial Intelligence, Robotics and Automation in Space*, volume 440, page 77, 1999.

[108] H. Kurokawa, E. Yoshida, K. Tomita, A. Kamimura, S. Murata, and S. Kokaji. Self-reconfigurable m-tran structures and walker generation. *Robotics and Autonomous Systems*, 54(2):142–149, 2006.

[109] F. Kyota, T. Watabe, S. Saito, and M. Nakajima. Detection and evaluation of grasping positions for autonomous agents. In *Cyberworlds, 2005. International Conference on*, pages 8–pp. IEEE, 2005.

[110] A. S. Lab. The alice microrobot. http://www.hizook.com/projects/alice, Aug. 2014.

[111] D. Laboratory. Autonoumous robotic systems. http://www.draper.com/, 2015.

[112] J.-W. Li, M.-H. Jin, and H. Liu. A new algorithm for three-finger force-closure grasp of polygonal objects. In *Robotics and Automation, 2003. Proceedings. ICRA'03. IEEE International Conference on*, volume 2, pages 1800–1804. IEEE, 2003.

[113] N. A. Limited. Robot wheels. http://www.microrobo.com/100mm-mecanum-wheel-right-w092.html, 2014.

[114] B. S. Lin and S.-M. Song. Dynamic modeling, stability, and energy efficiency of a quadrupedal walking machine. *Journal of Robotic Systems*, 18(11):657–670, 2001.

[115] S.-C. LIU, D.-L. TAN, and G.-J. LIU. Robust leader-follower formation control of mobile robots based on a second order kinematics model. *Acta Automatica Sinica*, 33(9):947–955, 2007.

[116] Y.-H. Liu. Qualitative test and force optimization of 3-d frictional form-closure grasps using linear programming. *Robotics and Automation, IEEE Transactions on*, 15(1):163–173, 1999.

[117] P. Lucidarme, O. Simonin, et al. Implementation and evaluation of a satisfaction/altruism based architecture for multi-robot systems. In *Robotics and Automation, 2002. Proceedings. ICRA'02. IEEE International Conference on*, volume 1, pages 1007–1012. IEEE, 2002.

[118] J. D. Martens and W. S. Newman. Stabilization of a mobile robot climbing stairs. In *Robotics and Automation, 1994. Proceedings., 1994 IEEE International Conference on*, pages 2501–2507. IEEE, 1994.

[119] M. J. Mataric, M. Nilsson, and K. T. Simsarin. Cooperative multi-robot box-pushing. In *Intelligent Robots and Systems 95.'Human Robot Interaction and Cooperative Robots', Proceedings. 1995 IEEE/RSJ International Conference on*, volume 3, pages 556–561. IEEE, 1995.

[120] E. Mattar. A survey of bio-inspired robotics hands implementation: New directions in dexterous manipulation. *Robotics and Autonomous Systems*, 61(5):517–544, 2013.

[121] R. B. McGhee and A. A. Frank. On the stability properties of quadruped creeping gaits. *Mathematical Biosciences*, 3:331–351, 1968.

[122] H. Mehrjerdi, J. Ghommam, and M. Saad. Nonlinear coordination control for a group of mobile robots using a virtual structure. *Mechatronics*, 21(7):1147 – 1155, 2011.

[123] V.-D. Nguyen. Constructing stable grasps in 3d. In *Robotics and Automation. Proceedings. 1987 IEEE International Conference on*, volume 4, pages 234–239. IEEE, 1987.

[124] M. Nieuwenhuisen, M. Schadler, and S. Behnke. Predictive potential field-based collision avoidance for multicopters. *ISPRS-International Archives of the Photogrammetry, Remote Sensing and Spatial Information Sciences*, 1(2):293–298, 2013.

[125] N. J. Nilsson. A mobius automation: An application of artificial intelligence techniques. In *Proceedings of the 1st International Joint Conference on Artificial Intelligence*, IJCAI'69, pages 509–520, San Francisco, CA, USA, 1969. Morgan Kaufmann Publishers Inc.

[126] F. of Engineering. The oddbot omni-directionnal mobile platform. http://homepages.engineering.auckland.ac.nz/~pxu012/mechatronics2012/group5/hardware/default.html, 2015.

[127] P. Ogren, E. Fiorelli, and N. E. Leonard. Formations with a mission: Stable coordination of vehicle group maneuvers. In *Symposium on mathematical theory of networks and systems*, 2002.

[128] D. E. Orin, R. B. McGhee, and V. Jaswa. Interactive compute-control of a six-legged robot vehicle with optimization of stability, terrain adaptibility and energy. In *Decision and Control including the 15th Symposium on Adaptive Processes, 1976 IEEE Conference on*, volume 15, pages 382–391. IEEE, 1976.

[129] L. E. Parker. Lifelong adaptation in heterogeneous multi-robot teams: Response to continual variation in individual robot performance. *Autonomous Robots*, 8(3):239–267, 2000.

[130] Z. Peng. *Formation Control of Multiple Nonholonomic Wheeled Mobile Robots*. PhD thesis, Ecole Centrale de Lille, 2013.

[131] G. Pessotto. Articulated bed with lifting mechanism, July 13 2011. EP Patent 2,108,288.

[132] F. G. Pin and S. M. Killough. A new family of omnidirectional and holonomic wheeled platforms for mobile robots. *Robotics and Automation, IEEE Transactions on*, 10(4):480–489, 1994.

[133] N. Pino. A screw and pantograph lifting jack, particularly for a motor vehicle, Nov. 21 2001. EP Patent 0,771,757.

[134] A. Plamondon, A. Delisle, S. Bellefeuille, D. Denis, D. Gagnon, and C. Larivière. Lifting strategies of expert and novice workers during a repetitive palletizing task. *Applied ergonomics*, 45(3):471–481, 2014.

[135] F. Pourboghrat. Exponential stabilization of nonholonomic mobile robots. *Computers & Electrical Engineering*, 28(5):349–359, 2002.

[136] Probst. Boulder grab mechanical. http://www.speedyservices.com/73_5075-h-boulder-grab-mechanical-fvz-uni-1-5t-swl, 2015.

[137] T. M. Quasny, L. D. Pyeatt, and J. L. Moore. Curvature-velocity method for differentially steered robots. In *Modelling, Identification and Control*, pages 618–622, 2003.

[138] C. Queiroz, N. Gonçalves, and P. Menezes. A study on static gaits for a four leg robot. In *Proc. CONTROL 2000-UK ACC Int. Conf. on Control*, 1999.

[139] D. Rabinowitz, R. Bridger, and M. Lambert. Lifting technique and abdominal belt usage: a biomechanical, physiological and subjective investigation. *Safety science*, 28(3):155–164, 1998.

[140] K. S. Raghuwaiya, S. Singh, and J. Vanualailai. Formation control of mobile robots. *World Academy of Science, Engineering and Technology*, 60:762–767, 2011.

[141] M. Raibert, K. Blankespoor, G. Nelson, R. Playter, et al. Bigdog, the rough-terrain quadruped robot. In *Proceedings of the 17th World Congress*, volume 17, pages 10822–10825, 2008.

[142] W. Ren and N. Sorensen. Distributed coordination architecture for multi-robot formation control. *Robotics and Autonomous Systems*, 56(4):324–333, 2008.

[143] M. Riedel, M. Nefzi, and B. Corves. Grasp planning for a reconfigurable parallel robot with an underactuated arm structure. 2010.

[144] RoboMatter. Robotics education store. http://robomatter.com/, 2015.

[145] A. Sadowska, T. v. den Broek, H. Huijberts, N. van de Wouw, D. Kostić, and H. Nijmeijer. A virtual structure approach to formation control of unicycle mobile robots using mutual coupling. *International Journal of Control*, 84(11):1886–1902, 2011.

[146] A. D. Sadowska. *Formation control of nonholonomic mobile robots: the virtual structure approach*. PhD thesis, Queen Mary University of London, 2012.

[147] A. Sahbani, S. El-Khoury, and P. Bidaud. An overview of 3d object grasp synthesis algorithms. *Robotics and Autonomous Systems*, 60(3):326–336, 2012.

[148] J. Sasaki, J. Ota, E. Yoshida, D. Kurabayashi, and T. Arai. Cooperating grasping of a large object by multiple mobile robots. In *Robotics and Automation, 1995. Proceedings., 1995 IEEE International Conference on*, volume 1, pages 1205–1210. IEEE, 1995.

[149] D. A. Schipper. *Mobile Autonomous Robot Twente, a mechatronics design approach*. Twente University Press, 2001.

[150] J. T. Schwartz and M. Sharir. On the piano movers' problem: Iii. coordinating the motion of several independent bodies: the special case of circular bodies moving amidst polygonal barriers. *The International Journal of Robotics Research*, 2(3):46–75, 1983.

[151] B. Sezen. Modeling automated guided vehicle systems in material handling= otomatikleştirilmiş rehberli araç sistemlerinin transport tekniğinde modellemesi. *Doğuş Üniversitesi Dergisi*, 4(2):207–216, 2011.

[152] R. Siegwart, P. Lamon, T. Estier, M. Lauria, and R. Piguet. Innovative design for wheeled locomotion in rough terrain. *Robotics and Autonomous systems*, 40(2):151–162, 2002.

[153] R. Siegwart, I. R. Nourbakhsh, and D. Scaramuzza. *Introduction to autonomous mobile robots*. MIT press, 2011.

[154] R. Simmons. The curvature-velocity method for local obstacle avoidance. In *Robotics and Automation, 1996. Proceedings., 1996 IEEE International Conference on*, volume 4, pages 3375–3382. IEEE, 1996.

[155] O. Simonin, A. Liégeois, and P. Rongier. An architecture for reactive cooperation of mobile distributed robots. In *Distributed Autonomous Robotic Systems 4*, pages 35–44. Springer, 2000.

[156] M. G. Slack. Navigation templates: mediating qualitative guidance and quantitative control in mobile robots. *Systems, Man and Cybernetics, IEEE Transactions on*, 23(2):452–466, 1993.

[157] Softdesign. Automated guided vehicles (agv). http://www.softdesign.se/newversion/english/agvindex.asp?gclid=CImA0K7c1sACFYmE2wodzy8AtQ, Aug. 2014.

[158] K. Stoy. Using situated communication in distributed autonomous mobile robotics. In *SCAI-01: Proceedings of the Seventh Scandinavian Conference on Artificial Intelligence*, pages 44–52, 2001.

[159] A. Stuart and A. R. Humphries. *Dynamical systems and numerical analysis*, volume 2. Cambridge University Press, 1998.

[160] T. Sugar and V. Kumar. Decentralized control of cooperating mobile manipulators. In *Robotics and Automation, 1998. Proceedings. 1998 IEEE International Conference on*, volume 4, pages 2916–2921. IEEE, 1998.

[161] S. Sugita, K. Ogami, M. Guarnieri, S. Hirose, and K. Takita. A study on the mechanism and locomotion strategy for new snake-like robot active cord mechanism-slime model 1 acm-s1. *Journal of Robotics and Mechatronics*, 20(2):302–309, 2008.

[162] H. G. Tanner, S. G. Loizou, and K. J. Kyriakopoulos. Nonholonomic stabilization with collision avoidance for mobile robots. In *IROS*, pages 1220–1225, 2001.

[163] T. Thueer and R. Siegwart. Mobility evaluation of wheeled all-terrain robots. *Robotics and autonomous systems*, 58(5):508–519, 2010.

[164] D. J. Todd. *Walking machines: an introduction to legged robots*. Chapman & Hall, 1985.

[165] A. A. Transeth, R. I. Leine, C. Glocker, K. Y. Pettersen, and P. Liljeback. Snake robot obstacle-aided locomotion: Modeling, simulations, and experiments. *Robotics, IEEE Transactions on*, 24(1):88–104, 2008.

[166] D. G. Ullman. *The mechanical design process*, volume 2. McGraw-Hill New York, 1992.

[167] I. Ulrich and J. Borenstein. Vfh+: Reliable obstacle avoidance for fast mobile robots. In *Robotics and Automation, 1998. Proceedings. 1998 IEEE International Conference*, volume 2, pages 1572–1577. IEEE, 1998.

[168] S. M. C. university press. differential drive. http://planning.cs.uiuc.edu/node659.html, 2014.

[169] T. van den Broek, N. van de Wouw, and H. Nijmeijer. A virtual structure approach to formation control of unicycle mobile robots. *Eindhoven University of Technology, the Netherlands, Tech. Rep. DCT*, 2009, 2009.

[170] T. H. van den Broek, N. van de Wouw, and H. Nijmeijer. Formation control of unicycle mobile robots: a virtual structure approach. In *Decision and Control, 2009 held jointly with the 2009 28th Chinese Control Conference. CDC/CCC 2009. Proceedings of the 48th IEEE Conference on*, pages 8328–8333. IEEE, 2009.

[171] F. Van Oirschot. Patient lifting device, June 7 2013. US Patent App. 13/912,726.

[172] J. Vilca, L. Adouane, and Y. Mezouar. Adaptive leader-follower formation in cluttered environment using dynamic target reconfiguration. In *Distributed Autonomous Robotic Systems*.

[173] J. Vilca, L. Adouane, Y. Mezouar, and P. Lebraly. An overall control strategy based on target reaching for the navigation of an urban electric vehicle. In *Intelligent Robots and Systems (IROS), 2013 IEEE/RSJ International Conference on*, pages 728–734. IEEE, 2013.

[174] I. F. Vis. Survey of research in the design and control of automated guided vehicle systems. *European Journal of Operational Research*, 170(3):677–709, 2006.

[175] R. Volpe, J. Balaram, T. Ohm, and R. Ivlev. Rocky 7: A next generation mars rover prototype. *Advanced Robotics*, 11(4):341–358, 1996.

[176] J.-Y. Wang, J.-S. Zhao, F.-L. Chu, and Z.-J. Feng. Innovative design of the lifting mechanisms for forklift trucks. *Mechanism and Machine Theory*, 45(12):1892–1896, 2010.

[177] Z. Wang, X. Ding, A. Rovetta, and A. Giusti. Mobility analysis of the typical gait of a radial symmetrical six-legged robot. *Mechatronics*, 21(7):1133–1146, 2011.

[178] P. Wells and D. Deguire. Talon: A universal unmanned ground vehicle platform, enabling the mission to be the focus. In *Defense and Security*, pages 747–757. International Society for Optics and Photonics, 2005.

[179] D. Wettergreen, D. Bapna, M. Maimone, and G. Thomas. Developing nomad for robotic exploration of the atacama desert. *Robotics and Autonomous Systems*, 26(2):127–148, 1999.

[180] D. Wettergreen, M. Bualat, D. Christian, K. Schwehr, H. Thomas, D. Tucker, and E. Zbinden. Operating nomad during the atacama desert trek. In *Field and Service Robotics*, pages 82–89. Springer, 1998.

[181] J. White, J. Coughlan, M. Harvey, R. Upton, and K. Walker. Taking andros [a robot] for a walk [remote technology]. 1989.

[182] J. R. White, T. Sunagawa, and T. Nakajima. Hazardous-duty robots-experiences and needs. In *Intelligent Robots and Systems' 89. The Autonomous Mobile Robots and Its Applications. IROS'89. Proceedings., IEEE/RSJ International Workshop on*, pages 262–267. IEEE, 1989.

[183] B. H. Wilcox, T. Litwin, J. Biesiadecki, J. Matthews, M. Heverly, J. Morrison, J. Townsend, N. Ahmad, A. Sirota, and B. Cooper. Athlete: A cargo handling and manipulation robot for the moon. *Journal of Field Robotics*, 24(5):421–434, 2007.

[184] J. Wu and Z. Jiang. Formation control of multiple mobile robots via switching strategy. *Int. J. of Information and Systems Sciences, 5 (6)*, pages 210–218, 2009.

[185] H. Yamaguchi, M. Mori, and A. Kawakami. Control of a five-axle, three-steering coupled-vehicle system and its experimental verification. In *World Congress*, volume 18, pages 12976–12984, 2011.

[186] A. Yamashita, M. Fukuchi, J. Ota, T. Arai, and H. Asama. Motion planning for cooperative transportation of a large object by multiple mobile robots in a 3d environment. In *Robotics and Automation, 2000. Proceedings. ICRA'00. IEEE International Conference on*, volume 4, pages 3144–3151. IEEE, 2000.

[187] A. Yamashita, J. Sasaki, J. Ota, and T. Arai. Cooperative manipulation of objects by multiple mobile robots with tools. In *Proceedings of the 4th Japan-France/2nd Asia-Europe Congress on Mechatronics*, volume 310, page 315. Citeseer, 1998.

[188] A. Yassi. Repetitive strain injuries. *The Lancet*, 349(9056):943–947, 1997.

[189] M. Yim, W.-M. Shen, B. Salemi, D. Rus, M. Moll, H. Lipson, E. Klavins, and G. S. Chirikjian. Modular self-reconfigurable robot systems. *IEEE Robotics & Automation Magazine*, 14(1):2–11, 2007.

[190] T. Yoshikawa. Multifingered robot hands: Control for grasping and manipulation. *Annual Reviews in Control*, 34(2):199–208, 2010.

[191] R. Zapata, P. Lépinay, and P. Thompson. Reactive behaviors of fast mobile robots. *Journal of Robotic Systems*, 11(1):13–20, 1994.

Abstract: Our goal in the proposed work is to design and control a group of similar mobile robots with a simple architecture, called m-bot. Several m-bots can grip a payload, in order to co-manipulate and transport it, whatever its shape and mass. The resulting robot is called a p-bot and is capable to solve the so-called "removal-man task" to transport a payload. Reconfiguring the p-bot by adjusting the number of m-bots allows to manipulate heavy objects and to manage objects with any shape, particularly if they are larger than a single m-bot. Obstacle avoidance is addressed and mechanical stability of the p-bot and its payload is permanently guaranteed. A proposed kinematic architecture for a manipulation mechanism is studied. This mechanism allows to lift a payload and put it on the m-bot body in order to be transported. The mobile platform has a free steering motion allowing the system manoeuvre in any direction. An optimal positioning of the m-bots around the payload ensures a successful task achievement without loss of stability for the overall system. The positioning algorithm respects the **F**orce **C**losure **G**rasping (**FCG**) criterion which ensures the payload stability during the manipulation phase. It respects also the **S**tatic **S**tability **M**argin (**SSM**) criterion which guarantees the payload stability during the transport. Finally it considers also the **R**estricted **A**reas (**RA**) that could not be reached by the robots to grab the payload. A predefined control law is then used to ensure the **T**arget **R**eaching (**TR**) phase of each m-bot to its desired position around the payload and to track a **V**irtual **S**tructure (**VS**), during the transportation phase, in which each elementary robot has to keep the desired position relative to the payload. Simulation results for an object of any shape, described by a parametric curve, are presented. Additional 3D simulation results with a multi-body dynamic software and experiments by manufactured prototypes validate our proposal.

Keyword: Cooperative mobile robots, Control architecture, Payload transport and co-manipulation, Lifting mechanism, Force closure grasping, Static stability margin, Restricted areas, Obstacle avoidance, Target reaching, Virtual structure navigation.

Résumé: L'objectif du travail proposé est de concevoir et commander un groupe des robots mobiles similaires et d'architecture simple appelés m-bots (mono-robots). Plusieurs m-bots ont la capacité de saisir ensemble un objet afin d'assurer sa co-manipulation et son transport quelle que soit sa forme et sa masse. Le robot résultant est appelé p-bot (poly-robot) et est capable d'effectuer des tâches de déménageur pour le transport d'objets génériques. La reconfigurabilité du p-bot par l'ajustement du nombre des m-bots utilisés permet de manipuler des objets lourds et des objets de formes quelconques (particulièrement s'ils sont plus larges qu'un seul m-bot). Sont considérés dans ce travail l'évitement d'obstacle ainsi que la stabilité du p-bot incluant la charge à transporter. Une cinématique pour un mécanisme de manipulation a été proposée et étudiée. Ce dernier assure le levage de la charge et son dépôt sur le corps des robots pour la transporter. Plusieurs variantes d'actionnement ont été étudiées : passif, avec compliance et actionné. Un algorithme de positionnement optimal des m-bots autour de l'objet à manipuler a été proposé afin d'assurer la réussite de la tâche à effectuer par les robots. Cet algorithme respecte le critère de "Force Closure Grasping" qui assure la stabilité de la charge durant la phase de manipulation. Il maintient aussi une marge de stabilité statique qui assure la stabilité de l'objet durant la phase de transport. Enfin, l'algorithme respecte le critère des zones inaccessibles qui ne peuvent pas être atteintes par les m-bots. Une loi de commande a été utilisée afin d'atteindre les positions désirées pour les m-bots et d'assurer la navigation en formation, durant la phase du transport, durant laquelle chaque robot élémentaire doit maintenir une position désirée par rapport à l'objet transporté. Des résultats de simulation pour un objet de forme quelconque, décrite par une courbe paramétrique, sont présentés. Des simulations 3D en dynamique multi-corps ainsi que des expériences menées sur les prototypes réalisés ont permis de valider nos propositions.

Mots-clés: Robots mobiles coopératifs, Architecture de contrôle/commande, Co-manipulation et transport de charge, Mécanisme de levage, Synthèse dimensionnelle, Force Closure Grasping, Marge de stabilité statique, Évitement d'obstacles, Atteinte des cibles, Navigation en formation.